UNIVERSITÉ DE RENNES 1

THÈSE DE DOCTORAT DE

L'UNIVERSITÉ DE RENNES 1

ÉCOLE DOCTORALE N° 601
Mathématiques et Sciences et Technologies
de l'Information et de la Communication
Spécialité : Télécommunications

Par

Remun KOIRALA

Fonctions conjointes de localisation et de communication dans les réseaux 5G en bandes millimétriques

Thèse présentée et soutenue au CEA-Leti, Grenoble, le 24 janvier 2020
Unités de recherche : CEA-Leti Grenoble et Institut d'Electronique et de Télécommunications de Rennes (UMR CNRS 6164), en cotutelle avec l'Université de Bologne

Rapporteurs avant soutenance :

Gonzalo Seco-Granados	Professeur, Universitat Autònoma de Barcelona, Espagne
Dirk Slock	Professeur, EURECOM, France

Composition du Jury :

Examinateurs :	Geneviève Baudoin	Professeur, ESIEE, France
	Henk Wymeersch	Professeur, Chalmers University of Technology, Suède
	Giuseppe Abreu	Professeur, Jacobs University Bremen, Allemagne
Dir. de thèse :	Bernard Uguen	Professeur, Université de Rennes 1, France
Co-dir. de thèse :	Davide Dardari	Professeur, Università di Bologna, Italie
Encadrant de thèse :	Benoît Denis	Ingénieur de Recherche, CEA-Leti, France

Université de Rennes 1
Università di Bologna
CEA-Leti

Doctoral Thesis

Joint Localization and Communication in 5G Millimeter Wave Networks

---

Author:
Remun Koirala

Supervisor:
Dr. Benoît Denis
Thesis Directors:
Prof. Dr. Bernard Uguen
Prof. Dr. Davide Dardari

"*Until the end.*"

Abstract

In this thesis, we investigate different facets of localization and communication services motivated by the symbiosis between them in the millimeter wave (mm-Wave) context for the fifth generation (5G) of wireless communications. Our aim is twofold: first, show that this duality is mutually beneficial to both services, and second, aim towards a co-existence to capture these benefits in order to bring forth mm-Wave as a strong contender for 5G. First, we look into how beamforming, an integral part of mm-Wave communications, can aid in improving the localization performance. After characterizing the localization performance in terms of Cramér-Rao lower bound (CRLB), we show that with optimized beamforming, the estimation of localization variables (delay, angle of departure (AoD) and angle of arrival(AoA)) improves. Then we consider the problem of co-existence of the two services together in the same system while sharing time and frequency resources. We study the non-trivial trade-off between the performances of the two services during this resource budgeting. Then, relying on this trade-off, we design an optimal resource allocation scheme while also optimizing the beamwidth in order to ascertain high performance in terms of both localization and communication. In the same context, we also look into different applications of this improved location information namely initial access, channel estimation and simultaneous localization and communication (SLAM). We show that the related performances improve in terms of quality, latency and/or complexity in comparison to the conventional methods.

Acknowledgements

First and foremost, I would like to express my sincere gratitude to my supervisor *Dr. Benoît Denis* for his support, enthusiasm, patience and dedication towards every aspect of my Ph.D. studies. I would like to thank him for being available irrespective of the time or day. He allowed me a lot of freedom to divulge into different research aspects while simultaneously ensuring that I do not deviate too much. In addition, he covered me almost in almost all the bureaucratic aspects of my Ph.D. (as complicated as it can be) thus allowing me to stay focused on my research. Without his guidance, this research and this dissertation would not have seen the light and I am eternally grateful to him for these three years.

Additionally, I would also like to express my thanks to my thesis directors *Prof. Dr. Bernard Uguen* and *Prof. Dr. Davide Dardari* for their continuous support and guidance during the course of these three years. They provided me with both technical feedback that helped me maintain the quality of my work and moral support that motivated me to keep going forward.

I gratefully acknowledge the funding received towards this work in part by European H2020 project SECREDAS, which is funded through the specific ECSEL Joint Undertaking research and innovation program (GA No. 783119).

Moreover, I would like to extend my sincere gratitude towards *Prof. Dr. Henk Wymeersch* for lending me his expertise and always providing me with new ideas and constructive support during our collaboration. I am grateful for his friendly guidance, patience and for always being available during our work together. I learnt a great deal from him.

Similarly, I would also like to thank *Dr. Antonio De Domenico* and *Gourab Ghatak* for their significant efforts during our collaboration. I enjoyed all our discussions and it was a pleasure to work with them.

I would also like to take this moment to thank *Prof. Dr. Giuseppe Abreu* for being an inspirational figure during my time at Jacobs University. He was the person who taught me all the fundamental aspects and details of research. Without the personal and intellectual growth I had under him, I would not be in this position today.

I would also like to thank *Prof. Dr. Geneviève Baudoin*, *Prof. Dr. Gonzalo Seco-Granados*, *Prof. Dr. Dirk Slock*, *Prof. Dr. Henk Wymeersch* and *Prof. Dr. Giuseppe Abreu* for agreeing to take part in the dissertation committee.

I gratefully acknowledge all my friends who have helped me during the past three years. I am especially grateful to *Papuli* with whom I have shared an unforgettable journey for 8 years. A big thanks to my friends in Grenoble *Luiz*, *Moises*, *Federico*, *Sandip*, *Walter*, *Ujjwol*, *Shriprem*, *Kyunghwa*, *Bikash*, *Bikram*, *Angela*, *Nieves*, *Ekki*, *Hakim*, *Imane*, *Aleksandra*, *Ibtissam*, *Subash* and *Sudishna* for helping me ease in the life of Grenoble very well. I am also grateful to all my friends in Germany, *Bishesh*, *Karish*, *Abhinandan*, *Monita*, *Anuraag*, *Grishma*, *Jason* and *Pritam* for still managing to find the time to spend with me during these three years despite the distance. Likewise, I would like to thank *Paras*, *Krishna*, *Neeraj* and *Sadeep* for always motivating me to keep going. The times I spent with you all are precious to me and will always be in my memory.

I would, further, like to express my sincere gratitude towards my German family, *Ina Ahrens* and *Bernd Giesecke*, who have always been so welcoming towards me and have been a vital part of my life in Europe. They have helped me fill the cultural gap between my home and Europe and have really become my second family. Thank you for being there for me for the past 8 years.

I would also like to say a heartfelt thank you to my late grandfather *Komal Mudvari* and my grandmother *Maiya Mudvari* for being such an important part of my childhood and growing up.

Last but not the least, I owe a huge debt of gratitude to my mother *Rekha Koirala*, my father *Madhav Prasad Koirala* and my brother *Devyanshu Koirala* for all the sacrifices, love, support, encouragement and motivation they have provided me throughout my life. They have always shown enthusiasm towards every one of my small achievements and it has only helped me move forward with even more vigour. Without your immense support, I would not be in this position and I am extremely grateful to you.

Contents

List of Figures

List of Tables

Acronyms

1G	first generation.
2D	two dimensional.
2G	second generation.
3D	three dimensional.
3G	third generation.
3GPP	3rd Generation Partnership Project.
4G	fourth generation.
5G	fifth generation.
AoA	angle-of-arrival.
AoD	angle-of-departure.
BCRLB	Bayesian Cramér-Rao lower bound.
BP	belief propagation.
BS	base station.
CBF	conventional beamformer.
CDF	cumulative distribution function.
CRLB	Cramér-Rao lower bound.
D2D	device-to-device.
DAC	digital-to-analog converter.
EB	exabytes.
eMBB	enhanced mobile broadband.
ESPRIT	estimation of signal parameters via rotational invariance.
FIM	Fisher information matrix.
FSPL	free space pathloss.
GNSS	global navigation satellite system.
GPS	Global Positioning System.
IoT	internet of things.

ITU International Telecommunication Union.

LOS line-of-sight.

MC Monte Carlo.
MIMO Multiple-input multiple-output.
mm-Wave millimeter wave.
mMTC massive machine type communication.
MS mobile station.
MUSIC multiple signal classification.

NLOS non-line-of-sight.
NMSE normalized mean square error.

OEB orientation error bound.
OFDM orthogonal frequency-division multiplexing.
OMP orthogonal matching pursuit.

PEB position error bound.
PPP Poisson point process.

QoS quality of service.

RAT radio access technique.
RF radio frequency.
RMSE root mean squared error.
RSSI received signal-strength indicator.

SDP semidefinite problem.
SINR signal-to-interference-plus-noise ratio.
SLAM simultaneous localization and mapping.
SNR signal-to-noise ratio.
SOEB squared orientation error bound.
SOMP simultaneous orthogonal matching pursuit.
SPEB squared position error bound.

TDoA time difference of arrival.
ToA time of arrival.

UE user equipment.
ULA uniform linear array.
URLLC ultra-reliable low latency communication.

V2V vehicle-to-vehicle.

Wi-Fi wireless fidelity.

List of Notations

$\mathbb{R}$	domain of real numbers
$\mathbb{C}$	domain of complex numbers
$\boldsymbol{x}$	vector notation
$\boldsymbol{X}$	matrix notation
$(\cdot)^T$	transpose of a vector or a matrix
$(\cdot)^H$	conjugate transpose of a vector or a matrix
$(\cdot)^{-1}$	inverse of a matrix
$\text{diag}(\boldsymbol{x})$	diagonal matrix with entries from $\boldsymbol{x}$
$\text{diag}(\boldsymbol{X}_1, \boldsymbol{X}_2)$	block diagonal matrix with $\boldsymbol{X}_1$ and $\boldsymbol{X}_2$ as the block components
$\otimes$	Kronecker product
$\text{trace}(\cdot)$	trace of a matrix
$\text{vec}(\cdot)$	vectorization of a matrix
$\text{rank}(\cdot)$	rank of a matrix
$\mathbb{E}[\cdot]$	expectation operator
$\|\| \cdot \|\|_p$	p-norm of a vector or a matrix
$\Re(\cdot)$	real operator
$\Im(\cdot)$	imaginary operator
$\lceil \cdot \rceil$	ceiling operator
$\lfloor \cdot \rfloor$	floor operator
$\boldsymbol{I}_N$	identity matrix of size $N \times N$
$\boldsymbol{0}_N$	zero matrix of size $N \times N$
$\boldsymbol{e}_n$	Euclidean space standard basis vector with n-th element as 1

List of Symbols

ULA antenna model

$\boldsymbol{a}_{Tx}$	ULA antenna response vector at transmitter	
$\boldsymbol{a}_{Rx}$	ULA antenna response vector at receiver	
N_t	Number of antenna elements in transmitter antenna array	
N_r	Number of antenna elements in receiver antenna array	
G_{Tx}	Transmitter antenna gain	
G_{Rx}	Receiver antenna gain	

Beamforming model

$\boldsymbol{f}$	Transmit beamforming column vector	
$\boldsymbol{w}$	Receive beamforming column vector	
γ_{Tx}	Main lobe transmitting antenna gain in the sectorized model	
ω_{Tx}	Main lobe beamwidth of the transmitting antenna	rad
γ_{Rx}	Main lobe receiving antenna gain in the sectorized model	
ω_{Rx}	Main lobe beamwidth of the receiving antenna	rad
g	Side-lobe antenna gain in the sectorized model	

mm-Wave channel model

h	Complex channel coefficient	
h_R	Real part of the complex channel coefficient	
h_I	Imaginary part of the complex channel coefficient	
θ	Angle of departure	rad
ϕ	Angle of arrival	rad
τ	Time delay	s
α_L	LOS path loss exponent	
α_N	NLOS path loss exponent	

mm-Wave network geometry

ξ	BS process	
λ	BS process intensity	
d_S	Radius of the LOS ball	m

d_a	Distance between the serving and the nearest interfering BS	m
h_B	Height of the BS	m

Signal model

P_{Tx}	BS transmit power	dBm
$s(t)$	Transmitted signal	
f_c	Center frequency of transmitted signal	Hz
λ_c	Wavelength of transmitted signal	m
B	Bandwidth of the transmitted signal	Hz
c	Speed of light	ms^{-1}
N_0	Noise power spectral density	dBm/Hz
σ_N^2	Total noise power	dBm

Dedicated to:

My parents

Madhav Prasad Koirala & Rekha Koirala

and

My brother

Devyanshu Koirala.

Chapter 1

Introduction

1.1 5G claims and requirements

Since its conception in early 1980s, we have been witnessing recurrent revolutionary leaps being made in the field of wireless communication networks [1]. The first generation (1G) of mobile communication was characterized by analog transmission of speech signals. The proneness of these analog signals to noise paved the way for the first digital system realized in second generation (2G) systems, offering digital speech transmission and low data rate services (*e.g.* short messaging service) with the downlink peak rate of up to 1.2 Mbps. Then the start of century oversaw a considerable advancement in the technology with the introduction of the third generation (3G) with services such as high speed internet access, audio and video streaming capabilities, accompanied by the rapid and massive deployment of navigation technologies such as Global Positioning System (GPS) with downlink peak rate of up to 42 Mbps. The success brought in by 3G has been further emboldened by the new heights of achievable data rate (up to 1Gbps downlink peak rate) improving even further user experience in the fourth generation (4G) systems.

Despite the huge technological progress in-between the generations, the common theme in this evolution, however, is clear: accommodating the ever increasing traffic and throughput demands of data-driven applications for better user experience. As evidenced in Fig. 1.1, mobile data traffic is expected to increase to an unprecedented level of 131 exabytes (EB) per month in 2024, as compared to just 3 EB a decade earlier [2]. In addition, the same report predicts an increase of global mobile subscriptions to 8.8 billion in 2024 in comparison with 6.8 billion within the same time frame. This growth in mobile data traffic and number of devices has put forth a huge challenge for the wireless service providers in the form of "global spectrum crunch" [3].

Hence, with the 4G technology approaching maturity, the wireless research community has been actively involved in envisioning the blueprint and setting standards

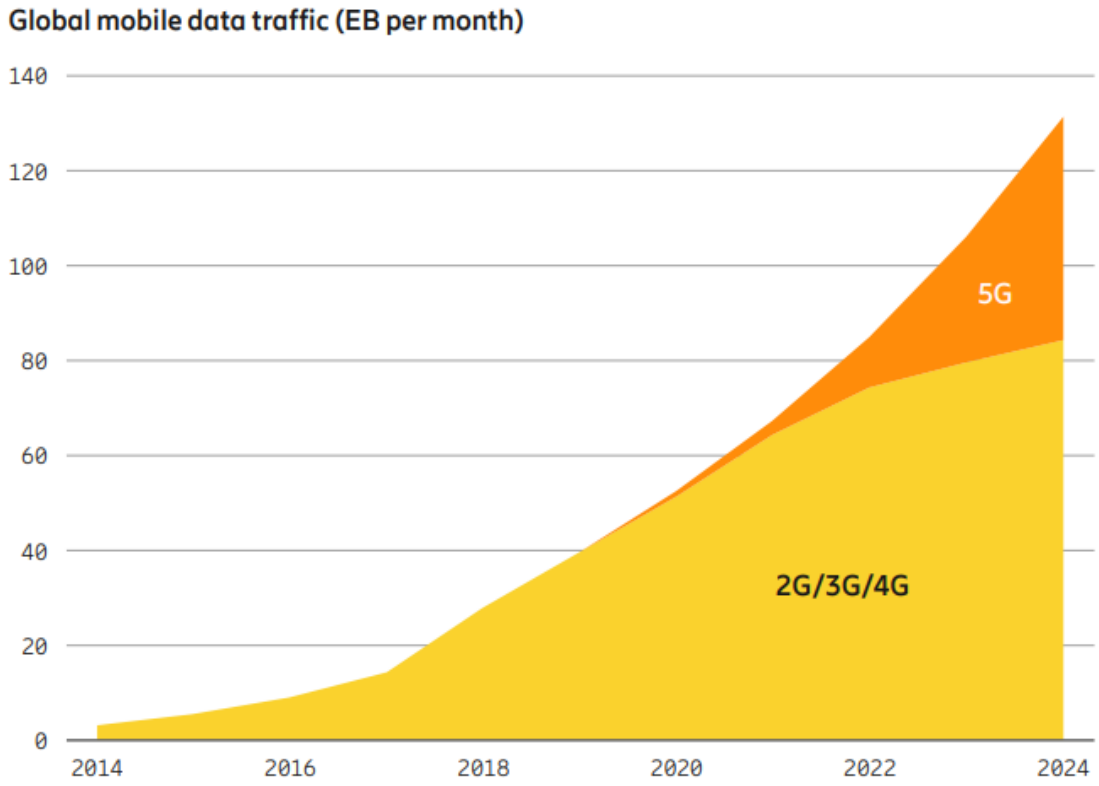

FIGURE 1.1: Global data traffic growth: past, present and future [2].

of fifth generation (5G) wireless networks. 5G promises to meet the expected demands of low-latency, high-rates, reliable and low-cost mobile connectivity and in the process open access to a plethora of new services and use cases, broadly categorized into three service categories including enhanced mobile broadband (eMBB), ultra-reliable low latency communication (URLLC) and massive machine type communication (mMTC) [4, 5].

- **eMBB**: eMBB use cases encompass the data driven use cases, requiring high data rate and a wide-area coverage even with high user mobility. *E.g.* Data heavy multimedia streaming, cloud gaming, augmented and virtual reality.
- **URLLC**: URLLC use cases consider applications requiring reliably delivering packets with stringent latency and quality of service (QoS) requirements. *E.g.* Remote medical surgery, inter-vehicular communications and the tactile internet.
- **mMTC**: mMTC use cases involve massive numbers of connected devices, and are typically expected to be energy efficient. *E.g.* massive internet of things (IoT), large sensor networks.

To fulfill the needs of these use cases, the key requirements identified for a 5G system are as follows [6, 7, 8, 9]:

1. **Ultra fast** with minimum of 20 Gbps peak downlink data rate for eMBB case as compared to 1 Gbps peak rate in 4G.

2. **Low latency** with 1 ms round trip latency for URLLC and 4 ms for eMBB as compared to about 15 ms in 4G [10].

3. **Ultra reliable** with 99.999% perceived availability. Additionally almost 100% perceived coverage.

4. **Massive Connectivity** with 1 million devices per km^2 in mMTC usage scenario as compared to a hundred thousand in 4G.

5. **Energy Efficient** with 90 % reduction in network energy usage and reduction in power consumption by devices. High sleep ratio and long sleep duration for the eMBB case.

6. **Mobility** with ability to achieve the defined QoS for up to 500 km/h as compared to 350 km/h in 4G.

1.2 Overview of 5G mm-Wave technology

The above mentioned list of requirements for 5G pose challenges in diverse areas. Hence, 5G will not be based on a single technology, but an integration of various technologies to deal with these requirements. In the following sections, we will detail some of the key technologies and techniques that have been identified for 5G, with a particular focus on the millimeter wave (mm-Wave) domain.

1.2.1 Millimeter waves

Revisiting the fundamental motives that have necessitated this migration towards the fifth generation of wireless systems, the question arises on how one can achieve an increase the network capacity. The answer lies in the core laws of information theory, more precisely, formulated in the Shannon-Hartley theorem [11].

The theorem provides an upper bound on the amount of error free data that can be transmitted over a noisy communication channel for a given bandwidth. More specifically,

$$C = B \log_2 \left(1 + \frac{S}{N}\right), \tag{1.1}$$

FIGURE 1.2: Spectrum availability in mm-Wave frequencies [12].

where, C is the channel capacity, B is the bandwidth of the channel, S denotes the denotes the received power of the desired signal and N is the average noise power over the bandwidth. The theorem establishes that the achievable rate is always less than the channel capacity C.

From the above equation, the obvious approaches to increase the channel capacity are to either increase the bandwidth, increase the received power or reduce the noise power at the receiver. Since for the currently utilized bandwidth, the technology is already approaching towards the Shannon limit, the linear proportionality of the bandwidth with channel capacity makes it an appealing approach to increase the system's capacity.

However, as established earlier, the existing sub-6 GHz microwave frequency band has been overly congested and as a result, the interest has been burgeoning towards exploring the previously largely underused high frequency millimeter wave (mm-Wave) band from 30 GHz[1] to 300 GHz in the electromagnetic spectrum [9, 13] as shown in Fig. 1.2. In mm-Wave band, the viable frequency bands of interest as recommended by International Telecommunication Union (ITU) [12] shows a vast amount of spectrum available for utilization, ideal to allow high data rate to multiple users at the same time. It is estimated that from this new access to the mm-Wave band, we can expect 3-10 times (depending on the region) increase in the total allocated spectrum within the next five years [14].

Reaping this amount of easily available spectrum, however, is not devoid of any challenge. The propagation characteristics of the radio signals at very high frequencies (and hence with small wavelengths) is a serious impediment to the potential benefits that we discussed before. In particular, mm-Wave signals are highly affected by higher pathloss, propagation loss due to environmental conditions such as rain, fog and atmospheric gases and its susceptibility to blockages [13, 15, 16].

[1] Actually, the first mm-Wave systems start operating around 24-26 GHz.

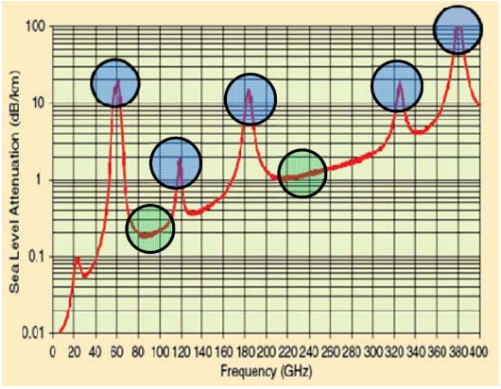

FIGURE 1.3: Atmospheric absorption across mm-wave frequencies in dB/km [13].

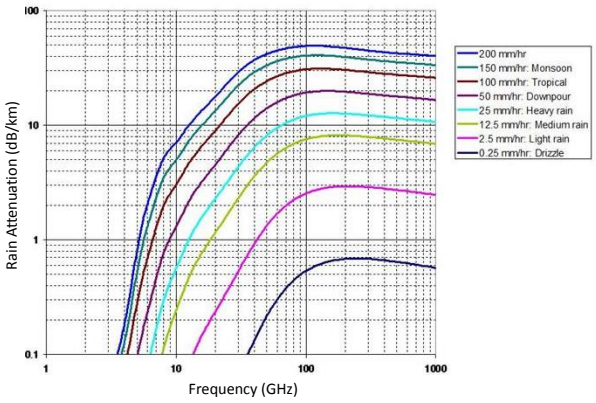

FIGURE 1.4: Rain attenuation in dB/km across frequency at different rainfall rates [17].

Free space pathloss

The free space pathloss (FSPL) can be defined as the attenuation of energy between two radiators in a free space. The pathloss between two antennas separated by a distance d is given by the Friis transmission formula [18]:

$$PL = \frac{1}{G_{Tx}G_{Rx}}\left(\frac{4\pi df}{c}\right)^2, \tag{1.2}$$

where, f is frequency of the transmitted signal, c is the speed of light and G_{Tx} and G_{Rx} are the transmit and recieve antenna gains respectively. In the case of isotropic transmission (*i.e.* $G_{Tx} = G_{Rx} = 1$), we can see in the above equation $PL \propto f^2$, thus coming to the conclusion that at high frequencies of the mm-Wave signal, the pathloss is significantly higher.

Environmental effects

In addition to the FSPL, environmental factors such as atmospheric absorption by gases such as oxygen and water vapour as seen in Fig. 1.3 and rainfall as seen in Fig. 1.4 also play a significant role in the mm-Wave signal propagation. The figures above show that the attenuation due to environmental factors (usually measured in [dB/km]) are frequency dependent. The attenuation due to atmospheric gases is worse especially for the frequency around 60 GHz, 120 GHz and 180 GHz. Similarly, the signal propagation in rainy conditions also depends upon the frequency and rate of rainfall with higher attenuation with increasing frequency and intensity of rainfall. The attenuation due to these effects makes it challenging particularly for outdoor communications.

Blockages

Apart from the previously mentioned FSPL and environmental effects, the sensitivity to blockages in another serious hindrance for mm-Wave signal propagation. mm-Wave signals are especially susceptible to blockages due to high penetration loss and negligible diffraction effects [19, 20]. For instance, the attenuation due to penetration loss through a 10 cm concrete at 3 GHz is 17.7 dB compared to a significant 175 dB at 40 GHz [20]. It can also be noted that there are significant differences between line-of-sight (LOS) and non-line-of-sight (NLOS) pathloss characteristics. The authors in [13] measured an average pathloss exponent of 2.55 in a LOS environment as compared to a significant 5.76 in NLOS cases in downtown New York City. Hence, these effects due to blockages can seriously pose issues regarding coverage for instance inside an indoor environment.

In the context of mm-Wave, however, the propagation loss are not as much pronounced due to short transmission distances [21]. Deliberately limiting the cell size to 100-200m, and hence densifying the access network, contributes to minimize the high propagation losses inherent to mm-Wave propagation [13]. We have already established that the FSPL scales quadratically with the propagation distance, hence shorter propagation distance reduces the attenuation. Moreover, as we can see in Figs. 1.3 and 1.4, in the case of 80 GHz frequency, the attenuation due to atmospheric absorption is expected to be just .2 dB/km and heavy rain is expected to be around 10 dB/km. Considering the propagation distance of 200m, the attenuation loss is just 0.04 dB and 2 dB due to atmospheric absorption and heavy rain respectively, which does not pose a significant enough threat to transmission at such frequencies.

Additionally, countering the effects of attenuation by exploiting the transmission and reception directionality with the help of beamforming has also been deemed as a very effective solution. In equation (1.2), we can leverage on the fact that $PL \propto \frac{1}{G_{Tx}G_{Rx}}$ and boost the transmit and receive antenna gains in preferred directions with the help of beamforming to mitigate the pathloss effects. Multiple-input multiple-output (MIMO), in the context of 5G, has been deemed as a key technology to exploit the potential gain due to beamforming. In the following section, we will further elaborate the relevance of beamforming and directionality with the help of MIMO in the context of mm-Wave communications.

1.2.2 MIMO and beamforming

It is well established that transmitting signals of shorter wavelengths, for instance in the case of mm-Wave, for physical reasons allow for a smaller antenna size [22]. Exploiting this reduced size, instead of using only one antenna, MIMO in the context of mm-Wave has the potential to employ a very large number of antenna elements together to enable a very powerful transmission technique known as beamforming [23]. Using multiple antenna elements in an antenna array helps in radiating the signal power towards a particular desired direction with certain beamwidth, instead of transmitting to all the directions as in the single antenna case. Moreover, it is also possible to receive the signal only from particular directions with the congruent technique at the receiver, referred to as combining[2].

This radiation pattern is achieved with the help of constructive and destructive interference between the same signals radiating from different antenna elements with varying phase and/or amplitude. In addition, the pattern also depends upon the number, the geometrical arrangement (for *e.g.* linear, circular, spherical, rectangular, 3D) and the inter-element spacing of the antennas in the array. Moreover, it is also possible to change the radiation direction by simply changing the phases and/or amplitude of the antenna elements (also referred to as beam steering).

As a consequence, mm-Wave MIMO technology allows for a remarkable deviation from the traditional omni-directional to the highly directional transmission with the help of antenna arrays at both transmitting and receiving end helping to compensate for the large propagation loss. Furthermore, with the help of beam-steering, it is possible to circumvent the problem of direct path blockage by steering the beam towards other non-direct paths giving possibilities to NLOS communications. Hence, in addition to the smaller cell sizes, beamforming with the help of highly directional and steerable antennas has been accepted as an important solution to the attenuation problem induced by high frequency signal characteristics in the step towards unleashing the full capabilities of mm-Wave based communications [24]. An example of very commonly used array configurations (also pertinent to this thesis) is uniform linear array (ULA).

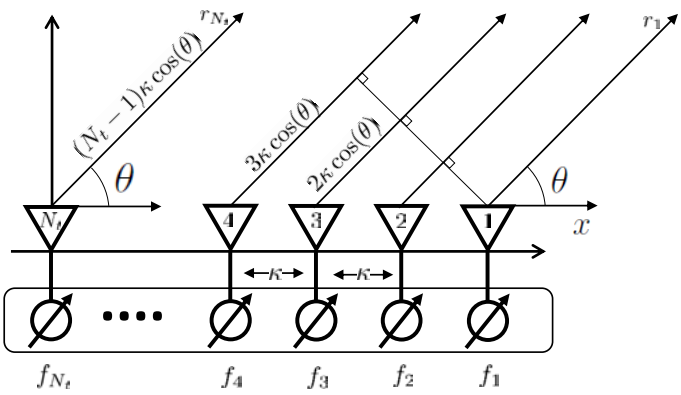

FIGURE 1.5: An example of a ULA array model with N_t antenna elements separated by a distance κ transmitting with AoD θ with the beamforming vector $\boldsymbol{f} = [f_1, f_2, \cdots f_{N_t}]^T$.

Uniform linear array

ULA is considered as one of the simplest and most widely adopted antenna array type characterized on the basis of antenna element arrangement. As the name suggests, ULA is formed by placing N_t uniformly distanced antennas along a line with inter-element distance κ, usually equal to $\lambda/2$, as illustrated in Fig. 1.5. Assume $x_n = (n-1)\kappa$ to be the position of n-th antenna element in the figure.

Consider a point user at a distance r_n and angle θ from the n-th antenna array that receives the transmitted signal s with wavelength λ and frequency f. Here, we make a "far field assumption" and consider that the destination point is sufficiently far away to assume the paths from each antenna element to the point is parallel. As indicated in the figure, the excess time of flight of the signal transmitted from the n-th antenna is $(n-1)\kappa\cos(\theta)$. Since $r_n = ct_n$, where t_n is the time taken for the signal from the n-th antenna to reach the destination, the phase shift can then be written as:

$$a_n = e^{j2\pi f t_n} = e^{\frac{j2\pi c t_n}{\lambda}} = e^{\frac{j2\pi r_n}{\lambda}}. \tag{1.3}$$

Hence the vector of received signals from all the antennas can be written as:

$$\boldsymbol{r} = \left[s e^{\frac{j2\pi r_1}{\lambda}}, s e^{\frac{j2\pi r_2}{\lambda}}, \cdots, s e^{\frac{j2\pi r_{N_t}}{\lambda}} \right]^T. \tag{1.4}$$

[2]Even though we only focus on the beamforming techniques in this section, all the ideas and techniques relevant to beamforming can be reciprocated for combining as well. In this thesis, we refer to combining also as beamforming at the receiver.

Thus normalizing with respect to the signal power and the phase of the first antenna element, we can have the normalized ULA response vector $\boldsymbol{a}_{Tx}(\theta)$ as:

$$\boldsymbol{a}_{Tx}(\theta) = \frac{1}{N_t}\frac{s^*}{||s||_2^2}e^{-\frac{j2\pi r_1}{\lambda}}\boldsymbol{r} = \frac{1}{N_t}\left[1, e^{\frac{j2\pi(r_2-r_1)}{\lambda}}, \cdots, e^{\frac{j2\pi(r_{N_t}-r_1)}{\lambda}}\right]^T \tag{1.5a}$$

$$= \frac{1}{N_t}\left[1, e^{\frac{j2\pi\kappa\cos(\theta)}{\lambda}}, \cdots, e^{\frac{j2\pi(N_t-1)\kappa\cos(\theta)}{\lambda}}\right]^T, \tag{1.5b}$$

where, we have the relation $r_1 - r_n = (n-1)\kappa\cos(\theta)$.

We can change the radiation pattern from the antenna by modifying the amplitude and phase of each antenna. Considering a ULA of N_t antenna elements and beamforming weights (in a precoding sense) f_n at each array element, the radiation pattern is given by the following equation.

$$y = \boldsymbol{f}^H\boldsymbol{a}_{Tx}(\theta), \tag{1.6}$$

where $\boldsymbol{f} = [f_1, f_2, \cdots, f_{N_t}]^T \in \mathbb{C}^{N_t}$.

MIMO beamforming architectures

We have established that exploiting the spatial beamforming with the help of antenna arrays enables the possibility to counter the significant propagation loss. In addition, the multiple antennas also allow for spatial multiplexing with the help of multi-stream transmissions [25]. Both of these features help to improve the spectral efficiency, and hence MIMO has been touted as a very strong enabler of mm-Wave technology.

However, there are of course practical limitations such as hardware complexity and power consumption limits to keep up with while using these arrays in real systems. Depending on the number of radio frequency (RF) chains used, number of data streams to be transmitted, and whether the weighting for beamforming is done in digital or analog domain, the MIMO beamforming architecture can be divided into three categories [24, 26].

- **Digital Beamforming:** Digital beamforming is the most complex and cost intensive beamforming architectures. The beamforming is done in baseband in digital domain, and requires 1 RF chain and 1 digital-to-analog converter (DAC) per antenna element. Even though, such implementation fully unlocks the multi-stream transmission capabilities of MIMO, the cost and power consumption are still very high for practical implementation. In addition, the

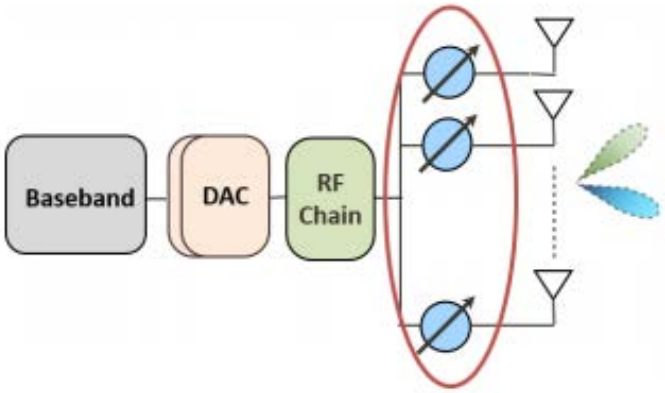

(a.)

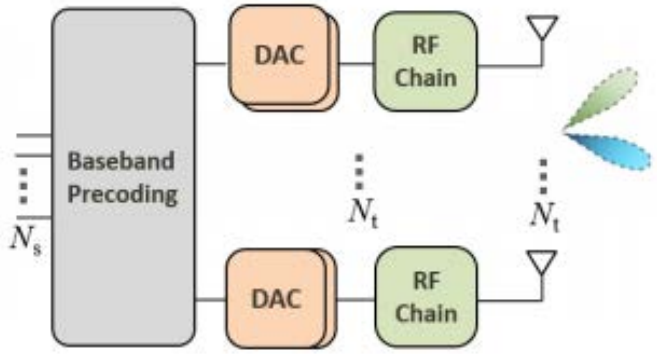

(b.)

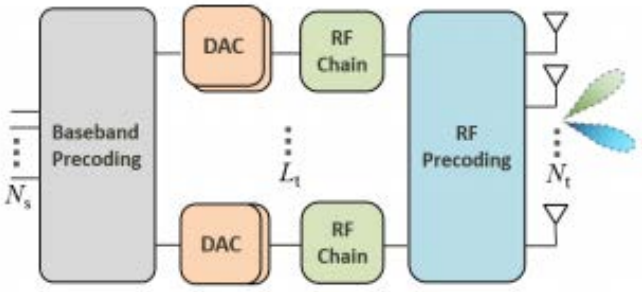

(c.)

FIGURE 1.6: MIMO architecture at mm-Wave based on (a) analog (b) digital and (c) hybrid beamforming [24].

large number of antenna elements packed in a small space inhibits such implementation due to physical space constraint.

- **Analog Beamforming:** In contrast, analog beamforming is one of the simplest and most cost efficient MIMO techniques. The beamforming weights are applied in the analog domain and only 1 RF chain and DAC is required which helps to reduce the hardware and power consumption cost significantly. One limitation using this architecture is the inability to exploit multi-stream transmission. Due to the simplicity of implementation, in this thesis we focus mainly on the analog beamforming architecture, especially since we plan on using the technique at the mobile station (MS) end as well where power and cost efficiency can be of the essence.

- **Hybrid Beamforming:** As a compromise, hybrid architecture combines the features of analog and digital architecture to extract the benefits of both. The beamforming is split in both the analog RF and the digital baseband domain in the case. Such an architecture supports transmission of multiple streams, but the number of streams are much less than the number of antennas. This reduces the number of RF chains and DACs required and hence more efficient than its digital counterpart.

We have established that exploiting directionality and hence beamforming and the different beamforming architectures for transmission can be an effective solution to fulfill the requirements of the next generation of wireless communications. However, irrespective of the types of antenna used or the signal processing techniques applied with MIMO, one major issue with the fundamental idea of beamforming is that the transmitter needs to have the knowledge of the location-dependent channel between itself and the receiver. In the next section, we will look in detail the channel model and parameters used in the MIMO systems.

1.2.3 mm-Wave MIMO channel model

Consider a mm-Wave MIMO model with N_t and N_r antenna elements at the transmitting and receiving end respectively. Then the MIMO multipath channel model $\boldsymbol{H} \in \mathbb{C}^{N_r \times N_t}$ with L propagation paths[3] can be expressed as a linear sum of channel

[3]The propagation paths are in-fact clusters of rays sharing common spatial/temporal characteristic. However, while modelling the channel, it is common in literature to represent a cluster by an effective path [27].

contributions from each path, written as [24, 28]:

$$\boldsymbol{H}(t) = \sqrt{\frac{N_t N_r}{\xi}} \sum_{l=0}^{L} h_l \boldsymbol{a}_{Rx}(\phi_l) \boldsymbol{a}_{Tx}^H(\theta_l) \delta(t - \tau_l) \tag{1.7}$$

where, θ_l and ϕ_l are the the angles with respect to reference directions (referred to as the orientations of the transmitting and the receiving node) of the l-th path from transmit and receive antenna array respectively, referred to as angle-of-departure (AoD) and angle-of-arrival (AoA). Similarly, τ_l represents the time delay between the signal transmission and reception through the l-th path. Likewise, the complex channel coefficient of the l-th path is defined by h_l and ξ represents the average pathloss between the transmitter and the receiver.

Adopting ULA as the antenna array, the transmit antenna response $\boldsymbol{a}_{Tx}(\theta)$ is formulated as in equation (1.5). We can similarly formulate the receive antenna response $\boldsymbol{a}_{Rx}(\phi)$ by replacing θ with ϕ and N_t with N_r in the equation (1.5).

Representing the channel in frequency domain, we can write equation (1.7) as:

$$\boldsymbol{H}(f) = \sqrt{\frac{N_t N_r}{\xi}} \sum_{l=0}^{L} h_l \boldsymbol{a}_{Rx}(\phi_l) \boldsymbol{a}_{Tx}^H(\theta_l) e^{-j2\pi\tau_l f} \tag{1.8}$$

In a nutshell, the intrinsically directional nature of mm-Wave MIMO communication tends to accentuate the susceptibility and dependency of key radio channel variables to both relative location and orientation. In order to comprehend the channel between two nodes, it is of utmost importance that we understand the location dependent variables (*i.e.* AoD, AoA and the distance), not only of the direct path between the transmitter and the receiver, but also of the indirect paths, or equivalently the position and orientation of the receiver and the position of the scatterers that contribute to the multipath components. Hence, localizing the user (and possibly, the scatterers in the physical environment) is one of the most important pieces of the 5G puzzle that needs to be identified to fully exploit the potentials of beamforming and hence mm-Wave and MIMO technologies.

1.3 Localization: Overview and prospects in 5G

In the last few decades, with the growing popularity of location based services, localization[4] with the help of radio signals has been recognized as a very important

[4]In this thesis, the term localization is used to refer to both the position and orientation estimation. Likewise positioning or position estimation refers to knowing the relative or absolute

functionality. After the conception of satellite based navigation systems with Transit [29] in 1960s, the significance grew especially with the global navigation satellite system (GNSS) systems such as GPS and Galileo [30]. With the advancement in the wireless communication technologies, localization in cellular domain gained considerable attention, especially starting from 4G systems, and led to the opening of new avenues in terms of location based services, for *e.g.* augmented reality with motion tracking, location based pervasive gaming[31], healthcare [32], and location dependent advertising [33]. Hence, we can claim that localization services have already established itself as an indispensable part of the wireless scenario.

In the cases of 3G and 4G cellular systems, the most popular localization techniques are primarily based on:

1. **Distance estimation** through techniques such as received signal-strength indicator (RSSI), time of arrival (ToA), time difference of arrival (TDoA) and delay[5] estimation between the reference and the terminal node[6] which can feed multi-lateration techniques for positioning.

2. **Angle estimation** with the help of AoA estimation techniques such as subspace based methods (*e.g.* multiple signal classification (MUSIC), estimation of signal parameters via rotational invariance (ESPRIT)) that can in turn feed multi-angulation techniques for positioning.

However, there are some serious challenges faced by localization in 3G and 4G (and in general in sub-6 GHz based) systems, namely, prevalence of the multipath components [34, 35], requirement of multiple anchor nodes, high processing complexity.

- **Prevalence of multipath components:** The multipath components correspond to replicas of the emitted signal (i.e., echos resulting from multiple electromagnetic interactions within the propagation environment, such as reflection, diffraction, etc), often overlapping with the useful signal components. These additional signal components create an adverse condition for both delay and angle estimation. For the case of RSSI, the multipath creates a great variation in received power due to the position of the terminal node. Similarly, ToA and TDoA based methods also suffers from additional biases during the

location of a node, whereas orientation estimation refers to estimating the heading of the user with respect to a reference direction.

[5]In this thesis, the term delay is interchangeably used as "absolute time of flight", which is affected by clock phase uncertainty in a real system but this can be solved out by implementing multi-way cooperative handshake protocols.

[6]Here, the terminal node is referred to the node whose location we are interested in estimating.

estimation process (for instance during matched filtering). Likewise correlated signals arriving from multiple directions can create an error during AoA estimation if the angular resolution is not very high.

- **Requirement of multiple anchor nodes:** Multi-lateration and multi-angulation techniques for location estimation rely on combining the individual distance and angle measurements by each anchor nodes. Hence, for such localization techniques to work accurately, we not only need the deployment of multiple anchor nodes, but also good placement of the anchors [36].

- **Processing Complexity:** For the localization techniques requiring complex architectures such as large number antenna arrays, large number of anchor nodes and/or a large number of nodes to be positioned simultaneously, the processing complexity can be very high [37, 38]. The localization algorithms for such complex requirements require high processing capacity which is not always the case. Such high processing, further, is generally cost and energy inefficient.

However, with the help of the technologies relevant to 5G as described earlier, these localization related issues native to the current generation of wireless technology can not only be alleviated, but in turn, localization has the potential to establish itself as a crucial component of 5G. In the following sections, we will first define performance metrics for localization performance characterization that we will use in this thesis and then describe how the innate features of 5G can aid in localization.

1.3.1 Intrinsic 5G mm-Wave benefits with respect to localization

We have already discussed in the earlier sections how the features of mm-Wave and MIMO can play an important role in 5G communications. However, in addition to communication, the localization accuracy that can be achieved with mm-Wave is very high, as it can be seen in table 1.1. In the table, we can see that the the physical layers operating in sub-6 GHz band (802.11a/g, 802.11n and 802.11ac) have considerably lower raw resolution as compared to the one operating in mm-Wave band (802.11ad). This is due to some of the intrinsic features of this technology, as shown below, that can inherently improve localization as well [33, 41, 42, 43].

Physical Layer	Bandwidth	Raw Resolution
IEEE 802.11a/g Wi-Fi	20 MHz	15m
IEEE 802.11n	40 MHz	7.5m
IEEE 802.11ac	<160 MHz	>1.9m
UWB	>500 MHz	0.6m
IEEE 802.11ad	**> 2 GHz**	**<15cm**

TABLE 1.1: Popular physical layers used in localization, their frequency bandwidth, and the raw sample spatial resolution each offers. The raw resolution is defined as the distance light travels between sampling instants at that bandwidth (Raw resolution = Speed of light / Bandwidth) [39, 40].

Reference	Measurement Scenario	Average No. of Clusters	
		LOS	NLOS
3GPP model [45]	UMi street canyon scenario	12	19
[13]	28 GHz urban scenario	7.2	6.8
[46]	60 GHz indoor scenario	10	10
[47]	60 GHz indoor scenario	3.5	2.2

TABLE 1.2: Comparison of average number of mm-Wave multipath clusters measured with different measurement scenarios.

Sparse multipath channel

We have already established that the high frequency mm-Wave signals suffer from propagation loss due to high pathloss and blockage. This property results in fewer clustered multipath components (group of multipath components with unique AoD and AoA distributed around a mean delay), and hence results in a spatially sparse channel. In Table 1.2, we have shown the comparison between the number of clusters measured during different campaigns. We can see that the number of clusters are in real world measurements are lower than the one recommended in the 3rd Generation Partnership Project (3GPP) channel model. Hence, less perturbation and bias in the received signal due to few multipath components is certainly a favourable property for localization. On the other hand, it also means that it is easier to track the few multipath components, and even use them as constructive information for improving localization [44] (*e.g.*, to compensate for the blockage of the direct path).

Large bandwidth availability

5G systems have the possibility to exploit large bandwidths. This large bandwidth allows for a finer degree of time-delay resolution [48] permitting a fine delay estimation, as well as multipath resolution. We have established that the multipath components are highly dependent on the position of transmitter, receiver and the

scattering environment. Hence, if we can resolve and track multipath, we can use the signal to position (and possibly track) not only the transmitter and receiver, but also physical features belonging to the environment (i.e., scatterers), thus contributing to mapping the latter. In this regard, recent results [49] show that there is a net gain in localization information (in terms of Fisher information matrix (FIM)) in the presence of tractable multipath components. Furthermore, the authors show that localization is feasible even in the absence of direct path with few multipath components. Similarly, in [50], the authors describe a particle filter based simultaneous localization and mapping (SLAM) approach exploiting the multipath measurements with wide-band signals.

Large number of antennas

Similarly, another property of 5G systems affecting localization is the possibility to rely on a large number of antennas. The resulting ability to beamform improves the signal-to-noise ratio (SNR) of the received signal in general, and hence, contributes positively to the estimation of the location-dependent variables such as delay, AoD and AoA. In [51, 52], the authors have shown that the theoretical bounds on localization performances for estimating the mentioned location dependent variables depends directly on the received signal-to-noise ratio (SNR). Moreover, large numbers of antennas also provide higher angular resolution in the spatial domain. Considering the multipath components are sparse, they are likely to arrive from fewer specific directions. As a result of this property, in addition to using the time-delay property, the multipath resolution can be performed in spatial domain as well, jointly aiding localization, mapping and tracking.

Ultra dense networks

Another 5G feature that is advantageous to localization corresponds to ultra dense networks. A denser base station (BS) network reduces the distance between the base station (BS) and the terminal node, increasing the LOS connectivity probability. For instance, according to the 3GPP channel model between 0.5 to 100 GHz in [53], the LOS probability is always 1 within certain BS-terminal distance whereas it gradually decreases after crossing the threshold. This increased probability of direct path improves the location estimation. Besides, the ultra dense networks also provide an option to rely on a large number of geo-referenced BSs playing the role of anchors for absolute positioning (assuming multi-BS connectivity).

D2D communications

Finally, the device-to-device (D2D) technology is another feature native to 5G that could aid in localization. D2D communication, naturally profiting from close proximity with the user nodes due to low pathloss, latency and reliable links, enables cooperative localization [54, 55]. Such D2D links can be used to extract reliable localization information in a distributed manner even in the absence of direct path, as each such devices can act as an anchor node. This information can be very useful especially in scenarios requiring quick, frequent and reliable localization information of the neighbouring nodes, for instance in the case of self driving applications with the help of vehicle-to-vehicle (V2V) links [43].

1.4 Duality between mm-Wave localization and communication

In the previous section, we established that location information can be an important piece in the case of 5G. We discussed how different features inherent to 5G (and in particular 5G mm-Wave communications) and the related technologies could turn out to be a boon for localization. However, this relationship between communication and localization is not just unilateral. In contrast, due to the features of the technologies relevant to 5G, localization has the potential to feature indispensably in various facets of 5G communications, fostering a strong symbiotic duality between localization and communication services. Such interdependence between the two services is illustrated in Fig. 1.7 and described below.

1.4.1 Beamforming optimization

Beamforming optimization is one of the perfect examples exhibiting the interdependence between localization and communication services.

We have already established that beamforming is an important enabling technology for 5G in order to counter the previously mentioned propagation loss effects at a high frequency with higher SNR for both communication and localization services. Depending on the types of services, the beamforming optimization (*i.e.* with regards to both beam direction and width) can be performed with different targets in mind. For instance, in the case of communication oriented beamforming, the target could be rate [56] or SNR [57] maximization whereas for localization oriented beamforming, minimization of error in estimating particular location dependent variables [58] or some localization error cost function [59]. In [58], the

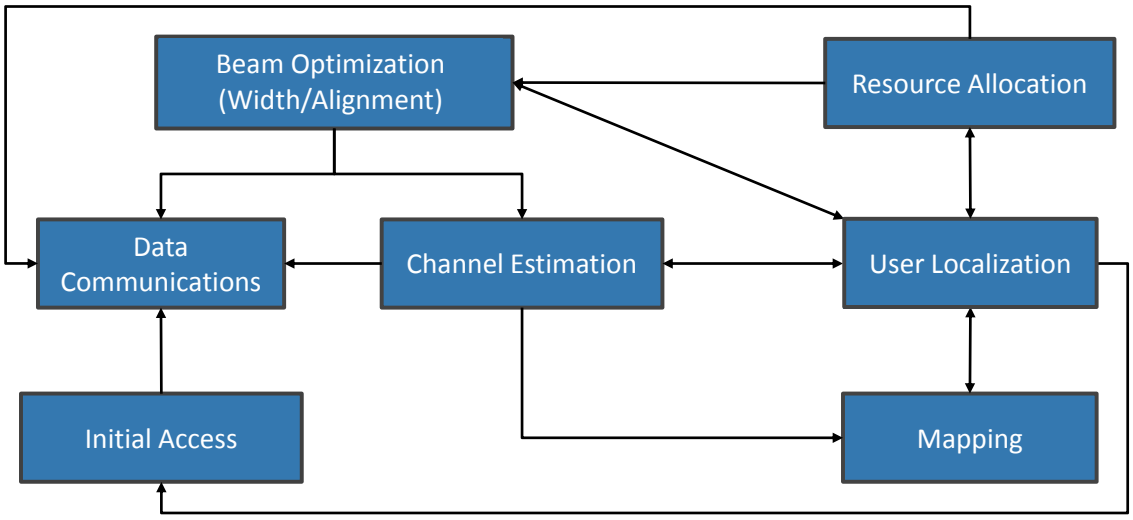

FIGURE 1.7: Illustration of the interdependence between localization and communication services in different facets of 5G.

authors perform beamforming optimization to jointly minimize the Cramér-Rao lower bound (CRLB) for estimating AoD and AoA whereas in [59], the authors consider minimization of squared position error bound (SPEB) of the user.

However, the required terminal node location is one of the major impediments to the optimization process. In the best case scenario, one perfectly knows the position of the terminal node, as then it enables the transmitter to beamform in the corresponding direction with very thin beamwidth, allowing for very high transmission rates. In other cases, the transmitter either has to locate the mobile node to indirectly, for instance by means of a sector search based on beam sweeping methods [56, 60] with overhead, or use localization services and technologies [61]. Hence, the availability of accurate localization information can be advantageous to optimizing the beam and reciprocally, a well optimized beam can help generate accurate localization estimates.

1.4.2 Resource allocation

Similarly, resource allocation is another factor that inter-locks the localization and communication functionalities.

At a macro level, in a system providing both localization and communication services, optimally budgeting the resources such as time or frequency, depending on the type of application, is of utmost importance in order to fulfill the service requirements. For instance, in [62], the authors consider the data-rate and localization-error trade-off in a single user system with both localization and communication functionalities while sharing time resources.

Moreover, in a joint localization and communication framework, the information from the localization phase could be used later in the communication phase. In such a scenario, we could divide resources between the services with a certain target in terms of the localization quality, such that we fulfill the data communication QoS requirements.

Similarly, at a micro level, we can perform resource allocation in terms of power allocation and in conjunction with beamforming especially, based on multi-user and/or multi-path considerations. Depending on the certainty of the user location in a multi-user scenario, or the accuracy of the scatterer's location and the channel coefficient of each path in a multi-path scenario, the beam power can be split into different directions in order to achieve some localization or communication targets, as in [61].

1.4.3 Initial access

Initial access - a procedure by which the mobile user establishes a link layer connection with a base station - is another key link between the localization and communication services. We can say that initial access procedure is an even bigger challenge in 5G as compared to previous generations due to the added dimension of directionality. Besides the challenges of the past generations, the mobile node needs to establish a directional link with the transmitter. A common method in practice to establish this link is either through exhaustive [60, 63] or through iteratively finer[64] spatial scanning. A major problem with these methods is latency, as scanning the entire space adds up to large delays, contradicting the idea of low latency communications and user tracking under mobility in 5G. Hence, the localization functionality could be an integral part of the initial access procedure in an attempt to avoid the bottleneck caused by delays in spatial search based initial access.

1.4.4 Channel estimation and environment mapping

We have already mentioned before that the channel at high frequencies has a highly specular and geometric behaviour (very close to optical geometry actually), which strongly depends on the configuration of the radio link relatively to its physical environment. Accordingly, in the model described in equation (1.8), the mm-Wave channel is dependent on the location dependent variables such as delay, AoD and AoA of all the paths including the direct one and the indirect ones. Hence, localizing the user and the scattering points could facilitate a better and faster channel estimation, which is even more relevant under user mobility, as evidenced by [65]

and it can eventually further aid in improving throughput for data communications, while capturing the "quasi-deterministic" location-dependent channel evolution as a function of time. Alternatively, one can leverage on the estimation of the mm-Wave channel, capitalizing on the channel sparsity with techniques such as compressive sensing, to perform environment mapping with SLAM, as done in [51].

1.5 Research methodology

Based on the previous analysis, the combination of localization and communication functionalities appears as a key in the quest towards unravelling the full potential of 5G mm-Wave systems. Motivated by this aspect, in our Ph.D. investigations, we explore the intricacies of this interdependence, in various aspects and from various perspectives. In this section, we outline the adopted research methodology and highlight the key steps, along with related contributions, which will be further detailed in the following chapters.

In chapter 2, we start with the study of the two way relationship between user localization and beamforming optimization. In this chapter we primarily study beamforming optimization while considering a minimization of the resulting localization error. We first solve the optimization problem in a simplified scenario considering a single user single carrier case. We then advance to a multi-carrier scenario and solve the problem for a multi-user case. In the process, we study the optimal power allocation across the subcarriers in order to the improve estimation of the location dependent variables across the users depending on the channel between them and the BS.

Then, in chapter 3 we focus on how localization and communication services can be accommodated in the same system given an a-priori resource budget. We firstly consider a framework comprising both localization and communication services independent of each other where we evaluate the trade-off arising from the different resource sharing strategies, in terms of time and frequency in particular. Then, moving on to a framework where the two services are interdependent, we characterize a trade-off considering the resource budgeting between the two service and also study how beamwidth can play an important role.

Consequently, in chapter 4, we extend this idea to formulate and solve simultaneously the resource allocation and beamwidth optimization problems in a framework consisting of joint localization and communication services. In addition, we also dig into the initial access problem, assessing the stringent low latency requirements of 5G. In this context, we exploit the localization techniques in the initial beam

selection procedure as a part of the initial access and compare our methods with the popular state-of-the-art beam selection and training methods.

Still capitalizing on the acquisition of location-dependent information, in chapter 5 we then investigate the problems of multipath channel estimation and SLAM using AoD and AoA measurements. In the first case, we present a localization aided channel estimation algorithm where we exploit the geometric nature of the mm-Wave multipath channel. In the latter, we then use the angle estimates to map jointly the positions of the user and the scatters in a multipath environment, while considering multiple BSs. In both cases, we compare our scheme with the state-of-the art.

Finally, we conclude our thesis in chapter 6 and then present the perspectives for future work.

1.6 Related contributions

Below, we present a list of related personal patents, journals and conference papers under the purview of this thesis.

Patents proposed:

[p1] "Optimal beamwidth selection and resource allocation in position assisted mm-wave network", **R. Koirala**, G. Ghatak, B. Denis, A. De Domenico

[p2] "Iterative beam training method for assessing a mm-Wave network", **R. Koirala**, G. Ghatak, B. Denis, A. De Domenico

Journal papers:

[j1] **R. Koirala**, B. Denis, D. Dardari, B. Uguen, H. Wymeersch, "Positioning and Throughput Trade-off for Multi-user Multi-carrier mm-Wave MIMO", in IEEE Access, vol. 7, pp. 167099-167112, 2019

[j2] **R. Koirala**, G. Ghatak, A. De Domenico, B. Denis, D. Dardari, B. Uguen, M. Coupechoux, "Joint Beamwidth Optimization and Resource Partitioning Scheme for Positioning Assisted mm-Wave Communication", submitted to IEEE Transactions on Wireless Communications

Conference papers:

[c1] **R. Koirala**, B. Denis, D. Dardari, B. Uguen, "Localization Bound based Beamforming Optimization for multicarrier mmWave MIMO", Proc. IEEE WPNC, Bremen, Oct. 2017

[c2] G. Ghatak, **R. Koirala**, A. De Domenico, B. Denis, D. Dardari, B. Uguen, "Positioning Data-Rate Trade-off in mm-Wave Small Cells and Service Differentiation for 5G Networks", in Proc. IEEE VTC-Spring, Porto, June 2018

[c3] **R. Koirala**, B. Denis, B. Uguen, D. Dardari, H. Wymeersch, "Localization Optimal Multi-user Beamforming for Multi-Carrier mmWave MIMO Systems", Proc. IEEE PIMRC, Bologna, Sept. 2018

[c4] **R. Koirala**, G. Ghatak, B. Denis, B. Uguen, D. Dardari, A. De Domenico, "Throughput Characterization and Beamwidth Selection for Positioning-Assisted mmWave Service", Proc. IEEE ASILOMAR, Pacific Grove, Oct. 2018

[c5] **R. Koirala**, B. Denis, B. Uguen, D. Dardari and H. Wymeersch, "Localization and Communication Resource Budgeting for Multi-user mm-Wave MIMO", Proc. IEEE WPNC, Bremen, Oct. 2019

[c6] **R. Koirala**, B. Uguen, D. Dardari, H. Wymeersch and B. Denis, "Localization Aided Multipath Channel Estimation for Millimeter Wave Systems", submitted to IEEE ICC, Dublin, June 2020

[c7] **R. Koirala**, B. Denis, B. Uguen, D. Dardari and H. Wymeersch, " Simultaneous Localization and Mapping in Millimeter Wave Networks with Angle Measurements", submitted to IEEE ICC, Dublin, June 2020

Chapter 2

Localization-oriented beamforming

2.1 Introduction

Beamforming, and in particular, its role in mitigating the propagation attenuation effects in the case of high frequency mm-Wave makes it an enabling technology availing us the benefits of high frequency communications as described in the previous chapter. With this in mind, the most natural path of action in the research community was to dig into various ways and means to facilitate and optimize beamforming strategies. The focus in the beamforming literature initially was emphasized mainly for the purpose of communications [24] for different beamforming architectures and objectives.

Incorporating beams to perform initial access and establish a reliable connection between the transmitter and the receiver was one of the primary challenges posed by the requirement of beamforming in mm-Wave communications [66]. The idea here was to design a dictionary of beams spanning different directions and beamwidths at both transmitting and receiving ends. Then the beams for initial access were selected based on the best link between all the possible combination of the said beams. In standards like IEEE 802.11ad [60], such codebook based initial access strategy has been implemented with the consideration of analog beamforming. The protocol initially involves large searching sectors, which then iteratively converge towards smaller sectors. In [66], such sequential scanning protocol was described for the case of hybrid beamforming architecture. With the ability to simultaneous beamform in multiple directions, the search duration could be significantly reduced due to parallel beam searching. We study such localization aided initial access scheme in detail in chapter 4.

The focus was then to find an optimal beamforming solution in order to maximize some communication oriented goal, with the coarse knowledge of the position and orientation of the user derived from for instance the initial access phase, initially

in a single-user scenario. For instance, the authors in [57, 67] present a beamforming optimization strategy for maximizing SNR in the case of single stream analog beamforming. Similarly in [56], the authors design a multi-resolution beam codebook with different beamwidths and devise an algorithm to maximize the throughput with hybrid beamforming. Likewise in [68], the authors present an optimal hybrid beamforming solution by maximizing the mutual information of a mm-Wave channel. Now, moving on to the multi-user scenario, the authors in [69] present a beamforming optimization, while considering a multi-user sum rate maximization problem. In the same context, the authors in [70] present a beamforming optimization policy that aims at minimizing transmit power while fulfilling each user's signal-to-interference-plus-noise ratio (SINR) requirements.

However, contrarily to such communication oriented beamforming studies, there has been a dearth of works concerning localization oriented beamforming optimization. We have already evidenced in chapter 1 that localization in 5G and especially in the context of mm-Wave communication can play an indispensable role when compared to the previous generations of wireless communications. Hence, in light of this, in this chapter we study localization bound based optimal beamforming in mm-Wave scenario for both single- and multi-user scenarios. In doing so, we also propose strategies to allocate power across the subcarriers in a multi-carrier scenario in order to minimize the localization error and various ways in which we can address the beamforming optimization problem in a multi-user scenario. In the following section, we present a list of related contributions from the recent state of the art.

2.2 Related works

The earlier works on mm-Wave localization to the best of our knowledge were primarily aimed at characterizing the performance bounds of location-dependent variables estimation, mostly in terms of their Cramér-Rao lower bound (CRLB), for instance in [51, 52, 71, 72]. In [52], the authors derive the CRLB for estimating delay, AoD and AoA in a simplistic single-user, single path and single carrier scenario considering ULA antenna model. Following up, in [51], the authors then provide the bound for a single-user, multipath scenario with multiple subcarriers. Likewise in [71], the authors provide the CRLB for delay, AoD and AoA estimation in a three dimensional (3D) multipath scenario without considering any particular antenna array configuration. The authors finally present the error bounds while considering different antenna arrays. Similarly, in [72], the authors derive a similar

CRLB formulation in a two dimensional (2D) multipath scenario, while making strong asymptotic assumptions regarding the occupied bandwidth and the number of transmit and receive antenna elements. The authors present the final result in terms of equivalent Fisher information matrix (FIM) where the result is presented in terms of position and orientation estimation and not in terms of delay, AoD and AoA like in previous cases.

Using these theoretical performance bounds, recent works in the literature have also been dedicated towards finding the localization optimal beamformers (in a precoding sense). In particular, the authors in [58] study the localization bounds based beamforming in a simplistic single-user single-carrier MIMO scenario while considering a digital beamforming model. The authors formulate the problem as a robust beamforming optimization problem where the minimum between the position error bound (PEB) and orientation error bound (OEB) is minimized. Similarly, following from [72], the authors in [59] propose a beamforming strategies to minimize a localization error expressed in the form of the SPEB in a single-user scenario while considering LOS path. This SPEB is shown to be equivalent to a linear combination of the CRLB terms associated with delay and AoD estimates.

2.3 Methodology and organization

Taking the recent literature into consideration, we present the list of limitation we have identified and how we plan to deal with them in this chapter.

- Firstly, to the best of our knowledge, leveraging multiple subcarriers in a localization oriented beamforming optimization problem has not been considered before in the literature. Hence, we study how beamforming power can be allocated across the spectrum in order to jointly minimize the performance bounds of delay and AoA.

- Further extending the beamforming optimization analysis levering multiple subcarriers, we then consider a problem with single BS and single-user where we estimate all the channel parameters (delay, AoD, AoA and complex channel coefficients). The difficulty in considering all the channel parameters lies in the fact that CRLB is not in closed form, and consequently, it is difficult to derive the beamforming power allocation insights. Motivated by this problem, we show that we can tackle this issue by exploiting the beamforming power allocation per subcarrier, by assuming a symmetric data transmission across the spectrum.

- With the help of the previous CRLB, we derive a heuristic localization error cost function as an appropriately weighted function of SPEB and squared orientation error bound (SOEB). Our derivations show that such an error function can be represented as weighted linear combinations of CRLBs of delay, AoD and AoA. Our motive then is to study the role of not only the frequency dimension, but also each location dependent variable in the beamforming optimization problem. Hence, we investigate them by solving the beamforming optimization problem by adjusting the weights associated to each in the cost function.

- After addressing the single-user beamforming optimization problem, we then extend our study towards the multiple user scenario, which to the best of our knowledge, has not been considered in the literature. In the multi-user scenario, unlike in the previously formulated single-user optimization problem, there is an additional issue concerning allocation of the beam power for each user. Hence, we then study the beamforming optimization problem while considering the various beam allocation fairness criteria for the multiple users.

This chapter is organized as follows. In section 2.4, we explain the choice of using CRLB, PEB and OEB to characterize localization performance. In section 2.5 we deal with the localization bound optimal beamforming optimization problem considering joint estimation of delay and AoA. In section 2.5.1, we introduce the single-user system model, reformulate the FIM for our scenario and accordingly the CRLB for estimating delay and AoA. We then present the solution of the beamforming optimization problem in a multi-carrier mm-Wave case in section 2.5.2. In section 2.5.3, we show the simulation results and their analysis for the localization bound based single-user beamforming optimization problem. In section 2.6, we deal with the multi-user localization optimal beamforming optimization problem. In section 2.6.1 we introduce the new system model for the multi-user scenario. In section 2.6.2, we present the FIM and CRLB derivation for both single- and multi- carrier cases. We formulate a heuristic localization error, which is used as a key performance indicator to then formulate and solve the localization based optimization problem. In section 2.6.3 we provide and discuss various illustrations of optimized beamforming results in a canonical scenario. We finally summarize the main findings of these investigations and conclude the chapter in section 2.7.

2.4 Bound based localization performance characterization

In the literature, it is common to characterize localization performance using CRLB which is the inverse of FIM. The FIM is a way of measuring the amount of information present in a random variable about a parameter. Likewise, CRLB provides the lower bound on the variance of an unbiased estimator. In section 2.2, we have already described the various works that characterize the CRLB in terms of localization variables such as delay, AoD and AoA in the context of mm-Wave.

However, when we are characterizing localization error, we typically look for error in terms of position and orientation estimation and not in terms of individual localization variable. For this purpose, PEB and OEB are practical measures of the localization accuracy. PEB characterizes the error bound concerning the position of the user, taking into consideration both the distance and AoD measurements. Likewise, OEB characterizes the error in user's orientation, considering the AoA measurements.

Both these metrics are widely used in the literature not only in the mmWave context, but while considering other systems as well. For instance, in [73, 74] the authors characterize the localization error in a multi-agent non-cooperative and cooperative scenarios respectively in terms of SPEB. Likewise, [58] also uses PEB and OEB to characterize the localization error in a beamforming optimization study. Similarly, the authors in [62] use PEB and OEB to characterize the localization error in a localization-communication resource allocation study for single users.

When it comes to the tightness of the bounds, CRLB is tight especially at average to high SNR [51]. In [51], the authors propose a compressive sensing based algorithm in both LOS and NLOS scenarios. The authors show the proposed algorithm, for SNR above -20dB in LOS scenario and -10dB in NLOS scenario, approaches the theoretical bound. Hence, especially in the average to high SNR scenario, which is a reasonable assumption in mm-Wave scenario, such bounds can be used as metrics of performance characterization.

2.5 Beamforming optimization in a single-user scenario

In this section, we study optimal beamforming policy to minimize the CRLB of joint AoA and time delay estimation for a multicarrier mm-Wave system. Considering one single BS with rough a-priori knowledge of channel coefficients and location

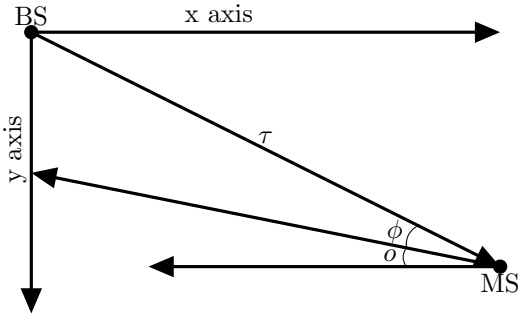

FIGURE 2.1: System model for single-user scenario with AoA (ϕ), time delay (τ) and orientation o.

information of the MS, we show that it is possible to improve the accuracy of AoA and time delay estimation, and hence of MS positioning, by means of optimized beamforming. Mathematical formulation of the CRLB is first introduced and the related optimization problem is solved for a each single subcarrier independently. Then we propose a solution optimizing the beamformer jointly for the multicarrier system. In the process, we also show the effect of frequency diversity and spectrum occupancy on localization performance.

2.5.1 System model

Consider a mm-Wave MIMO system consisting of N_t transmitting antennas and N_r receiving antennas at the BS and the MS, respectively. We consider the BS and the MS to be in LOS and also assume a downlink transmission between them. At every time slot, the BS transmits N orthogonal frequency-division multiplexing (OFDM) symbols corresponding to the number of orthogonal subcarriers, denoted by s_n for the n-th subcarrier. The system operates at the center frequency f_c with the total bandwidth B.

The transmitted signal per subcarrier is given by $\boldsymbol{f}_n s_n$ where $\boldsymbol{f}_n \in \mathbb{C}^{N_t}$ is the beamforming vector per subcarrier. The complex channel response for a multi-carrier case (like in [51, 56]) $\boldsymbol{H}_n \in \mathbb{C}^{N_r \times N_t}$ for the system is given by:

$$\boldsymbol{H}_n = \sqrt{\frac{N_t N_r}{\xi}} h\, e^{-j2\pi\tau\frac{nB}{N}}\, \boldsymbol{a}_{Rx,n}(\phi)\boldsymbol{a}^H_{Tx,n}(\theta), \tag{2.1}$$

with complex channel gain h, pathloss ξ, delay τ, BS antenna array response $\boldsymbol{a}_{Tx,n}(\theta) \in \mathbb{C}^{N_t}$ and MS antenna array response $\boldsymbol{a}_{Rx,n}(\phi) \in \mathbb{C}^{N_r}$ which depends on the arrangement of the elements in the antenna array, AoD (θ) and AoA (ϕ) (relative to a certain orientation o). In this section, for simplicity and without the loss of generality, we use ULA as the antenna array model with array elements

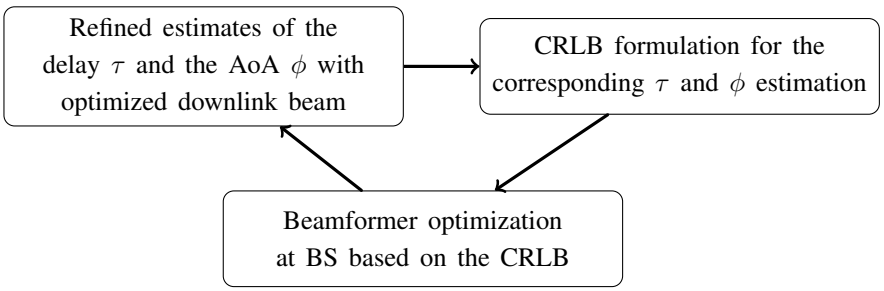

FIGURE 2.2: Block diagram for localization accuracy refining with beamforming in a dynamic tracking scenario.

separated by a distance κ and given by

$$\boldsymbol{a}_{Tx,n}(\theta) = \frac{1}{\sqrt{N_t}} \left[1, e^{j\frac{2\pi}{\lambda_n}\kappa\cos(\theta)}, \cdots, e^{j(N_t-1)\frac{2\pi}{\lambda_n}\kappa\cos(\theta)}\right]^T, \tag{2.2}$$

where λ_n is the wavelength corresponding to the frequency of the n-th subcarrier. Likewise, one can simply replace N_t by N_r and θ by ϕ in (2.2) to get $\boldsymbol{a}_{Rx,n}(\phi)$. At the receiver, the $N_r \times 1$ received signal vector is

$$\boldsymbol{y}_n = \boldsymbol{H}_n \boldsymbol{f}_n s_n + \boldsymbol{n}_n = \boldsymbol{\mu}_n + \boldsymbol{n}_n, \tag{2.3}$$

where $\boldsymbol{n}_n$ is the complex Gaussian noise defined by the circularly symmetric complex Gaussian random vector, with variance (per element of the vector) N_0 ($N_0/2$ per real and imaginary dimension).

In our work we consider the joint AoA and time delay estimation, which in 2D is sufficient for either absolute MS positioning with the knowledge of MS orientation or just relative positioning without. The delay estimation can be performed with methods such as downlink ToA or two way TDoA measurements and the AoA estimation can be performed with subspace based angle measurement methods such as MUSIC or ESPRIT in downlink.

2.5.2 Beamforming optimization

In this work, we are interested in finding the optimal beamformer per subcarrier $\boldsymbol{f}_n^*$ which assists in minimizing the delay and AoA estimation error at the receiver. The advantage of such CRLB based beamforming optimization can be, for instance, as shown in figure 2.2, in a dynamic MS tracking scenario feeding the system with the coarse estimates of AoA and delay, the new AoA and delay parameters can be more accurately estimated in every cycle creating some sort of virtuous loop.

As formulated in [51], the FIM for the model with all the subcarriers is provided by the summation of FIM for individual subcarriers.

$$\boldsymbol{J} = \sum_{n=1}^{N} \boldsymbol{J}_n. \tag{2.4}$$

However for problem simplification, in the following, we will first solve the optimal beamforming problem for a given subcarrier n and also for notational simplicity, we will denote $\boldsymbol{a}_{Tx,n}(\theta)$ as $\boldsymbol{a}_{Tx,n}$ and $\boldsymbol{a}_{Rx,n}(\phi)$ as $\boldsymbol{a}_{Rx,n}$.

FIM reformulation for a single subcarrier

The FIM, the inverse of CRLB, for delay-AoA estimation [51, 75] for n-th subcarrier can be particularized to our scenario as

$$\boldsymbol{J}_n = \begin{bmatrix} \psi_n(\tau,\tau) & \psi_n(\tau,\phi) \\ \psi_n(\tau,\phi) & \psi_n(\phi,\phi) \end{bmatrix} \tag{2.5}$$

where

$$\psi_n(\tau,\tau) = \alpha_n |a_{Tx,\boldsymbol{f},n}|^2, \tag{2.6a}$$
$$\psi_n(\tau,\phi) = \gamma_n |a_{Tx,\boldsymbol{f},n}|^2, \tag{2.6b}$$
$$\psi_n(\phi,\phi) = \beta_n |a_{Tx,\boldsymbol{f},n}|^2, \tag{2.6c}$$

and,

$$\alpha_n = 8\pi^2\sigma \sqrt{\frac{N_t N_r}{\xi}} \frac{n^2 B^2}{N^2} = \alpha n^2, \tag{2.7a}$$
$$\gamma_n = 8\pi^2\sigma \frac{\kappa \sin(\phi) n B}{\lambda_n N} \sqrt{\frac{N_t}{\xi N_r}} \sum_{i=0}^{N_r-1} i = \gamma \frac{n}{\lambda_n}, \tag{2.7b}$$
$$\beta_n = 8\pi^2\sigma \frac{\kappa^2 \sin^2(\phi)}{\lambda_n^2} \sqrt{\frac{N_t}{\xi N_r}} \sum_{i=0}^{N_r-1} i^2 = \beta \frac{1}{\lambda_n^2}, \tag{2.7c}$$

where σ, in this section, is defined as a SNR indicator given by $\frac{|x|^2|h|^2}{N_0}$. In equation (2.6), $a_{Tx,\boldsymbol{f},n} = \boldsymbol{a}_{Tx,n}^H(\theta)\boldsymbol{f}_n$ is the joint beamforming and TX antenna response. Note that all the terms of the matrix $\boldsymbol{J}_n$ depend on n and hence on the position of the subcarrier in the spectrum.

CRLB reformulation for a single subcarrier

In equation (2.6), we reformulate $||a_{Tx,\boldsymbol{f},n}||_2^2$ as

$$||a_{Tx,\boldsymbol{f},n}||_2^2 = \boldsymbol{a}_{Tx,n}^H \boldsymbol{f_n}\, \boldsymbol{f_n}^H \boldsymbol{a}_{Tx,n} = \boldsymbol{a}_{Tx,n}^H \boldsymbol{F}_n \boldsymbol{a}_{Tx,n}. \tag{2.8}$$

This formulation of the beamformer in equation (2.8) simplifies the optimization problem that will be presented later in this section.

The CRLB, which is again defined as the inverse of the FIM, can be formulated from (2.5) for respectively delay and AoA estimation as follows:

$$\boldsymbol{J}_{\tau,n}^{-1} = \frac{\beta_n \boldsymbol{a}_{Tx,n}^H \boldsymbol{F}_n \boldsymbol{a}_{Tx,n}}{(\alpha_n\beta_n - \gamma_n^2)(\boldsymbol{a}_{Tx,n}^H \boldsymbol{F}_n \boldsymbol{a}_{Tx,n})^2} = \frac{k_1}{\boldsymbol{a}_{Tx,n}^H \boldsymbol{F}_n \boldsymbol{a}_{Tx,n}}, \tag{2.9}$$

where,

$$k_1 = \frac{N^2\zeta_2}{8\pi^2\sigma n^2 B^2 \sqrt{\frac{N_t}{\xi N_r}}\,(N_r\zeta_2 - \zeta_1^2)}, \tag{2.10}$$

and,

$$\boldsymbol{J}_{\phi,n}^{-1} = \frac{\alpha_n \boldsymbol{a}_{Tx,n}^H \boldsymbol{F}_n \boldsymbol{a}_{Tx,n}}{(\alpha_n\beta_n - \gamma_n^2)(\boldsymbol{a}_{Tx,n}^H \boldsymbol{F}_n \boldsymbol{a}_{Tx,n})^2} = \frac{k_2}{\boldsymbol{a}_{Tx,n}^H \boldsymbol{F}_n \boldsymbol{a}_{Tx,n}}, \tag{2.11}$$

where,

$$k_2 = \frac{\lambda_n^2}{8\pi^2\sigma \sqrt{\frac{N_t}{\xi N_r}}\kappa^2 \sin^2(\phi)\,(N_r\zeta_2 - \zeta_1^2)}, \tag{2.12}$$

where, for $m \in \{1, 2\}$ we define

$$\zeta_m = \sum_{i=0}^{N_r-1} i^m. \tag{2.13}$$

Optimization problem for a single subcarrier

Recalling the main objective, the idea is to find the optimal beamformer that minimizes the CRLB for delay and AoA estimation. Since equations (2.9) and (2.11) both contain the same expression at the denominator, but different constants at the numerator, it is clear that $\boldsymbol{a}_{Tx,n}^H \boldsymbol{F}_n \boldsymbol{a}_{Tx,n}$ must be maximized in order to minimize the CRLB of both τ and ϕ given that the coefficients k_1 and k_2 are positive, which is proved in Appendix A.1. The equivalent expression in the equations also means that the min-max approach used in [58] is equivalent to just maximization of $\boldsymbol{a}_{Tx,n}^H \boldsymbol{F}_n \boldsymbol{a}_{Tx,n}$. For a given subcarrier n, we thus lay the optimization problem as

follows.

$$\min_{\boldsymbol{F}_n} \quad \text{trace}(-\boldsymbol{A}_{Tx,n}\boldsymbol{F}_n). \tag{2.14a}$$

$$\text{subject to:} \quad \text{trace}(\boldsymbol{F}_n) = 1, \tag{2.14b}$$

$$\boldsymbol{F}_n \succeq 0, \tag{2.14c}$$

$$\text{rank}(\boldsymbol{F}_n) = 1, \tag{2.14d}$$

where, $\boldsymbol{A}_{Tx,n} = \boldsymbol{a}_{Tx,n}\boldsymbol{a}_{Tx,n}^H$. Note that $-\boldsymbol{a}_{Tx,n}^H\boldsymbol{F}_n\boldsymbol{a}_{Tx,n}$ can be formulated as equation (2.14a) in the semidefinite problem (SDP) form and the objective function and constraints except for (2.14d) are clearly convex. Constraint (2.14d) is a non-convex constraint. In the literature it is common to solve the problem by dropping the latter and then, after obtaining the optimal beamforming vector $\boldsymbol{f}_n^*$, approximate $\boldsymbol{F}_n$ to rank-1 matrix. The constraint in equation (2.14b) is imposed to ensure that the transmitted signal is within the spectral mask allowed by the transmission regulation. Similarly, the constraint in equation (2.14c) comes as a result of the structure of $\boldsymbol{F}_n$ in equation (2.8).

CRLB reformulation for multiple subcarriers

Let $x_n = \boldsymbol{a}_{Tx,n}^H\boldsymbol{F}_n\boldsymbol{a}_{Tx,n}$. From equation (2.4), the equation for FIM including all the subcarriers is now given by

$$\boldsymbol{J} = \begin{bmatrix} \alpha\sum_n n^2 x_n & \gamma\sum_n \frac{n}{\lambda_n}x_n \\ \gamma\sum_n \frac{n}{\lambda_n}x_n & \beta\sum_n \frac{1}{\lambda_n^2}x_n \end{bmatrix}, \tag{2.15}$$

where the coefficients α, β and γ are defined in equation (2.7). We can further simplify the matrix as:

$$\boldsymbol{J} = \begin{bmatrix} \boldsymbol{a}^T\boldsymbol{x} & \boldsymbol{c}^T\boldsymbol{x} \\ \boldsymbol{c}^T\boldsymbol{x} & \boldsymbol{b}^T\boldsymbol{x} \end{bmatrix}, \tag{2.16}$$

where,

$$\boldsymbol{a} = \begin{bmatrix} \alpha & 4\alpha & \cdots & N^2\alpha \end{bmatrix}^T, \tag{2.17a}$$

$$\boldsymbol{b} = \begin{bmatrix} \frac{\beta}{\lambda_1^2} & \frac{\beta}{\lambda_2^2} & \cdots & \frac{\beta}{\lambda_N^2} \end{bmatrix}^T, \tag{2.17b}$$

$$\boldsymbol{c} = \begin{bmatrix} \frac{\gamma}{\lambda_1} & \frac{2\gamma}{\lambda_2} & \cdots & \frac{N\gamma}{\lambda_N} \end{bmatrix}^T, \tag{2.17c}$$

$$\boldsymbol{x} = \begin{bmatrix} x_1 & x_2 & \cdots & x_N \end{bmatrix}^T. \tag{2.17d}$$

Then from the matrix in equation (2.16), we can derive the CRLB for both delay and AoA as

$$\boldsymbol{J}_{\tau}^{-1} = \frac{\boldsymbol{b}^T\boldsymbol{x}}{\boldsymbol{x}^T\boldsymbol{a}\boldsymbol{b}^T\boldsymbol{x} - \boldsymbol{x}^T\boldsymbol{c}\boldsymbol{c}^T\boldsymbol{x}} = \frac{\boldsymbol{b}^T\boldsymbol{x}}{\boldsymbol{x}^T\boldsymbol{Z}\boldsymbol{x}}, \tag{2.18}$$

and,

$$\boldsymbol{J}_{\phi}^{-1} = \frac{\boldsymbol{a}^T\boldsymbol{x}}{\boldsymbol{x}^T\boldsymbol{a}\boldsymbol{b}^T\boldsymbol{x} - \boldsymbol{x}^T\boldsymbol{c}\boldsymbol{c}^T\boldsymbol{x}} = \frac{\boldsymbol{a}^T\boldsymbol{x}}{\boldsymbol{x}^T\boldsymbol{Z}\boldsymbol{x}}, \tag{2.19}$$

where, $\boldsymbol{Z} = \boldsymbol{a}\boldsymbol{b}^T - \boldsymbol{c}\boldsymbol{c}^T$. Here, in equations (2.18) and (2.19), since $\boldsymbol{a}$, $\boldsymbol{b}$ and $\boldsymbol{x}$ are always positive by construction, the numerators are always positive. In Appendix A.2, we prove that the denominator $\boldsymbol{x}^T\boldsymbol{Z}\boldsymbol{x}$ is always positive, and hence the negative of the expression is convex with respect to $\boldsymbol{x}$.

Optimization problem for multiple subcarriers

Equations (2.18) and (2.19) are non-convex with respect to $\boldsymbol{x}$, but one can come up with an equivalent convex reformulation, and thus, convex optimization problem for the multicarrier case can be formulated as follows.

$$\max_{\boldsymbol{x}} \quad \boldsymbol{a}^T\boldsymbol{x} \text{ or } \boldsymbol{b}^T\boldsymbol{x}, \tag{2.20a}$$

$$\text{subject to:} \quad \mathbf{1}_N^T\boldsymbol{x} < N, \tag{2.20b}$$

$$0 \leq \boldsymbol{x} \leq 1, \tag{2.20c}$$

where $\mathbf{1}_N = \begin{bmatrix} 1 & 1 & \cdots & 1 \end{bmatrix}^T$ of length N.

The optimization problem in hand is a linear programming problem and since both the coefficients $\boldsymbol{a}$ and $\boldsymbol{b}$ in (2.18) and (2.19) are increasing for higher subcarrier indices, the CRLB minimization problem for both the equations can be formulated as (2.20a).

The optimization problem in equation (2.20) can be viewed as the energy allocation problem across the subcarriers constrained on the limited energy available (provided by equation (2.20b)) that can be distributed across the subcarriers, judging by which subcarrier is more valuable for minimizing the CRLB. In addition to the energy limitation across the subcarriers, equation(2.20c) provides us with the constraint to limit the transmitted power to the spectral mask.

After solving the energy allocation problem across the subcarriers, for the optimal energy available at each subcarrier x_n^*, we solve the optimization problem discussed in equation (2.14) to find the same beamforming optimization problem as that in equation (2.14) per subcarrier independently as follows.

$$\min_{\boldsymbol{F}_n} \quad \text{trace}(-\boldsymbol{A}_{Tx,n}\boldsymbol{F}_n). \tag{2.21a}$$

$$\text{subject to:} \quad \text{trace}(\boldsymbol{F}_n) = x_n^*, \tag{2.21b}$$

$$\boldsymbol{F}_n \succeq 0. \tag{2.21c}$$

Recovery of beamforming vector

After completing the optimization problem in equations (2.20) and (2.21), one would still need to recover the optimal beamforming vector $\boldsymbol{f}_n^*$ from the matrix $\boldsymbol{F}_n^*$ which is, as evident from equation (2.8), a rank-1 complex matrix. In [76], the authors have shown that the best rank-1 approximation of a matrix $\boldsymbol{F}_n^*$ in 2-norm sense is provided by:

$$\boldsymbol{f}_k^* = \sqrt{\lambda}\boldsymbol{v}, \tag{2.22}$$

where λ is the biggest eigenvalue of the matrix $\boldsymbol{F}_n^*$ and $\boldsymbol{v}$ is the corresponding eigenvector.

2.5.3 Numerical results

System parameters and simulation setup

In these first simulations, we use $f_c = 38$ GHz and a large bandwidth $B = 1$ GHz with $N = 64$ subcarriers. For the antenna array, we use the ULA model with $N_t = 30$ and $N_r = 30$ elements. The inter-element spacing between the antenna array at both transmitter and receiver is set to a constant $\kappa = 0.5\lambda_c$ where $\lambda_c = \frac{c}{f_c}$ and c is the speed of light. We assume that the BS roughly knows the relative MS position. We assume that the orientation $o = 0^o$ and hence $\phi = 80^o$ and the distance between the nodes as reflected by τ is 50 m unless otherwise specified.

In our simulations, we consider the following mm-Wave pathloss model with parameters from [77].

$$\xi(d)[dB] = \xi(d_0) + 10\alpha\,(d/d_0) + X_\sigma, \tag{2.23}$$

where, $\xi(d_0)$ is the free space path loss given by $10\log_{10}\left(\frac{4\pi d_0}{\lambda_c}\right)^2$ for a reference distance $d_0 = 1m$ for our case. Parameters $\alpha = 1.9$ and $\sigma = 4.6$ are the path loss exponent and the standard deviation of the shadow factor X_σ (a zero mean Gaussian random variable), respectively.

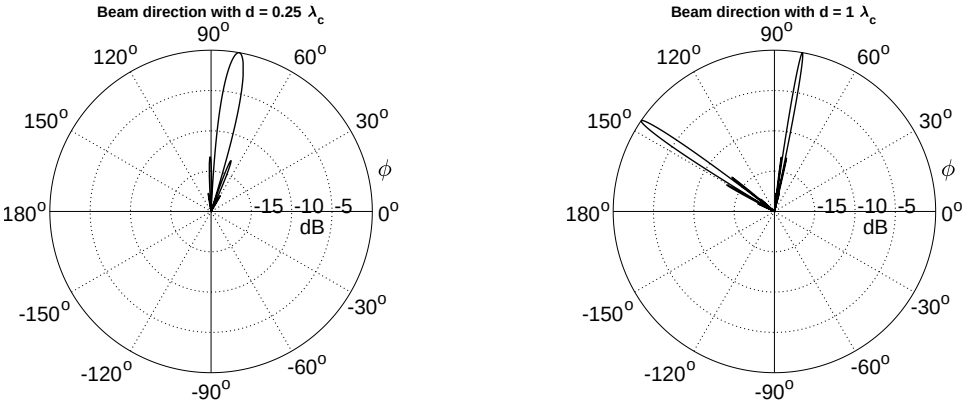

FIGURE 2.3: Normalized beam direction with optimal beamformer for $\theta = 80^o$ $||a_{Tx,\boldsymbol{f}^*,n}||_2^2$ varied with possible directions in a planar coordinate for (A) $\kappa = 0.5\lambda_c$ and (b) $\kappa = \lambda_c$.

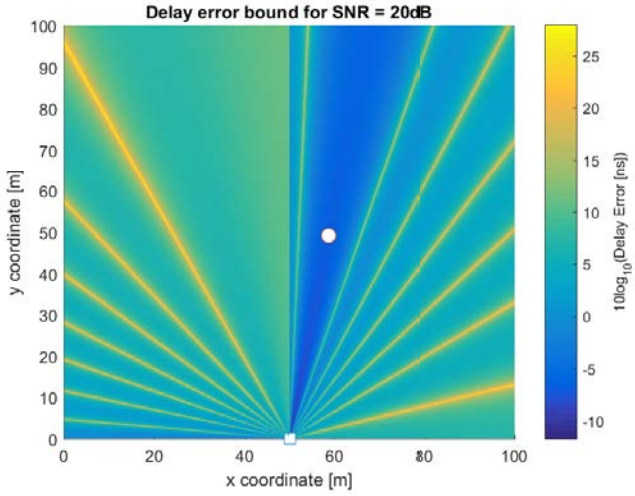

FIGURE 2.4: Delay error bound after beamforming optimization for MS position (white circle) at distance 50m and 80^o from BS (white square).

Results and analysis

Figures 2.3a and 2.3b show the normalized optimal beamforming direction given by $||a_{Tx,\boldsymbol{f},n}||_2^2$ for the above-mentioned scenario with different inter-element distances for transmit antennas. However, it is very important to set carefully the parameters as it can be seen in figure 2.3b. For instance, the effect of having a large inter-element distance leads to the presence of grating lobes and results in transmitting some energy in the unwanted direction. In [78], it has been shown that to avoid angular oversampling, κ must be below the nyquist sampling rate $\kappa \leq \frac{\lambda_c}{2}$.

In figures 2.4 and 2.5, we illustrate the estimation error bounds for delay and AoA, defined by $\sqrt{J_\tau^{-1}}$ and $\sqrt{J_\phi^{-1}}$ respectively, in dB scale, for a fixed MS location (60, 50) and BS location (50, 0) after beamformer optimization. It can be noted

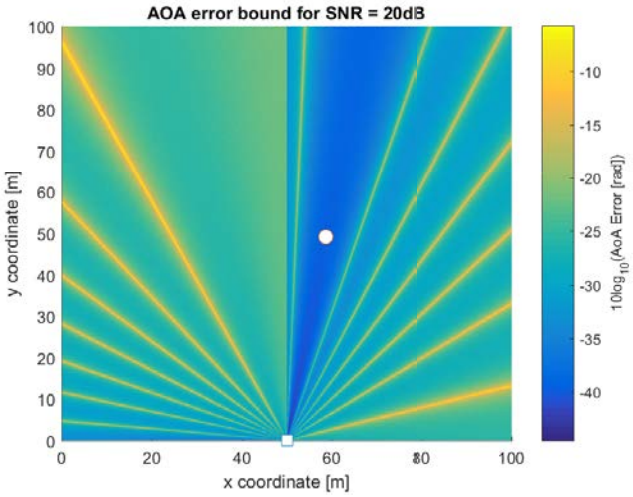

FIGURE 2.5: AoA error bound after beamforming optimization for MS position (white circle) at distance 50m and 80^o from BS (white square).

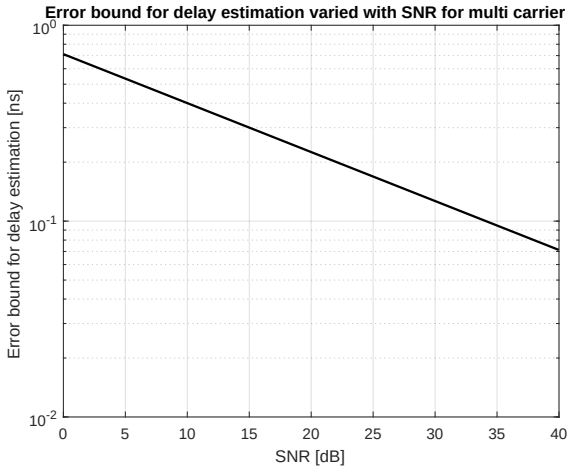

FIGURE 2.6: Error Bound for the estimation of τ for multicarrier system ($N = 64$) as a function of SNR.

that the error bound for both the delay and AoA estimates follows a non trivial spatial pattern which is due to the side lobe pattern from the antenna. For instance, for the sector containing MS in the scenario, the error is more than 10dB lower as compared to outside the sector, due to beamforming.

Likewise, in figures 2.6 and 2.7, we show theoretical bounds for estimations of time delay and AoA respectively for the multicarrier case with $N = 64$ subcarriers as a function of the SNR. It can be noted that with optimal beamforming, even for small SNR, the error bound for both delay (in range of less than 1ns) and AoA (in the range of less that 0.1 rad) is low.

Finally in figures 2.8 and 2.9 we show the previously defined delay and AoA error for different MS positions (i.e., for each point of the map, we consider a virtual MS is

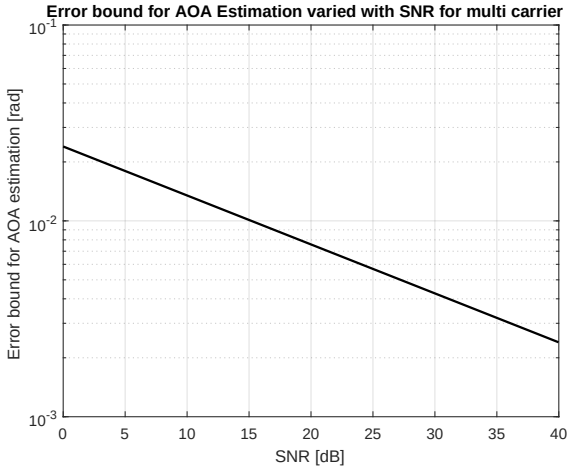

FIGURE 2.7: Error Bound for the estimation of ϕ for multicarrier system ($N = 64$) as a function of SNR.

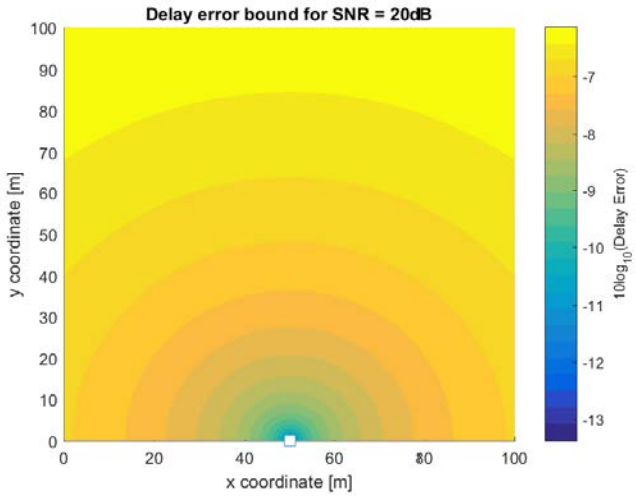

FIGURE 2.8: Delay error bound after beamforming optimization for different MS position by BS (white square).

occupying this point and the beamforming optimization is performed accordingly). For delay error bound, the error pattern is isotropic with the effects of the increasing pathloss along with distance. For AoA however, the pattern is different due to the constant MS orientation throughout all the possible MS positions. For the given scenario, the minimum, average and maximum delay estimation errors are 0.0459 ns, 0.2032 ns and 0.2434 ns respectively and the corresponding AoA estimation errors are 2.3852×10^{-5} rad, 1.4950×10^{-4} rad and 0.0522 rad respectively.

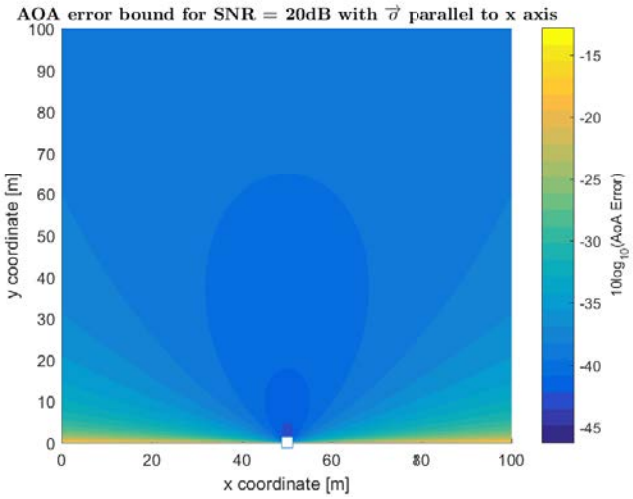

FIGURE 2.9: AoA error bound after beamforming optimization for different MS position by BS (white square) for a fixed MS orientation parallel to x axis.

2.6 Beamforming optimization in a multi-user scenario

Following the localization optimal beamforming study in the single-user scenario considering joint delay and AoA estimation, in this section, we extend the model to a multi-user scenario. In this section, we study optimal beamforming strategies for a mm-Wave system consisting of multiple users, while still relying on localization performance bounds. We consider a single BS with prior coarse knowledge of the users' positions and orientations similarly as in section 2.5 and formulate the optimal beamforming problem in order to minimize a localization error cost function. In addition to following a similar beamforming optimization strategy as in section 2.5, we further incorporate AoD on top of AoA, delay and channel coefficient estimates. With the estimates of all the channel parameters including the AoD, we can absolutely position all the users in the multi-user scenario. We first formulate the simplified CRLB of estimation parameters, taking advantage of multiple subcarriers, and then formulate the localization error for optimization of the beamformer. Then, finally, we evaluate the resulting position and orientation error bounds after optimization for different fairness strategies.

2.6.1 System model

Consider a mm-Wave downlink scenario consisting of a BS node located at $\boldsymbol{p} = \begin{bmatrix} p_x, p_y \end{bmatrix}^T \in \mathbb{R}^2$ and U users, each user u located at $\boldsymbol{q}_u = \begin{bmatrix} q_{x,u}, q_{y,u} \end{bmatrix}^T \in \mathbb{R}^2$ as shown in Fig. 2.10. Assume that the BS and each user is equipped with a ULA antenna

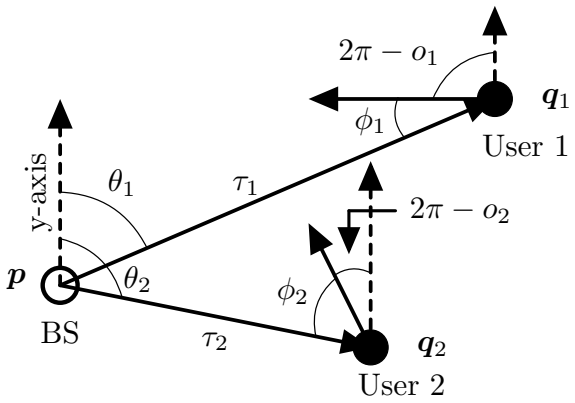

FIGURE 2.10: Example of canonical scenario with 1 BS and 2 users with orientations o_1 and o_2 at locations $\boldsymbol{q}_1$ and $\boldsymbol{q}_2$ respectively.

with N_t and N_r antenna elements respectively. Likewise, as illustrated in Fig. 2.10, the orientation of u-th user (relative to the y axis) is given by $\boldsymbol{o}_u \in [0, 2\pi)$.

The complex signal at a generic time instance is transmitted across N subcarriers centered around frequency f_c with bandwidth B and duration T_s and is denoted by s_n for the n-th subcarrier where $n \in \mathcal{N} = \left\{\frac{-N}{2}, \cdots, \frac{N}{2}\right\}$. The i-th element of the previous is denoted as n_i where $i = 1, \cdots N$.

Let $\boldsymbol{f}_n \in \mathbb{C}^{N_t}$ denote the beamformer in the precoding sense for the n-th subcarrier. We consider limited beamforming power $0 \leq \text{trace}(\boldsymbol{f}_n \boldsymbol{f}_n^H) \leq 1$ to satisfy the spectral mask set by regulations as in the previous section. We consider uniquely the direct path, assuming a LOS propagation model [52, 59]. The $N_r \times N_t$ complex channel matrix, for the n-th subcarrier between the BS and user-u is denoted by $\boldsymbol{H}_{u,n}$ and is formulated as in [56].

$$\boldsymbol{H}_{u,n} = \sqrt{\frac{N_t N_r}{\xi_u}} h_u \, e^{-j2\pi\tau_u \frac{nB}{N}} \boldsymbol{a}_{\text{Rx},u}(\phi_u) \boldsymbol{a}_{\text{Tx},u}^H(\theta_u), \tag{2.24}$$

where $h_u \in \mathbb{C}$ is the complex channel coefficient, ξ_u is the path-loss between the BS and the user, and τ_u, θ_u and ϕ_u are the delay, AoD and AoA respectively associated with user u. Both the transmitting $\boldsymbol{a}_{\text{Tx},u}(\theta_u) \in \mathbb{C}^{N_t}$ and receiving $\boldsymbol{a}_{\text{Rx},u}(\phi_u) \in \mathbb{C}^{N_r}$ antennas are assumed to be ULA. Assuming odd numbers of antenna elements and the centroid of the array as the reference point (as compared to considering the first antenna element as reference point in (2.2)), the antenna array response can be expressed as,

$$\boldsymbol{a}_{\text{Tx},u} = \frac{1}{\sqrt{N_t}} \left[e^{-j\left(\frac{N_t+1}{2}-1\right)\frac{2\pi}{\lambda_c}\kappa\cos(\theta_u)}, \cdots, 1, \cdots, e^{-j\left(\frac{N_t+1}{2}-N_t\right)\frac{2\pi}{\lambda_c}\kappa\cos(\theta_u)} \right]^T. \tag{2.25}$$

under the same notations as in the previous single-user section. For the ease of

notation, we write $\boldsymbol{a}_{\mathrm{Tx},u}(\theta_u)$ as $\boldsymbol{a}_{\mathrm{Tx},u}$ and do the same for $\boldsymbol{a}_{\mathrm{Rx},u}(\phi_u)$. Likewise, $\boldsymbol{a}_{\mathrm{Rx}}(\phi_u)$ can be expressed by simply replacing θ_u by ϕ_u and N_t by N_r in equation (2.25). Unlike in the previous section, in this section, we consider a narrow-band model meaning $B \ll f_c$. In such case, we can assume no beam squinting effects for both transmit and receive antenna responses. Hence, in contrast to the equation (2.2), the antenna array responses in this section are considered independent of subcarrier frequencies[1].

We consider the received and post processed signal $y_{u,n} \in \mathbb{C}$ at the user-u after whitening and combining as

$$y_{u,n} = \sqrt{P_{\mathrm{Tx},u}}\boldsymbol{w}_u^H \boldsymbol{H}_{u,n}\boldsymbol{f}_n s_n + \tilde{n}_n, \tag{2.26}$$

where, $P_{\mathrm{Tx},u}$ is the transmitted power at the user and $\tilde{n}_n \in \mathbb{C}$ is the zero-mean Gaussian with a power spectral density of N_0 ($N_0/2$ per real and imaginary dimension) and $\boldsymbol{w}_u \in \mathbb{C}^{N_r}$ is the combiner vector at the mobile user.

2.6.2 Beamforming optimization

Here, we will derive the FIM associated with joint delay, AoD and AoA estimates, firstly for the n-th subcarrier and then generalize it for all the subcarriers and then, subsequently, derive the corresponding CRLBs. Then, we will derive an equivalent localization error cost function and formulate the beamforming optimization problem accordingly. During the beamforming optimization, we first characterize the localization error and the corresponding beamforming optimization problem for a single-user case and extrapolate it to characterize the optimization problem for multi-user scenario.

FIM for a single subcarrier

We define the new set of parameters $\boldsymbol{\eta}_u = \begin{bmatrix}\tau_u & \theta_u & \phi_u & h_{R,u} & h_{I,u}\end{bmatrix}$ comprising the estimation variables where $h_{R,u}$ and $h_{I,u}$ respectively represent the real and imaginary parts of the complex the channel coefficient. Then, the FIM $\boldsymbol{J}_{n,u} \in \mathbb{R}^{5\times 5}$ characterizing the estimation of these parameters has been derived in [51, 58, 75] as

[1]We make this assumption in order to keep the expressions relatively simple in line with other works in the literature [58, 59].

$$\boldsymbol{J}_{u,n} = \begin{bmatrix} \psi_n(\tau_u,\tau_u) & \psi_n(\tau_u,\theta_u) & \psi_n(\tau_u,\phi_u) & \psi_n(\tau_u,h_{R,u}) & \psi_n(\tau_u,h_{I,u}) \\ \psi_n(\theta_u,\tau_u) & \psi_n(\theta_u,\theta_u) & \psi_n(\theta_u,\phi_u) & \psi_n(\theta_u,h_{R,u}) & \psi_n(\theta_u,h_{I,u}) \\ \psi_n(\phi_u,\tau_u) & \psi_n(\phi_u,\theta_u) & \psi_n(\phi_u,\phi_u) & \psi_n(\phi_u,h_{R,u}) & \psi_n(\phi_u,h_{I,u}) \\ \psi_n(h_{R,u},\tau_u) & \psi_n(h_{R,u},\theta_u) & \psi_n(h_{R,u},\phi_u) & \psi_n(h_{R,u},h_{R,u}) & \psi_n(h_{R,u},h_{I,u}) \\ \psi_n(h_{I,u},\tau_u) & \psi_n(h_{I,u},\theta_u) & \psi_n(h_{I,u},\phi_u) & \psi_n(h_{I,u},h_{R,u}) & \psi_n(h_{I,u},h_{I,u}) \end{bmatrix}, \tag{2.27}$$

where the values of the matrix entries are given in Appendix A.3.

FIM for multiple subcarriers

The FIM for the multi-carrier case can be extended from equation (2.5) as follows.

$$\boldsymbol{J}_u = \sum_{n=-N/2}^{N/2} \boldsymbol{J}_{u,n}. \tag{2.28}$$

Considering a symmetric power density of the transmitted signal (with respect to the central frequency) after beamforming by assuming $\boldsymbol{f}_{-n} = \boldsymbol{f}_n$ and $s_{-n} = s_n$, we can reformulate the FIM according to Appendix A.4. By considering these assumptions, we significantly reduce the complexity of inverting the matrix for the derivation of CRLB, although we reduce the transmit diversity by a factor 2.

CRLB formulation for multiple subcarriers

The symmetry assumption in the transmitted signal decouples the delay estimation with the rest of estimation variables in the FIM in equation (2.28), and hence, we can simply invert the delay Fisher information to get the CRLB for delay estimation. For the AoD and AoA, we can use Schur's complement similar to [58] and find the CRLBs, as follows.

$$\psi^{-1}(\tau_u,\tau_u) = \frac{\alpha_{\tau,u}}{\boldsymbol{a}_{\mathrm{Tx},u}^H \boldsymbol{X}_\tau \boldsymbol{a}_{\mathrm{Tx},u}}, \tag{2.29a}$$

$$\psi^{-1}(\theta_u,\theta_u) = \frac{\alpha_{\theta,u}}{\left(\dot{\boldsymbol{a}}_{\mathrm{Tx},u}^H \boldsymbol{X} \dot{\boldsymbol{a}}_{\mathrm{Tx},u} - \frac{|\dot{\boldsymbol{a}}_{\mathrm{Tx},u}^H \boldsymbol{X} \boldsymbol{a}_{\mathrm{Tx},u}|^2}{\boldsymbol{a}_{\mathrm{Tx},u}^H \boldsymbol{X} \boldsymbol{a}_{\mathrm{Tx},u}}\right)}, \tag{2.29b}$$

$$\psi^{-1}(\phi_u,\phi_u) = \frac{\alpha_{\phi,u}}{\boldsymbol{a}_{\mathrm{Tx},u}^H \boldsymbol{X} \boldsymbol{a}_{\mathrm{Tx},u}}. \tag{2.29c}$$

where, the variables $\alpha_{\tau,u} = (4\pi^2 \sigma_u d_{0,u} |h_u|^2)^{-1}$, $\alpha_{\theta,u} = (d_{0,u}\sigma_u |h_u|^2)^{-1}$, $\alpha_{\phi,u} = \left(\sigma_u |h_u|^2 \left(d_{2,u} - \frac{d_{1,u}^2}{d_{0,u}}\right)\right)^{-1}$ and $\dot{\boldsymbol{a}}_{\mathrm{Tx},u}$, σ_u and $d_{i,u}$ for $i \in \{0,1,2\}$ are the intermediary

variables fully defined in Appendices A.3 and A.4. We also define the beamformer dependent variables $\boldsymbol{X}_\tau = \sum_{n=-N/2}^{N/2} |s_n|^2 n^2 \boldsymbol{F}_n$, $\boldsymbol{X} = \sum_{n=-N/2}^{N/2} |s_n|^2 \boldsymbol{F}_n$ and $\boldsymbol{F}_n = \boldsymbol{f}_n \boldsymbol{f}_n^H$.

SPEB and SOEB

In this section we introduce SPEB and SOEB which we can derive from the FIM in equation (2.28). SPEB and equivalently PEB characterizes the error bound concerning the position of the user, taking into consideration both the distance and AoD measurements. Likewise, SOEB and hence OEB characterizes the error in user's orientation, considering the AoA measurements. Both these metrics characterizing the localization error are widely used in the literature not only in the mm-Wave context, but while considering other systems as well [73, 74]. Hence, we introduce these metrics, as they will be used later in this chapter and thesis.

Let $\boldsymbol{\mu}_u = [p_{x,u}, p_{y,u}, o_u, h_{R,u}, h_{I,u}]$ be the vector comprising the new estimation variables representing user u's 2D absolute Cartesian coordinates and absolute orientation, along with the real and imaginary channel coefficients respectively. As derived in [51] and [62], the FIM in terms of the new parameters can be written as

$$\boldsymbol{J}_{\mu,u} = \boldsymbol{T}_u \boldsymbol{J}_u(\boldsymbol{X}_N) \boldsymbol{T}_u^T, \tag{2.30}$$

where $\boldsymbol{T}_u$ is the Jacobian of $\boldsymbol{\mu}_u$ with respect to the original estimation variables in $\boldsymbol{\eta}_u$ formulated in equation (A.12).

Hence, we define SPEB and SOEB for user u as follows.

$$\mathrm{SPEB}_u = \mathrm{trace}\left(\boldsymbol{J}^{-1}_{\mu,u,1:2,1:2}(\boldsymbol{X}_N)\right). \tag{2.31}$$

$$\mathrm{SOEB}_u = \boldsymbol{J}^{-1}_{\mu,u,3,3}(\boldsymbol{X}_N). \tag{2.32}$$

Localization error for a single-user

In this section, we derive an equivalent overall localization error resulting from the combined SPEB and SOEB. As we can see in the derivation in Appendix A.5, the localization error can be formulated as a weighted linear combination of corresponding unitary CRLBs of the three location-dependent variables.

$$L_u(\boldsymbol{X}, \boldsymbol{X}_\tau) = \beta_\tau \psi^{-1}(\tau_u, \tau_u) + \beta_\theta \psi^{-1}(\theta_u, \theta_u) + \beta_\phi \psi^{-1}(\phi_u, \phi_u). \tag{2.33}$$

Here, in order to have a general optimization framework, we replace the weights with the tunable parameters[2] β_τ, β_θ, $\beta_\phi \geq 0$ for each estimation variable, namely delay, AoD, AoA respectively. The goal is to find the beamformer that minimizes this localization error. With the generalized localization error formulation in equation (2.33), we can analyze the effect of each estimation parameter independently onto beamforming by adjusting the a-priori application-dependent weights.

We can however notice that there are two different variables $\boldsymbol{X}$ and $\boldsymbol{X}_\tau$ in the formulation of the localization error, in equation (2.33). In order to maintain one unique optimization variable in the equation, we can restructure the latter as follows.

Let $M = N_t \times N$. Using the Kronecker product, we define vectors $\boldsymbol{a}_u = \boldsymbol{s} \otimes \boldsymbol{a}_{\mathrm{Tx},u}$, $\dot{\boldsymbol{a}}_u = \boldsymbol{s} \otimes \dot{\boldsymbol{a}}_{\mathrm{Tx},u}$ and $\boldsymbol{a}_{N,u} = \boldsymbol{s}_N \otimes \boldsymbol{a}_{\mathrm{Tx},u}$, where $\boldsymbol{s} = \begin{bmatrix} |s_{n_1}| & |s_{n_2}| & \cdots & |s_{n_N}| \end{bmatrix}^T$, $\boldsymbol{s}_N = \begin{bmatrix} n_1^2|s_{n_1}| & n_2^2|s_{n_2}| & \cdots & n_N^2|s_{n_N}| \end{bmatrix}^T$ and $\boldsymbol{X}_N \in \mathbb{C}^{M \times M}$ is defined as the block diagonal matrix consisting of the matrix $\boldsymbol{F}_n$ over each subcarrier, expressed as

$$\boldsymbol{X}_N = \begin{bmatrix} \boldsymbol{F}_{n_1} & & & \\ & \boldsymbol{F}_{n_2} & & \\ & & \ddots & \\ & & & \boldsymbol{F}_{n_N} \end{bmatrix}. \tag{2.34}$$

Hence, the localization error can be reformulated as

$$L_u(\boldsymbol{X}_N) = \frac{\beta_\tau \alpha_{\tau,u}}{\boldsymbol{a}_{N,u}^H \boldsymbol{X}_N \boldsymbol{a}_{N,u}} + \frac{\beta_\theta \alpha_{\theta,u}}{\left(\dot{\boldsymbol{a}}_u^H \boldsymbol{X}_N \dot{\boldsymbol{a}}_u - \frac{|\dot{\boldsymbol{a}}_u^H \boldsymbol{X}_N \boldsymbol{a}_u|^2}{\boldsymbol{a}_u^H \boldsymbol{X}_N \boldsymbol{a}_u} \right)} + \frac{\beta_\phi \alpha_{\phi,u}}{\boldsymbol{a}_u^H \boldsymbol{X}_N \boldsymbol{a}_u}. \tag{2.35}$$

[2]With the new parameters, the localization error formulated in Appendix A.5 becomes a special case of the formulation in equation (2.33) when $\beta_\tau = k_{\tau,u}$, $\beta_\theta = k_{\theta,u}$ and $\beta_\phi = k_{\phi,u}$. It must also be noted that the CRLB of the estimation variables are interrelated, as explained in [58]. It is inevitable that if we estimate a variable, we can estimate another one as well. The weights do not define the exclusivity of estimation of particular parameters, but rather the estimation variable on which the focus is. A motivation behind the introduction of the general cost function in equation (2.33) is that some applications might be more sensitive to angle or ranging errors than the absolute position error. In such cases, one can adjust the weights β to tune the cost function depending on application requirements.

The goal now is to state an optimization problem which minimizes the localization error under a power constraint. This problem can be formulated as:

$$\min_{\boldsymbol{X}_N} \quad L_u(\boldsymbol{X}_N), \tag{2.36a}$$

$$\text{subject to:}$$

$$\text{trace}(\boldsymbol{\mathcal{I}}_i^T \boldsymbol{X}_N \boldsymbol{\mathcal{I}}_i) \leq 1, \qquad \forall i, \tag{2.36b}$$

$$\text{trace}(\boldsymbol{\mathcal{I}}_i^T \boldsymbol{X}_N \boldsymbol{\mathcal{I}}_i) \geq 0, \qquad \forall i, \tag{2.36c}$$

$$\boldsymbol{\mathcal{I}}_i^T \boldsymbol{X}_N \boldsymbol{\mathcal{I}}_j = \boldsymbol{0}_{N_t}, \quad \forall i, j : i \neq j, \tag{2.36d}$$

$$\text{trace}(\boldsymbol{X}_N) = K, \tag{2.36e}$$

$$\boldsymbol{X}_N \succeq 0, \tag{2.36f}$$

$$\text{rank}(\boldsymbol{\mathcal{I}}_i^T \boldsymbol{X}_N \boldsymbol{\mathcal{I}}_i) = 1 \qquad \forall i. \tag{2.36g}$$

where $i, j \in \{1, 2, \cdots, N\}$, $\boldsymbol{0}_{N_t} \in \mathbb{R}^{N_t \times N_t}$ represents the zero matrix sized $N_t \times N_t$ and $\boldsymbol{\mathcal{I}}_n \in \mathbb{R}^{N_t \times M}$ represents a matrix consisting of identity matrix $\boldsymbol{I}_{N_t}$ of size $N_t \times N_t$ in n-th block position and $\boldsymbol{0}_{N_t}$ in the rest of the block positions; in other words,

$$\boldsymbol{\mathcal{I}}_n = \boldsymbol{e}_n \otimes \boldsymbol{I}_{N_t} \tag{2.37}$$

where $\boldsymbol{e}_n \in \mathbb{R}^{N \times 1}$ is the N-dimensional Euclidean space standard basis vector whose values are all 0s except the n-th element, which is equal to 1.

The constraints from equations (2.36b) and (2.36c) define the power constraint at each subcarrier as assumed in the system model. Likewise, equation (2.36d) enforces the block diagonality constraint in the matrix $\boldsymbol{X}_N$. Equation (2.36e) represents the total power constraint across all the subcarriers and by the virtue of equation (2.36b), we know that $K \leq N$. Similarly, from the positive semidefinite structure of the individual blocks $\boldsymbol{F}_n$ in $\boldsymbol{X}_N$, we can conclude that $\boldsymbol{X}_N$ is positive semidefinite as well and the rank of each block is 1.

The objective function along with some constraints in this equation, however, are non-convex. It is possible to reformulate it into a convex optimization problem by

introducing different slack variables $\zeta_\tau, \zeta_\theta, \zeta_\phi$ and represent the problem as follows:

$$\max_{\boldsymbol{X}_N, \zeta_\theta, \zeta_\phi, \zeta_\tau} \quad \beta_\theta \zeta_\theta + \beta_\phi \zeta_\phi + \beta_\tau \zeta_\tau, \tag{2.38a}$$

subject to:

$$\frac{\boldsymbol{a}_{N,u}^H \boldsymbol{X}_N \boldsymbol{a}_{N,u}}{\alpha_{\tau,u}} \geq \zeta_\tau, \tag{2.38b}$$

$$\frac{1}{\alpha_{\theta,u}} \left(\dot{\boldsymbol{a}}_u^H \boldsymbol{X}_N \dot{\boldsymbol{a}}_u - \frac{|\dot{\boldsymbol{a}}_u^H \boldsymbol{X}_N \boldsymbol{a}_u|^2}{\boldsymbol{a}_u^H \boldsymbol{X}_N \boldsymbol{a}_u} \right) \geq \zeta_\theta, \tag{2.38c}$$

$$\frac{\boldsymbol{a}_u^H \boldsymbol{X}_N \boldsymbol{a}_u}{\alpha_{\phi,u}} \geq \zeta_\phi, \tag{2.38d}$$

(2.36b)-(2.36g).

Note that the constraints from equations (2.38b) and (2.38d) are affine. From [79] and Appendix A.6, we can simplify and cast the hyperbolic constraint in equation (2.38c) as

$$\left\| \begin{bmatrix} 2\Re(\dot{\boldsymbol{a}}_u{}^H \boldsymbol{X}_N \boldsymbol{a}_u) \\ 2\Im(\dot{\boldsymbol{a}}_u{}^H \boldsymbol{X}_N \boldsymbol{a}_u) \\ \dot{\boldsymbol{a}}_u^H \boldsymbol{X}_N \dot{\boldsymbol{a}}_u - \zeta_\theta \alpha_{\theta,u} - \boldsymbol{a}_u^H \boldsymbol{X}_N \boldsymbol{a}_u \end{bmatrix} \right\|_2 \leq \dot{\boldsymbol{a}}_u^H \boldsymbol{X}_N \dot{\boldsymbol{a}}_u - \zeta_\theta \alpha_{\theta,u} + \boldsymbol{a}_u^H \boldsymbol{X}_N \boldsymbol{a}_u. \tag{2.39}$$

where $\Re(\cdot)$ and $\Im(\cdot)$ represents the real and imaginary operators.

The objective function and all the constraints in equation (2.38), except the rank constraint in equation (2.36g), are convex. In order to solve first a (sub-)problem after dropping the incriminated constraint. Then, based on the first step optimization result, one gets the best rank-1 approximation for the matrix of interest. The rank-1 approximation of the matrix $\boldsymbol{F}_n^*$ can be done in the same way as in equation (2.22).

Localization error for multiple users

Similarly, for a multi-user case, we define the overall localization error as a function of the localization errors per user.

$$L(\boldsymbol{X}_N) = f\left(L_1(\boldsymbol{X}_N), L_2(\boldsymbol{X}_N), \cdots L_U(\boldsymbol{X}_N)\right). \tag{2.40}$$

For this multi-user scenario, we consider fairness criteria based beamforming strategies according to which we define the function $f(\cdot)$. The idea is to allocate power to different users based on their positions with the help of beamforming optimization in order to minimize the localization error.

1. **Min-max fairness strategy:** In this strategy, we ensure a minimum localization error requirement for each user. In doing so, we are limited by the worst user, hence the optimal solution would lead to the minimization of the localization error of the user with the maximum error. In this case, the objective function $L(\boldsymbol{X}_N)$ would be $\max\left(L_1(\boldsymbol{X}_N), L_2(\boldsymbol{X}_N), \cdots, L_U(\boldsymbol{X}_N)\right)$.

   The optimization problem is thus formulated accordingly, as follows:

$$\max_{\boldsymbol{X}_N, \zeta_\theta, \zeta_\phi, \zeta_\tau} \quad \beta_\theta \zeta_\theta + \beta_\phi \zeta_\phi + \beta_\tau \zeta_\tau \tag{2.41a}$$

   subject to:

$$\frac{\boldsymbol{a}_{N,u}^H \boldsymbol{X}_N \boldsymbol{a}_{N,u}}{\alpha_{\tau,u}} \geq \zeta_\tau, \quad \forall u \tag{2.41b}$$

$$\left\| \begin{bmatrix} 2\Re(\dot{\boldsymbol{a}}_u{}^H \boldsymbol{X}_N \boldsymbol{a}_u) \\ 2\Im(\dot{\boldsymbol{a}}_u{}^H \boldsymbol{X}_N \boldsymbol{a}_u) \\ \dot{\boldsymbol{a}}_u^H \boldsymbol{X}_N \dot{\boldsymbol{a}}_u - \zeta_\theta \alpha_{\theta,u} - \boldsymbol{a}_u^H \boldsymbol{X}_N \boldsymbol{a}_u \end{bmatrix} \right\|_2 \leq \dot{\boldsymbol{a}}_u^H \boldsymbol{X}_N \dot{\boldsymbol{a}}_u - \zeta_\theta \alpha_{\theta,u} + \boldsymbol{a}_u^H \boldsymbol{X}_N \boldsymbol{a}_u, \quad \forall u \tag{2.41c}$$

$$\frac{\boldsymbol{a}_u^H \boldsymbol{X}_N \boldsymbol{a}_u}{\alpha_{\phi,u}} \geq \zeta_\phi, \quad \forall u \tag{2.41d}$$

   (2.36b)-(2.36g)

   Note that the constraints in (2.41b)-(2.41d) have the same CRLB requirement for each of the estimation parameters (ζ_τ, ζ_θ and ζ_ϕ) for each user. This condition serves to maximize the performance of the worst user.

2. **Proportional fairness strategy:** Alternatively, we can have a proportionally fair beamforming where better users receive proportionally more power and hence have lower localization errors compared to worse users. We use sum log as the function $f(\cdot)$ in equation (2.40) and then have the CRLB requirements for each user in order to achieve this proportionality while distributing the power. It has been shown that the diminishing returns property of the log function can be used to achieve proportional fairness [80]. The objective function, in this case, would be $\sum_{u=1}^{U} \log\left(L_u(\boldsymbol{X}_N)\right)$.

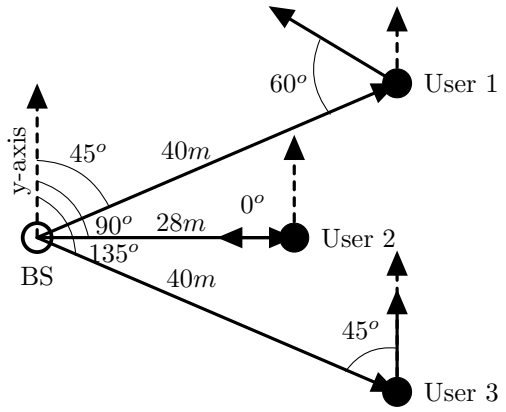

FIGURE 2.11: Example of canonical scenario with a BS and 3 users positioned at different distances from the BS with different orientation.

The optimization problem can be written as

$$\max_{\boldsymbol{X}_N,\zeta_{\theta,u},\zeta_{\phi,u},\zeta_{\tau,u}} \sum_{u=1}^{U} \log(\beta_\theta \zeta_{u,\theta} + \beta_\phi \zeta_{u,\phi} + \beta_\tau \zeta_{u,\tau}) \tag{2.42a}$$

subject to:

$$\frac{\boldsymbol{a}_{n,u}^H \boldsymbol{X}_N \boldsymbol{a}_{n,u}}{\alpha_{\tau,u}} \geq \zeta_{\tau,u}, \qquad \forall u \tag{2.42b}$$

$$\left\| \begin{bmatrix} 2\Re(\dot{\boldsymbol{a}}_u{}^H \boldsymbol{X}_N \boldsymbol{a}_u) \\ 2\Im(\dot{\boldsymbol{a}}_u{}^H \boldsymbol{X}_N \boldsymbol{a}_u) \\ \dot{\boldsymbol{a}}_u^H \boldsymbol{X}_N \dot{\boldsymbol{a}}_u - \zeta_{\theta,u}\alpha_{\theta,u} - \boldsymbol{a}_u^H \boldsymbol{X}_N \boldsymbol{a}_u \end{bmatrix} \right\|_2 \leq \dot{\boldsymbol{a}}_u^H \boldsymbol{X}_N \dot{\boldsymbol{a}}_u - \zeta_{\theta,u}\alpha_{\theta,u} + \boldsymbol{a}_u^H \boldsymbol{X}_N \boldsymbol{a}_u, \forall u \tag{2.42c}$$

$$\frac{\boldsymbol{a}_u^H \boldsymbol{X}_N \boldsymbol{a}_u}{\alpha_{\theta,u}} \geq \zeta_{\phi,u}, \quad \forall u \tag{2.42d}$$

(2.36b)-(2.36g)

Since we solved the optimization problems in equations (2.41) and (2.42) without the rank constraints to maintain the convexity, we perform the rank-1 approximation of matrix $\boldsymbol{F}_n^*$ as for the single-user case in equation (2.22).

2.6.3 Numerical results

In this section we provide some illustrations of optimized beamformers in a canonical multi-user scenario.

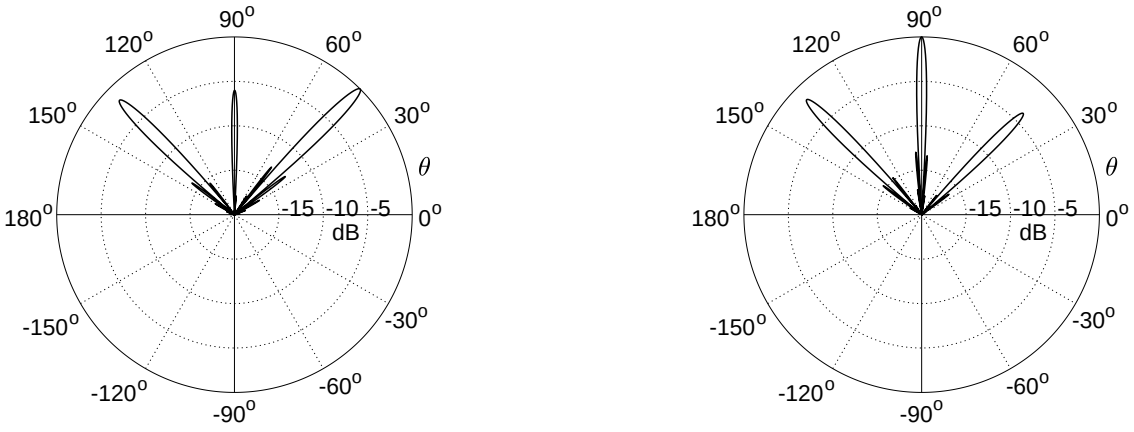

FIGURE 2.12: Example of normalized beam direction for a localization error optimized beamformer in the multi-user case, according to (a) min-max and (b) proportional fairness strategies

System parameters and simulation setup

Let us consider a mm-Wave BS operating at $f_c = 38$ GHz with bandwidth $B = 300$ MHz. We fix the antenna elements number for both BS and user to $N_t = N_r = 30$ elements. We consider both BS and user antennas to have a gain of 13 dBi and an inter-element distance of $\kappa = 0.5\lambda_c$. The path loss $\xi(d_u)$ between the BS and any mobile user at a distance of d_u from the BS is given as by equation (2.23).

We consider the illustrating canonical scenario shown in Fig. 2.11 as the system model, unless otherwise specified.

Results and analysis

In Fig. 2.12, we show the normalized beam gains as a function of BS transmission directions as a result of localization error optimal multi-user beamforming in the above canonical scenario. We observe variable levels of power transmitted in the directions of the three distinct users depending on the fairness strategy considered. From Fig. 2.11, we observe that User 2 is the best user due to its proximity and orientation towards the base station followed by User 3 which is at the same distance as User 1, but with a different orientation. This is evident in Fig. 2.12, as with the min-max fairness strategy User 1 is allocated relatively more power compared to with the proportional fairness strategy.

Using the same localization error optimal beamforming model, in Fig. 2.13 and 2.14 we can see the effect of β_τ on the subcarriers allocation. As discussed earlier, during localization, we consider symmetric power allocation across subcarriers (with

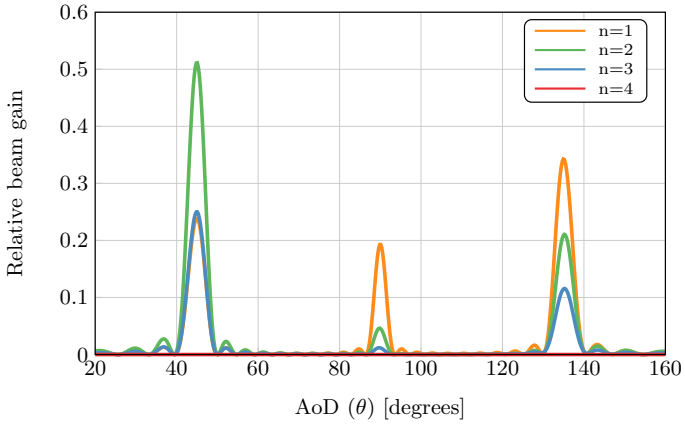

FIGURE 2.13: Example of normalized beam gain (with respect to total gain) with min-max fairness strategy as a function of the direction in the multi-user case with $\beta_\tau = 1$, $\beta_\theta = 1$ and $\beta_\phi = 1$.

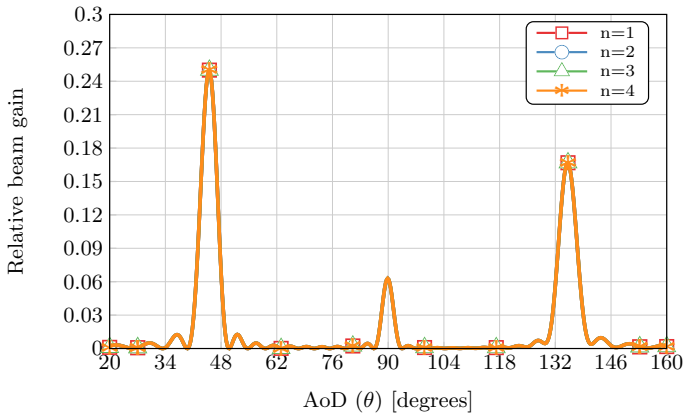

FIGURE 2.14: Example of normalized beam gain (with respect to total gain) with min-max fairness strategy as a function of the direction in the multi-user case with $\beta_\tau = 0$, $\beta_\theta = 1$ and $\beta_\phi = 1$.

respect to the center frequency of the occupied spectrum) to facilitate the statement and resolution of the optimization problem we derived. Hence, to avoid repetition due to the underlying symmetry in our analysis, we only consider the repeated subcarriers in the simulations. We consider 8 subcarriers for simulation in this scenario, but only look at 4 of them numbered as $n = \{1, 2, 3, 4\}$. We limit the total power K to 2.5 units and optimize the beamformer with $\beta_\tau = 0$ or $\beta_\tau > 0$. When $\beta_\tau > 0$, we can observe that in Fig. 2.13, the first subcarrier has no power allocated and the remaining subcarriers have unequal power distribution. However, for the other case where $\beta_\tau = 0$, we have equal allocation across all the subcarriers, as illustrated by Fig. 2.14. The subcarrier power distribution for the two cases are presented in Fig. 2.15. It is clear that for $\beta_\tau > 0$, the optimal beamformer would allocate all the power to the two extremities of the spectrum. The reason is that, for delay estimation, performance would benefit

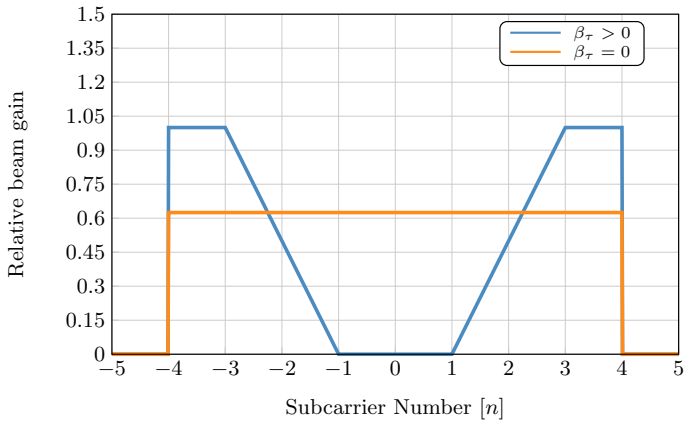

FIGURE 2.15: Power allocation per subcarrier for different values of β_τ.

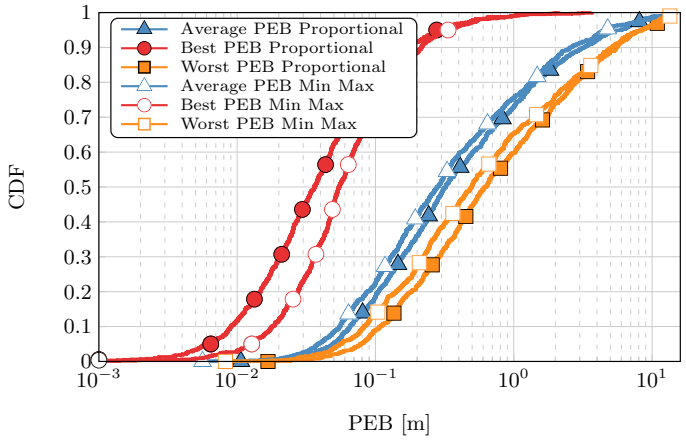

FIGURE 2.16: Empirical CDF of the PEB per user (best, worst and average performance) for different fairness strategies over 1000 MC trials.

from higher resolution provided by a larger equivalent bandwidth (from using more distant frequency components). Hence in the figure, under the spectral power mask constraint (with $0 \leq \text{trace}(\boldsymbol{f}_n \boldsymbol{f}_n^H) \leq 1$), the optimal power allocation solution is vertical water-filling starting from the ends of the spectrum. In contrast, for AoD and AoA estimation, since the frequency plays no role according to the underlying model, there is a uniform power allocation over all the subcarriers.

Figs. 2.16 and 2.17 show the empirical cumulative distribution function (CDF) of best case, worst case and average PEB and OEB over users per trial in the multi-user scenario, over 1000 Monte Carlo (MC) simulation trials of the user positions consisting of three random users positions/orientations (per trial) evaluated with both proportional and min-max fairness strategies. In each occupied position of each MC trial, we use the localization error optimal beamforming to characterize the best PEB as the one with minimum PEB, the worst PEB as the one with maximum PEB and the average PEB as the mean PEB over all three users (and similarly for OEB). We can observe that the CDFs of best, worst and average PEB and OEB

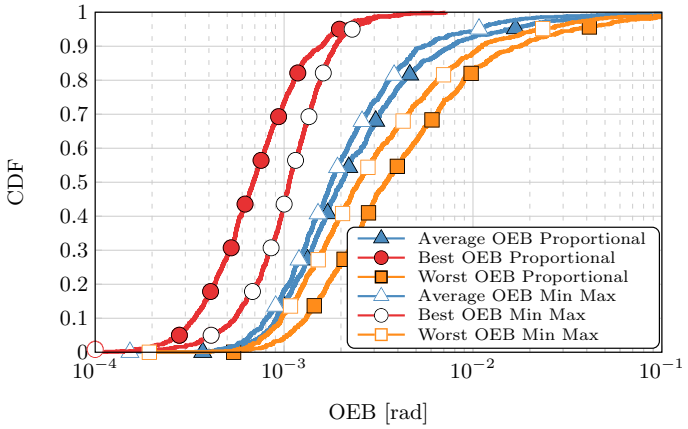

FIGURE 2.17: Empirical CDF of the OEB per user (best, worst and average performance) for different fairness strategies over 1000 MC trials.

are close to each other for all the cases. Even then, we can see that the proportional fairness, as expected, performs better for the best user whereas worse for the worst user and in average. It is also evident that the min-max fairness improves the worst user performance, whereas the proportional fairness improves further the best user. Based on this observation, we can suggest that, if the dispersion is large between the worst and the best user, it is better to use the proportional fairness scheme such that the localization performance of the best user does not degrade too much whereas for a lower dispersion, min-max optimization improves the overall performance more.

2.7 Chapter conclusions

In this chapter, we characterized the typical mm-Wave localization errors based on theoretical performance bounds for both single- and multi-user cases and solved a localization-oriented beamforming optimization problem accordingly.

We firstly tackled the problem for a single-user case, where we investigated the optimal beamforming problem for jointly minimizing delay and AoA estimation. While dealing with the single-user case in a multi-carrier mm-Wave system, we firstly solved the beamforming optimization problem that jointly minimizes the delay and AoA performance bounds. In the process, we formulated the problem as a power allocation problem across the subcarriers to achieve the minimum CRLB. As a result of the optimization, we showed that, theoretically, we can achieve highly accurate estimates of delay and AoA.

We then considered the multi-user scenario where we derived the localization error in terms of SPEB and SOEB and accordingly formulated the beamforming optimization problem minimizing the error. In the process, we reformulated the

FIM for the joint estimation of all the channel parameters in a multi-carrier case and consequently, showed that with certain conditions on the transmission, we can achieve a closed form solution for the CRLB in terms of delay, AoD and AoA. Furthermore, from the formulated localization error, we understood the importance of optimal power allocation in the frequency spectrum during the localization phase, especially for delay estimation, and then determined the optimal beamforming solution. Then, while optimizing the beamformer for the multi-user scenario, we suggested two distinct strategies for power allocation, based on different definitions of fairness among users, namely min-max and proportional fairness strategies. We showed that each proposal offers a distinct solution that can be advantageous on its own depending on the use case scenario.

Despite the findings, we acknowledge that there are some limitations in the study. Firstly, we only consider a simplistic channel path model with only the direct path. It is true that in mm-Wave systems, due to their propagation characteristic as mentioned in chapter 1, the channel is sparse. However, multipath model would to provide a more complete analysis in the case of both single- and multi-user optimization. We consider beamforming considering multipath model in the context of channel estimation in chapter 5 and further mention the possible exploration into the multipath channel in chapter 6.

Similarly, in the channel model, we do not consider the possibilities of blockages, even though it is a problem for the signals at mm-Wave frequencies, as described in chapter 1. In conjunction with the multipath model, the blockage models could be adopted in the future work, as described in chapter 6.

Likewise, in this chapter we consider coarse knowledge of user position and orientation without explicitly characterizing the error in initial estimation. Considering such a probabilistic initial estimation would allow us to optimize the width of the beam in addition to the direction. For instance, if the confidence in the position and orientation estimate of the user is high, we can transmit a beam with small width due to the reduced risk of beam alignment errors thus enabling high data rate and *vice versa*. We have characterized such error in the estimates of the position and orientation, and accordingly the optimization of beam direction and width, in chapters 3, 4 and 5.

Chapter 3

Localization-Communication services trade-off study

3.1 Introduction

Unlike with the technologies of previous generations, the localization service in the case of mm-Wave systems can play an even more crucial role as is can not only fulfill its role of standalone service but also aid in different aspects of communication. For instance, in our previous chapter, we have already showcased the importance of beamforming and thus directionality to mitigate pathloss effects in such mm-Wave systems. We can exploit localization services to estimate the position(s) and orientation(s) of the user(s) and use the direction information for efficient beamforming [58, 59]. In our chapter 1, we have investigated how we can beamform leveraging upon the localization error in both single- and multi-user scenarios. Likewise, we can exploit localization to reduce latency in initial access [61] and channel estimation [65], as we will see later in chapters 4 and 5 respectively.

Reciprocally, we have seen in chapter 1 that some of the intrinsic features of mm-Wave communication can also be highly advantageous for accurate and precise localization, as backed up by the localization resolution figures in table 1.1. The inherent properties of mm-Wave such as sparse channel, high bandwidth, large number of antenna elements and highly dense networks provide favourable conditions for very accurate localization. For instance, in [81], the authors show that even in the absence of the direct path, the PEB performance in mm-Wave is still accurate enough. Similarly, in [42], the authors demonstrate the positive impact of network densification on the positioning error.

Hence, considering such inter-relation between the localization and communication services, it is highly likely that the two services not only exist as two separate entities in the context of 5G, but will co-exist symbiotically within the same system. In the light of the previous remark, it is important to investigate different aspects

of such co-existence in order to build a framework incorporating and even inter-operating both services, as efficiently as possible. To achieve this, in this chapter, we look into how we can split resources between the two services, in particular time and frequency, in a quest to find an equilibrium for their optimal co-existence.

In this chapter, we study the localization and communication services as both standalone and joint[1] functionalities of a system in order to achieve the required QoS objectives. In the process, we also aim towards considering a mm-Wave network scenario with many BSs, unlike the single BS assumption made in chapter 2. In order to isolate the effects of considering standalone and joint services from the number of BSs assumption, we gradually complexify the network through this and the next chapter. Specifically, in this chapter we evaluate the localization and communication performances firstly in the standalone scenario and then in a joint scenario both in a single BS scenario. Then, we consider the joint services scenario in a mm-Wave network scenario with multiple BSs, however with deterministic deployment where we consider a constant distance between the deployed BSs. In the chapter 4, we will finally arrive to a probabilistic network deployment in a similar joint services scenario.

3.2 Related works

In the context of mm-Wave localization, as we have detailed in section 2.2, the authors in [51, 52, 71, 72] have comprehensively characterized the localization performance limits in terms of CRLB. In [51], the authors present an algorithm to estimate the position and orientation of the user and verify that even in low SNR, the algorithm can approach the PEB and OEB.

In the context of mm-Wave communication services, the authors in [82] have characterized the downlink communication performance in random wireless networks in terms of SINR coverage probability and rate coverage probability, using stochastic geometry [83, 84]. For such a model, the positions of the BSs can be modeled either using homogeneous Poisson point process (PPP) [85] or using repulsive point process [86]. Recently, the authors in [87] investigated a more realistic scenario, where the mm-Wave BSs are deployed along the roads of a city.

[1]In this thesis, in the context of localization and communication functionalities, the term *standalone* refers to the scenario when the two services act independently of each other. In contrast, the term *joint* is used to refer to the scenario when the communication service exploits the positional or directional information from the localization service.

In the context of joint localization and communication functionalities, the authors in [88] have studied a distributed antenna system providing both data communication and positioning functionalities in sub-6 GHz systems. The authors assumed that the user equipments (UEs) know the positions of the BSs and attempt to estimate their own positions based on the received signals. Similarly, Garcia *et al.* in [65] have studied a location-aided initial access strategy for mm-Wave networks, in which the information of UE locations enables to speed up the channel estimation and beamforming procedures. Likewise, in [62], the authors investigate the resource allocation in terms of time in mm-Wave network based on localization performance bounds. The authors extend this study in [89] to a multi-user scenario where the trade-off between the two standalone services is studied in terms of sum-rate and PEB. Likewise, in [90], the authors present an iterative localization based beam selection algorithm where the transmitter, in each iteration, selects a refined finer beam based on position and orientation estimation. The refined beam again improves the estimation and the process continues in a virtuous loop. Extending this idea, in [91], the authors present the beam selection algorithm at both transmitter and receiving ends.

3.3 Methodology and organization

Considering the advancements in the literature regarding specifically the multi-service aspects, in this section, we present our motivations behind this work and introduce the structure of the chapter.

- To the best of our knowledge, resource sharing between the localization and communication services has not been considered in a multi-user scenario. Motivated by this limitation and our work on localization oriented beamforming in chapter 2, we study the trade-off between the two standalone services in a mm-Wave system as a result of sharing time and frequency resources.

- After assessing the system level performance with standalone services, we then shift our attention to the resource allocation scheme in a joint localization and communication scenario where localization and communication phases are inter-dependent on each other. Even though resource allocation between communication and localization standalone services has already been considered before in the literature, to the best of our knowledge, it has not been envisaged yet in a joint scenario.

- In such a system, we then study not only the optimal allocation of time and frequency resources, but also look into the implication of localization accuracy and hence beam alignment errors in the communication phase. Specifically, taking advantage of the localization error characterization, we study the effects of beamwidth adjustment in the beam alignment error and consequently in the data service aspect.

The rest of the chapter is organized as follows. In section 3.4 we study the trade-off between the localization and communication functionalities when they are treated as standalone services. In section 3.4.1, we introduce the system model of the standalone services. Then, in sections 3.4.2 and 3.4.3, we study the different ways in which time and frequency can be budgeted between the two services. Finally, we illustrate the trade-off *via* simulations. We then move on to a system endowed with joint localization and communication functionalities in section 3.5. For such a system, we present the network geometry and communication model in section 3.5.1. Then, in sections 3.5.2 and 3.5.3 we present the analysis and numerical results while sharing time and frequency resources respectively between the two services. We finally conclude the chapter in 3.6.

3.4 Standalone localization and communication services

In this section, we will study the trade-off arising due to resource allocation, in particular time and frequency (or analogously energy and power respectively), in a multi-user mm-Wave system supporting both localization and communication services. In such a multi-service system, budgeting more resources for the data service than for localization would indeed imply higher data rates but also, adversely, higher position and orientation estimation errors. Based on theoretical localization performance bounds and on the expression of the average data rate per user, we herein investigate and compare various ways the two different services could be operated depending on when the multiple users are assessed.

3.4.1 System model

We consider a two-dimensional mm-Wave communication scenario with a single BS and U users, exactly as described in chapter 2 section 2.6.1. We also consider the BS provides both communication and localization functionalities with a limited time

and frequency budgets. In the previous chapter, we have already defined the localization optimal beamformers and we have also stated that communication oriented beamformers have been already studied in the literature. Hence, considering both localization and communication functionalities, the idea is to investigate a trade-off between the two services while sharing resources between them in both single-user and multi-user cases. For a fixed resource budget, based on the trade-off and a-priori QoS requirement for each service, we determine the optimal split between the resources.

In this section, for the localization phase, we consider the multi-user localization error optimal beamforming from section 2.6.2. Let $\boldsymbol{X}_{L,u}^*$ and $\boldsymbol{X}_L^*$ represent the optimal localization beamformers $\boldsymbol{X}_N$ from equations (2.38) in a single-user case and (2.41) or (2.42) in a multi-user case respectively. For the communication phase, we consider the beamformer maximizing the sum-rate for the multiple users similar to [89] as derived in appendix B.1. In consistency with the localization phase, we consider using an analog beamforming architecture with 1 RF chain[2] transmitting one stream of data at a time. Similarly, let $\boldsymbol{X}_{C,u}^*$ represent the data rate optimal beamformer from equation (B.6). Also, the FIM $\boldsymbol{J}_{\mu,u}$ is defined in equation (2.30)

3.4.2 Frequency sharing

In this strategy, we share the available sub-carriers for both localization and communication simultaneously for the full duration of time T as shown in Fig. 3.1. Let $\mathcal{N}_L$ and $\mathcal{N}_C$ represent the sets of subcarriers dedicated for localization and communication respectively and $N_L = |\mathcal{N}_L|$ and $N_C = |\mathcal{N}_C|$ represent the cardinality of the two sets. We further need to split the subcarriers allocated to the communication phase into U parts, represented as $\mathcal{N}_{C,u}, \forall u$, such that we can beamform all the U users relying on different subcarriers. Since we do not consider any effect of sub-carriers power allocation on the rate[3], we can split the frequency among the users arbitrarily. The sets $\mathcal{N}_L$ and $\mathcal{N}_C$ are mutually exclusive and $\bigcup_{u=1}^{U} \mathcal{N}_{C,u} = \mathcal{N}_C$. Let us define matrices $\boldsymbol{Y}_L = \text{diag}(\boldsymbol{Y}_{L,1}, \boldsymbol{Y}_{L,2}, \cdots, \boldsymbol{Y}_{L,N}) \in \mathbb{R}^{M \times M}$

[2]Note that the primary focus of this work is on beamforming optimization for the localization phase. In this section we look at a simple example relying on an analog architecture in the communication phase for the resource allocation trade-off study. However, the choice of a beamforming architecture and the optimal beamformer for communication can be independent as any type of solution can be implemented on top of our beamforming optimization framework.

[3]We have this assumption from the channel model from equation (2.24) where we considered a frequency flat spectrum in order to have a general system level overview of the effects of resource sharing. In the equation, we can consider frequency dependent channel coefficient to have a more realistic model. In that case, we need to further optimize the sub-carrier allocation to particular users depending on the channel coefficient per user.

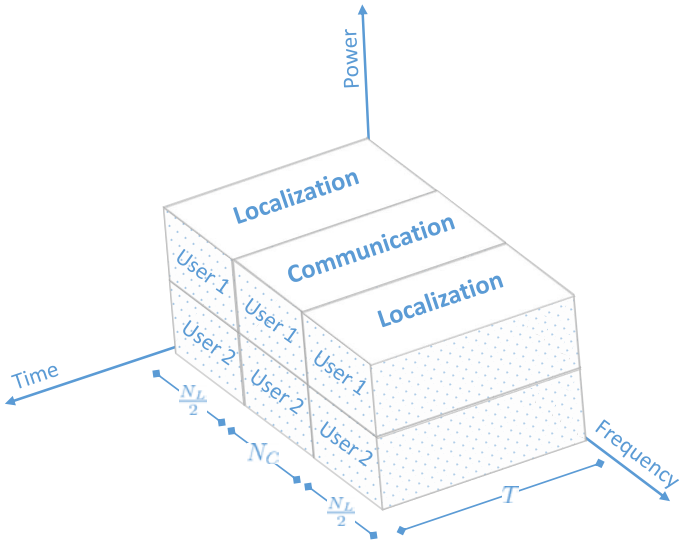

FIGURE 3.1: Frequency division framework for localization and communication services.

and $Y_{C,u} = \text{diag}(\boldsymbol{Y}_{C,u,1}, \boldsymbol{Y}_{C,u,2}, \cdots, \boldsymbol{Y}_{C,u,N}) \in \mathbb{R}^{M\times M}$ where

$$\boldsymbol{Y}_{L,n} = \begin{cases} \boldsymbol{I}_{N_t}, & \text{if } n \in \mathcal{N}_L \\ \boldsymbol{0}_{N_t}, & \text{otherwise.} \end{cases} \tag{3.1}$$

$$\boldsymbol{Y}_{C,u,n} = \begin{cases} \boldsymbol{I}_{N_t}, & \text{if } n \in \mathcal{N}_{C,u} \\ \boldsymbol{0}_{N_t}, & \text{otherwise.} \end{cases} \tag{3.2}$$

Then, we can define the average data rate as

$$R = \frac{1}{U}\sum_{u=1}^{U} \log_2\left(1 + \frac{\boldsymbol{a}_{\zeta,u}^H \boldsymbol{Y}_C \boldsymbol{X}_C^* \boldsymbol{Y}_C^T \boldsymbol{a}_{\zeta,u}}{N_0}\right), \tag{3.3}$$

where,

$$\boldsymbol{a}_{\zeta,u} = \begin{bmatrix} \zeta_u |s_{n_1}| \boldsymbol{a}_{\text{Tx},u}^T & \cdots & \zeta_u |s_{n_N}| \boldsymbol{a}_{\text{Tx},u}^T \end{bmatrix}^T \in \mathbb{C}^M, \tag{3.4}$$

and $\zeta_u = \sqrt{\frac{P_{\text{Tx}}}{xi_u}} |h_u| |\boldsymbol{w}_u^H \boldsymbol{a}_{\text{Rx},u}|$.

Similarly, the average PEB and OEB per user for the multi-user case can be written as

$$\text{PEB} = \frac{1}{U}\sum_{u=1}^{U} \sqrt{\frac{T_s}{T} \text{trace}\left(\boldsymbol{J}_{\mu,u,1:2,1:2}^{-1}\left(\boldsymbol{Y}_L \boldsymbol{X}_L^* \boldsymbol{Y}_L^T\right)\right)}, \tag{3.5}$$

and,

$$\text{OEB} = \frac{1}{U}\sum_{u=1}^{U} \sqrt{\frac{T_s}{T} \boldsymbol{J}_{\mu,u,3,3}^{-1}\left(\boldsymbol{Y}_L \boldsymbol{X}_L^* \boldsymbol{Y}_L^T\right)}, \tag{3.6}$$

where as defined in section 2.6.1, T_s is the symbol duration. In T_L amount of

localization time, the gain in information is T_L/T_s as reflected in equations (3.5) and (3.6).

The formulation $\boldsymbol{Y}_C \boldsymbol{X}_{C,u}^* \boldsymbol{Y}_C^T$ nullifies the beamformer related to the sub-carriers not dedicated for communication (and likewise $\boldsymbol{Y}_L$ for localization). Accordingly, the individual sub-carriers, and thus the total power budgeted over the entire occupied bandwidth, can be split to cover the two different services.

3.4.3 Time sharing

After the frequency sharing between the services, now we consider a system where time is split between them. Consider a system level framework with total time budget of $T = T_L + T_C$, where T_L is the total time budgeted for localization, and the rest of the time T_C is allocated for communication. We investigate the trade-off between localization and communication performances as a result of time sharing between the two services.

For the multi-user scenario, we use two different schemes, namely the simultaneous and the sequential[4] localization and communication framework. In the former, we simultaneously localize all the users in the first phase and then simultaneously communicate with them. In the latter, we perform localization and communication for the first user independently and then for the second independently and so on.

Simultaneous multi-user assessment

We firstly look into a scheme assessing the multiple users simultaneously. In this strategy, all the users are simultaneously localized for a complete localization time duration of T_L, even though allocating simultaneous localization pilots to different users means that each localization signal has reduced power as shown in Fig. 3.2. Likewise, we have the same situation for the communication phase in this scenario. In this case we use the optimal beamforming vector for multiple users $\boldsymbol{X}_L^*$ and $\boldsymbol{X}_C^*$ for both localization and communication services respectively. We then look at the resulting average performance per user while considering data rate, PEB and OEB. The detailed derivations for the latter can be found in equations (2.31) and (2.32).

The average rate per user is

$$R = \frac{1}{U} \frac{T_C}{T} \sum_{u=1}^{U} \frac{T_u^*}{T_C} \log_2 \left(1 + \frac{\boldsymbol{a}_{\zeta,u}^H \boldsymbol{X}_{C,u}^* \boldsymbol{a}_{\zeta,u}}{N_0} \right). \tag{3.7}$$

[4]Here, the words simultaneous and sequential shall be intended in terms of multi-user assessment (and not in terms of communication or localization functionalities). The word "simultaneous" refers to a scenario when all the users are assessed at once, and "sequential" refers to the scenario when the users are assessed one by one.

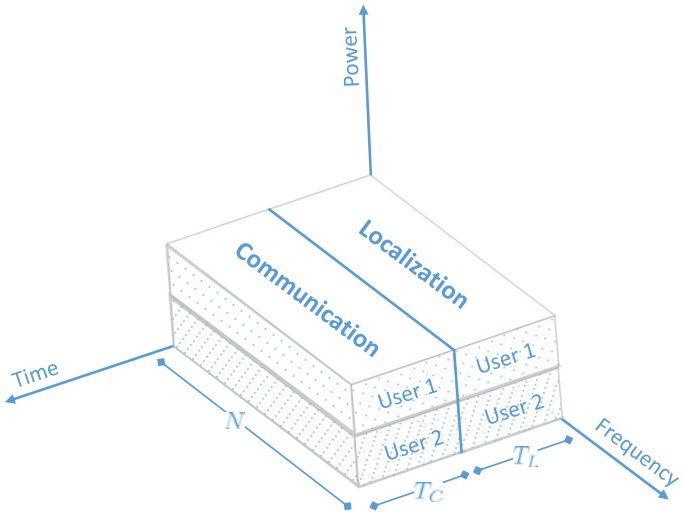

FIGURE 3.2: Time division framework for localization and communication services with simultaneous multi-user assessment.

Similarly, the average PEB and OEB per user with localization time limited to T_L can be written as[5]

$$\text{PEB} = \frac{1}{U}\sum_{u=1}^{U}\sqrt{\frac{T_s}{T_L}\text{trace}\left(\boldsymbol{J}^{-1}_{\mu,u,1:2,1:2}(\boldsymbol{X}^*_L)\right)}, \tag{3.8}$$

and,

$$\text{OEB} = \frac{1}{U}\sum_{u=1}^{U}\sqrt{\frac{T_s}{T_L}\boldsymbol{J}^{-1}_{\mu,u,3,3}(\boldsymbol{X}^*_L)}. \tag{3.9}$$

Sequential multi-user assessment

Then, moving on to the sequential multi-user assessment, we localize and communicate with one single-user at a time, while assessing multiple users one by one. In this strategy, for both localization and communication phases, at each time instance, one single user is served with maximum power but only for a reduced time duration of T_L/U and T_C/U for localization and communication respectively as shown in Fig. 3.3, thus respecting the same overall constraints on time T_L and T_C as in the previous allocation scheme. In other words, we basically use the single-user time division strategy for U consecutive periods, once for each user. The average rate per user can be written as equation (3.7).

[5]The FIM in [62] is considered for a signal with duration T_s. Since we consider a localization time of T_L, we consider the information increase by a factor of T_L/T_s (e.g., equivalently, performing a coherent integration of successive observations/estimates would reduce noise by the same factor).

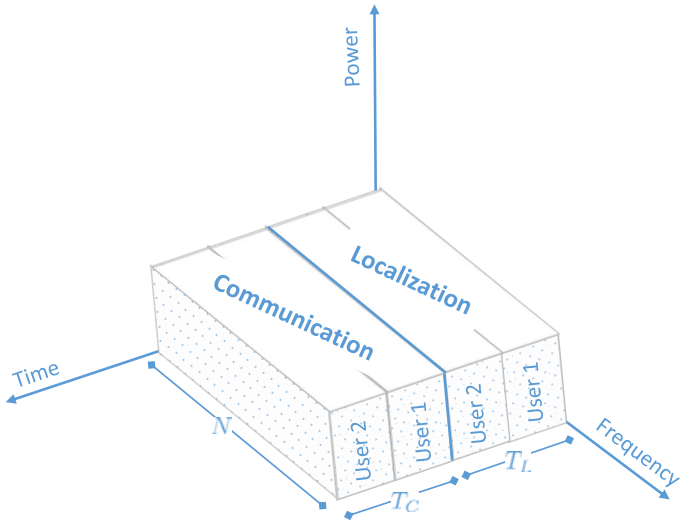

FIGURE 3.3: Time division in a localization and communication framework with sequential multi-user assessment.

Similarly, the average PEB and OEB per user with the localization time limited to T_L/U can be written as

$$\text{PEB} = \frac{1}{U}\sum_{u=1}^{U}\sqrt{\frac{UT_s}{T_L}\text{trace}\left(\boldsymbol{J}^{-1}_{\mu,u,1:2,1:2}(\boldsymbol{X}^*_{L,u})\right)}, \tag{3.10}$$

and,

$$\text{OEB} = \frac{1}{U}\sum_{u=1}^{U}\sqrt{\frac{UT_s}{T_L}\boldsymbol{J}^{-1}_{\mu,u,3,3}(\boldsymbol{X}^*_{L,u})}. \tag{3.11}$$

3.4.4 Numerical results

Let us consider a mm-Wave BS operating at $f_c = 38$ GHz with bandwidth $B = 300$ MHz. We fix the antenna elements number for both the BS and the user to $N_t = N_r = 30$ elements. We consider both the BS and the user antennas to have a gain of 13 dBi and an inter-element distance $\kappa = 0.5\lambda_c$. The path loss ξ_u between the BS and any mobile user at a distance d_u from the BS is given as in equation (2.23).

In Fig. 3.4 (and respectively Fig. 3.5), we represent the corresponding trade-off between PEB (and respectively OEB) according to different resources sharing strategies and the average rate. Here, we use the localization optimal beamforming for obtaining the PEB and OEB and the data rate optimal beamforming for obtaining the average rate, as clarified in sections 3.4.2 and 3.4.3. In case of frequency division, we dedicate the peripheral parts of the spectrum to localization services for better delay estimation as concluded in chapter 2. From the equations of data rate, PEB and OEB, one can intuitively understand the effect of frequency

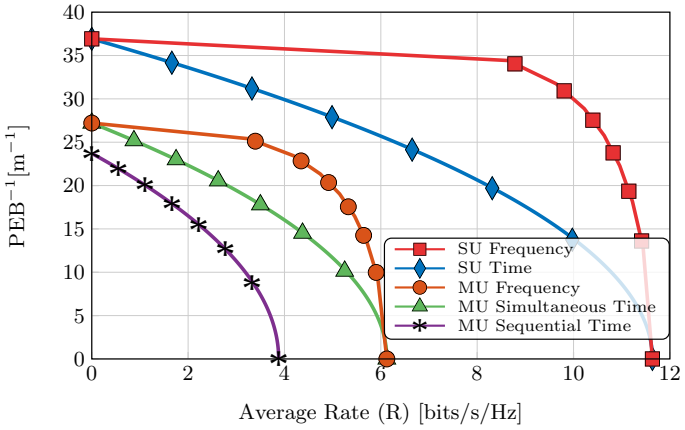

FIGURE 3.4: Inverse of PEB vs. average rate trade-off for both frequency and time division strategies among the 3 users.

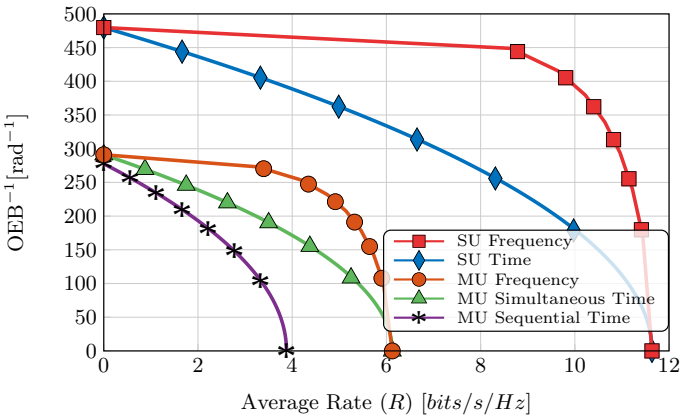

FIGURE 3.5: Inverse of OEB vs. average rate trade-off for both frequency and time division strategies among the 3 users.

and time sharing. With a larger proportion of time split for the localization phase, we can send more localization pilot signals and get better average PEB and OEB performance. We can notice that PEB and OEB decrease by a factor of $\sqrt{1/T_L}$ and the average rate decreases by a factor of $(T - T_L)/T$ as we increase T_L. Similarly, with more time allocated for communication, we get higher data rates for communication as expected. Likewise, increasing the number of sub-carriers allocated for localization, we get better average PEB and OEB performances, but the resulting allocation of a low number of sub-carriers for communication decreases the rate performance.

From Figs. 3.4 and 3.5, we can firstly observe that for single-user, the PEB is smaller and the data rate is higher. Since there are no beams in other directions unlike for the multi-user case, more power is received by the user. Similarly, it is better for the BS to localize and communicate with all the users simultaneously

rather than sequentially while targeting localization and communication with individual users. Moreover, we can see that for both PEB and OEB, it is better to share frequency rather than time to get a better performance. Allocating localization pilots on the extremities of the spectrum improves localization performance (in particular delay performance) while there is no advantageous temporal allocation for either of the phases while sharing time. Here, in the single-user frequency division and multi-user frequency division, we use the peripheral parts of the spectrum for localization and the remaining central part for communication, and hence we can see the performance gain for PEB and OEB with optimal power allocation in frequency rather than in time.

The operating point on each trade-off curve then depends on the QoS requirement for each service. Given a particular system scenario and a total resource budget, we can pin-point the feasible region in the trade-off curve that satisfies the QoS requirement for each of the localization and communication service and then find the optimal resource split for the frequency and time division.

3.5 Joint localization and communication services

In contrast to the standalone localization and communication services considered in the previous section, in this section we investigate a system where localization and communication services are inter-dependent. We have already established in the previous chapters that the importance of directionality in 5G suggests that localization and communication services would most likely be tightly intertwined. With this in mind, we need to characterize how the localization service can be infused with the data communication service in order to efficiently achieve the outlined targets of 5G. In this system, unlike in the standalone case, the data service phase utilizes the information from localization phase to transmit the data to the UE. More specifically, the directional information for beamforming in the data phase is exploited from the localization phase. Hence, here, we scrutinize the prospects of joint localization and communication while sharing, as in the previous section, frequency/power and time/energy resources.

3.5.1 System model

Network geometry and BS characteristics

In this joint localization and communication framework, we consider an urban scenario with dense multi-radio access technique (RAT) BSs deployed along the streets

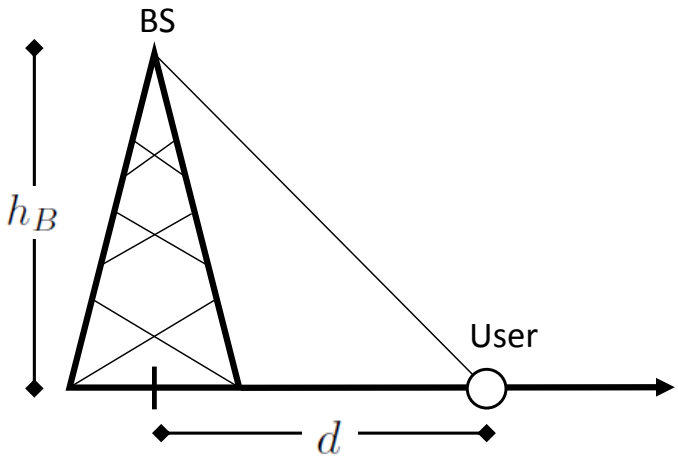

FIGURE 3.6: Model depicting the 1D deployment scenario consisting of 1 BS and 1 user node.

of a city with tall buildings contributing to a dense blocking environment. We assume that the distribution of BS positions in each street is modeled as a one-dimensional[6] PPP ξ with intensity λ [m^{-1}]. Each BS is assumed to be of known height h_B and equipped with directional antennas with beamwidth ω. The transmit power of the BSs is assumed to be P_{Tx}. Without loss of generality we perform our analysis from the perspective of a typical user located at the origin, which associates with the BS that provides the highest downlink power. Accordingly, the distribution of the distance d of the typical user from the base of the serving BS is given by [83]:

$$f_d(x) = 2\lambda \exp(-2\lambda x). \tag{3.12}$$

Path-loss model

We consider a Nakagami fading with parameter n_0 and variance 1 to model the low local scattering for communication [93]. At the receiver located at the origin, the power received from a BS located at a distance d including the pathloss is given by:

$$P_{Rx} = \frac{|h|^2 K P_{Tx} G_{Tx} G_{Rx}}{(d^2 + h_B^2)^{\alpha/2}}, \tag{3.13}$$

where $K = \lambda_c^2/4\pi^2$ is the path loss coefficient, λ_c is the wavelength corresponding to the center frequency of the transmitted signal, h represents the fast-fading, α

[6]The 1D model assumed in this chapter is relevant for the case where the cellular deployment is envisioned to be along roads. As an example, Verizon and AT&T have both announced plans to deploy 5G infrastructure on lampposts for mobile access [92], respectively. In such scenario, the 1D model assumed in our work can be utilized by a network operator to derive system design insights and to further fine-tune the deployment parameters.

is the path loss exponent and $G_{Tx} = |\boldsymbol{a}_{Tx}^H \boldsymbol{f}|^2$ and $G_{Rx} = |\boldsymbol{w}^H \boldsymbol{a}_{Rx}|^2$ represent the directional antenna gains at the transmitter and the receiver respectively.

Received signal model

Let $s(t)$ be the signal transmitted by the BS. The signal received at the user can be written as:

$$y(t) = \sqrt{P_{Rx}} s(t - \tau) + n(t), \tag{3.14}$$

where, $\tau = \sqrt{d^2 + h_B^2}/c$ with d being the true distance from the base of the BS to the user and $n(t)$ is the zero mean Gaussian noise with two-sided power spectral density $N_0/2$ and corresponding power $\sigma_N^2 = N_0 B$. We further assume the transmit signal $s(t)$ with duration T_s has flat spectrum with $|S(f)|^2 = T_s/(2\pi B)$ where B is the bandwidth of the system, similarly to [62].

3.5.2 Frequency sharing

With respect to the joint localization and communication framework, we look into a system where the localization and communication services share frequency resources or power and, accordingly, study the trade-off between the localization and the data rate performance. In this section, based on the localization performances in terms of localization error bounds, we firstly define the probability of beam alignment errors. Then, leveraging on the tools of stochastic geometry, we present an average characterization of the localization and communication performance of this network, by exploiting the a-priori knowledge about the distribution of the distances of the users from the BSs while considering the aforementioned beam alignment errors. Finally, we prescribe the network operator a scheme to select the beamwidth and the power splitting factor between the localization and communication functions to address different QoS requirements, while limiting cellular outage.

Transmission policy and model

We assume a communication scheme where the transmit power of the BS is divided into two parts: one associated with positioning and the other allotted for data communication. Such power split can be achieved by splitting the spectrum into localization and communication parts. The power allocated for localization determines the number of control symbols used for this function, whereas the remaining power is utilized for control and data symbols of the communication phase. We acknowledge that it is possible to utilize the native communication signal for positioning

services. However, we use a dedicated waveform designed for better localization performance (e.g., see [94] for a discussion on localization specific waveforms). Hence, splitting of the transmit power becomes necessary to characterize and optimize the operating trade-off between communication and localization functionalities.

Accordingly, if the total transmit power is P_{Tx}, and β is the fraction of power used for data services, the corresponding transmit power for localization is $P_L = (1-\beta)P_{Tx}$. Consequently, the transmit power for data service is $P_C = \beta P_{Tx}$. Let the SNR for the distance estimation and the data communication phases be represented by SNR_L and SNR_C, respectively. We also assume that both localization and communication services are performed for a total duration of T.

In this work, we consider the estimation of the delay in the localization phase, and accordingly use it to characterize the beam alignment error (as in our one-dimensional scenario delay and AoD are directly related to each other). Likewise, we also assume that the network is equipped with efficient interference management capabilities (e.g., spatio-temporal frequency reuse), so that the performance of the users is noise-limited[7]. In next sections and chapters, we introduce further localization estimation variables and interference analysis for completeness.

Positioning error, data rate coverage and beam selection error

In this section, we first characterize the minimum variance of the error in the estimation of the distance of the typical user from the serving BS. Then, we derive the SNR coverage and the rate coverage probabilities.

Distance estimation analysis: Let the power spectral density of the transmit signal be symmetric [62] and equal to $T_s/2\pi B$, where, T_s and B are respectively the time duration and the bandwidth of the transmitted signal $s(t)$. The symmetry, consequently, decouples the Fisher information of the distance, i.e., $J_{d,d}$ from the rest of the estimation parameters, as shown in chapter 2 and [62]. This is also the reason we have not considered the channel coefficients yet as an estimation parameter for the FIM. We will do so in chapter 4 while also considering AoA estimation for UE side beam alignment. With the received signal model in equation (3.14) we can write the FIM for delay estimation, as derived in [62, 96] and in appendix C.1, as

$$J_{d,d} = \zeta \frac{1}{(h_B^2 + d^2)^{\alpha/2}}, \tag{3.15}$$

[7]Although the assumption of the network being noise-limited simplifies the analysis, Singh *et al.* [95] have shown the validity of this assumption in outdoor mm-Wave mesh networks.

where $\zeta = (2KP_LTG_{Rx}G_{Tx}|h|^2B^2\pi^2)/3c^2\sigma_N^2$.

Now using the distribution of d from (3.12), the expectation of the Fisher information (or the average information over all possible true distances) is calculated as:

$$J_D = \mathbb{E}_d\left[J_{d,d}\right] = 2\lambda\zeta \int_1^\infty \frac{e^{-2\lambda x}}{(h_B^2 + x^2)^{\alpha/2}} dx. \tag{3.16}$$

For the special case of path loss exponent $\alpha = 2$ (under a LOS assumption), J_D evaluates to (3.17), where Ei is the exponential integral [97].

$$J_D = 2\lambda\zeta \left(\frac{i(e^{-i2\lambda h_B} Ei(i2\lambda h) - e^{i2\lambda h_B} Ei(-i2\lambda h_B))}{2h_B} + 2\lambda \log(2\lambda) - 1 \right). \tag{3.17}$$

Likewise, the prior information resulting from the a-priori knowledge of the distribution of d can be calculated as:

$$J_P = \mathbb{E}\left[\log(f_d(x))\right] = \int_0^\infty \log\left(f_d(x)\right) f_d(x) dx, \tag{3.18a}$$

$$= \int_0^\infty \log\left(2\lambda \exp\left(-2\lambda x\right)\right) 2\lambda \exp\left(-2\lambda x\right) dx, \tag{3.18b}$$

$$= \log(2\lambda) - 1. \tag{3.18c}$$

Finally, the Bayesian information can be obtained as $J_B = J_D + J_P$ according to [96]. Consequently, the Bayesian Cramér-Rao lower bound (BCRLB) and Jeffrey's prior corresponding to the Bayesian information are calculated as $\frac{1}{J_B}$ and $\sqrt{J_B}$, respectively. Intuitively, higher the Jeffrey's prior (or lower the BCRLB) is, better the estimation efficiency will be. From (3.17), we see that a higher Jeffrey's prior is facilitated by a larger value of P_L, i.e., a smaller β.

Coverage and rate analysis: Now, moving on to the data-service procedure, the SNR based on the path-loss model in the section 3.5.1 is:

$$\mathrm{SNR}_C = \frac{|h|^2 K G_{Tx} G_{Rx} P_C}{\sigma_N^2} (d^2 + h_B^2)^{-\frac{\alpha}{2}}. \tag{3.19}$$

Accordingly, let us define the SNR coverage probability of the typical user at a threshold γ, as the probability that the SNR is greater than γ. It represents the fraction of the users under coverage in the network. Then, the SNR coverage

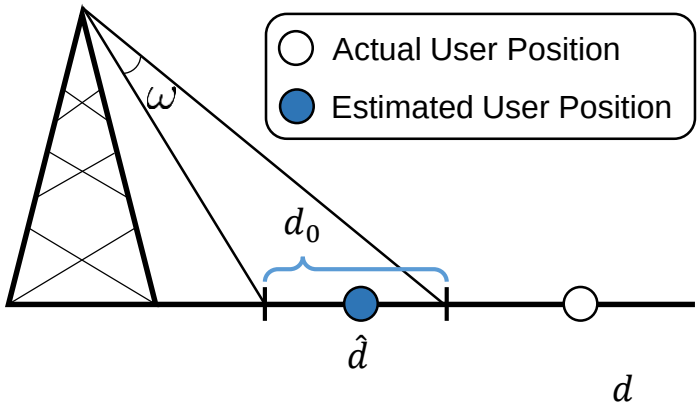

FIGURE 3.7: Illustration of beam selection error.

probability is computed as follows:

$$\mathbb{P}\left(\mathrm{SNR}_C \geq \gamma\right) = \mathbb{P}\left(\frac{|h|^2 K G_{Tx} G_{Rx} P_C}{\sigma_N^2} \sqrt{(x^2 + h_B^2)}^{-\alpha} \geq \gamma\right), \tag{3.20a}$$

$$= \mathbb{P}\left(|h|^2 \geq \frac{\gamma \sigma_N^2}{P_C K G_{Tx} G_{Rx} (x^2 + h_B^2)^{-\frac{\alpha}{2}}}\right), \tag{3.20b}$$

$$= \sum_{n=1}^{n_0} (-1)^{n+1} \binom{n_0}{n} \mathbb{E}_x \left[\exp\left(-\frac{n\gamma\sigma_N^2}{P_C K G_{Tx} G_{Rx} (x^2 + h_B^2)^{-\frac{\alpha}{2}}}\right)\right], \tag{3.20c}$$

$$= \sum_{n=1}^{n_0} (-1)^{n+1} \binom{n_0}{n} 2\lambda \int_0^\infty \exp\left(-\frac{n\gamma\sigma_N^2 (x^2 + h_B^2)^{\frac{\alpha}{2}}}{P_C K G_{Tx} G_{Rx}}\right) \exp\left(-2\lambda x\right) dx, \tag{3.20d}$$

where, x is the random variable representing d. Hence, evaluating the integral, the coverage probability can be formulated as follows:

$$\mathcal{P}_C(\gamma) = \sum_{n=1}^{n_0} (-1)^{n+1} \binom{n_0}{n} 2\lambda \exp\left(2\lambda - \frac{h_B^2 n\gamma}{G_1}\right) \left[\frac{\sqrt{\pi}}{2} \left(\sqrt{\frac{G_1}{n\gamma}} - \frac{G_1}{n\gamma} \mathrm{erf}\left(\frac{h_B^2 n\gamma}{G_1}\right)\right)\right], \tag{3.21}$$

where $G_1 = P_C K G_{Tx} G_{Rx} / \sigma_n^2$ for notational simplicity.

Now, similar to the SNR coverage probability, the rate coverage probability at a threshold r_0 is defined as the probability that the downlink data rate of the typical user is greater than r_0. The rate coverage probability can be computed as:

$$\mathcal{P}_R(r_0) = \mathbb{P}\left(R \geq r_0\right) = \mathbb{P}\left(\mathrm{SNR}_C \geq 2^{\frac{r_0}{B}} - 1\right), \tag{3.22a}$$

$$= \mathcal{P}_C\left(2^{\frac{r_0}{B}} - 1\right). \tag{3.22b}$$

Beam selection error characterization: We assume that through the localization procedure, the user is positioned at $\hat{d}$. Consider the BS with an antenna beamwidth ω, serving the user located at an estimated $\hat{d}$, covers a region of length d_0 on the ground in Fig. 3.7. Using simple trigonometric calculations, we have:

$$d_0 = \frac{2\tan\left(\frac{\omega}{2}\right)\left[1+\frac{\hat{d}^2}{h_B^2}\right]}{1-\frac{\hat{d}^2}{h_B^2}\tan^2\frac{\omega}{2}}. \tag{3.23}$$

The beam selection can occur in the absence of dynamic beam-alignment on both sides of the radio link. Assuming that the user's antenna is always oriented towards the BS, or equivalently, in case the user is operating with an omni-directional antenna, beam selection error will occur in case the distance of the actual user position on the ground is more than $d_0/2$ from the estimated position for a given beamwidth of ω.

Let us assume that the estimation error for the user localization is symmetric about its mean. Consequently, we bound the probability of the beam selection error as follows:

$$\mathcal{P}_{BS}(d) = \mathbb{P}\left(|d-\hat{d}| \geq \frac{d_0}{2}\right) \overset{(a)}{\leq} \frac{2\sigma_d^2}{d_0} \overset{(b)}{=} \frac{2}{J_B d_0}, \tag{3.24}$$

where $\hat{d}$ is the estimated distance of the user. Here (a) follows from Chebyshev's inequality assuming σ_d^2 as the variance of estimating the user at $\hat{d}$. The step (b) holds of a minimum-variance unbiased estimator (MVUE)[8].

Based on this, we can then bound the mean beam selection error by taking the expectation over d, as follows:

$$\bar{\mathcal{P}}_{BS} = \mathbb{E}_d\left[\mathcal{P}_{BS}(d)\right] \leq \mathbb{E}_d\left[\frac{2}{J_B d_0}\right]. \tag{3.25}$$

Numerical results

In this section, we present some numerical results based on the analytical framework presented above. First, we present how the SNR coverage probability changes with the power splitting factor (β). Subsequently, we study the trade-off between localization and data rate as a function of β. Then, with the help of two examples,

[8]For instance, in [51], the authors demonstrate that in both LOS and NLOS conditions, the algorithm attains CRLB even at low SNR in the mm-Wave scenario.

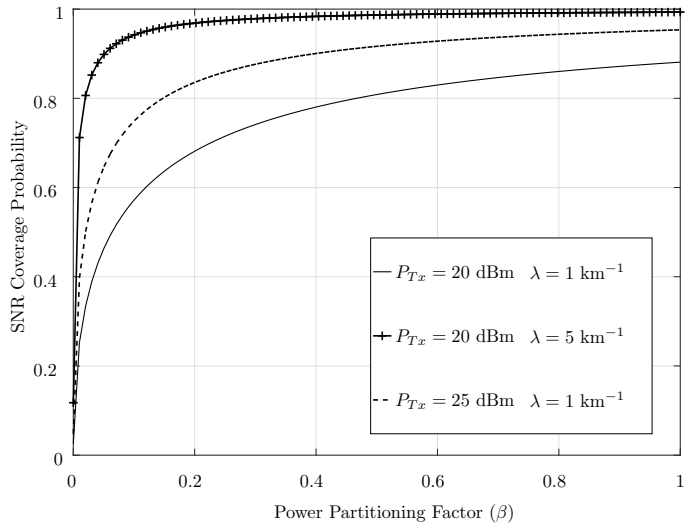

FIGURE 3.8: SNR coverage probabilities for a threshold of $\gamma = -10$ dB vs the fractional power split for different λ.

we describe our power partitioning scheme. In the following analysis, we assume $G_{Tx}G_{Rx} = 10$ dBi and $n_0 = 3$.

SNR coverage probability: In Fig. 3.8 we plot the SNR coverage probability $\mathcal{P}_C$ with respect to β at a threshold of $\gamma = -10$ dB. As β increases, the SNR coverage probability increases due to more power allocated to the data transmission phase. This provides a guideline to select a minimum operating β for a given deployment density, such that the outage is limited. As an example, to limit a service outage below 20%, with a BS deployment of 1 km^{-1} and a power budget of $P = 25$ dBm, the minimum β is 0.15, whereas with a power budget of $P = 20$ dBm, the minimum β is 0.5.

More interestingly, this analysis provides the operator with dimensioning rules in terms of the deployment density of the BSs for a given power budget. For example, in order to support services with an outage tolerance of 10%, with a power budget of 20 dBm, a deployment density of 1 km^{-1} does not suffice, and the operator must necessarily deploy more BSs.

Beam selection error: In Fig. 3.9 we plot the mean beam selection error with respect to the beamwidth of the transmit antenna of the BSs. As expected, the larger the beamwidth and the higher the SNR, the lower the selection error. For example, for a tolerable beam selection error of 0.02% with SNR = -15 dB and $\lambda = 5$ km^{-1}, the minimum antenna beamwidth should be 8 degrees.

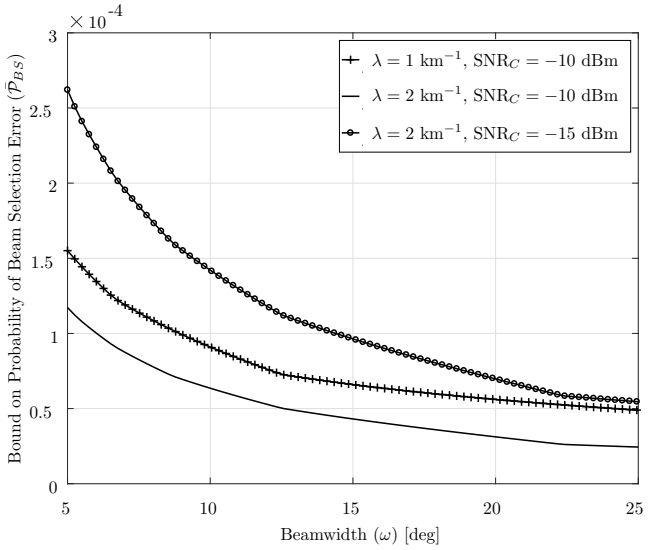

FIGURE 3.9: Beam selection error with respect to beamwidth of the transmit antenna.

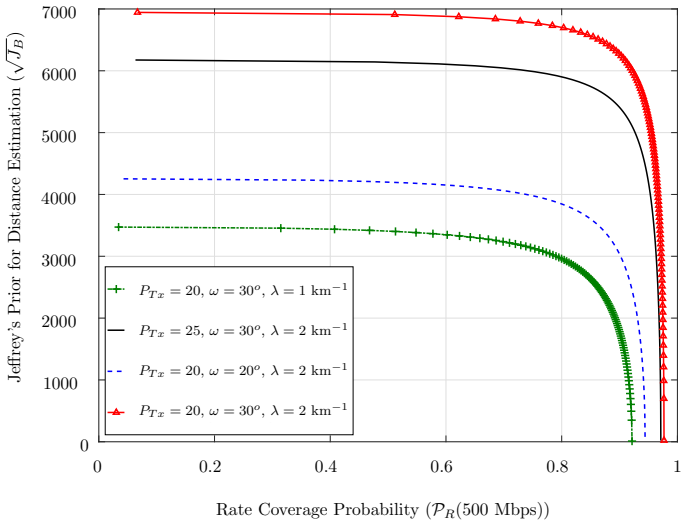

FIGURE 3.10: Distance estimation error vs rate coverage probability for different power budget.

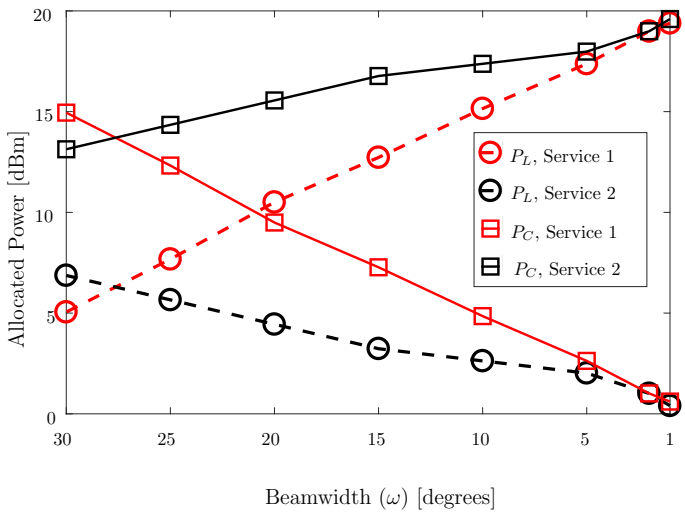

FIGURE 3.11: Power allocation for the two services for different operating beamwidths.

Distance estimation - data rate trade-off: In Fig. 3.10 we plot the trade-off between the efficiency of the distance estimation of the user, represented by its Jeffrey's prior[9], and the rate coverage probability at a rate threshold of 500 Mbps. Each position in the plot for a given deployment parameter corresponds to a particular β. Thus for a given power budget, deployment density, and operating beamwidth, the performance of the system is determined by a particular operating characteristic, i.e., a trade-off between the positioning efficiency and data rate performance. For a particular operating characteristic, as we increase β, we improve the rate coverage probability at the cost of degrading the localization efficiency; whereas, decreasing β has the opposite effect. Accordingly, there exists a non-trivial trade-off between distance estimation and the data rate performance of the system. Next, we propose a scheme for selecting an optimal β, given an operating beamwidth.

QoS aware network parameter setting: We propose the following scheme for setting the network parameters. First, for a given power budget, deployment density and operating beamwidth, the corresponding operating characteristic (i.e., a trade-off curve from Fig. 3.10) is selected. Next, for the chosen operating characteristic, the minimum β_{min} is chosen to satisfy the required outage constraint. Then, for a given positioning error constraint, the maximum value of β, i.e., β_{max} is selected. Finally, we select $\beta_{min} \leq \beta \leq \beta_{max}$ to address the specific QoS requirements.

In what follows, we explain the total power distribution based on the QoS requirements, for a varying degree of beam selection error. We assume a network with $\lambda = 2$ km^{-1} and a BS power budget of $P_{Tx} = 20$ dBm providing two services:

[9]The estimation error is calculated as the inverse of the Jeffrey's prior.

- Service 1 has a outage tolerance of 10%.
- Service 2 has a positioning error tolerance of 5 cm.

We study the power partitioning scheme under different operating beamwidths. Intuitively, for a less stringent beam selection requirement, the operating beamwidth can be smaller. This can be exploited either to improve positioning accuracy or enhance the data-rate, as per the required QoS.

For service 1, the operator should set β equal to β_{min} which fulfills the outage requirement from Fig. 3.10 corresponding to the corresponding beamwidth ω such that the beam selection error is satisfied from Fig. 3.9. Then, if the operating beamwidth ω can be decreased, while maintaining the rate coverage requirement, more power can be allotted for localization and consequently, less power for the data service phase.

On the other hand, for Service 2, the operator should set β equal to β_{max} satisfying the positioning error constraint and ω that satisfies the beam selection error requirement. Therefore, similarly to Service 1, a thinner beamwidth can facilitate a larger P_C as shown in Fig. 3.11.

The stark difference in the two examples lies in the fact that the advantage of operating with a thinner beamwidth is exploited differently. With decreasing ω, for positioning based Service 1, P_L increases and P_C decreases, whereas the opposite is true for the high data-rate services (see Fig. 3.11).

It is worth mentioning that the inter-dependence of β and ω for controlling the positioning performance and the beam selection error is not trivial. As an example, for a required beam selection error constraint or for a required positioning error constraint, there exist non-unique (ω, β) pairs. Furthermore, it may happen that for a given ω and P_{Tx}, no feasible β exists that satisfies the positioning and beam selection error constraints simultaneously, thereby necessitating a higher BS power budget.

3.5.3 Time sharing

After the frequency sharing framework with the aid of power splitting, we now look into the time sharing framework with the help of energy partition between the two phases, thus supporting the two services while still relying on the same system. With this consideration, similarly to the previous sections, we herein characterize a trade-off between the resource allocation for localization and communication. With larger resources devoted to localization, we achieve a lower beam selection error due to accurate position information, although the resulting limitation in communication

resources reduces the user data rate. Conversely, to obtain a better rate performance the system needs to increase the allocation for communication, consequently increasing the probability of beam selection error. We characterize localization performance bounds and downlink average rate performance of a mm-Wave network and accordingly introduce a possible multi-service optimization policy.

We consider the one-dimensional network model similarly to the previous section. In contrast to the previous sections, in this section we consider equi-spaced distribution of BSs, with inter-BS distance equal to a constant $d_a = 1/\lambda$ m. Accordingly, we consider the communication model considering interference. In the next chapter where we consider the problem of beamwidth optimization, we consider a probabilistic distribution of the inter-BS distance.

Transmission policy and model

In this subsection, we consider a joint localization and communication framework facilitated by a time frame split across the two phases as illustrated similarly to Fig. 3.2 or Fig. 3.3 but for a single user case. Of the total transmit time T, we allocate a fraction β for communication, i.e., $T_C = \beta T$, and the rest $(1 - \beta)$ to send the localization pilots, i.e., $T_L = (1 - \beta)T$. Since we consider a constant P_{Tx} and T, we use the terms energy and time allocation for both localization and communication phases interchangeably.

Without loss of generality we perform our analysis from the perspective of a typical user located at the origin, which associates with the BS that provides the highest downlink power in the sub-6GHz band. Accordingly, we refer to the associated BS as the serving BS. Unlike in the previous section, we assume that the user experiences interference from the BSs' other than the serving BS.

Similarly, unlike in the previous section, we also model blockage in this section by consider the possibility of the user being in both LOS and NLOS with respect to the serving BS by modelling the the blockage according to LOS ball model with radius d_S similar to [82, 98]. In the LOS ball model approximation, the user is assumed to be in LOS as long as it is inside the distance d_S from the BS, and in NLOS otherwise. We assume that the path loss coefficient α can be either α_L and α_N depending on whether the user is in LOS or NLOS.

The user is assumed to have access to the AoA and AoD information, but since we are considering one-dimensional model, we can represent the AoD in terms of d (and thus delay). Each BS, with height h_B, and user are equipped with mm-Wave ULA directional antennas both with N_t antenna elements with a BS antenna array

response given as follows:

$$\boldsymbol{a}_{Tx}(d) = \frac{1}{\sqrt{N_t}} \left[1, e^{j\frac{2\pi\kappa}{\lambda_c}\sin(\theta(d)}, \cdots, e^{j(M-1)\frac{2\pi\kappa}{\lambda_c}\sin(\theta(d)}\right], \tag{3.26}$$

where, κ is the inter-element distance in the antenna array and λ_c is the wavelength corresponding the center frequency f_c. For the receive antenna response $\boldsymbol{a}_{Rx}(\phi)$ at UE, simply replace $\theta(d)$ with ϕ and N_t with N_r in equation (3.26). Similarly, let $\boldsymbol{f} \in \mathbb{C}^{N_t \times 1}$ and $\boldsymbol{w} \in \mathbb{C}^{N_r \times 1}$ represent the transmit and receive beamforming vectors respectively.

In order to simplify the analysis of the data service phase, we approximate the beamforming by a sectorized beamforming model [99, 100], where the transmitted and received beams are divided into two sectors, a main lobe sector whose antenna gain depends on the beamwidth ω and a side lobe sector with a fixed gain. Here, the term main lobe stands for the angular region of the antenna pattern centered around the axis of maximum gain and aperture equal to the half-power beamwidth[10]. Accordingly, in the sectorized model, the antenna gain at the BS and the user side $G_x(\omega_x) = |\boldsymbol{a}_x^H(\theta(d))\boldsymbol{f}|^2$ or $|\boldsymbol{w}^H\boldsymbol{a}_x(\phi)|^2$, where $x \in \{Tx, Rx\}$, is given by [100] as:

$$G_x(\omega_x) = \begin{cases} \gamma_x(\omega_x) = G_0\frac{2\pi-(2\pi-\omega_x)\epsilon}{\omega_x}, & \text{in the main lobe,} \\ g = G_0\epsilon, & \text{otherwise,} \end{cases} \tag{3.27}$$

where G_0 is the antenna gain of an equivalent omni-directional beam (i.e., $\omega_x = 2\pi$) and ϵ is a small positive constant $\ll 1$.

Beam dictionary

We assume that each BS has a mm-Wave beamforming database. Specifically, each BS is capable of having beam dictionaries of different sizes, where each beam dictionary is composed by a set of beams characterized by the same width. Furthermore, we assume that the main lobes of different beams of the same dictionary are non-overlapping. Together, the beams of a dictionary provide complete coverage in the geographical coverage area (i.e., the Voronoi cell) of the BS as shown in Fig. 3.12. Consequently, the larger the number of beams in the dictionary, the smaller is the beamwidth. It must be noted that for a typical BS deployed along the road, the neighbouring BSs on either side may not be located at the same distances from it.

[10]Note that the width of the beam depends on the beamforming vectors $\boldsymbol{f}$ and $\boldsymbol{w}$. In our case of ULA, large number of antenna can guarantee a thin beam. Similarly, we can switch some antenna elements off in order to achieve other beamwidths. We can solve an optimization problem like in [91] to find the optimal beamforming corresponding to a particular beamwidth.

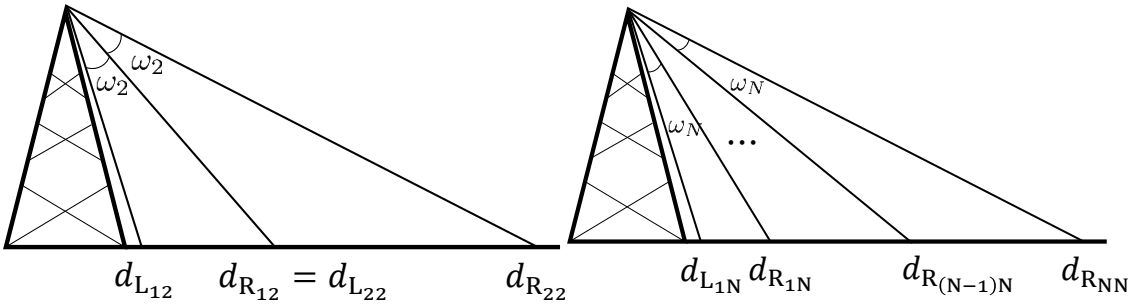

FIGURE 3.12: Illustration of the beam dictionary elements in case of (A) 2 beams and (B) N beams.

As a result, the beam dictionary maintained at the BSs would contain the cell size information for both the sides of them. Without loss of generality, in what follows, we focus on one side of the typical BS in this chapter as well as chapter 4.

Let $\omega_1 = \arctan\left(\frac{d_a}{2h_B}\right) - \arctan\left(\frac{d_{L_{11}}}{h_B}\right)$ be the beamwidth of the beam that provides total coverage of the area $d_a/2$, where $d_{L_{11}} = d_{L_{12}} = d_{L_{1N}}$ is the starting point of the coverage area (as illustrated in Fig. 3.12) and h_B is the height of the BS. Then, for the beam dictionary size k, the beamwidth is defined by $\omega_k = \omega_1/k$. Now, depending on this beamwidth ω_k and the total number of beams, the left and right boundaries of each main lobe coverage positions of the j-th beam ($1 \leq j \leq k$) are denoted as $d_{L_{jk}}$ and $d_{R_{jk}}$. The non-overlapping and adjacent assumption of the beams implies that $d_{R_{jk}} = d_{L_{(j+1)k}}$, $\forall j \leq k$.

Hence, we define the beam dictionary database $\mathcal{DB}$ of a mm-Wave BS as a lower triangular matrix consisting of all feasible beams for each beam dictionary. Each element $\mathcal{DB}_{k,j}$ of $\mathcal{DB}$, where $j \leq k$, consists of a tuple $(\omega_k, d_{L_{jk}}, d_{R_{jk}})$ corresponding to the j-th beam of the k-th beam dictionary. The elements of the tuple indicate respectively a) the width of the beam, b) the left boundary, and c) the right boundary of the main lobe of the beam (according to the *sectorized model*), as illustrated in (3.30). Then, for the k-th beam dictionary, the j-th beam has a coverage area $\mathcal{C}_{jk} = d_{R_{jk}} - d_{L_{jk}}$. The steps for designing the beam dictionary at a mm-Wave BS are:

1. After being deployed, the new BS exchanges inter-BS signals to discover its coarse geographical location on the street[11], with respect to its neighbouring mm-Wave BSs[12]. Using this information, a BS maps its own geographical coverage area with respect to its neighbors. As all the BSs are assumed to

[11]Such prior geo-referencing, anyway required for mapping geographical coverage, can also be performed in alternative ways such as the GPS.

[12]This information can be provided a-priori by the operator during the deployment phase.

have the same transmit power, the cell boundaries are midway between two neighboring BSs.

2. For each value of beam dictionary $k \in \{1, 2, \ldots, N\}$, the BS calculates the coverage areas of the associated beams as $\mathcal{C}_{j,k} = d_{R_{jk}} - d_{L_{jk}}$, where:

$$d_{R_{jk}} = h_B \tan\left(\arctan\left(\frac{d_{L_{jk}}}{h_B}\right) + j\omega_k\right), \quad j = 1, 2, \cdots, k, \tag{3.28}$$

$$d_{L_{jk}} = \begin{cases} d_{R_{(j-1)k}}, & j = 2, \cdots, k, \\ 0, & j = 1. \end{cases} \tag{3.29}$$

3. The resulting data-base is thus lower triangular matrix as follows:

$$\mathcal{DB} = \begin{bmatrix} (\omega_1, d_{L_{11}}, d_{R_{11}}) & 0 & 0 & \ldots & 0 \\ (\omega_2, d_{L_{12}}, d_{R_{12}}) & (\omega_2, d_{L_{22}}, d_{R_{22}}) & 0 & \ldots & 0 \\ \vdots & \vdots & \ddots & \ddots & \vdots \\ (\omega_N, d_{L_{1N}}, d_{R_{1N}}) & (\omega_N, d_{L_{2N}}, d_{R_{2N}}) & \ldots & \ldots & (\omega_N, d_{L_{NN}}, d_{R_{NN}}) \end{bmatrix}, \tag{3.30}$$

where the k-th row consists of the beam dictionary of size k beams and contains the information about the width and the main lobe coverage areas of the corresponding beams.

Localization phase

Contrarily to to the data communication phase, in the localization phase, we do not consider the effect of interference. This is primarily because we assume that the localization estimation occurs using signals transmitted in the control channel, which is assumed to be interference-free due to the usage of orthogonal resources for transmitting the pilots.

In this section, we characterize the CRLB in terms of distance like in section 3.5.2. FIM $\boldsymbol{J}$ from [52] and [62] for the estimation of the mentioned variables are given below. Considering that $T_L = (1 - \beta)T$ amount of time is allocated for localization,

$$J_{d,d} = \zeta G_{Rx}(\omega_{Rx}) G_{Tx}(\omega_{Tx}) \frac{B^2\pi^2}{3c^2}, \tag{3.31}$$

where, $\zeta = (2KP_{Tx}|h|^2(1-\beta)T)/(h_B^2 + d^2)\sigma_N^2$.

Hence, the CRLBs for the estimation of the distance can be written as follows:

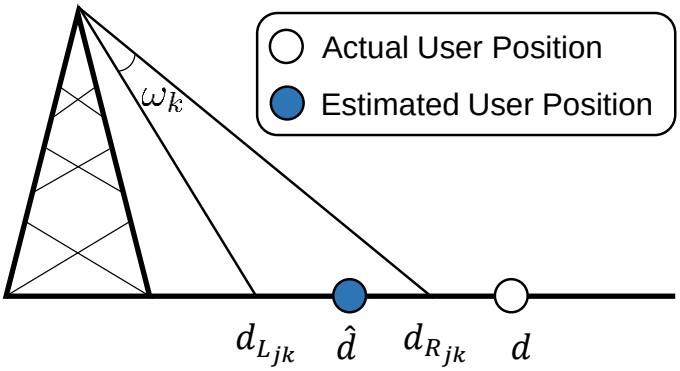

FIGURE 3.13: Illustration of beam selection error.

$$\sigma_d^2 = J_{d,d}^{-1} \tag{3.32}$$

Beam selection error

Without loss of generality, assume that the real position of the UE is $d_{L_{jk}} \leq d \leq d_{R_{jk}}$, and accordingly, for a given beam dictionary k, the j-th beam, whose coverage area is given by $\mathcal{C}_{j,k} = d_{R_{jk}} - d_{L_{jk}}$, should be assigned to it. However, due to ranging errors, the estimated distance of the user $\hat{d}$ is distributed as $\mathcal{N}(d, \sigma_d^2)$ similarly to [101], where σ_d^2 is defined in (3.32). Hence, a beam selection error occurs for the user when $\hat{d}$ is not inside the correct interval defined by $d_{L_{jk}}$ and $d_{R_{jk}}$ (see Fig. 3.13). Contrarily to the definition in the frequency sharing case in section 3.5.2, in this section, the beam selection error is defined with respect to the previously defined beam dictionary. Averaging out on the possible beams that can be selected depending on the relative distance of the typical user to BS, we have the following result.

The probability of beam selection error when the BS estimates the UE to be in the position $\hat{d}$ and selects a beam of width ω_k, is derived from appendix B.2 as:

$$\mathcal{P}_{BS,j,k}\left(d, \sigma_d^2\right) = \mathbb{P}\left(\hat{d} < d_{L_{jk}}\right) + \mathbb{P}\left(\hat{d} > d_{R_{jk}}\right) \tag{3.33a}$$

$$= 1 - \mathcal{Q}\left(\frac{d_{L_{jk}} - d}{\sigma_d}\right) + \mathcal{Q}\left(\frac{d_{R_{jk}} - d}{\sigma_d}\right), \tag{3.33b}$$

where, as defined earlier, $\mathcal{Q}(\cdot)$ is the Q-function.

In case of deterministic equi-spaced BS deployment, where the BSs are at a distance of $d_a = 1/\lambda$, the average beam selection error over all the possible UE

positions in case of N total beams is given by

$$\bar{\mathcal{P}}_{BS} = \sum_{j=1}^{k} \int_{d_{L_{jk}}}^{d_{R_{jk}}} \mathcal{P}_{BS,j,N}(x, \sigma_d^2) f_d(x) dx, \tag{3.34}$$

where,

$$k = \left\lceil \frac{1}{\omega_k} \arctan\left(\frac{\frac{1}{\lambda} - d_{L_{1N}}}{h_B} \right) \right\rceil. \tag{3.35}$$

Note that the wider the antenna beam, the larger is the value of $\mathcal{C}_{j,k}$. Thus, for a given distance estimation accuracy (i.e., σ_d), the beam selection error is smaller for a larger beamwidth since $\mathcal{P}_{BS,j,k}(x, \sigma_d^2)$ decreases with $\mathcal{C}_{j,k}$ in (3.33). On the other hand, with increasing ω_k, the value of σ_d increases because of the lower antenna gain. This increases the beam selection error.

Data service phase

In this section, first we characterize the SINR coverage probability of the typical UE considering the beam selection error into account. Based on that, we define the effective downlink data rate of the typical UE.

The SINR, according to the transmission policy, can be formulated as:

$$\text{SINR} = \frac{P_{Tx}|h|^2 K G_{Tx} G_{Rx} d^{-\alpha_L}}{\sigma_N^2 + P_{Tx} K g^2 \left(\sum_{i \in \xi_L \setminus 0} d_i^{-\alpha_L} |h_i|^2 + \sum_{i' \in \xi_N} d_{i'}^{-\alpha_N} |h_{i'}|^2 \right)} \tag{3.36}$$

where ξ_L and ξ_N represent the indices of the BSs in LOS and NLOS respectively, h_i and $h_{i'}$ represent the channel between the user and the i-th BS (LOS) and i'-th BS (NLOS) respectively.

The SINR coverage probability, as defined earlier, is probability that the typical user receives the transmitted signal with a SINR over a given threshold. Mathematically, it is characterized in appendix B.3 as follows:

$$\mathcal{P}_{C,j,k}(\gamma) = \int_{d_{L_{j,k}}}^{d_{R_{j,k}}} 2\lambda \left(\underbrace{\mathcal{P}_{BS_{j,k}}(x) \mathcal{T}_{BS}(x, \gamma)}_{\text{Beam Selection Error}} + \underbrace{\left(1 - \mathcal{P}_{BS_{j,k}}(x)\right) \mathcal{T}_0(x, \gamma)}_{\text{No Beam Selection Error}} \right) \exp\left(-2\lambda x\right) dx,$$

where, $P_{BS_{j,k}}$ is defined in equation (B.11), and

$$\mathcal{T}_0(x,\gamma) = \exp\left(-\frac{\gamma\sigma_N^2}{P_{Tx}Kg^2 z_0^{-\alpha_L}} - \mathcal{A}_{L0}(x,\gamma) - \mathcal{A}_{N0}(x,\gamma)\right), \tag{3.37a}$$

$$\mathcal{T}_{BS}(x,\gamma) = \exp\left(-\frac{\gamma\sigma_N^2}{P_{Tx}KGz_0^{-\alpha_L}} - \mathcal{A}_{LBS}(x,\gamma) - \mathcal{A}_{NBS}(x,\gamma)\right), \tag{3.37b}$$

in which $z_0 = \sqrt{x^2 + h_B^2}$ as defined in appendix B.3

$$\mathcal{A}_{L0}(x,\gamma) = \int_x^{d_S} \frac{\gamma g^2 (y^2+h_B^2)^{-\alpha_L/2}}{G^2 z_0^{-\alpha_L} + \gamma g^2 (y^2+h_B^2)^{-\alpha_L/2}} 2\lambda y dy, \tag{3.38a}$$

$$\mathcal{A}_{N0}(x,\gamma) = \int_{d_S}^{\infty} \frac{\gamma g^2 (y^2+h_B^2)^{-\alpha_N/2}}{G^2 z_0^{-\alpha_L} + \gamma g^2 (y^2+h_B^2)^{-\alpha_N/2}} 2\lambda (y-d_S) dy, \tag{3.38b}$$

$$\mathcal{A}_{LBS}(x,\gamma) = \int_x^{d_S} \frac{\gamma (y^2+h_B^2)^{-\alpha_L/2}}{z_0^{-\alpha_L} + \gamma (y^2+h_B^2)^{-\alpha_L/2}} 2\lambda y dy, \tag{3.38c}$$

$$\mathcal{A}_{NBS}(x,\gamma) = \int_{d_S}^{\infty} \frac{\gamma (y^2+h_B^2)^{-\alpha_N/2}}{z_0^{-\alpha_L} + \gamma (y^2+h_B^2)^{-\alpha_N/2}} 2\lambda (y-d_S) dy. \tag{3.38d}$$

Hence, the overall SINR coverage probability for a beamwidth ω_k is calculated as

$$\mathcal{P}_C(\gamma,k) = \sum_{j=1}^{k} \mathcal{P}_{C,j,k}(\gamma). \tag{3.39}$$

Considering that the data service phase consists of a fraction β of the total time of the positioning-communication scheme, we can obtain the effective rate coverage probability as below:

$$\mathcal{P}_R(r_0,\beta,k) = \mathbb{P}\left(\beta B \log_2(1+\text{SINR}) \geq r_0\right) \tag{3.40a}$$

$$= \mathbb{P}\left(SINR \geq 2^{\frac{r_0}{\beta B}} - 1\right) \tag{3.40b}$$

$$= \mathcal{P}_C\left(2^{\frac{r_0}{\beta B}} - 1, k\right) \tag{3.40c}$$

Numerical results

In this section, we present the simulation results to evaluate the beamwidth selection strategy for a mm-Wave small cell network with $\lambda = 10$ km^{-1} and 50 km^{-1} and $d_S = 100$ m operating at the center frequency f_c of 60 GHz with bandwidth B of 1 GHz. Moreover, assume $P_{Tx} = 1$ W, the transmit and receive main and side lobe antenna gains $G = 30$ dB and $g = -10$ dB and $\sigma_N^2 = -174$ dB/Hz. The LOS

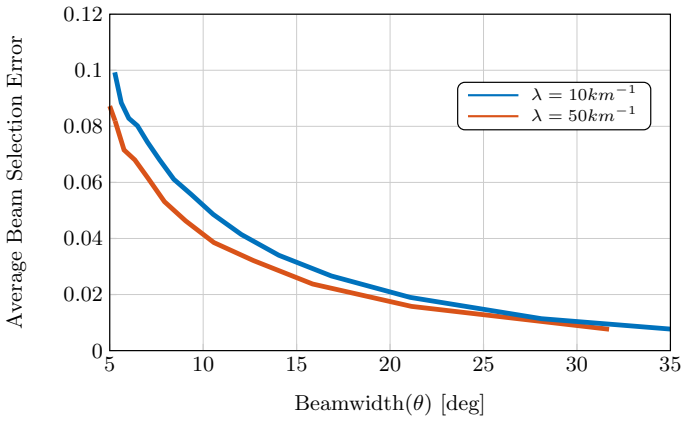

FIGURE 3.14: Average Beam Selection Error $\bar{\mathcal{P}}_{BS}$ varied with the beamwidth for different λs.

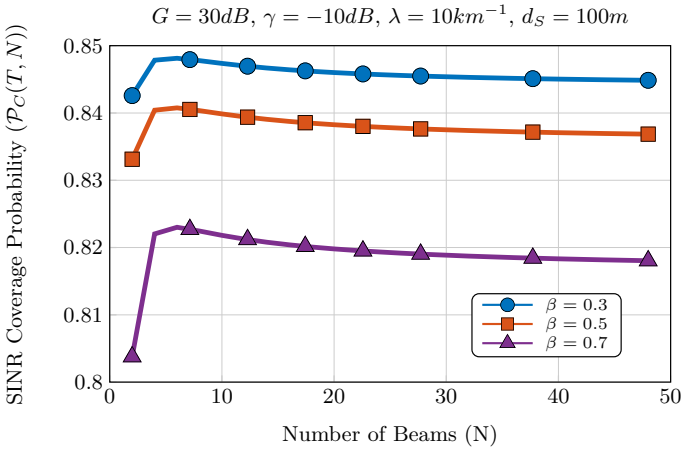

FIGURE 3.15: SINR Coverage Probability $\mathcal{P}_C(\gamma, N)$ varied with N for different βs.

and NLOS pathloss exponents are assumed to be $\alpha_L = 2$ and $\alpha_L = 4$ respectively. Similarly, the coefficient $K = 7.5 \times 10^{-7}$.

In Fig. 3.14 we present the average beam selection error for different numbers of beams. A wider beamwidth provides more coverage area for localizing the user, and hence, reduces the error due to the user being within the main lobe of the transmitted beam. Likewise, the figure also shows the effect of increasing the intensity of the PPP. With a lower number of BSs due to larger λ, the typical user has more probability of being far from the BS causing σ_d^2 to increase. Hence for smaller beamwidths, this inaccuracy in the knowledge of user position leads to a higher average beam selection error. However, for larger beamwidths, the larger coverage area compensates for this inaccuracy and hence both the plots with $\lambda = 10$ and 50km^{-1} converge towards each other.

Furthermore, in Fig. 3.15, we plot the SINR coverage probability as a function of the number of beams for different β. It can be noticed that increasing the time

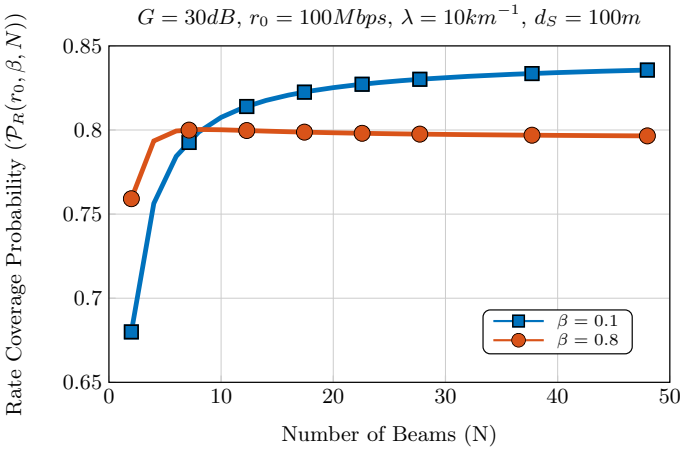

FIGURE 3.16: Rate Coverage Probability $\mathcal{P}_R(r_0, \beta, N)$ varied with N for different βs.

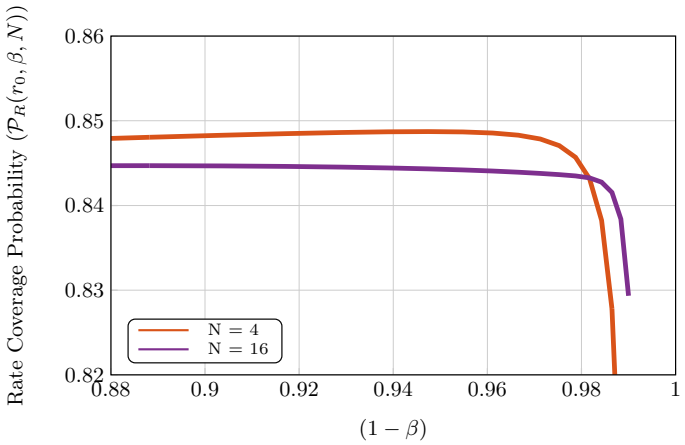

FIGURE 3.17: Rate Coverage Probability $\mathcal{P}_R(r_0, \beta, N)$ varied with $(1 - \beta)$ for different λs and N.

allocation for localization for a better localization performance increases the SINR coverage probability as it decreases the probability of having a beam selection error. For a certain β, when the number of beam increases and hence the beamwidths get thinner, there is a higher chance of beam selection error, in which case, the unwanted power received from interfering BSs decreases the SINR coverage probability.

Likewise, in Fig. 3.16 we can see the rate coverage probability with $r_0 = 100$ Mbps varying with different Ns for $\beta = 0.1$ and 0.8. For lower β, more precise localization improves the rate coverage probability even with thinner beamwidths. For larger β, the rate coverage probability first increases and then decreases with thinner beamwidth due to worse positioning.

Similarly, in Fig. 3.17, we can see the effect of favoring localization over communication with the same parameters as above. The rate coverage probability increases while increasing T_L except after 96% when T_C is so low that the rate coverage degrades very rapidly due to outage. Comparing the different numbers of

beams, using 16 beams instead of 4 is beneficial with respect to the rate coverage only after the user has been very accurately localized.

From the above figures, we can summarize that for a given λ, increasing N increases the beam selection error and even though it increases the SINR coverage probability initially. Too thin beams decreases this probability due to beam selection error and resulting interference from other BSs. Similarly, allocating a large portion of time for accurate user localization can help in achieving high rate coverage probability. Hence, from these analyses it is essential to optimally allocate the parameters ω and β for improving both localization and hence throughput performance at the user.

3.6 Chapter conclusions

In this chapter, we looked at different resource sharing schemes facilitating localization and communication functionalities in both standalone and joint frameworks.

We firstly evaluated the trade-off arising from the different resource sharing strategies over time and frequency, in particular, in a framework supporting both localization and communication as standalone services. In this multi-service system, budgeting more resources for the data service than for localization would indeed imply higher data rates but also, adversely, higher position and orientation estimation errors, which in turn, can be harmful to localization-based beam selection and alignment, and hence communication performances.

Beyond, we then studied a system supporting both localization and communication services jointly, where we not only investigated the effects of resource budgeting, unlike in the case of standalone services, but also assessed the impact of the localization performance on the communication phase arising from error in distance estimation and subsequently in the beam alignment.

We firstly studied the implications of frequency or power sharing between the two services where we derived dimensioning rules in terms of the density of BSs required to limit outage probability. We provided the operator with a beamwidth selection guideline to limit the beam alignment error probability and also studied the trade-off between the localization performance and the downlink data rate. Consequently, we presented a scheme for partitioning the transmit power depending on a-priori requirements. Finally, we studied the impact of time or equivalently energy sharing between the two phases. Through CRLB calculation, we characterized the best achievable variance of distance estimators. Then after the characterization of the uncertainty in distance estimation, we formulated the average beam selection

error and subsequently the SINR and rate coverage probabilities and showed that optimizing the beamwidth and the resources partitioning factor is important in order to facilitate the localization and communication functionalities simultaneously.

Regarding the limitations of our study, in section 3.4, we do not consider the inter-user interference in the communication phase while considering the rate optimization problem. Even if we do not expect that interference would have a significant effect on the trends of the trade-off, the consideration would make the analysis complete. Similarly, in section 3.4.2, we considered a noise-limited case where we assume that the UE has the capability to resolve the interference from the serving BS. We however considered the interference during rate analysis in section 3.5.3 and chapter 4. Similarly, in our model in section 3.5.3, we assumed that the inter-BS distance is equi-spaced for the trade-off study. In the next chapter, we will consider the BSs are distributed according to the PPP. Moreover, in section 3.5, while considering the alignment error due to erroneous localization, we only considered an error from the perspective of the BS considering that the beam of user is either omnidirectional or oriented towards the serving BS. We have included the beam alignment errors at both BS and user ends in chapter 4. Finally, in section 3.5.3, even though we consider the interference due to multiple BSs in the communication phase, we do not consider it in the localization phase. Even though we do not expect the analysis of the localization phase with interference will have a significant impact on the trends of the trade-off, we would like to address the scenario in the future. We have furthered this discussion in chapter 6.

Chapter 4

Beam optimization in a joint localization-communication system

4.1 Introduction

In the previous chapters, we have already seen that beamforming can significantly help both localization and communication functionalities in a system. Furthermore, in chapter 3, realizing that the two services are mutually beneficial to one another, we investigated different resource sharing schemes in order to accommodate the two services in the same system. In this context, in the standalone case, we have seen that the effects of resource budgeting were quite intuitive and thus anticipated. However, in the joint localization and communication case, the trade-off was much less trivial since the two services are deeply intricate.

Allocating too much resource to the localization is penalizing to the communication phase. However at the same time, as a result of accurate localization, we can transmit beams with thin width which allows for high rate performance. On the contrary, allocating a small amount of resource to the localization phase can mean that even though large amount of resources are available for the communication phase, the beam can be wrongly aligned due to erroneous user location estimation causing an outage. Hence, there is an equilibrium between the allocated resources and the consequent achievable data rate in the case of joint localization and communication framework which we will address in this chapter.

In addition, in this chapter, we also consider the problem of initial access - a process by which the mobile device or a UE establishes an initial link layer connection with the BS. In the previous generations of wireless systems, the initial access procedure consisted in the UE finding the most favourable BS and hence the cell with omnidirectional transmission to initiate the connection with [102]. However, due to directionality requirements in mm-Wave systems, it is essential to determine the direction of the UE from the BS and *vice versa*, to establish this connection

[66]. In the literature, the initial access schemes have been proposed with different cell search methods for mm-Wave including the exhaustive search where all the possible directions are evaluated and the iterative scheme that successively narrows the search area [103]. However, this new requirement to solve the problem of directionality in the initial access procedure induces a new problem in terms of latency, which in fact goes against the notion behind using mm-Wave technology for 5G. Motivated by this bottleneck, in this chapter, we also look into techniques for faster initial access aided by localization.

4.2 Related works

In the context of mm-Wave initial access, preliminary works are described in [63, 104] where the authors present the algorithms with exhaustive and random beam search based initial access schemes. To improve the latency of the above methods, the Desai *et al.* in [64] proposed an iterative algorithm where beams are initially with wide beamwidths and then gradually refined at each iteration to minimize the beam search space. In [105], the authors exploit the a-priori user's position information from external means such as GPS to minimize the beam search area and hence minimize the duration of initial access. Moreover, Ghatak *et al.* [106] have studied networks with co-existing mm-Wave and sub-6GHz RATs, in which the control signals sent in the sub-6GHz band are used to provide initial access to the mm-Wave nodes. However, they have not provided any algorithm for facilitating the initial access procedure.

With respect to localization and communication functionalities, we have already mentioned in chapter 3 that Destino *et al.* in [62, 89] have presented frameworks accommodating both localization and communication services in a single- and multi-user system respectively. In both papers, the authors describe the trade-off between data rate and PEB while partitioning time between the two. In the context of beamforming optimization (in terms of both alignment and width), in [65], the authors utilize a-priori user location information to initialize the iterative hierarchical beam alignment procedure. Likewise, in [61], the authors present a beam alignment optimization scheme between the transmitter and the receiver considering erroneous position estimations at both ends and scatterers. In this work, the authors describe a 2-step beam alignment algorithm, firstly at the transmitter independently and then at the receiver following the transmitter's decision. Recently in [107], the authors presented a beam alignment method where, under similar conditions as [61], the transmitter and receiver select the beams in a joint manner, thus outperforming

the 2-step method. Similarly, as described in section 3.2, the authors in [90, 91] present an iterative scheme for selecting the optimal beams at both transmitter and receiver based on localization estimation errors.

4.3 Methodology and organization

With respect to the related works from the literature reported in the previous section, in this section, we present the methodology of this chapter.

- Even though directionality is a key component in the mm-Wave initial access, to the best of our knowledge, there is no work directly exploiting localization during the cell search procedure. Moreover, the conventional cell search procedures in the mm-Wave context necessitates to search in a very large space and hence is inefficient in terms of latency. Motivated by these limitations, in this chapter we consider localization assisted initial beam selection procedure while aiming to reducing the search duration.

- As discussed in the previous chapter, even though there are some optimal resource allocation schemes in a standalone localization-communication case, to the best of our knowledge, there is a dearth of work concerning the joint localization-communication functionalities in terms of both resource allocation and beam optimization. Motivated by this and the interesting trade-off pointed out in chapter 3, in a joint localization and communication scenario, we look to jointly optimize the resource allocation and the transmit and receive beam. We intend to perform the beamforming optimization not only in terms of alignment but also the width which has not been addressed in the literature.

The rest of this chapter is organized as follows. In section 4.4, we present the system model for both initial access and the localization and communication phases. We present the channel and network models, and also define the beam alignment errors in this section. We then firstly consider the problem of localization aided initial access in section 4.5. Following, we then characterize the joint localization and communication performance in section 4.6. In section 4.7 we present the numerical results following our works on both initial access and joint localization and communication. We finally conclude the chapter in 4.8.

4.4 System model

4.4.1 Radio frame structure

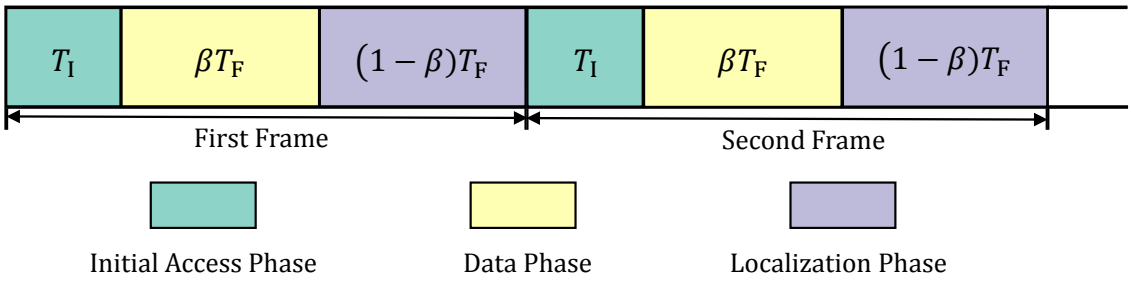

FIGURE 4.1: The proposed radio frame structure for localization assisted mm-Wave communications.

We consider a small cell network where multi-RAT BSs are deployed along the roads, similarly to the previous chapter, to provide a high speed data-access to the mobile users by jointly exploiting sub-6GHz and mm-Wave bands. In this context, we propose a new radio frame structure for joint communication and localization services, which is illustrated in Fig. 4.1. Each frame consists of an initial access phase of duration T_I in addition to the service phase of duration T_F similar to section 3.5.

The access phase provides reliable mm-Wave services to the new UEs in the system. Accordingly, in this phase, the initial beams at the BS and UE sides are refined in an iterative manner, until the localization information (ranging and AoA)[1] reaches a predefined resolution.

Then, the data and localization phases follow as depicted in Fig. 4.1. The service phase is further partitioned by a factor β into a data communication phase of length βT_F and a localization phase of length $(1-\beta)T_F$. Initially, the BS selects a transmit beam to maximize the effective data rate, which takes into account the localization errors as well, and satisfy the a-priori localization service requirements. In the following frames, the beam is further adapted to the newly obtained position[2] and orientation information in order to improve the system performance in terms of rate coverage. Thus, in the localization phase, the location information of the users are updated. For static users, this information is improved at each subsequent frame.

[1]For AoA estimation, we can choose one of the popular techniques such as Bartlett technique [108], Capon technique [109] or a subspace based techniques [110] (Multiple Signal Classification). For distance estimation, as a basic option, one can simply use RSSI based estimation in the mm-Wave band.

[2]Note that, as highlighted in the previous chapter, in the one dimensional scenario, for a known BS position, the position of the user and the distance from the base of the BS to the user are bijective functions.

For mobile users, the aim of this phase is to keep a track of the current location so as to facilitate beam-switching if needed. It is important to note that the beam pair that facilitates mm-Wave service in the initial access phase is different from the one in the service phase. The former is refined in an iterative manner in the initial access phase only depending on the initial localization performance to provide access to new UEs; whereas, the latter is obtained while trying to maximize the data rate performance.

In this work, like in chapter 3, we assume that the resources in the localization phase are perfectly multiplexed across active users, i.e., interference does not affect the localization performance.

Both downlink and uplink are included in our radio frame structure. Specifically, in the initial access and localization phases there is an exchange of downlink and uplink signals to enable precise estimation of the localization parameters. However, in this chapter, we analyse the performance of the data-phase exclusively during downlink communications.

4.4.2 Network geometry

Let us consider an urban scenario with multi-storied buildings resulting in a dense blocking environment similarly to section 3.5.1. The BSs deployed along the roads of the city are assumed to be of height h_B and having a transmit power of P_{Tx}. Their positions in each street are modeled as points of a one-dimensional PPP ξ, with intensity λ [m^{-1}].

The users are assumed to be static[3] and located uniformly on the roads with a density λ_U [m^{-1}]. Without loss of generality, we perform our analysis from the perspective of a BS located at the origin and an associated user located at a distance d from the BS as illustrated in Fig. 4.2. The user selects the serving BS following a RSSI based association. Unlike the deterministic deployment in section 3.5.3, in this chapter, for a BS located at the origin, the distance from the nearest neighbor (i.e, the closest BS) is given by:

$$f_{d_a}(x) = 2\lambda \exp(-2\lambda x). \tag{4.1}$$

[3]In this regard, it is important to highlight that mobility does not have a large impact on our protocol and performance evaluation methodology. As an example, let us assume vehicular users moving at a speed of 30 km per hour. With 1 ms of frame length, the distance covered by the user in-between frames is approximately 8 cm, which is considerably small with respect to the coverage area of any beam in the dictionary.

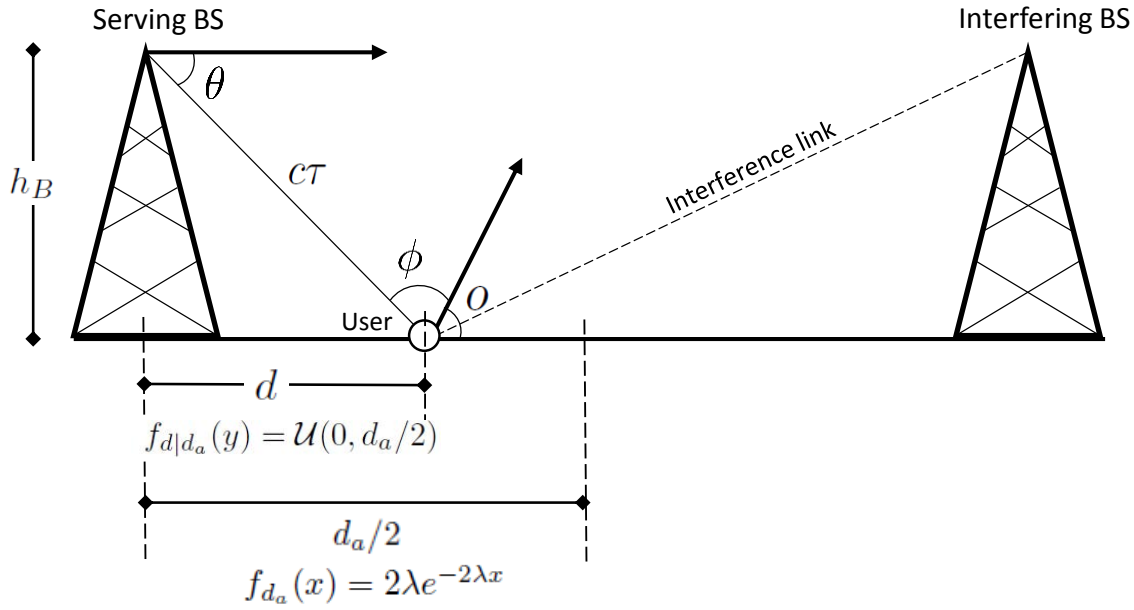

FIGURE 4.2: An example system model consisting of a serving BS, an interfering BS and a user node at distance d from the serving BS. The figure illustrates the relationship between the BS and user positions and the localization variables (distance d, AoD θ, AoA ϕ and the user orientation o).

Assuming that all the BSs have equal transmit power, the coverage area of the BS located at the origin is given by $d_a/2$ on either side of it, where d_a follows the distribution (4.1). Moreover, inside the coverage region of this BS, the location of a random user is uniformly distributed. Accordingly, the joint probability distribution of the distance d and the coverage area d_a is given by $f_{d_a,d}(x,y) = f_d(y|d_a = x)f_{d_a}(x)$ [83], where

$$f_d(y|d_a = x) = \begin{cases} x^{-1} & 0 \leq y \leq x, \\ 0 & \text{otherwise} \end{cases} . \tag{4.2}$$

Thus, each BS is associated with a Voronoi-cell service coverage area of length d_a, which is distributed as equation (4.1).

In the following, we denote the user orientation with respect to the reference x-axis as o, the AoA at the user as ϕ and the AoD at the BS as θ. As depicted in Fig. 4.2, the relations between the position of the BS and the user with the delay

τ, AoD, AoA and the user orientation are:

$$\tau = \sqrt{d^2 + h_B^2}/c, \tag{4.3a}$$

$$\omega = \cos^{-1}\left(d/\sqrt{d^2 + h_B^2}\right), \tag{4.3b}$$

$$\phi = \pi - \cos^{-1}\left(d/\sqrt{d^2 + h_B^2}\right) - o. \tag{4.3c}$$

It must be noted that in our 1D scenario, θ is dependent directly on d. We also assume that the orientation of the users are unknown, and accordingly, we consider that the distribution of the initial AoA of the user $f(\phi)$ is uniform between 0 and 2π.

4.4.3 Millimeter-wave beamforming

We assume that the BSs do not cater to multiple users or transmit multi-stream data, simultaneously. Accordingly, we assume the existence of a single RF chain with analog beamforming and, like in the other chapters in this thesis, ULA model with N_t and N_r antenna elements at the transmitter and receiver respectively. The responses of the transmit and receive array antennas are represented by $\boldsymbol{a}_{Tx}$ and $\boldsymbol{a}_{Rx}$ respectively as defined in equation (3.26). In order to simplify the analysis of the data service phase, we approximate the beamforming by a sectorized beamforming model similarly to section 3.5.3, where the transmitted and received beams are divided into two sectors, a main lobe sector whose antenna gain depends on the beamwidth ω and a side lobe sector with a fixed gain.

Let $\boldsymbol{f}(\omega_{Tx}) \in \mathbb{C}^{N_t}$ and $\boldsymbol{w}(\omega_{Rx}) \in \mathbb{C}^{N_r}$ represent the transmit and receive beamforming vectors. As defined in [111], the width of the beam can be controlled by changing the number of activated elements N_t and N_r in the antenna array. The method of changing the beamwidth is shown in [90, 91]. Accordingly, the sectorized beamforming model is the same as that already defined in equation (3.27). The beam dictionary in this chapter is exactly as defined in section 3.5.3.

4.4.4 Beam alignment errors

Following the description of the beam-dictionary, we define two critical metrics of the system, which we will use to characterize the performance of the localization phase.

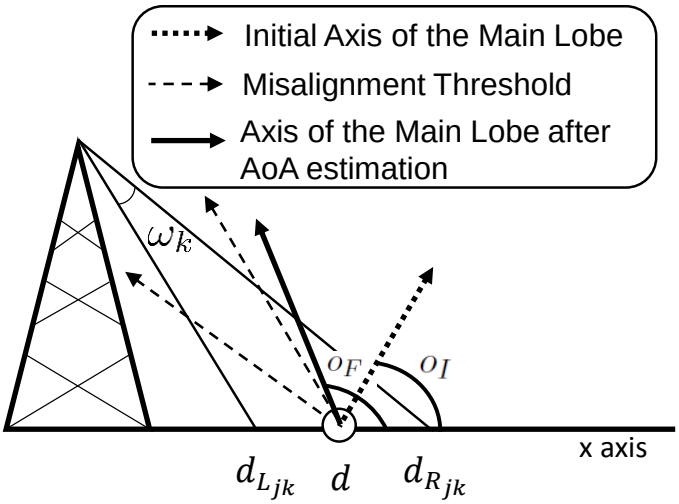

FIGURE 4.3

FIGURE 4.4: Illustration of the misalignment error.

Beam selection error

As already defined in section 3.5.3, the beam selection error is defined as the event that a UE located in $\mathcal{C}_{j,k}$ is estimated to be at $\hat{d}$, outside of $\mathcal{C}_{j,k}$, and accordingly, it is allotted a different beam than $(\omega_j, d_{L_{j,k}}, d_{R_{j,k}})$. Let us denote as σ_d^2 the variance of the distance estimation error; the probability of beam selection error ($\mathcal{P}_{BS}$), given that the UE is located at a distance d, is defined as

$$\mathcal{P}_{BS,j,k}\left(d, \sigma_d^2\right) = \mathbb{P}\left(\hat{d}(d, \sigma_d^2) \notin \mathcal{C}_{j,k} | d \in \mathcal{C}_{j,k}\right). \tag{4.4}$$

This event is depicted in Fig. 3.13.

Misalignment error

In comparison to the section 3.5, in this chapter, we further introduce the beam alignment error from the point of view of the UE referred to from hereon as the beam misalignment error. The beam misalignment error is defined as the event that, after the AoA estimation, the UE beamforms towards a direction such that the axes of the main lobe of the UE and BS antennas have an angular separation greater than a predefined threshold ν. Let us denote as o_I the initial user orientation and as $\hat{\phi}$ and σ_ϕ^2 the estimated AoA and the variance of the AoA estimation error, respectively. After the AoA estimation, the user reorients its main lobe towards the direction of $\hat{\phi}$ in order to align it towards the BS main lobe. The new orientation of the user main lobe is denoted by o_F in Fig. 4.3. The probability of misalignment

error, given that the UE is located a distance d (i.e., $\mathcal{P}_{MA}$) is then defined as

$$\mathcal{P}_{MA,j,k}(d,\phi,\sigma_\phi^2) = \mathbb{P}\left(|\phi - \hat{\phi}(d,\sigma_\phi^2)| \geq \nu(\omega_k,\omega_{Rx})\right). \tag{4.5}$$

This event is depicted in Fig. 4.3.

4.4.5 Blockage, pathloss, and signal propagation

Due to the presence of buildings and other obstacles, the communication links can either be in LOS or NLOS state. We assume a LOS ball model for characterizing the blockage, similar to that in section section 3.5.3 and [82], with a radius of d_S. Thus, all the BSs present within a distance d_S from the user are assumed to be in LOS, whereas, the BSs lying beyond d_S are assumed to be in NLOS. Accordingly, the LOS BS process is denoted by ξ_L and the NLOS BS process is denoted by ξ_N.

Furthermore, because of the low local scattering in mm-Wave communications, we consider a Nakagami fading h with parameter n_0 and variance equal to 1 [93] similarly to section 3.5.1. Additionally, we assume a pathloss model where the power at the receiver located at a distance d from the BS is given by $P_{Rx} = KP_{Tx}|h|^2 G_{Tx}(\omega_{Tx})G_{Rx}(\omega_{Rx})(d^2 + h_B^2)^{\frac{-\alpha}{2}}$, where K is the path loss coefficient, α is the path loss exponent. Here, similarly to chapter 3, we consider $G_{Tx}(\omega_{Tx}) = |\boldsymbol{a}_x^H(\theta(d))\boldsymbol{f}|^2$ and $G_{Rx}(\omega_{Rx}) = |\boldsymbol{w}^H\boldsymbol{a}_x(\phi)|^2$ are represented by the sectorized beamfoming model as mentioned earlier. In our model, $\alpha = \alpha_L$ or α_N depending on whether the link is in LOS or NLOS state, respectively.

Let us assume that the received signal suffers from a zero-mean additive Gaussian noise with two-sided noise power spectral density N_0 [dBm/Hz]. As a result the SINR in the data-communication phase is given by:

$$\text{SINR}_C = \frac{KP_{Tx}|h|^2 G_{Tx}(\omega_{Tx})G_{Rx}(\omega_{Rx})\left(h_B^2 + d^2\right)^{-\frac{\alpha}{2}}}{N_0 B + \sum_{i\in\mathcal{I}} KP_{Tx}|h_i|^2 g^2 \left(h_B^2 + d_i^2\right)^{-\frac{\alpha}{2}}}, \tag{4.6}$$

where $\mathcal{I}$ refers to the set of interfering BSs, h_i, and d_i represent the channel and distance respectively between the user and the i-th interfering BS. Here it is important to note that the BSs do not point their main lobe towards the coverage areas of other BSs. Consequently, for any given user, the interference power is sent from the side lobe of the interfering BSs, and never from the main lobe. Similarly, with our orientation estimation procedure, the users are assumed to beamform towards their serving BS. As a result, the gain from the interfering BSs is always g^2.

As stated previously, we do not consider the effect of interference in the localization phase. Hence, the SNR in the localization process is given as:

$$\mathrm{SNR}_L = \frac{K P_{Tx} |h|^2 G_{Tx}(\omega_{Tx}) G_{Rx}(\omega_{Rx})}{N_0 B} \left(h_B^2 + d^2\right)^{-\frac{\alpha}{2}}. \tag{4.7}$$

4.5 Initial access procedure

In this section, we discuss our initial beam-selection procedure for a user arriving in the mm-Wave network. In this procedure, the BS and the user select appropriate beam pairs with beamwidths ω_{Tx} and ω_{Rx} respectively, based on the localization accuracy required for the initial access.

1. When a new user arrives in the network, it associates with the BS that provides the highest downlink received power in the sub-6GHz band. The UE then makes a coarse initial estimation $\hat{d}$ of its distance from the serving BS which is characterized by an estimation-error variance σ_d^2. Without loss of generality, this initial localization can be obtained by means of technologies such as sub-6 GHz band (e.g., based on RSSI or ToA/TDoA measurements), external means such as GPS or wireless fidelity (Wi-Fi) or even with standalone mm-Wave band based distance estimation. The UE then relays this information to the BS.

2. Next, the BS and the UE switch to the mm-Wave band. The UE selects a mm-Wave beam of beamwidth ω_{Rx}, initially quasi-omnidirectional (with beamwidth $\pi/2$).

3. In $\mathcal{DB}$ (as defined in 3.5.3), for each beam dictionary k, there exists a beam j such that $d_{L_{jk}} \leq \hat{d} \leq d_{R_{jk}}$. Out of all such possible beam and beamwidth pairs j and k, the BS selects the pair with the largest beam dictionary size (i.e., the thinnest beam) that results in a beam selection error probability $\mathcal{P}_{BS,j,k}\left(d, \sigma_d^2\right)$ less than a threshold δ_{Tx}. Mathematically, $\omega_{Tx} = \omega_k$ such that

$$k = \max(i) : \mathcal{P}_{BS,j,i}\left(d, \sigma_d^2\right) \leq \delta_{Tx},\ i = 1, 2, \ldots, N, d_{L_{jk}} \leq \hat{d} \leq d_{R_{jk}}. \tag{4.8}$$

   The expression for beam selection error is derived in equation (4.11).

4. After this step, the BS sends downlink pilots in mm-Wave band, the UE updates $\hat{d}$ and σ_d^2 and transmits this information in the uplink. The BS then updates ω_{Tx} accordingly.

5. In parallel with the ranging estimation, the UE also measures the AoA of the BS signal $\hat{\phi}$, which is characterized by an estimation-error variance σ_{ϕ}^2. First, the user sets the angle of the maximum gain equal to $\hat{\phi}$; then, it fixes ω_{Rx} as the thinnest beam ω_i for which the misalignment error probability $\mathcal{P}_{MA,j,k}(d, \phi, \sigma_{\phi}^2)$ is less than a threshold δ_{Rx}, given that the BS selects the j-th beam of size ω_k. Mathematically,

$$\omega_{Rx} = \min(\omega_i) : \left[\mathcal{P}_{MA,j,k}(d, \phi, \sigma_{\phi}^2) \leq \delta_{Rx}\right], \text{and} 0 \leq \omega_i \leq \frac{\pi}{2}. \tag{4.9}$$

   The expression for misalignment error is derived in equation (4.12).

6. Let δ_{ϕ} and δ_d be the localization resolution requirements for reliable initial access; the refinement procedure terminates when either i) the BS beam and the UE beam simultaneously satisfy $\sigma_d^2 \leq \delta_d$ and $\sigma_{\phi}^2 \leq \delta_{\phi}$ or ii) a maximum number of iterations is reached.

7. When the termination conditions are not satisfied, the UE continues to measure the downlink pilots, and accordingly, the estimates of $\hat{d}$, σ_d^2, $\hat{\phi}$, and σ_{ϕ}^2 are updated. Following these new estimates, steps 3 and 5 are repeated for an improved initial beam selection.

We refer the reader to Fig. 4.5 for a description of the steps involved in the iterative loop for the initial access. It must be noted that the number of steps the initial beam-selection algorithm takes to terminate depends directly on the desired resolution of the localization. In other words, the more stringent the localization requirements of the initial access are, the more will be the number of steps of the initial beam-selection algorithm. Consequently, by tuning δ_d and δ_{ϕ}, the initial access delay can be controlled. There is thus an inherent trade-off between initial access delay and the accuracy of the UE localization, which we shall discuss in section 4.7.

The proposed initial-access scheme improves the latency for establishing mm-Wave connection in the system as compared to an exhaustive search solution (as we will see in the numerical results). However, in case the direct path between the user and the BS gets obstructed due to dynamic blockage, the localization performance would suffer and the system could experience beam selection errors. In the worst case, the user might have to re-initiate the initial-access procedure. With our algorithm, this situation can be prevented by adapting the beam size using the previously stored location estimate and the current estimation accuracy. Thus, integrating the estimation accuracy (e.g., the variance of the estimation error)

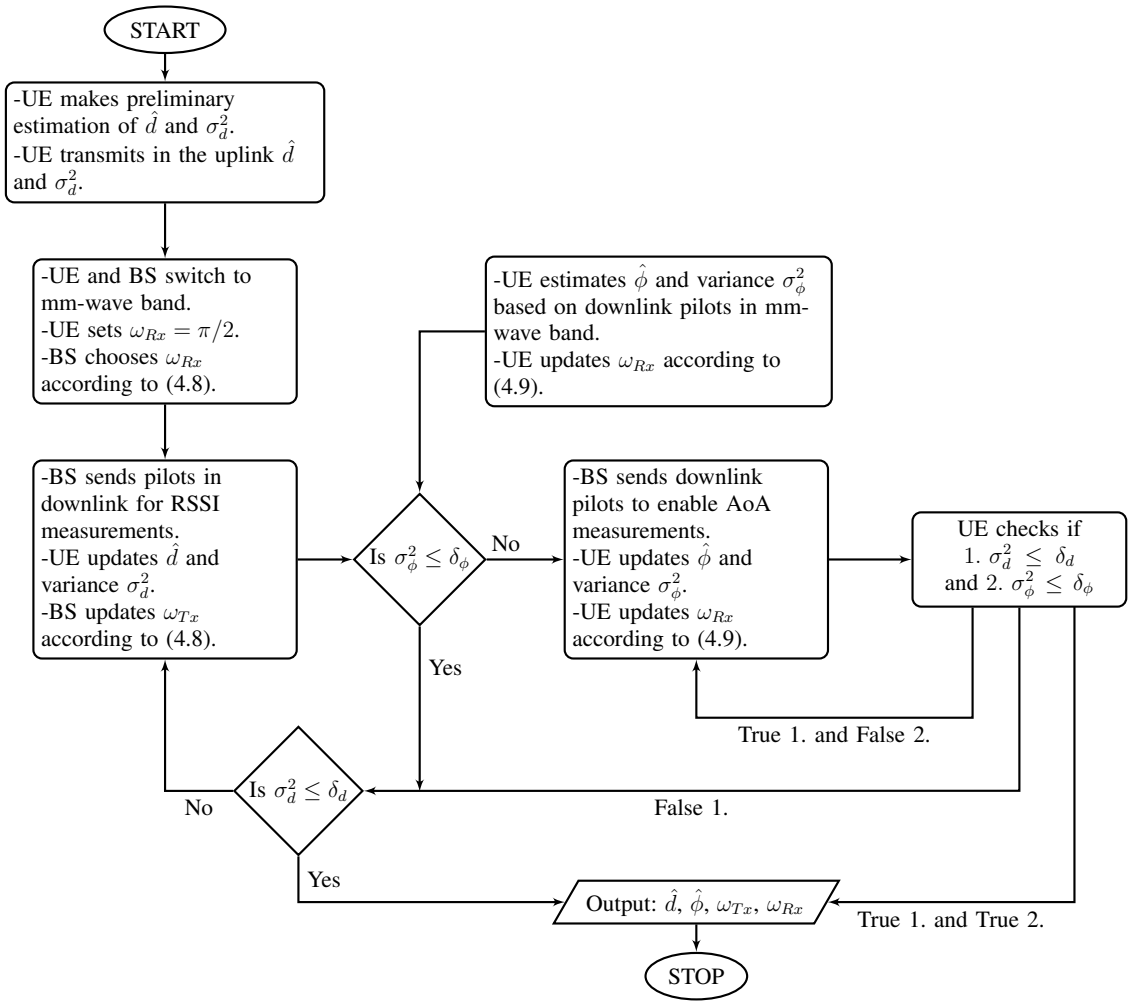

FIGURE 4.5: Flowchart representing the BS and user beam selection procedure as a part of the localization aided initial access procedure.

enables a fall-back solution that is not possible when using only location estimate. In case of using a simple exhaustive search, the entire set of beam combinations from the UE and the BS sides needs to be checked to re-establish the connection. Once the initial-access process is concluded, the system initiates the data and localization phases, which are defined and optimized in the subsequent sections.

4.6 Localization and communication performance

After the initial access phase, the system starts the service phase, which comprises two alternating phases: the communication/data service phase and the localization phase (see Fig. 4.1). In the localization phase, mm-Wave transmission is used to update the estimates of distance $\hat{d}$ and AoA of the signal received at the user $\hat{\phi}$, and potentially improve the localization accuracy. In the data service phase, the UE is served by the BS with a mm-Wave beam, which is selected from the dictionary according to the estimated user location. We propose a framework where the radio frames are divided into flexible sub-frames in order to address jointly the requirements of localization and data services. In this section, we mathematically characterize the performance metrics of localization (*v.i.z.*, position and orientation accuracy) and communication (in terms of downlink rate coverage), as a function of the resource partitioning factor (β) and the sizes of the beams (ω_{Tx}, ω_{Rx}), in order to optimize the radio frame design.

4.6.1 Localization phase

In this section, we model the accuracy of the localization in terms of the CRLBs of the estimated distance of the UE from the BS $\hat{d}$ and of the AoA $\hat{\phi}$ which will be further used for beam selection at the BS and beam alignment at the UE. Since we consider also the beam misalignment error at the UE, we need to consider the AoA estimation in addition to the distance estimation like in chapter 3. Then, using these tools, we characterize the beam selection error $\mathcal{P}_{BS}$ resulting from a distance estimation error and we model the misalignment $\mathcal{P}_{MA}$ between the user and the BS due to inaccuracy in the estimation of the AoA.

CRLB of the estimation parameters

Let the estimates be represented by the vector $\boldsymbol{\eta} = [d, \phi, h_R, h_I]$, where h_R and h_I respectively describe the real and imaginary parts of the channel between the UE

and the serving BS. In the previous chapter we did not consider the channel coefficients in the estimation variable, since then we only required distance estimation and, as mentioned before, considering a symmetric spectrum of the transmitted signal decouples the distance estimation from other channel parameters. However, since we are also considering AoA estimation in this case, we need to consider it for CRLB derivation.

The CRLBs for the estimation of the distance (by inverting the first element of $\boldsymbol{J}$) and the AoA (using Schur's decomposition [58]), as derived in appendix C.1, can written as follows:

$$\sigma_d^2 = \left(\zeta G_{Rx}(\omega_{Rx}) G_{Tx}(\omega_{Tx}) \frac{B^2\pi^2}{3c^2}\right)^{-1}, \tag{4.10a}$$

$$\sigma_\phi^2 = \left(\zeta G_{Tx}(\omega_{Tx}) \left(|\dot{\boldsymbol{a}}_{Rx}^H(\phi)\boldsymbol{w}(\omega_{Rx})|^2 - \frac{|\boldsymbol{a}_{Rx}^H(\phi)\boldsymbol{w}(\omega_{Rx})\boldsymbol{w}^H(\omega_{Rx})\dot{\boldsymbol{a}}_{Rx}(\phi)|^2}{G_{Rx}(\omega_{Rx})}\right)\right)^{-1}, \tag{4.10b}$$

where, $\zeta = 2\mathrm{SNR}_L B(1-\beta)T_F / G_{Tx}(\omega_{Tx})G_{Rx}(\omega_{Rx})$.

Note that the CRLBs of the estimation of the distance and the AoA are inversely proportional to ζ. Thus, the variance of the error in estimation decreases with increasing SNR_L and decreasing β. Accordingly, the higher the transmit power and/or the BS deployment density, the better the estimation performance. Similarly, larger bandwidth improves the distance estimation as it provides finer resolution for accurately analyzing the time of arrival of the received signal.

Beam selection error characterization

The beam selection error for the deterministic deployment scenario has been derived in the previous chapter in appendix B.2. Accordingly, the average beam selection error over all the possible UE positions in case of a total number of beams $N(y)$ (where y is the cell-size) with beamwidth ω_k[4] and probabilistic d_a is given by:

$$\bar{\mathcal{P}}_{BS} = \mathbb{E}_{d_a}\left[\sum_{j=1}^{N(d_a)} \bar{\mathcal{P}}_{BS,j,k}\right], \tag{4.11a}$$

$$= \int_0^\infty \left(\sum_{j=1}^{N(y)} \int_{d_{L_{jk}}}^{d_{R_{jk}}} \mathcal{P}_{BS,j,k}(x, \sigma_d^2) f_d(x) dx\right) f_{d_a}(y) dy, \tag{4.11b}$$

where $\bar{\mathcal{P}}_{BS,j,k}$ is defined in equation (B.12).

[4]Note that since in the service phase, we are only looking to optimize the beam from the perspective of the BS. Hence, we will denote the BS beam by ω_k in the following.

Misalignment error characterization

We assume that the UE estimates the AoA and then sets the axis of the main lobe of its antenna to $\hat{\phi}$. However, in case of erroneous estimate, there exists a possibility to wrongly align the beams (see Fig. 4.3). Let us assume that the user located at a distance d from the BS has an AoA ϕ with respect to the BS, and that is served by the j-th beam of size ω_k (i.e., $\omega_{Tx} = \omega_k$). Due to the noise affecting the received signal, the estimated AoA $\hat{\phi}$ is affected by random errors. Consequently, we assume that $\hat{\phi}$ is distributed as $\mathcal{N}\left(\phi, \sigma_\phi^2\right)$, where σ_ϕ^2 is defined in (4.10b). For our analysis, we define the BS-UE beam pair to be misaligned, if $|\phi - \hat{\phi}|$ is larger than a threshold $\nu(\omega_{Tx}, \omega_{Rx})$. In other words, in case the axes of the main lobe of the beams of the UE and the BS have an angular separation larger than the a-priori angular threshold $\nu(\omega_{Tx}, \omega_{Rx})$, we assume that the beams are misaligned.

The misalignment error probability for a UE at a distance d from the BS is given by

$$\mathcal{P}_{MA,j,k}(d, \phi, \sigma_\phi^2) = \mathbb{P}\left(\phi - \hat{\phi} \leq -\nu\right) + \mathbb{P}\left(\phi - \hat{\phi} \geq \nu\right), \tag{4.12a}$$

$$= 2\mathcal{Q}\left(\frac{\nu}{\sigma_\phi}\right). \tag{4.12b}$$

Then, the average misalignment probability is calculated by taking the expectation with respect to d and ϕ, i.e.,

$$\bar{\mathcal{P}}_{MA} = \mathbb{E}_{d,d_a,\phi}\left[\mathcal{P}_{MA}(d, \phi, \sigma_\phi^2)\right], \tag{4.13}$$

where the distribution of d is $f_d(y)$, and the distribution of ϕ is uniform between 0 and 2π as previously stated in the section 4.4.2. From equation (4.12), it can be observed that larger the threshold for misalignment, the lower is the misalignment probability. As the threshold is directly related to the transmit and receive beamwidths, in case of wider beamwidths, the probability of misalignment is lower.

4.6.2 Communication phase

In this section, first we characterize the performance of the typical UE considering beam-selection and misalignment errors. Then, we propose a methodology to jointly configure the split between the localization and data phases as well as the BS beam in order to optimize data and localization performance simultaneously. Accordingly,

in the following, we first model the effective SINR coverage probability and then we define the effective user data-rate.

Effective SINR coverage probability

Since the locations of the BSs are modeled as points of a 1D PPP, the locations of the users are assumed to be uniformly in the coverage area of the BSs, and the orientation of the users is assumed to be uniformly distributed between 0 and 2π, the SINR of a user is a random variable. Mathematically, the SINR coverage probability is characterized as follows. The SINR coverage probability of the typical user $\mathcal{P}_C\left(\gamma, j, \omega_k, \omega_{Rx}\right)$ served by the j-th beam of width ω_k is given by:

$$\mathcal{P}_C\left(\gamma, j, \omega_k, \omega_{Rx}\right) = \int_0^{2\pi} \int_{d_{L_{j,k}}}^{d_{R_{j,k}}} \left[\mathcal{P}_{BS,j,k}(x, \sigma_d^2)\mathcal{T}_{BS}(x, \gamma) + \left(1 - \mathcal{P}_{BS,j,k}(x, \sigma_d^2)\right)\right.$$
$$\left.\left(\left(1 - \mathcal{P}_{MA,j,k}(x, \phi, \sigma_\phi^2)\right)\mathcal{T}_0(x, \gamma) + \mathcal{P}_{MA,j,k}(x, \phi, \sigma_\phi^2)\mathcal{T}_{MA}(x, \gamma)\right)\right] f_d(x) f(\phi) dx d\phi, \tag{4.14}$$

where T_0 and $\mathcal{T}_{BS}$ are defined in equation (3.37) and

$$\mathcal{T}_{MA}(x, \gamma) = \exp\left(-\left(\frac{\gamma\sigma_N^2}{P_{Tx}K\gamma_{Tx}(\omega_k)g z_0^{-\alpha_L}} + \mathcal{A}_{LMA}\left(x, \gamma\right) + \mathcal{A}_{NMA}\left(x, \gamma\right)\right)\right), \tag{4.15}$$

in which $z_0 = \sqrt{x^2 + h_B^2}$, σ_d^2 is a function of x, σ_ϕ^2 is a function of x and ϕ, and

$$\mathcal{A}_{LMA}(x, \gamma) = \int_x^{d_S} \frac{\gamma g (y^2 + h_B^2)^{-\alpha_L/2} 2\lambda y}{\gamma_{Tx}(\omega_k) z_0^{-\alpha_L} + \gamma g (y^2 + h_B^2)^{-\alpha_L/2}} dy, \tag{4.16a}$$

$$\mathcal{A}_{NMA}(x, \gamma) = \int_{d_S}^{\infty} \frac{\gamma g (y^2 + h_B^2)^{-\alpha_N/2} 2\lambda (y - d_S)}{\gamma_{Tx}(\omega_k) z^{-\alpha_L} + \gamma g (y^2 + h_B^2)^{-\alpha_N/2}} dy. \tag{4.16b}$$

This derivation can be done similarly to the one in appendix B.3 with the inclusion of misalignment error. In (4.14) and appendix B.3, the term $\mathcal{T}_0(x, \gamma)$ corresponds to the case in which there is no beam selection error as well as no misalignment. In this case, we have $G_{Tx}(\omega_k) = \gamma_{Tx}(\omega_k)$ and $G_{Rx}(\omega_{Rx}) = \gamma_{Rx}(\omega_{Rx})$ resulting in a high coverage probability. The term $\mathcal{T}_{MA}(x, \gamma)$ represents the case where there is no beam selection error, but the BS-user beam pair suffers from misalignment. Here the coverage probability decreases as compared to $\mathcal{T}_0(x, \gamma)$ although $G_{Tx}(\omega_{Tx})$ remains the same, since here we have $G_{Rx}(\omega_{Rx}) = g$. Finally, the term $\mathcal{T}_{BS}(x, \gamma)$ refers to the case when there is a beam selection error. It must be noted that according to our assumption, in the case of beam selection error, we assume that the

beams are always misaligned. Here we have $G_{Tx}(\omega_k) = G_{Rx}(\omega_{Rx}) = g$.

In case of exhaustive-search, the users will not suffer from beam-selection or misalignment errors, i.e., for exhaustive-search, in (4.14) we have $\mathcal{P}_{BS,j,k}(x, \sigma_d^2) = 0$ and $\mathcal{P}_{MA,j,k}(x, \phi, \sigma_\phi^2) = 0$. Accordingly, the users will experience a better SINR, as discussed in the following: For a given value of ω_k and ω_{Rx}, an exhaustive-search based initial access algorithm will suffer from no beam selection error and no misalignment error. Consequently, the SINR coverage probability for an exhaustive search algorithm is given by:

$$\mathcal{P}_C\left(\gamma, j, \omega_k, \omega_{Rx}\right) = \int_0^{2\pi} \int_{d_{L_{j,k}}}^{d_{R_{j,k}}} \mathcal{T}_0(x, \gamma) f_d(x) f(\phi) dx d\phi. \tag{4.17}$$

In both the cases, the overall SINR coverage probability, considering all the N beams of size ω_k is:

$$\bar{\mathcal{P}}_C(\gamma, \omega_k, \omega_{Rx}) = \mathbb{E}_{d_a}\left[\sum_{j=1}^{N(d_a)} \mathcal{P}_C\left(\gamma, j, \omega_k, \omega_{Rx}\right)\right], \tag{4.18}$$

where the expectation is taken with respect to the inter-BS distance d_a given by equation (4.1).

Effective rate coverage probability

As the data phase uses β fraction of the total resources in the service phase T_F, we can compute the probability $\mathcal{P}_R(r_0, \beta, \omega_k, \omega_{Rx})$ that the effective rate is above given target rate threshold r_0 as below. For a given SINR coverage probability, the effective rate coverage probability is given by

$$\bar{\mathcal{P}}_R(r_0, \beta, \omega_k, \omega_{Rx}) = \mathbb{P}\left(\frac{\beta T_F}{T_I + T_F} B \log_2\left(1 + \mathrm{SINR}_C\right) \geq r_0\right), \tag{4.19a}$$

$$= \mathbb{P}\left(\mathrm{SINR}_C \geq 2^{\frac{r_0(T_I+T_F)}{\beta B T_F}} - 1\right), \tag{4.19b}$$

$$= \bar{\mathcal{P}}_C\left(2^{\frac{r_0(T_I+T_F)}{\beta B T_F}} - 1, \omega_k, \omega_{Rx}\right). \tag{4.19c}$$

4.6.3 Joint optimization of the beamwidth and radio frame structure

Given the characterization of the effective rate coverage probability, we present a framework for selecting, at the BS, the optimal beam with width ω_{Tx}^* from the

designed beam dictionary. First, we define the product of the beam selection and misalignment errors to jointly capture the effect of the localization errors, giving equally importance to both errors[5], and illustrate the trade-off between data service and localization, as

$$\mathcal{F}_C(\omega_k, \omega_{Rx}, \beta) = \bar{\mathcal{P}}_{BS} \cdot \bar{\mathcal{P}}_{MA}. \tag{4.20}$$

The proposed schematic is presented in the form of a two-stage optimization problem, as follows:

$$\omega_{Tx}^* = \underset{\omega_k}{argmax} \begin{bmatrix} \max\limits_{\beta} & \bar{\mathcal{P}}_R(r_0, \beta, \omega_k, \omega_{Rx}) \\ \text{subject to} & \mathcal{F}_C(\omega_k, \omega_{Rx}, \beta) \leq \mu \end{bmatrix}. \tag{4.21}$$

To solve this problem, in the first step, for a given ω_k, we select the value of β_k^* that maximizes the effective rate coverage probability subject to an a priori constraint (μ) on the joint error $\mathcal{F}_C$. This constraint can be a system parameter which defines the requirement of the localization service. In the subsequent frames, based on the new measurements, the estimates ($\hat{d}$ and $\hat{\phi}$) are updated and the measurement error variances (σ_d^2 and σ_ϕ^2) change. Accordingly, the BS beamwidth ω_{Tx}^* can be further updated by using equation (4.21). We emphasize that the optimal beamwidth thus calculated is different from the adaptive beamwidth value evaluated in the initial access phase. The former is calculated offline to maximize the data-rate given a set of system parameters, whereas, the latter is the beamwidth adapted for initial access to achieve the required resolution just in terms of distance and orientation.

4.7 Numerical results

Now we present numerical results related to the initial beam-selection and the localization-communication trade-offs developed in this chapter. The numerical results follow the analytical expressions derived in this chapter, where the beam-selection and misalignment errors are characterized by equations (4.11) and (4.12) respectively. The errors are incorporated into the SINR coverage probability expressions as derived in equation (4.14). Leveraging this, the rate coverage probability follows in equation (4.19).

[5]Other possibilities could have been chosen as i.) setting a threshold simultaneously on each error probability or ii.) using $\max(\bar{\mathcal{P}}_{BS}, \bar{\mathcal{P}}_{MA})$ for a robust optimization.

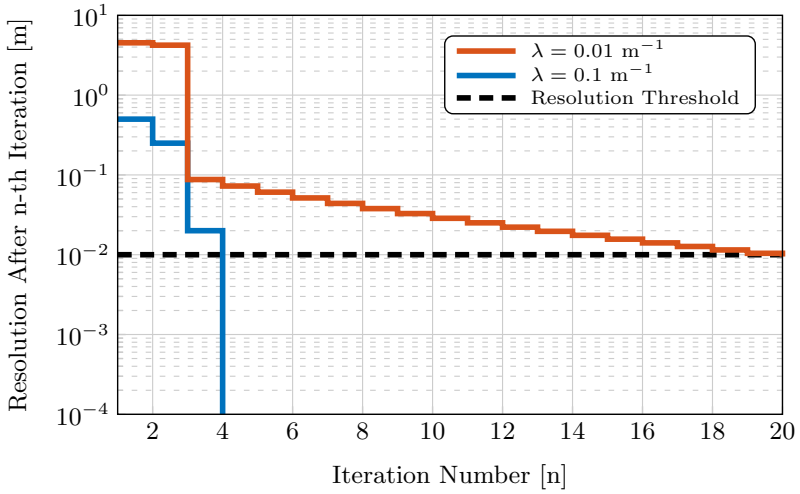

FIGURE 4.6: Resolution in the n-th step of the localization-based initial access strategy for different deployment densities.

4.7.1 Initial access phase

First, let us discuss the performance of the initial beam-selection strategy developed in section 4.5. In Fig. 4.6, we plot the enhancement in positioning resolution (characterized as the variance of the ranging error) with increasing the number of steps of our initial beam-selection algorithm. Here, we have assumed that $\delta_d = 0.01$m is the minimum resolution required to provide mm-Wave date-service. As expected, we note that for denser small cell deployments (e.g., $\lambda = 0.1$ m^{-1}) the algorithm stops at a lower number (here 4) of iterations, as compared to the sparser deployment scenarios. As the deployment becomes sparser (e.g., $\lambda = 0.01$ m^{-1}), a larger number of steps is required for the initial access procedure. This is precisely due to the fact that for denser deployments, SNR_L increases. Accordingly, a larger beamwidth is sufficient and hence, a lower number of iterations are required to meet the localization requirements.

Then, in Fig. 4.7 we compare the initial access delay of the proposed localization-bound based strategy with the one achieved by two well-known beam-sweeping solutions: exhaustive search and iterative search [56, 60, 112]. For the exhaustive search, we consider the beamwidth of the BS and the UE to be fixed and equal to ω_{Tx} and ω_{Rx}, respectively. Thus, the BS and the UE go through all the possible $\frac{2\pi}{\omega_{Tx}} \times \frac{2\pi}{\omega_{Rx}}$ beam combinations to select the beam pair that maximizes the SNR. The exhaustive search has been adopted in the standards IEEE 802.15.3c and IEEE 802.11ad [60]. On the other hand, for the case of iterative search (similar to bisection search in [113]), we assume that the BS initiates the procedure with $k = 2$ while the user uses an omnidirectional beam. In this iterative method, out of the two possible beams, the BS identifies the beam that results in the highest downlink SNR and

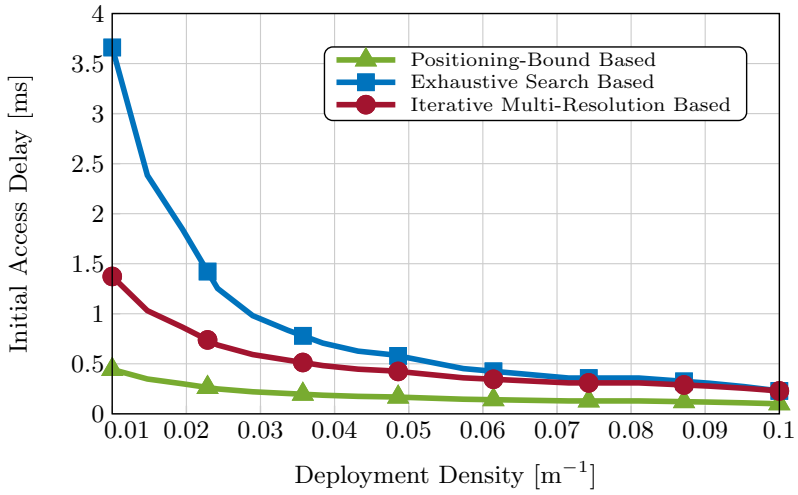

FIGURE 4.7: Comparison of the delay in initial access of our localization-based strategy to the iterative and exhaustive search strategies.

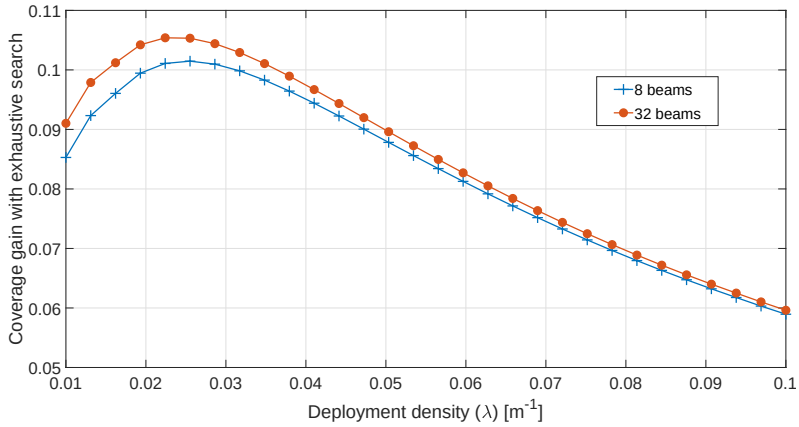

FIGURE 4.8: Gain in SINR coverage with an exhaustive search based initial-access algorithm for two beam dictionary sizes.

changes its search space to the region covered by that beam. Then, the BS halves its beam size and iteratively searches the new space. We assume that the initial beam-selection phase terminates when this process chooses the same beamwidth ω_{Tx} selected by our localization based algorithm. Thereafter, the BS fixes the selected beam and the UE carries out the same procedure for obtaining the user side beam.

In our system, similar to [112], we assume that i) one OFDM symbol length (including cyclic prefix) is 14.3 μs, ii) each synchronization signal occupies only one OFDM symbol, and iii) the beam reference signal is also transmitted in the same symbol to uniquely identify the beam index. Clearly, our strategy provides considerably faster initial access precisely due to the smaller number of steps than those required by the exhaustive and iterative search based schemes.

The number of iterations our algorithm takes to terminate is a direct measure of the delay in the initial beam-selection procedure. Specifically, we assume that

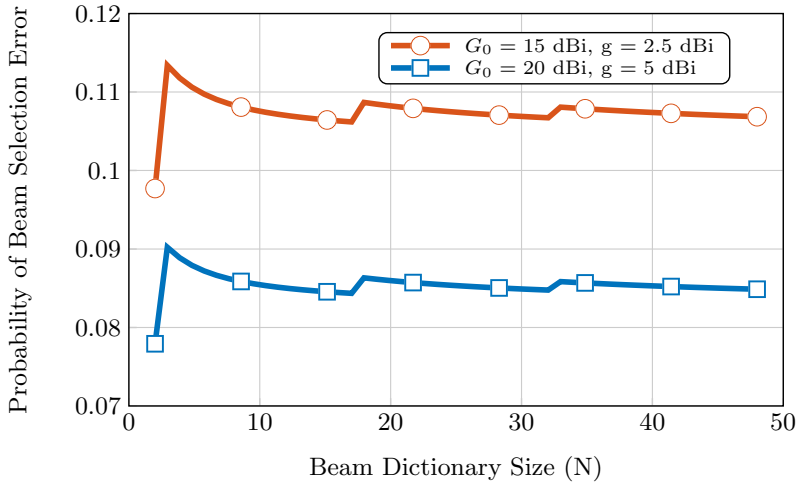

FIGURE 4.9: Probability of beam selection error vs the beam dictionary size for different antenna gains.

this delay is computed as the product of the sum of the required number of steps at the BS side and the UE side and the duration of one OFDM symbol. In Fig. 4.6, with $\lambda = 0.01$ m^{-1}, we observe that for a required $\delta_d = 0.01$ m, our algorithm terminates in 20 steps, which corresponds to a delay of about 5.7 ms. Whereas, if the positioning requirement was specified to be 0.1 m, the algorithm would have terminated in 3 steps, which corresponds to a initial beam-selection delay of about 1 ms. Thus, there exists a fundamental trade-off between the localization requirement (δ_d and δ_ϕ) and the delay in the initial beam-selection.

For a fair comparison, we emphasize that conventional algorithms such as the exhaustive search do not suffer from beam-selection and misalignment errors. This is shown in Fig. 4.8, where we plot the gain in SINR coverage with an exhaustive search based initial-access algorithm as compared to our proposed algorithm for two beam dictionary sizes. We observe that with a large number of beams, the SINR gain increases. This is precisely because a large beam dictionary size leads to smaller beam coverage, which in turn increases the beam selection error. More interestingly, we see that for dense deployment of BSs, the gain drops dramatically as the beam-selection and misalignment errors with the proposed initial-access scheme are limited.

4.7.2 Localization phase

The reduction in the initial beam-selection delay with the proposed algorithm is naturally associated with localization errors, which we discuss in this section.

In Fig. 4.9 we plot the beam selection error as a function of the beam-dictionary size (N) for different antenna gains. It must be noted that the effect of a larger

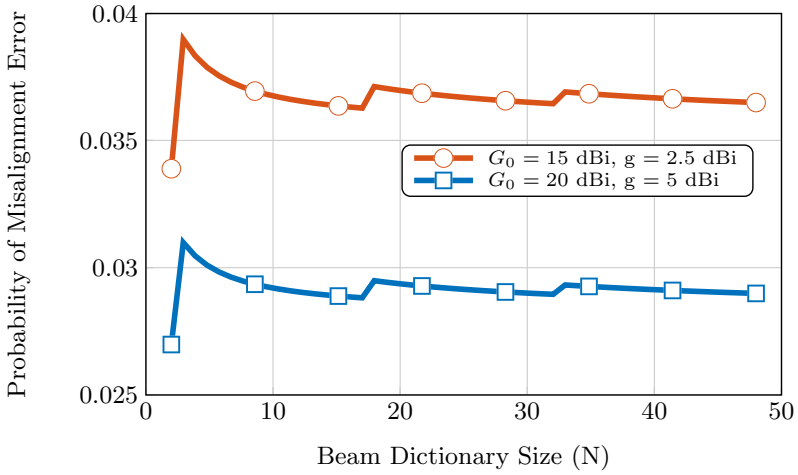

FIGURE 4.10: Probability of misalignment error vs the beam dictionary size for different antenna gains.

beamwidth on the beam selection error is non-trivial. Larger beamwidth results in a lower radiated power, which leads to a higher CRLB for distance estimation, which may lead to a higher beam selection error. However, a larger beamwidth also corresponds to a larger geographical area covered on ground by the beam (i.e., larger $\mathcal{C}_{k,j}$), which leads to a lower beam selection error.

As expected, the beam selection error is minimized for $N = 1$, when a single beam encompasses all the cell coverage area of the BS. The beam selection error would occur only when using a distance-based cell selection scheme, if the actual position of the UE is outside the coverage area of the serving BS. For $N \geq 2$, interestingly, we observe a stepped behavior of the probability of beam selection error with respect to the beam dictionary size. The beam selection error gradually decreases with increasing beam dictionary size due to the increasing antenna gain (see equation (3.27)). This behaviour continues until a certain value of beam dictionary size, where the beam width becomes so thin that the probability that the user lies outside the beam coverage area is high. This results in an increase in the probability of beam selection error, which then gradually decreases, when increasing the beam dictionary size, and so on. This brings forth an important characteristic of the system: for achieving a given beam selection error performance, multiple beam sizes can exist. This is precisely because of the fact that with the decreasing size of the beams, two conflicting phenomena occur: i) an improvement in the estimation performance owing to larger antenna gain and ii) a reduction of the geographical area covered by each beam.

Fig. 4.10 shows that the beam misalignment probability has the same peaky

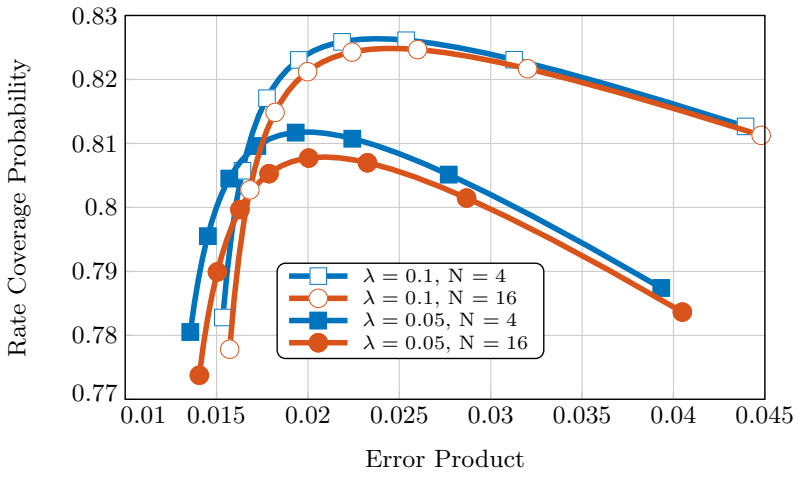

FIGURE 4.11: Rate coverage probability at 100 Mbps vs the joint error product bound.

trend of the beam selection error with respect to the beam dictionary size. Specifically, the misalignment probability gradually decreases with increasing N until a certain value after which the beam becomes so thin that the misalignment error increases.

4.7.3 Localization communication trade-off

In Fig. 4.11 we plot the rate coverage probability of the typical user with respect to the product of the beam selection and misalignment errors $\mathcal{F}_C(\omega_k, \omega_{Rx}, \beta)$ for different beam dictionary sizes. We vary the probability of beam selection error and the probability of misalignment by tuning the value of β. We observe that for all beam dictionary sizes, as the value of $\mathcal{F}_C(\omega_k, \omega_{Rx}, \beta)$ increases (i.e., as the localization estimation performance degrades), the rate coverage probability is initially improved. Thereafter, it reaches an optimal value for a certain $\mathcal{F}_C(\omega_k, \omega_{Rx}, \beta)$ and decreases on further increasing the value of $\mathcal{F}_C(\omega_k, \omega_{Rx}, \beta)$. This highlights the non-trivial trade-off between the localization and the data-rate performance in our system. This is all the more complex as the optimal value of β (and hence the rate coverage probability) depends on both the BS deployment density and the dictionary size. To achieve very low values of $\mathcal{F}_C(\omega_k, \omega_{Rx}, \beta)$, sufficient resources need to be allotted for the localization phase thus leading to efficient beam-selection and beam-alignment. A small increase in the value of $\mathcal{F}_C(\omega_k, \omega_{Rx}, \beta)$ does not result in a large degradation of the localization performance but, in contrast, enhances the data-rate as more resources are assigned to the data-communication phase.

However, further increasing the value of $\mathcal{F}_C(\omega_k, \omega_{Rx}, \beta)$ after a certain β (i.e., β^*) deteriorates the rate coverage. This is because poor localization leads to a high beam selection and beam-misalignment errors. As a result, the antenna gains at the

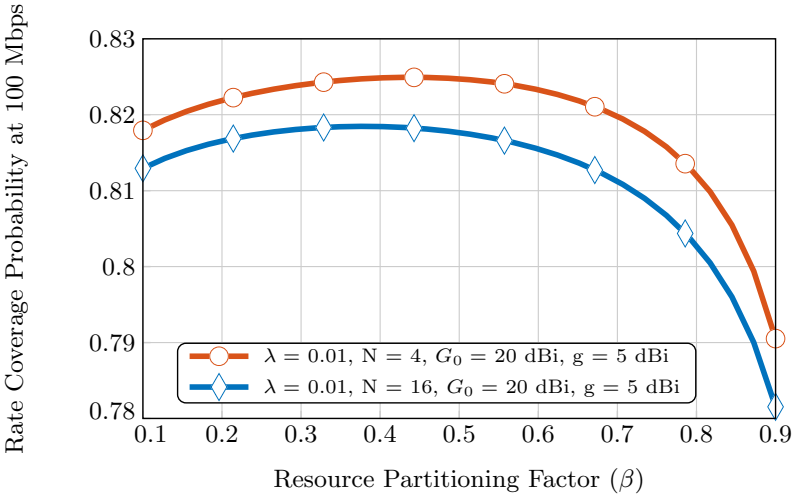

FIGURE 4.12: Rate coverage probability versus the resource partitioning factor for different beam dictionary sizes for $r_0 = 100$ Mbps.

transmitter and receiver sides decrease, which directly reduces the useful received signal power, while the interference power remains same. Overall, this leads to limited rate performance.

Another interesting observation in this figure, is the fact that, in order to achieve the same coverage performance, the joint beam-selection and misalignment error is slightly larger in case of larger beam-dictionaries. This is due to the thinner beams in larger beam-dictionaries, which increase the probabilities that the users lie outside the serving beam, or that the beams are misaligned. In the next section, we will see that this may not always be the case, i.e., depending on other system parameters such as the antenna gain and the deployment density, thinner beams can provide a better rate coverage.

4.7.4 Rate coverage performance and trends

In Figs. 4.12 and 4.13 we plot the rate coverage probability with respect to the resource partitioning factor β varying the antenna gain parameter G_0 and the BS deployment density for different rate requirement thresholds. First, we note again that there exists an optimal β^* for each beam dictionary size, for which the rate coverage probability is maximized. More interestingly, the value of β^* is not unique and is dependent not only on the dictionary size but also on the system parameters such as antenna gains. From Fig. 4.12 we can see that the optimum value of β decreases for higher N, i.e., thinner beamwidth. This is because with thinner beamwidth, the localization resources should be increased to limit the probability that the UE lies outside the coverage area of the beam.

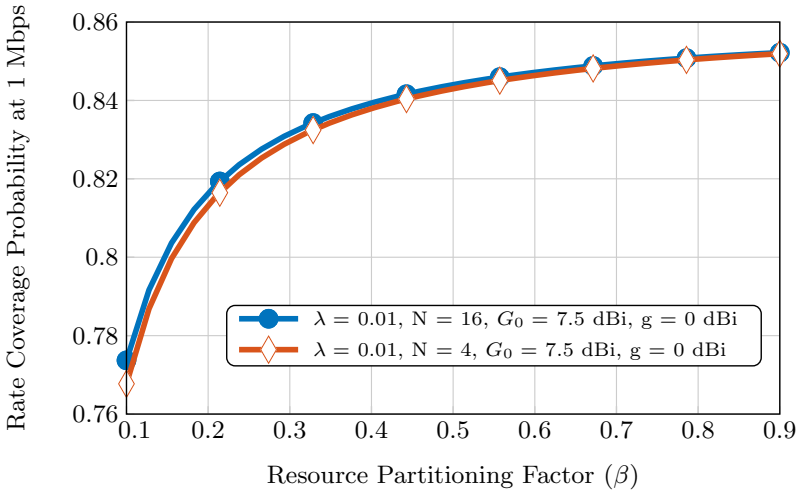

FIGURE 4.13: Rate coverage probability versus the resource partitioning factor for different beam dictionary sizes for $r_0 = 1$ Gbps.

When the antenna gain is smaller ($G_0 = 7.5$ dBi), we see in Fig. 4.13 that the rate coverage (at 1 Mbps contrary to 100 Mbps as before) increases with β. With $G_0 = 15$ dBi, the positioning accuracy is limited (for any value of β), while increasing β simply increases the communication resources, thereby augmenting the coverage. In this case, a smaller beamwidth (with $N = 16$) provides better coverage than a larger beamwidth (with $N = 4$), since with limited localization accuracy, the rate coverage simply increases with decreasing ω due to higher radiated power.

4.7.5 Optimal partitioning factor and beam dictionary size

In this section, we discuss the results obtained solving the transmit beamwidth and radio frame structure problem presented in equation (4.21). In Fig. 4.14 we plot the optimal values of β with respect to the BS deployment density λ and the noise power N_0B [dBW]. With low noise power (e.g., -50 dBW) the optimal value of β is closer to 1 for higher λ. This is due to the fact that for low noise power and densely deployed BSs, even a limited amount of resources allocated to the localization phase results in a good localization performance. Thus, the optimal solution is to allocate large resources to the data phase for enhancing the rate coverage. On the other hand, for sparsely deployed BSs, larger amount of resources are required for efficient localization and the value of β decreases, even for the case of low noise.

Interestingly, in the case of high noise (e.g., N_0B = -20 dBW), when increasing the small cell density, the optimal β increases at first and then decreases. This is due to the fact that for dense deployment of BSs, in case of high noise power, the effect of the beam selection error is notable due to the concurrent large interference

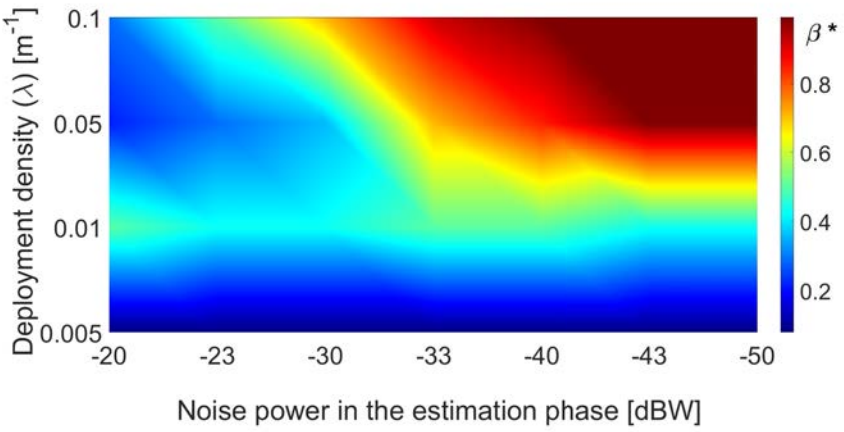

FIGURE 4.14: Optimal value of β with respect to deployment density and noise.

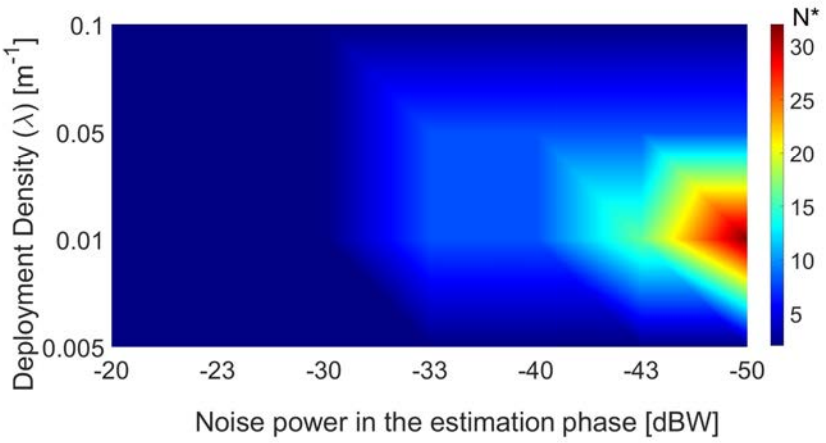

FIGURE 4.15: Optimal beam-dictionary size with respect to deployment density and the noise.

(since interfering BSs are closer due to higher density). This requires a lower value of optimal β to facilitate efficient localization and reduce localization errors. Thus for higher noise, the behaviour of optimal β is not monotonous with respect to the deployment density.

In Fig. 4.15 we plot the optimal beam-dictionary size with respect to λ and N_0B. For high noise power, large beams (i.e., smaller dictionaries) must be used so as that the beam selection error is limited. In case the noise is low (e.g. -50 dBW), the optimal size of the beam dictionary at first increases with the deployment density, due to the fact that larger antenna gains improve the rate coverage. However, after a certain point (i.e., for very dense deployments), the optimal beam-dictionary size decreases to limit the beam selection errors, which would have a large impact on the user performance due to the concurrent high interference.

4.8 Chapter conclusions

In this chapter, we studied a mm-Wave system deployed along the roads of a city to support localization and communication services simultaneously. We proposed a novel localization bound-assisted initial beam-selection method for the mobile users, which reduces the latency of initial access by upto 75%. Then the localization performance bounds were used to derive the downlink data-rate of the network in a system supporting jointly the localization and communication services. Our results highlight that increasing the resources allocated to the localization functions may or may not enhance the user data-rate. As a result, the study of the optimal resource partitioning factor is non-trivial. Consequently, we highlighted and explored the main trends in the optimal resource partitioning factor and mm-Wave beamwidth with respect to the rate coverage probability, with varying BS deployment density, antenna gain, and noise. Finally, we provided several key system-design insights and guidelines based on our results.

Regarding the limitations of this work, firstly, we only considered the LOS path. In the initial access phase, this consideration implies that, in the case of blockages, the terminating condition *i.e.* the minimum CRLB requirement does not get fulfilled until the blockage is resolved. In the data service phase, the direct path blockage implies that we are in outage. Instead of relying only on the direct path, we can utilize other non-direct paths in order to be more robust against the blockages. We have elaborated such a model in chapter 6. In this work, even though we consider a one dimensional road scenario, we do not explicitly consider a mobility model for the vehicles and we have justified this choice in section 4.4.2. However, incorporating a mobility model on top of our framework would provide more robustness to our framework and can be addressed in the future. We have described the idea in chapter 6. Similarly, we acknowledge that interference, whose effects onto localization performance are herein neglected, could be better modelled and assessed in future works, as also accounted for in chapter 6.

Chapter 5

Applications of multipath angles estimation

5.1 Introduction

In the previous chapters, we have studied general frameworks enabling the estimation of various location dependent variables. In chapter 2, we saw that with the right beam alignment, we can improve the localization performance. Similarly, in chapters 3 and 4, we found out that beyond beam alignment considerations, beamwidth optimization also plays an important role with respect to localization performance and accordingly, contributes to improve further location-aided data communication performance, in terms of both latency and throughput. In the same context, in this chapter, we will investigate two representative applications relying on such estimated localization variables.

Contrarily to previous chapters, in this chapter we will not consider delay, but only angular variables (AoD and AoA), which can be exploited at different levels and stages of the mm-Wave system as shown in Fig. 1.7. The reason for this choice is twofold. Firstly, as already motivated in the previous chapters, directionality is a natural element of the mm-Wave technology. The need to overcome high power attenuation as a function of the distance and the possibility to integrate many small antennas at high frequencies make the angular information a rather natural but crucial element of mm-Wave systems. Secondly, delay based localization methods such as ToA or TDoA require tight synchronization [114, 115], whereas angle based methods relax this constraint.

In this chapter, we will present two applications facilitated by angular measurements, namely channel estimation and SLAM.

One major challenge of mm-Wave beamforming (and beyond, of beam alignment) is that the transmitter needs to have a fairly good knowledge of channel

information with respect to the receiver so as to transmit the beam with the adequate width in the right direction, as we have illustrated in earlier chapters. In this demanding context, estimating the channel between the transmitter and the receiver, that is to say, estimating the parameters of multipath components (delays, AoAs, AoDs and channel coefficients), is thus of the highest importance. In this chapter, we will study how the sparse and geometric nature of the mm-Wave channel can be exploited, by means of angular information, so as to minimize the number of required measurements (and hence the duration) performed by the transmitter and the receiver beam pair compared to conventional methods. This method is inspired -and somehow can be fed by- the beam alignment and width selection method proposed in chapter 4, once it has reached its steady-state regime[1] of the algorithm.

After channel estimation, we then focus on the problem of SLAM in a multi-BS multipath scenario. The mm-Wave propagation channel is sparse by nature, as mentioned earlier, meaning that there are only few multipath components. Consequently, in mm-Wave system, it has been shown that it is possible to estimate the delays, AoAs and AoDs of the main multipath components [116]. Thus, one can leverage the location-dependent information conveyed by each component to aid the localization process [49]. Beyond, knowing the positions of the scatterers[2] generating these multipath contributions, in addition to localizing the user, offers a unique opportunity to map the physical environment. Hence, in the latter part of this work, we investigate the possibility of both localizing the user and mapping the environment, while still being based uniquely on angular measurements for the same reasons as previously explained.

5.2 Related works

With regards to channel estimation, in the literature, this problem has been addressed from the perspective of two distinct stages, namely the beam training stage and the estimation algorithm stage. Firstly, in the beam training, the most straightforward approach is to exhaustively search the best beams in terms of received power, by testing all possible angular directions on both transmitter's and receiver's sides [60]. Furthermore, the authors in [56] and [117] propose an iterative multi-resolution beam training procedure, where larger beams are used first,

[1] By steady state regime, we mean the state when the BS and user beam start to converge due to improved localization in the initial access algorithm.

[2] In this chapter, we consider term scatterers which can either diffract or reflect the signal to the receiver.

before converging iteratively to a beamwidth corresponding to the a-priori required spatial resolution. Likewise the authors in [65] propose a similar iterative beam training process fed by AoD and AoA in presence of prior location information. Similarly, in [118], the authors devise a channel estimation strategy employing different beam patterns in different directions. The latter two strategies reduce the channel estimation duration in comparison to the exhaustive case, which is critical in case of 5G applications due to both their latency requirements and the necessity to operate at mm-Wave, possibly under mobility. Secondly, in the estimation stage, most of the contributions are based on compressive sensing techniques, exploiting the aforementioned sparsity of the mm-Wave channel, with algorithms such as orthogonal matching pursuit (OMP) [119, 120], simultaneous orthogonal matching pursuit (SOMP) [51] and L1-norm minimization [121].

Then, regarding the tracking of location dependent variables for both LOS and NLOS multipath components, the authors in [51] and [122] present an estimator that exploits the mm-Wave channel sparsity, by relying on SOMP and support detection based algorithms. Similarly, the authors in [123] and [124] present a SLAM algorithm based on the multiple location estimates of the user and the scatterers at different time instances. In [115], the authors describe a message passing based solution for estimating the position and orientation of the user and the positions of scattering points in both presence and absence of direct path. The authors show that even in NLOS, the positions of the scatterers can be reliably estimated. Likewise, in [125], the authors provide a belief propagation (BP) based approach to track features in the environment in a dynamic vehicular scenario. The authors perform the message passing in a distributed way that necessitates passing large number of messages at each BSs. The authors in [126] propose a BP based algorithm to solve the data association problem (*i.e.* associating measurements to the correct sources) and propose a solver with low complexity. As suggested earlier, since the methods relying on time-based measurements require tight synchronization [114, 115], cooperative localization using only AoA information was proposed in [127]. Similarly, in [128], the authors investigate indoor localization with only AoA measurements.

5.3 Methodology and organization

Motivated by the previous literature analysis, we present the research method and the axes of investigation followed in this chapter.

- During the channel estimation procedure, the main limitations of the popular beam training methods such as the exhaustive or the iterative multi-resolution

based methods lie in the necessity to search in the whole beam space, which takes up a lot of time. This ends up being a bottleneck particularly in the context of low latency 5G applications and in dynamic channel estimation scenarios. Motivated by this limitation, we instead look to exploit the angular information of the mm-Wave system to aid the multipath channel estimation process and reduce the latency.

- In the literature, the works on SLAM firstly consider delay estimation. We have already argued before that in absence of tight synchronization, the estimates can be erroneous. In the light of this remark, in our work, we consider only AoD and AoA measurements to localize both the user and the scatterers.

- In the same context, most of the works reported in the literature consider performing the message passing in a distributed way, as mentioned earlier. Such an approach could lead to huge communication overhead. In contrast, in our work, we look into a centralized approach in order to avoid this communication overhead and ease data association.

The rest of this chapter is organized as follows. In section 5.4, we deal with the problem of localization aided multipath channel estimation. In this context, in section 5.4.1, we present the system model including the deployment scenario, channel model, communication model and angles estimation model. In section 5.4.2, we formulate the channel estimation problem, design the beam, and finally present the algorithm. In section 5.4.3 we present the comparison of the performance of our algorithm with the conventional methods. We then consider the problem of SLAM in section 5.5. In this context, we present, firstly, the system model in section 5.5.1 and then formulate the factor graph in section 5.5.2. From the factor graph, we design and specify a message passing algorithm, while highlighting its main specificities in section 5.5.3 including the comparison with conventional methods. Through simulations, we evaluate and compare the performance of our proposal with that of a conventional approach in section 5.5.4. We finally conclude the chapter in section 5.6.

5.4 Multipath channel estimation with angle measurements

In this section, we firstly present a low latency multipath mm-Wave channel estimation algorithm where the beam training phase is aided by angles estimation. First,

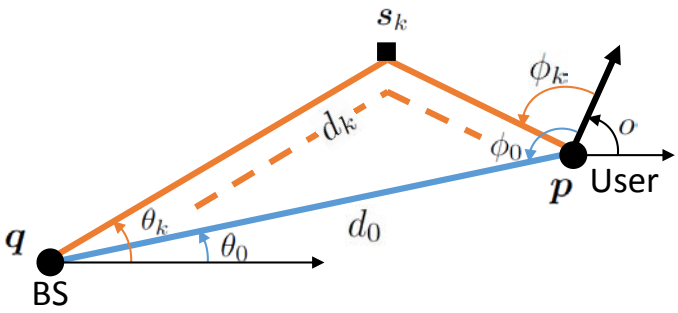

FIGURE 5.1: Illustration of the system model with a BS, a user and k-th scatterer located at positions $\boldsymbol{q}$, $\boldsymbol{p}$ and $\boldsymbol{s}_k$ respectively. The distance between the BS and the user through direct path is d_0 and through the k-th scatterer is d_k. The AoD and AoA for the k-th path are θ_k and ϕ_k respectively.

during the beam training procedure, we perform AoD and AoA measurements, estimate the corresponding variances and based on them, design both downlink and uplink beams. We then perform the acquisition of received signals with these beams and accordingly design the sensing matrix, while also iteratively refining the angles estimation and the beams for the next measurements. Finally, exploiting both the sparseness and the intrinsic geometric nature of the mm-Wave channel, we apply compressive sensing tools so as to complete the estimation procedure. One underlying expectation is that the corresponding estimation error decreases rapidly in comparison with other conventional approaches.

5.4.1 System model

Deployment scenario

Consider a mm-Wave downlink scenario with a BS and a user, equipped respectively with N_t antennas and N_r antennas and operating at the carrier frequency f_c (and the corresponding wavelength λ_c) with bandwidth B, and L scatterers, as illustrated in Fig. 5.1. The BS, the user and the k-th scatterer are located at positions $\boldsymbol{q} = [q_x, q_y]^T$, $\boldsymbol{p} = [p_x, p_y]^T$ and $\boldsymbol{s} = [s_{k,x}, s_{k,y}]^T$ respectively. The BS position is assumed to be known, whereas that of both the user and the scatterers are unknown a-priori. The BS is assumed to have a known orientation, whereas the user is arbitrarily oriented towards an angle $o \in (0, 2\pi]$ with respect to the reference x-axis.

Channel model

The $N_r \times N_t$ complex channel matrix between the BS and the user is denoted by $\boldsymbol{H}$ and is formulated as in [56], similarly to equation (1.8) as:

$$\boldsymbol{H} = \sqrt{\frac{N_r N_t}{\xi}} \sum_{k=0}^{L} h_k e^{-\frac{j2\pi\tau_k}{T_s}} \boldsymbol{a}_{Rx}(\phi_k)\boldsymbol{a}_{Tx}^H(\theta_k), \tag{5.1}$$

where h_k, $\tau_k = d_k/c$, θ_k and ϕ_k are respectively the complex channel coefficient, the time delay, the AoD and the AoA of the k-th path between the BS and the user and $T_s = 1/B$ is the sampling period. Like in the previous chapters, we consider a ULA model for the antenna array.

We can reformulate equation (5.1) similarly to [56] as

$$\boldsymbol{H} = \sqrt{\frac{N_r N_t}{\xi}} \boldsymbol{A}_{Rx} \boldsymbol{\Lambda} \boldsymbol{A}_{Tx}^H, \tag{5.2}$$

where,

$$\boldsymbol{A}_{Tx} = \left[\boldsymbol{a}_{Tx}(\theta_0), \cdots, \boldsymbol{a}_{Tx}(\theta_L)\right], \tag{5.3a}$$

$$\boldsymbol{A}_{Rx} = \left[\boldsymbol{a}_{Rx}(\phi_0), \cdots, \boldsymbol{a}_{Rx}(\phi_L)\right], \tag{5.3b}$$

$$\boldsymbol{\Lambda} = \operatorname{diag}\left(h_0 e^{-\frac{j2\pi\tau_0}{T_s}}, \cdots, h_L e^{-\frac{j2\pi\tau_L}{T_s}}\right). \tag{5.3c}$$

Communication model

Consider a downlink scenario between the BS and the user. If the BS uses a beamforming vector $\boldsymbol{f}_p$ and the mobile device uses a combining vector $\boldsymbol{w}_q$, the resulting received signal can be written similarly to equation (2.3) as:

$$y_{q,p} = \boldsymbol{w}_q^H \boldsymbol{H} \boldsymbol{f}_p s_p + n_{q,p}, \tag{5.4}$$

where, s_p is the transmitted symbol such that $\mathbb{E}\left[s_p\right] = P_{Tx}$, where P_{Tx} is the average power used per transmission, and $n_{q,p}$ is a Gaussian distributed noise with zero mean and bilateral power spectrum density $N_0/2$ per real dimension. Considering M_B and M_U vectors at the BS and the user respectively, the received signal can be written in a multipath scenario as

$$\boldsymbol{Y} = \boldsymbol{W}^H \boldsymbol{H} \boldsymbol{F} \boldsymbol{S} + \boldsymbol{N}, \tag{5.5}$$

where $\boldsymbol{W} = [\boldsymbol{w}_1, \boldsymbol{w}_2, \cdots, \boldsymbol{w}_{M_U}]$ and $\boldsymbol{F} = [\boldsymbol{f}_1, \boldsymbol{f}_2, \cdots, \boldsymbol{f}_{M_B}]$. Similarly to [56], we assume that for the channel estimation phase, all the transmitted symbols are equal and hence $\boldsymbol{S} = \sqrt{P_{Tx}}\boldsymbol{I}_{M_B}$, where $\boldsymbol{I}_{M_B}$ is an identity matrix of size M_B, and hence

$$\boldsymbol{Y} = \sqrt{P_{Tx}}\boldsymbol{W}^H\boldsymbol{H}\boldsymbol{F} + \boldsymbol{N}. \tag{5.6}$$

AoD and AoA estimation

We assume that the BS and the user have access to the estimates of AoD and AoA respectively for every k-th path[3], which can be expressed as:

$$\hat{\theta}_k = \theta_k + e_{\theta_k}, \tag{5.7a}$$

$$\hat{\phi}_k = \phi_k + e_{\phi_k}, \tag{5.7b}$$

where

$$\theta_k = \begin{cases} \arccos\left(\frac{p_x - q_x}{||\boldsymbol{p}-\boldsymbol{q}||_2}\right) & k = 0 \\ \arccos\left(\frac{s_{k,x} - q_x}{||\boldsymbol{s}_k-\boldsymbol{q}||_2}\right) & \text{otherwise,} \end{cases} \tag{5.8a}$$

$$\phi_k = \begin{cases} \pi + \arccos\left(\frac{p_x - q_x}{||\boldsymbol{p}-\boldsymbol{q}||_2}\right) - o & k = 0 \\ \pi - \arccos\left(\frac{p_x - s_{k,x}}{||\boldsymbol{p}-\boldsymbol{s}_k||_2}\right) - o & \text{otherwise,} \end{cases} \tag{5.8b}$$

and e_{θ_k} and e_{ϕ_k} are the estimation errors regarding θ_k and ϕ_k respectively. It was shown in [116] that under conditions such as a large number of transmit and receive antennas and a large bandwidth, which is reasonable in mm-Wave, the error for both AoD and AoA can be assumed as independent per path. Moreover, we assume that the random measurement noise terms are Gaussian distributed with zero mean and known variances[4] σ_θ^2 and σ_ϕ^2 [101].

[3]The angle estimations can be realized through well known subspace based AoA estimation techniques [110] such as MUSIC or ESPRIT. The BS can estimate the AoA with downlink measurements. Considering that for a given path, the AoD in downlink at the BS is the same as the AoA in uplink from the perspective of the user, the latter can estimate AoD with uplink measurements. In this chapter, by AoD, we refer to the uplink AoA. The sparse nature of the mm-Wave channel means that there are few distinct paths and the angles in each path can be estimated with high resolution due to the large number of antenna elements [43]

[4]The variance of estimation depends on the estimator and factors such as SNR, bandwidth and number of antenna elements. Such variances can be known a-priori, by means of e.g., theoretical bounds calculation, empirical statistics drawn over sequences of real measurements, or even through simulations.

5.4.2 AoD and AoA aided channel estimation

The objective of channel estimation is to estimate the matrix $\boldsymbol{H}$ in a multipath scenario. Equivalently, one can estimate the channel coefficient and the three location dependent variables (i.e., delay, AoD and AoA) for each path. In this section, we firstly state the channel estimation problem as a sparse problem. We then introduce the same sectorized beamforming model as in equation (3.27) to simplify the previous channel estimation problem. Finally, we propose the localization aided channel estimation algorithm.

Channel estimation problem

Vectorizing equation (5.6), we can write

$$\boldsymbol{y}_v = \mathrm{vec}(\boldsymbol{Y}) = \sqrt{P_{Tx}}\mathrm{vec}(\boldsymbol{W}^H\boldsymbol{H}\boldsymbol{F}) + \mathrm{vec}(\boldsymbol{N}), \tag{5.9a}$$

$$= \zeta(\boldsymbol{F}^T \otimes \boldsymbol{W}^H)(\boldsymbol{A}_{Tx}^* \otimes \boldsymbol{A}_{Rx})\mathrm{vec}(\boldsymbol{\Lambda}) + \boldsymbol{n}_v, \tag{5.9b}$$

$$= \zeta(\boldsymbol{F}^T\boldsymbol{A}_{Tx}^* \otimes \boldsymbol{W}^H\boldsymbol{A}_{Rx})\boldsymbol{x} + \boldsymbol{n}_v, \tag{5.9c}$$

where $\zeta = \sqrt{N_r N_t P_{Tx}/\xi}$, $\boldsymbol{x} = \mathrm{vec}(\boldsymbol{\Lambda})$ and $\boldsymbol{n}_v = \mathrm{vec}(\boldsymbol{N})$.

In order to present a sparse formulation of the estimation problem, consider a grid of N_B discrete AoD and N_U AoA directions taken uniformly between 0 and 2π, with the i-th grid direction represented by $\tilde{\theta}_i$ and $\tilde{\phi}_i$ for AoD and AoA respectively. Mathematically, $\tilde{\theta}_i = 2\pi(i-1)/N_B$ and $\tilde{\phi}_i = 2\pi(i-1)/N_U$. Assume,

$$\tilde{\boldsymbol{A}}_{Tx} = \left[\boldsymbol{a}_{Tx}(\tilde{\theta}_1), \cdots, \boldsymbol{a}_{Tx}(\tilde{\theta}_{N_B})\right], \tag{5.10a}$$

$$\tilde{\boldsymbol{A}}_{Rx} = \left[\boldsymbol{a}_{Rx}(\tilde{\phi}_1), \cdots, \boldsymbol{a}_{Rx}(\tilde{\phi}_{N_U})\right]. \tag{5.10b}$$

Similarly to [56, equation (17)], we can now reformulate equation (5.9c) as a sparse problem:

$$\boldsymbol{y}_v = \zeta(\boldsymbol{F}^T\tilde{\boldsymbol{A}}_{Tx}^* \otimes \boldsymbol{W}^H\tilde{\boldsymbol{A}}_{Rx})\boldsymbol{x} + \boldsymbol{n}_v = \zeta\boldsymbol{M}\boldsymbol{x} + \boldsymbol{n}_v, \tag{5.11}$$

where $\boldsymbol{M}$ is the sensing matrix and the j-th element in the vector $\boldsymbol{y}_v$ is

$$y_j = \zeta(\boldsymbol{f}_p^T\tilde{\boldsymbol{A}}_{Tx}^* \otimes \boldsymbol{w}_q^H\tilde{\boldsymbol{A}}_{Rx})\boldsymbol{x} + n_j = \zeta\boldsymbol{M}(j,:)\boldsymbol{x} + n_j, \tag{5.12}$$

where the j-th measurement is performed with the beamforming vector $\boldsymbol{f}_p$ and the combining vector $\boldsymbol{w}_q$, and $\boldsymbol{M}(j,:)$ represents the j-th row of the sensing matrix.

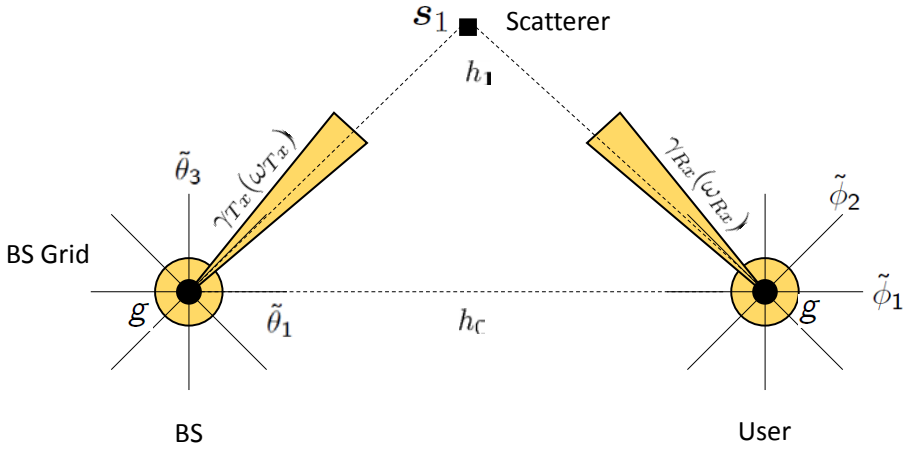

FIGURE 5.2: Example scenario with $N_B = N_U = 8$ with both BS and user main lobe directed towards $\boldsymbol{s}_1$.

Likewise

$$\boldsymbol{f}_p^T \tilde{\boldsymbol{A}}_{Tx}^* = \left[\boldsymbol{a}_{Tx}^H(\tilde{\theta}_1)\boldsymbol{f}_p, \cdots, \boldsymbol{a}_{Tx}^H(\tilde{\theta}_{N_B})\boldsymbol{f}_p\right], \tag{5.13a}$$

$$\boldsymbol{w}_q^H \tilde{\boldsymbol{A}}_{Rx} = \left[\boldsymbol{w}_q^H \boldsymbol{a}_{Rx}(\tilde{\phi}_1), \cdots, \boldsymbol{w}_q^H \boldsymbol{a}_{Rx}(\tilde{\phi}_{N_U})\right]. \tag{5.13b}$$

Equation (5.13a) (and equivalently, equation (5.13b)) represents the gain due to the beamforming vector $\boldsymbol{f}_p$ in all the grid directions. Hence, $\boldsymbol{f}_p^T \tilde{\boldsymbol{A}}_{Tx}^* \otimes \boldsymbol{w}_q^H \tilde{\boldsymbol{A}}_{Rx}$ represents the gain due to $\boldsymbol{f}_p$ and $\boldsymbol{w}_q$ in all the BS and user grid combinations (*i.e.* $N_B \times N_U$ combinations).

Sectorized beamforming model

We approximate the beamforming model, like in chapters 3 and 4 by the sectorized model, where the transmitted and received beams are divided into a main lobe sector and a side lobe sector. The antenna gain $G_x(\omega_x)$, where $x \in \{Tx, Rx\}$ at the BS side *i.e.* $|\boldsymbol{f}^H \boldsymbol{a}_x(\theta_k)|^2$ and user side *i.e.* $|\boldsymbol{w}^H \boldsymbol{a}_x(\phi_k)|^2$ can be approximated by equation (3.27).

Sensing matrix design

From equations (5.12) and (3.27), each element of the sensing matrix $\boldsymbol{M}$ can have four distinct values: $\sqrt{\gamma_{Tx}(\omega_{Tx})\gamma_{Rx}(\omega_{Rx})}$, $\sqrt{\gamma_{Tx}(\omega_{Tx})g}$, $\sqrt{g\gamma_{Rx}(\omega_{Rx})}$ and $\sqrt{g^2}$ depending on the beam alignment and beamwidths.

Consider an example scenario as illustrated in Fig. 5.2 with $N_B = N_U = 8$. We have beams from the BS and the user with widths ω_{Tx} and ω_{Rx} respectively, both directed at a scatterer located at $\boldsymbol{s}_1$. Let $\boldsymbol{m}_{BS} = \boldsymbol{f}^T \tilde{\boldsymbol{A}}_{Tx}^*$ and $\boldsymbol{m}_{MS} = \boldsymbol{w}^H \tilde{\boldsymbol{A}}_{Rx}$.

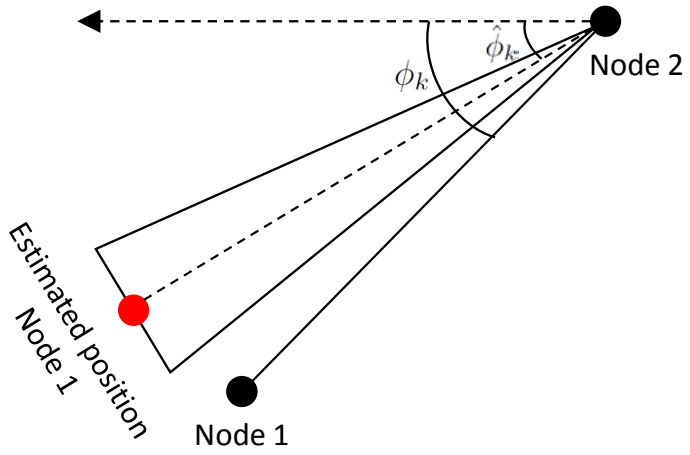

FIGURE 5.3: Illustration of beam misalignment error due to erroneous estimation of $\hat{\phi}_k$ such that Node 1 is not within the transmitted beam. Node 1 might be receiver or scatterer depending on whether it corresponds to the direct path or not.

Then, the received signal is

$$y = \zeta \sum_{k=0}^{L} \sqrt{G_{Rx}(\omega_{Rx,k})} \sqrt{G_{Tx}(\omega_{Tx,k})} h_k + n, \tag{5.14a}$$

$$= \zeta \left[\sqrt{\gamma_{Tx}(\omega_{Tx,1}) \gamma_{Rx}(\omega_{Rx,1})} h_1 + \sqrt{g^2} h_0 \right] + n, \tag{5.14b}$$

and each row of the sensing matrix is calculated as

$$\boldsymbol{m}_{Tx} = [\sqrt{g}, \sqrt{\gamma_{Tx}(\omega_{Tx})}, \sqrt{g}, \sqrt{g}, \sqrt{g}, \sqrt{g}, \sqrt{g}, \sqrt{g}], \tag{5.15a}$$

$$\boldsymbol{m}_{Rx} = [\sqrt{g}, \sqrt{g}, \sqrt{g}, \sqrt{\gamma_{Rx}(\omega_{Rx})}, \sqrt{g}, \sqrt{g}, \sqrt{g}, \sqrt{g}], \tag{5.15b}$$

$$\boldsymbol{M}(j,:) = \boldsymbol{m}_{Tx} \otimes \boldsymbol{m}_{Rx}. \tag{5.15c}$$

AoD and AoA aided beam design

Now based on the angles estimate from equation (5.7), for each path, we design the optimal beamwidth ω_{Tx} and ω_{Rx} at both BS and user respectively in such a way to minimize the beam misalignment error per path. We define the misalignment error as the event that the scatterer (or correspondingly the receiving node in case of direct path transmission) does not fall within the main beam lobe from the transmitting (or receiving) node due to estimation errors. This event is depicted in Fig. 5.3.

Based on this new definition of the misalignment error in a multipath context, we

design the beamwidth[5] $\omega_{Tx,k}$ with respect to the k-th path such that the probability of misalignment error is a constant ϵ_{Tx}, i.e.,

$$\mathcal{P}\left(\hat{\theta}_k - \frac{\omega_{Tx,k}}{2} \leq \theta \leq \hat{\theta}_k + \frac{\omega_{Tx,k}}{2}\right) = \epsilon_{Tx}. \tag{5.16}$$

Accordingly,

$$\omega_{Tx,k} = 2\Phi^{-1}\left(\frac{\epsilon_{Tx}+1}{2}\right)\sigma_\theta, \tag{5.17}$$

where $\Phi^{-1}(x)$ is the inverse function of the CDF of standard normal distribution. Likewise,

$$\omega_{Rx,k} = 2\Phi^{-1}\left(\frac{\epsilon_{Rx}+1}{2}\right)\sigma_\phi. \tag{5.18}$$

Channel estimation algorithm

Overall, the proposed localization aided channel estimation algorithm can be summarized by the following steps.

Initialization:

I. Determine initial estimates of AoD $\hat{\theta}_k^{(1)}$ and AoA $\hat{\phi}_k^{(1)}$ at the BS and MS respectively for all the paths and their corresponding variances $\sigma^2_{\theta_k}$ and $\sigma^2_{\phi_k}$.

Beam Training Phase:

II. $i \leftarrow 1$

III. For each estimated $\hat{\theta}_{k_1}^{(i)}$ and $\hat{\phi}_{k_2}^{(i)}$ pair, $\forall k_1, k_2 \in \{0, 1, \cdots L\}$ and corresponding $\sigma^2_{\theta_{k_1}}$ and $\sigma^2_{\phi_{k_2}}$:

1. Calculate the beamwidth $\omega^{(i)}_{Tx,k_1}$ and $\omega^{(i)}_{Rx,k_2}$ for BS and MS beams according to equations (5.17) and (5.18) respectively.
2. Set the BS and MS beams towards $\hat{\theta}^{(i)}_{k_1}$ and $\hat{\phi}^{(i)}_{k_2}$ respectively with widths $\omega^{(i)}_{Tx,k_1}$ and $\omega^{(i)}_{Rx,k_2}$.
3. With these beams, acquire the received signal y_i, according to equation (5.14a).
4. Calculate the corresponding row of the sensing matrix $\boldsymbol{M}(i,:)$, as in equation (5.15c).

[5] In practice, the ability of an antenna to beamform with a certain width depends on the number and the geometry of the antenna elements. In our scenario, we assume that both BS and MS have enough elements to support small beamwidth.

5. If $|y_i|^2 \geq \gamma_i$:
   i. With downlink transmission towards $\hat{\theta}_{k_1}^{(i)}$ with beamwidth $\omega_{Tx,k_1}^{(i)}$, the BS estimates the refined AoA $\hat{\phi}_k^{(i+1)}$.
   ii. With uplink transmission towards $\hat{\phi}_{k_1}^{(i)}$ with beamwidth $\omega_{Tx,k_1}^{(i)}$, the user estimates the refined AoD $\hat{\theta}_k^{(i+1)}$.
   iii. Update the estimation variances $\sigma_{\theta_k}^2$ and $\sigma_{\phi_k}^2$.

IV. Go to step III unless the terminating condition[6] is satisfied and $i \leftarrow i+1$.

Estimation Algorithm Phase:

V. $\boldsymbol{z} \leftarrow \text{OMP}(\boldsymbol{M}, \boldsymbol{y})$ and reshape $\boldsymbol{z}$ from $N_B N_U \times 1$ vector to a $N_B \times N_U$ matrix.

$$\hat{\boldsymbol{\Lambda}} = \text{reshape}\left(\boldsymbol{z}, [N_B, N_U]\right). \tag{5.19}$$

VI. **Output:** $\hat{\boldsymbol{H}} = \tilde{\boldsymbol{A}}_{Rx} \hat{\boldsymbol{\Lambda}} \tilde{\boldsymbol{A}}_{Tx}^H$

In summary, we firstly initialize the algorithm with coarse estimates of the AoDs and AoAs along with their variances for all the paths. For each AoD and AoA, we then calculate the beamwidths such that we limit the misalignment error probabilities to ϵ_{Tx} and ϵ_{Rx} (with respect to the scatterer in case of secondary path) at the transmitter and the receiver respectively. We then sequentially transmit for every pair of AoD and AoA, in total $(L+1)^2$ pairs, with the calculated beamwidths and measure the received signals and the corresponding row of the sensing matrix according to equations (5.14a) and (5.15c) respectively. Following, we refine AoDs and AoAs, as well as the corresponding variances, for each path with the new beamwidth. We only perform this step if the BS and user beam pairs are corresponding to either the direct path or the same scatterer, hence $L+1$ times. In order to decide when to perform this step, we threshold the received signal power on γ_i, which is a function of $\omega_{Tx,k_1}^{(i)}$ and $\omega_{Rx,k_2}^{(i)}$, such that we only measure the angles when both the main lobes are aligned towards either each another or the same scatterer. This beam refining and measuring process is iteratively repeated until some application dependent terminating condition is fulfilled. The sparsity of mm-Wave channel ensures that the sensing matrix is sparse, and hence we use some compressive sensing algorithm such as OMP in this case to finally estimate the channel.

[6]The terminating condition can be application dependent. It can be, for *e.g.*, the minimum beamwidth constraint, the total channel estimation duration constraint, *etc.*

5.4.3 Numerical results

In our work, we assume an analog beamforming architecture on both BS and user sides with only 1 RF chain operating at $f_c = 28$ GHz with bandwidth $B = 500$ MHz. We assume the transmit power $P_{Tx} = 30$ dBm and the noise power density at the received signal $N_0 = -174$ dBm/Hz. We consider 1 BS with known position ($\boldsymbol{q} = [0, 0]^T$) and orientation ($o = 0^o$), and $L = 3$ scatterers (and accordingly, 4 paths). Moreover, we assume the $N_B = N_U = 360$ grid points at both the BS and the user respectively. For determining the beamwidth, we consider $\epsilon_{Tx} = \epsilon_{Rx} = 0.99$.

We compare our proposed localization assisted channel estimation method with that resulting from two well-known solutions, namely exhaustive search and iterative multi-resolution search [56, 60]. For the exhaustive search, we consider the beamwidths of the BS and the user to be fixed and equal to ω_{Tx}^{Ex} and ω_{Rx}^{Ex} respectively. Thus, with these widths, the BS and the user go through all the possible combinations of beams throughout the search area in order to complete the beam training process. On the other hand, for the case of iterative multi-resolution based search, we implement the multipath channel estimation algorithm in [56], where we start with an initial beamwidth of $\pi/2$ rad and iteratively bisect the beamwidth and sweep to converge to finer resolution. After the beam training step, we use OMP according to step V. from the above algorithm, in the estimation phase for both the cases. Like in chapter 4, we assume that each transmission can be completed within 14.3μs which is equal to one OFDM symbol length [112]. We characterize the error in channel estimation in terms of normalized mean square error (NMSE), defined as NMSE $= ||\boldsymbol{H} - \hat{\boldsymbol{H}}||_2^2 / ||\boldsymbol{H}||_2^2$, where, $||\cdot||_2$ represents the 2-norm.

In Fig. 5.4, we can see the minimum beamwidth that can be achieved within a given duration. For instance, during x μs, we can transmit $n = \lfloor x/14.3 \rfloor$ beam pairs. For the case of exhaustive search based channel estimation, since we need to search the entire $\pi/2$ space in x μs, the minimum beamwidth that we can use is $\omega_{Tx}^{\text{Ex}} = \omega_{Rx}^{\text{Ex}} = \pi/2n$ rad. In case of iterative search, the minimum beamwidth we can achieve during n steps is given by $\omega_{Tx}^{It} = \omega_{Rx}^{It} = \pi/2 \log_2(n)$, since the search sector grows to the power of 2 at each bisection. For the localization based method, the minimum beamwidth with n possible beam pairs depends on how fast the beamwidth converges at each iteration and hence, on the variance of estimated AoD and AoA. Since the previous variances, and thus the beamwidths, vary for each path, for the localization based method, we plot both the minimum and maximum beamwidths allocated at each iteration. In our simulations, in order to have a closed

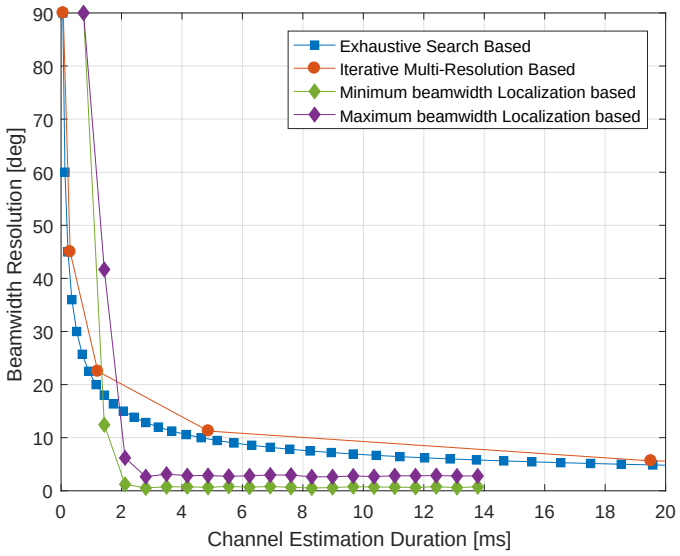

FIGURE 5.4: Beamwidth achieved for different channel estimation methods varied with total channel estimation duration.

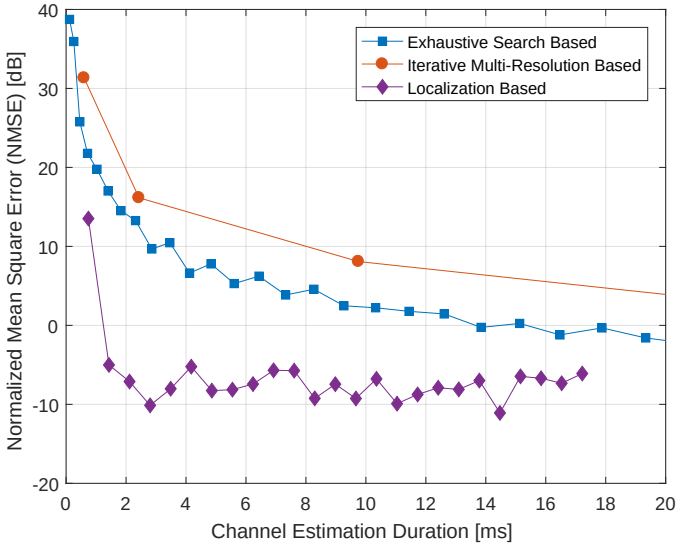

FIGURE 5.5: NMSE comparison for different channel estimation methods varied with total channel estimation duration.

form expression of the variances, we assume an estimator meeting the CRLB[7] when estimating of AoD and AoA, as derived in [51]. In Fig. 5.4 we can see that the beamwidth in the proposed localization assisted algorithm decreases much more quickly than in other cases.

In Fig. 5.5, we also present the NMSE of channel estimation for each method for different channel estimation durations and with different beamwidths corresponding to these estimation durations, as shown in Fig. 5.4. In this figure, we can observe that with the proposed localization based method, the estimation error, similar to the beamwidth, decreases more rapidly than the other methods. The reason for this is that in the proposed method, we directly use the relevant beams even though there is a small probability of misalignment. However, in the exhaustive and iterative search based methods, a lot of time is spoilt while searching all the sectors including those which do not provide any relevant information. This gain in latency could be crucial especially in the context of low latency 5G applications and in dynamic channel estimation scenarios, for *e.g.*, tracking a mobile user.

5.5 SLAM with angle measurements

Following our work on channel estimation, in this section, we look into a BP based SLAM approach suitable for mm-Wave networks. This approach leverages AoA and AoD information[8] with respect to multiple scatterers[9]. Considering measurements from multiple BS and scatterers, seen as multiple sources, we solve out the data association problem from a centralized BP perspective, while jointly estimating the positions of both the mobile and scatterers.

5.5.1 System model

Consider a 2D scenario with N BSs and a single user as illustrated in Fig. 5.6. The positions of the BSs are assumed to be known, located at $\boldsymbol{x}_1, \boldsymbol{x}_2, \cdots, \boldsymbol{x}_N$ in

[7]Although CRLB represents a lower bound on the variance of an unbiased estimator and hence, the best case scenario, the authors in [51] show that it is possible for an estimator to achieve the bound even at low SNR.

[8]Such information can be achieved by various algorithms such as, as described earlier, MUSIC or ESPRIT, or even following the channel estimation algorithm. For instance, in [51], the authors present a iterative expectation maximization algorithm in order to extract the localization information from the estimated channel. A similar method can be implemented in conjunction with the previously presented channel estimation algorithm in order to estimate the angles.

[9]For the sake of positioning each scattering point out of AoA and AoD measurements, we assume a single interaction with the latter point along each secondary path for simplicity, thus preserving the unicity of the solution (*i.e.*, rather than assuming multi-bounce interactions per path). This assumption is realistic in the mm-Wave context since multi-bounce paths would be too attenuated and likely not even detected on the receiver side.

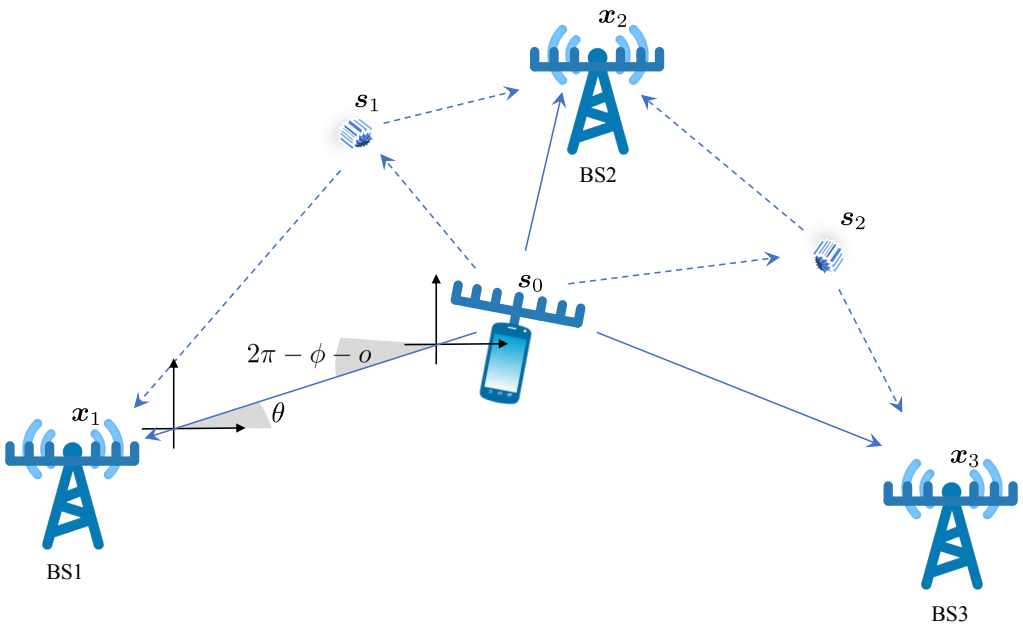

FIGURE 5.6: Example system model with 3 BS positioned at $\boldsymbol{x}_1$, $\boldsymbol{x}_2$ and $\boldsymbol{x}_3$ and 1 user positioned at $\boldsymbol{s}_0$ with orientation o along with two scatterers at $\boldsymbol{s}_1$ and $\boldsymbol{s}_2$ and the AoD and AoA of the LOS paths with respect to BS1.

a common coordinate system. Likewise, the user is assumed to be positioned at $\boldsymbol{s}_0$ with a known orientation[10] o. In the scenario, we also assume L scattering points (and hence $L+1$ total possible paths between a BS and the mobile user), with respective positions $\boldsymbol{s}_1, \boldsymbol{s}_2, \cdots, \boldsymbol{s}_L$. Both the positions of the user and the scatterers are unknown. We assume that each BS i can measure the AoD and AoA corresponding to $\hat{L}_i$ different paths, contrarily to [49] where, in addition to the angle measurements, the authors also include delay-based distance measurements for each path. We also assume that L is known, there are no false alarms[11], *i.e.* $\hat{L}_i \leq L+1$, and the measurements can be sorted in any arbitrary order with respect to the $L+1$ total paths.

$$\mathcal{Z}^{(i)} = [\boldsymbol{z}_1^{(i)}, \cdots, \boldsymbol{z}_l^{(i)}, \cdots, \boldsymbol{z}_{\hat{L}_i}^{(i)}], \tag{5.20}$$

where $l \in \{1, 2, \cdots, \hat{L}_i\}$ denotes the measurement index of i-th BS corresponding to a set of estimates of AoD ($\hat{\theta}$) and AoA ($\hat{\phi}$). We also assume that we have access to the measurement covariance matrix ($\boldsymbol{\Sigma}_l^{(i)}$) corresponding to the measurements of

[10]For simplicity, we consider that the orientation of the user is known. The absolute heading can be extracted from some orientation estimators, for instance, inertial measurement unit (IMU) and magnetometer in the mobile phone [123].

[11]This consideration excludes the possibility of any measurements not associated with the user, N BSs and L scatterers. For the problem formulation including the possibility of false alarm, see [126].

AoD and AoA between the i-th BS and the l-th scatterer. We consider that all the measurements $\boldsymbol{z}_l^{(i)}$ are independent. Mathematically,

$$\boldsymbol{z}_l^{(i)} = [\hat{\theta}_l^{(i)}, \hat{\phi}_l^{(i)}] \sim \mathcal{N}\left([\theta_l^{(i)}, \phi_l^{(i)}], \boldsymbol{\Sigma}_l^{(i)}\right). \tag{5.21}$$

The measurements for all the N BSs can be grouped together as $\boldsymbol{Z} = [\mathcal{Z}^{(1)}, \cdots, \mathcal{Z}^{(N)}]$.

The main task now is to thus calculate the posterior distribution $p(s_k|\boldsymbol{Z})$, where $k \in \{0, 1, \cdots, L\}$. However, since the order of the measurements at each BS is random, in the process of calculating the posterior distribution, we also need to solve the data association problem, where we associate each measurement with the corresponding path (and hence the source).

5.5.2 Factor graph formulation

Data association auxiliary variables

For the purpose of data association, following a similar approach to [125], we introduce the set $\mathcal{M} = \otimes_{i=1}^{N}\{1, \cdots, \hat{L}_i\}$ with its cardinality $P = \prod_{i=1}^{N} \hat{L}_i$, $\boldsymbol{a}_k \in \mathcal{M}$ and $b_{\boldsymbol{m}} = \{0, 1, \cdots, L\}, \forall \boldsymbol{m} \in \mathcal{M}$. Each element of the set $\mathcal{M}$, referred to in this chapter as a measurement vector, is a vector of length N containing all the possible permutations of measurement indices; $\boldsymbol{a}_k$ indicates which measurement vector corresponds to the source k. Reciprocally, $b_{\boldsymbol{m}}$ indicates which source corresponds to a measurement vector. Both $\boldsymbol{a}$ and b can be mapped one-to-one, meaning that the knowledge of either of the variables is sufficient to know the other. Mathematically, this relation is expressed as

$$\psi(\boldsymbol{a}_k, b_{\boldsymbol{m}}) = \begin{cases} 0 & \boldsymbol{a}_k = \boldsymbol{m}, b_{\boldsymbol{m}} \neq k \text{ or } \boldsymbol{a}_k \neq \boldsymbol{m}, b_{\boldsymbol{m}} = k, \\ 1 & \text{otherwise.} \end{cases} \tag{5.22}$$

Contrary to [125], where the data association is performed in a distributed way at each BS, we assume that the association in our case is done in a centralized way and hence, unlike in [125], the association variables $\boldsymbol{a}$ and b in our work are not scalars.

Factor graph of joint distribution

Our objective is to find the marginal probability of $\boldsymbol{s}_k$ while also solving out the data association problem. We have a posterior distribution formulation as follows:

$$p(\boldsymbol{s}_{0:L}, \boldsymbol{a}, \boldsymbol{b}|\boldsymbol{Z}) \propto p(\boldsymbol{Z}|\boldsymbol{s}_{0:L}, \boldsymbol{a}, \boldsymbol{b})\Psi(\boldsymbol{a}, \boldsymbol{b}) \prod_{k=0}^{L} p(\boldsymbol{s}_k), \tag{5.23}$$

where, $p(\boldsymbol{s}_k)$ is the prior distribution on the position of the sources, $\boldsymbol{a}$ and $\boldsymbol{b}$ contain all the association variables $\boldsymbol{a}_k$ and $b_{\boldsymbol{m}}$, and $\psi(\boldsymbol{a}, \boldsymbol{b})$ can be formulated similarly to [125, 126] from (5.22):

$$\Psi(\boldsymbol{a}, \boldsymbol{b}) = \prod_{k=0}^{L} \prod_{\boldsymbol{m}\in\mathcal{M}} \psi(\boldsymbol{a}_k, b_{\boldsymbol{m}}). \tag{5.24}$$

The measurement likelihood $p(\boldsymbol{Z}|s_{0:L}, \boldsymbol{a}, \boldsymbol{b})$ can be formulated as:

$$p(\boldsymbol{Z}|\boldsymbol{s}_{0:L}, \boldsymbol{a}, \boldsymbol{b}) = \prod_{i=1}^{N} p(\mathcal{Z}^{(i)}|\boldsymbol{s}_{0:L}, \boldsymbol{a}, \boldsymbol{b}), \tag{5.25a}$$

$$\propto \prod_{k=0}^{L} \prod_{i=1}^{N} p\left(\boldsymbol{z}^i_{[\boldsymbol{a}_k]_i}|\boldsymbol{s}_0, \boldsymbol{s}_k\right), \tag{5.25b}$$

$$\propto \prod_{k=0}^{L} v(\boldsymbol{a}_k, \boldsymbol{s}_0, \boldsymbol{s}_k), \tag{5.25c}$$

where, $p(\boldsymbol{z}^i_{[\boldsymbol{a}_k]_i}|\boldsymbol{s}_0, \boldsymbol{s}_k)$ is a Gaussian distributed variable, as per equation (5.21):

$$p(\boldsymbol{z}^i_{[\boldsymbol{a}_k]_i}|\boldsymbol{s}_0, \boldsymbol{s}_k) \propto \exp\big(- \|[\hat{\theta}^{(i)}_{[\boldsymbol{a}_k]_i}, \hat{\phi}^{(i)}_{[\boldsymbol{a}_k]_i}] - \boldsymbol{h}(\boldsymbol{s}_0, \boldsymbol{s}_k)\|_{\Sigma^{(i)}_{[\boldsymbol{a}_k]_i}}\big), \tag{5.26}$$

where $||\boldsymbol{x}||_{\boldsymbol{A}} = \boldsymbol{x}^T\boldsymbol{A}\boldsymbol{x}$ and $\boldsymbol{h}(\boldsymbol{s}_0, \boldsymbol{s}_k)$ is a nonlinear function transforming the location of the user $\boldsymbol{s}_0$ in the case of direct path and both the user $\boldsymbol{s}_0$ and the scatterer $\boldsymbol{s}_l$ in the case of non-direct path to the corresponding AoD and AoA variables.

Note that from equation (5.25b), one does not have the dependence on $\boldsymbol{b}$, as the equation (5.25a) is conditioned on the knowledge of both $\boldsymbol{a}$ and $\boldsymbol{b}$ and since $\boldsymbol{a}$ and $\boldsymbol{b}$ are injective-only, knowing one is enough to recover the other. The corresponding factor graph of the posterior distribution is given in Fig. 5.7.

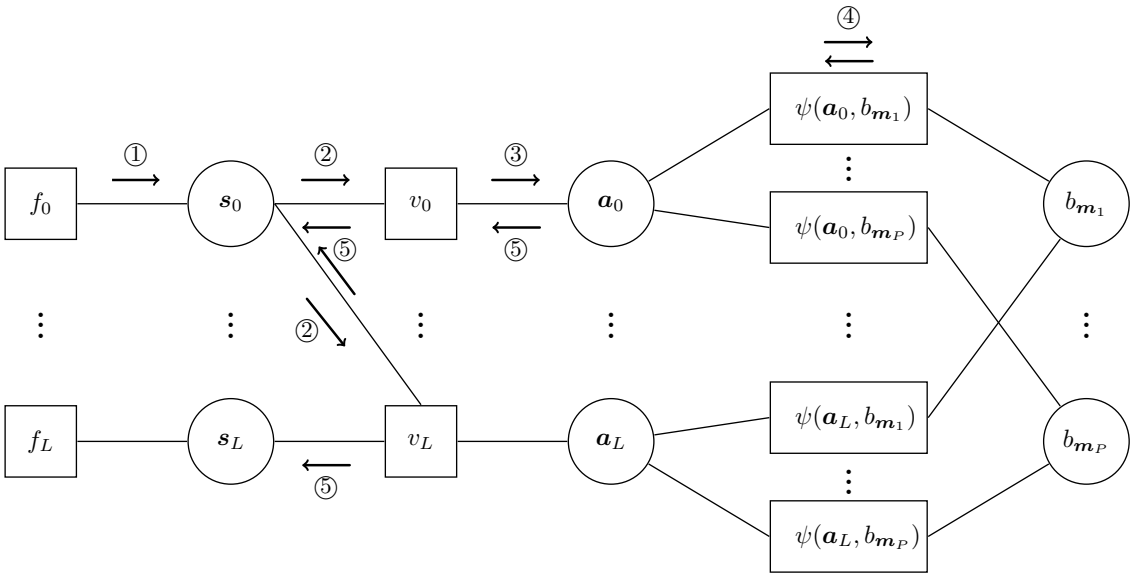

FIGURE 5.7: Factor graph representation of the posterior distribution in equation (5.23). In the graph, we have introduced the short form notation f_k to represent $p(s_k)$, v_k to represent $v(a_k, s_0, s_k)$ and $\boldsymbol{m}_p$, $p = 1, \cdots, P$ represents the p-th element of the set $\mathcal{M}$. The factor and variable nodes are represented inside squares and circles respectively.

5.5.3 Message passing via BP

BP for marginalization

We find the marginal $p(\boldsymbol{s}_k|\boldsymbol{Z})$ using the BP message passing algorithm on the factor graph [129], starting from the root nodes $p(\boldsymbol{s}_k)$ to the leaf node[12]. BP proceeds by passing messages between variables and factors defined by $\mu_{v\to f}(v)$ and $\mu_{f\to v}(v)$, respectively, where v is a variable and f is a factor. The marginal $p(\boldsymbol{s}_k|\boldsymbol{Z})$ can then be found as

$$p(\boldsymbol{s}_k|\boldsymbol{Z}) \propto \mu_{\boldsymbol{s}_k\to f}(\boldsymbol{s}_k) \times \mu_{f\to \boldsymbol{s}_k}(\boldsymbol{s}_k), \tag{5.27}$$

for any connected factor f.

Message passing schedule

We now show the message passing steps from the root nodes f_k through the nodes back to the leaf node f_k. The root node f_k or $p(\boldsymbol{s}_k)$ contains the a-priori distribution of the position of $\boldsymbol{s}_k$. In the following, we consider the indices $1 \leq k' \leq L$ and $0 \leq k \leq L$.

[12]Note that the factor graph in Fig. 5.7 consists of loops in between the variables $\boldsymbol{a}$ and $\boldsymbol{b}$. In such loopy cases, BP can still be used by passing the messages until the latter converge. Even though such convergence can not be guaranteed, it has been shown that this kind of method often arrives at a reasonable estimate [130].

① In the first step, we pass the a-priori distributions to the corresponding position variables.

$$\mu_{f_k \to \boldsymbol{s}_k}(\boldsymbol{s}_k) = f_k(\boldsymbol{s}_k). \tag{5.28}$$

② In the second step, we have no message from $\mu_{v_k \to \boldsymbol{s}_0}$ yet, so we initialize $\mu_{v_k \to \boldsymbol{s}_0} = 1, \forall k$. Hence, the messages from $\boldsymbol{s}_k$ to v_k can be written as:

$$\mu_{\boldsymbol{s}_0 \to v_k}(\boldsymbol{s}_0) = f_0(\boldsymbol{s}_0) \prod_{k' \neq k}^{L} \mu_{v_{k'} \to s_0}(\boldsymbol{s}_0) = f_0(\boldsymbol{s}_0), \tag{5.29a}$$

$$\mu_{\boldsymbol{s}_{k'} \to v_{k'}}(\boldsymbol{s}_{k'}) = f_{k'}(\boldsymbol{s}_{k'}). \tag{5.29b}$$

③ Next, we compute the outgoing messages from the factor node v_k to the variable node $\boldsymbol{a}_k$.

$$\mu_{v_0 \to \boldsymbol{a}_0}(\boldsymbol{a}_0) = \int v(\boldsymbol{a}_0, \boldsymbol{s}_0) \mu_{\boldsymbol{s}_0 \to v_0}(\boldsymbol{s}_0) \, \mathrm{d}\boldsymbol{s}_0, \tag{5.30a}$$

$$\mu_{v_{k'} \to \boldsymbol{a}_{k'}}(\boldsymbol{a}_{k'}) = \iint v(a_{k'}, \boldsymbol{s}_0, \boldsymbol{s}_{k'}) \mu_{\boldsymbol{s}_{k'} \to v_{k'}} \, \mathrm{d}\boldsymbol{s}_{k'} \, d\boldsymbol{s}_0. \tag{5.30b}$$

From equation (5.25c), we can see that v_k is already formulated as the product of distributions over all the BSs. Hence, in this step, the messages can be passed in a centralized way, unlike in [125] where the factor graph is formulated so that the messages need to be passed through each BS separately.

④ Then, we move the message forward to the data association loop. For notational simplicity, we represent the factor node $\psi(\boldsymbol{a}_k, b_m)$ by $\psi_{k,m}$. We start by initializing the messages $\mu^{(0)}_{\psi_{k,m} \to \boldsymbol{a}_k}(\boldsymbol{a}_k) = 1$. We can then execute multiple iterations. The message in the p-th iteration can be written as [126]:

$$\mu^{(p)}_{\boldsymbol{a}_k \to \psi_{k,\boldsymbol{m}}}(\boldsymbol{a}_k) = \mu_{v_k \to \boldsymbol{a}_k}(\boldsymbol{a}_k) \prod_{\boldsymbol{m}' \neq \boldsymbol{m}} \mu^{(p-1)}_{\psi_{\boldsymbol{m}',k} \to \boldsymbol{a}_k}(\boldsymbol{a}_k), \tag{5.31a}$$

$$\mu^{(p)}_{\psi_{k,\boldsymbol{m}} \to b_{\boldsymbol{m}}}(b_{\boldsymbol{m}}) = \sum_{\boldsymbol{a}_k} \psi_{k,\boldsymbol{m}} \mu^{(p)}_{\boldsymbol{a}_k \to \psi_{k,\boldsymbol{m}}}(\boldsymbol{a}_k), \tag{5.31b}$$

$$\mu^{(p)}_{b_{\boldsymbol{m}} \to \psi_{k,\boldsymbol{m}}}(b_{\boldsymbol{m}}) = \prod_{k' \neq k} \mu^{(p)}_{\psi_{k',\boldsymbol{m}} \to b_{\boldsymbol{m}}}(b_{\boldsymbol{m}}), \tag{5.31c}$$

$$\mu^{(p)}_{\psi_{k,\boldsymbol{m}} \to \boldsymbol{a}_k}(\boldsymbol{a}_k) = \sum_{\boldsymbol{b}_{\boldsymbol{m}}} \psi_{k,\boldsymbol{m}} \mu^{(p)}_{b_{\boldsymbol{m}} \to \psi_{k,\boldsymbol{m}}}(b_{\boldsymbol{m}}). \tag{5.31d}$$

⑤ After the data association loop, we have the message from $\boldsymbol{a}_k$ to v_k as:

$$\mu_{\boldsymbol{a}_k \to v_k}(\boldsymbol{a}_k) = \prod_{\boldsymbol{m}} \mu_{\psi_{k,\boldsymbol{m}} \to \boldsymbol{a}_k}(\boldsymbol{a}_k). \tag{5.32}$$

The next step is to calculate the messages $\mu_{v_k \to \boldsymbol{s}_k}(\boldsymbol{s}_k)$ and $\mu_{v_{k'} \to \boldsymbol{s}_0}(\boldsymbol{s}_0)$.

$$\mu_{v_0 \to \boldsymbol{s}_0}(\boldsymbol{s}_0) = \sum_{\boldsymbol{a}_0} v(\boldsymbol{a}_0, \boldsymbol{s}_0) \mu_{\boldsymbol{a}_0 \to v_0}(\boldsymbol{a}_0), \tag{5.33a}$$

$$\mu_{v_{k'} \to \boldsymbol{s}_0}(\boldsymbol{s}_0) = \int \sum_{\boldsymbol{a}_{k'}} v_{k'} \mu_{a_{k'} \to v_{k'}} \mu_{s_{k'} \to v_{k'}} \mathrm{d}\boldsymbol{s}_{k'}, \tag{5.33b}$$

$$\mu_{v_{k'} \to \boldsymbol{s}_{k'}}(\boldsymbol{s}_{k'}) = \int \sum_{\boldsymbol{a}_k} v_{k'} \mu_{a_{k'} \to v_{k'}} \mu_{\boldsymbol{s}_0 \to v_k} \mathrm{d}\boldsymbol{s}_0, \tag{5.33c}$$

where, $\mu_{\boldsymbol{s}_0 \to v_k}(\boldsymbol{s}_0) = \int \sum_{\boldsymbol{a}_0} v(\boldsymbol{a}_0, \boldsymbol{s}_0) \mu_{a_0 \to v_0}(\boldsymbol{a}_0) d\boldsymbol{s}_{k'}$.

⑥ Finally, the posterior beliefs can be computed as:

$$p(\boldsymbol{s}_0 | \boldsymbol{Z}) \propto \mu_{f_0 \to \boldsymbol{s}_0}(\boldsymbol{s}_0) \prod_k \mu_{v_k \to \boldsymbol{s}_0}(\boldsymbol{s}_0), \tag{5.34a}$$

$$p(\boldsymbol{s}_{k'} | \boldsymbol{Z}) \propto \mu_{f_{k'} \to \boldsymbol{s}_{k'}}(\boldsymbol{s}_{k'}) \mu_{v_{k'} \to \boldsymbol{s}_{k'}}(\boldsymbol{s}_{k'}). \tag{5.34b}$$

Particle implementation

As the integrals in the previous section cannot be solved in closed form, we approximate them using MC integration. Thereby we represent the messages as lists of weighted particles. We have to consider that the number of particles is enough to provide an accurate representation of the probability distributions and the weights are normalized such that their sum is 1. To compute the products in (5.34a)–(5.34b), we evaluate all messages only in the particles generated from the priors.

Centralized vs distributed approach

For benchmark purposes, we compare our proposed method against a distributed BP based SLAM method equivalent to that in [125][13]. For the distributed method, we introduce the set $\mathcal{M}_i = \{1, 2, \cdots, \hat{L}_i\}, \forall i$ for each i-th BS. We define $a_{k,i} \triangleq m_i \in \mathcal{M}_i$ indicating which measurement m_i corresponds to the source k at the i-th BS. Similarly, we define $b_{m_i,i} \triangleq k \in \{0, 1, \cdots, L\}$ indicating which source corresponds to the measurement m_i at the i-th BS. Note that contrarily to $\boldsymbol{a}_k$, $b_{\boldsymbol{m}}$ and $\boldsymbol{m}$ in our

[13] In the literature, it is common to consider such distributed methods especially for the data association problem [126, 131]

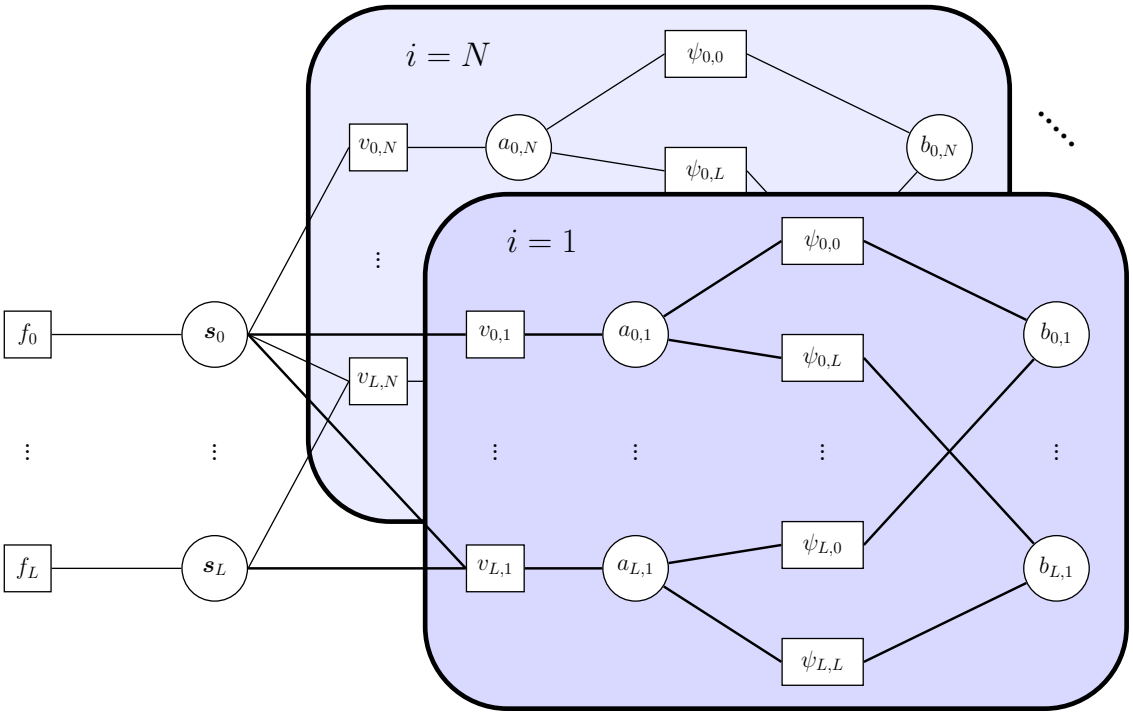

FIGURE 5.8: Factor graph with distributed BP (for performance comparison only). For notational convenience, $v_{k,i}$ represents $v(a_{k,i}, \boldsymbol{s}_0, \boldsymbol{s}_k)$ and $\psi_{k_1,k_2} = \psi(a_{k_1,i}, b_{k_2,i})$ $\forall i$.

proposed centralized methods, in this distributed method, $a_{k,i}$, $b_{m_i,i}$ and m_i are all scalars and the relation between a_i and b_i, the vector of data association variables, is in fact bijective. We further define

$$\Psi(\boldsymbol{a}, \boldsymbol{b}) = \prod_{i=1}^{N} \prod_{k=0}^{\hat{L}_i} \prod_{m_i \in \mathcal{M}_i} \psi(a_{k,i}, b_{m_i,i}). \tag{5.35}$$

where,

$$\psi(a_{l,i}, b_{m_i,i}) = \begin{cases} 0 & \boldsymbol{a}_{k,i} = m_i, b_{m_i,i} \neq k \text{ or } a_{k,i} \neq m_i, b_{m_i,i} = k, \\ 1 & \text{otherwise.} \end{cases} \tag{5.36}$$

Hence, following a formulation similar to the posterior distribution as (5.23), we can build a factor graph as illustrated in Fig. 5.8. We can compute the beliefs and accordingly the marginal similarly to the previous section.

5.5.4 Numerical results

In this section, we describe the simulation setup and parameters and then show the simulation of our proposed method. To benchmark our result, we then compare

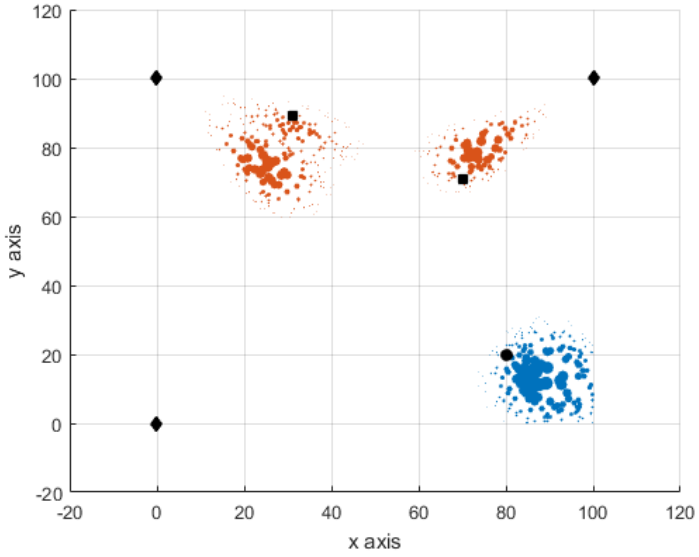

FIGURE 5.9: Marginal distribution with $\sigma_\theta^2 = \sigma_\phi^2 = 1$ deg^2 with the proposed method. The diamonds, squares and circle represent the true positions of the 3 BSs, 2 scatterers and the user respectively.

with a model inspired by the distributed BP approach in [125] shown on Fig. 5.8.

5.5.5 System parameters and simulation setup

We consider a scenario with $N = 3$ BSs, $L = 2$ scatterers and a user where all the BSs can measure all three paths (*i.e.* $\hat{L}_i = 3, \forall i$). We consider the locations of BSs are known with $\boldsymbol{x}_1 = [0, 0]$, $\boldsymbol{x}_2 = [0, 100]$, $\boldsymbol{x}_3 = [100, 100]$, whereas the user and the scatters are uniformly distributed within an area of 100 m $\times$ 100 m area.

We assume that the measurement covariance matrix is a diagonal matrix with the variance of estimating AoD σ_θ^2 equal to the variance of estimating the AoA σ_ϕ^2 for all the measurements. Similarly, while simulating the BP algorithm, we consider $N_{s_0} = N_{s_{k'}} = 2500$ particles (50 per dimension) to represent the distributions of the user and the scatterers.

In our simulations, we assume no prior knowledge of the positions of either the user or the scatterers and hence, we consider they are uniformly distributed within the deployment area. Hence, to replicate $p(\boldsymbol{s}_0)$ as particles, we can draw N_{s_0} sample points of $\boldsymbol{s}_0$ from the specified domain and assign the corresponding probability as weights, in this case a constant (and accordingly for $p(s_{k'})$).

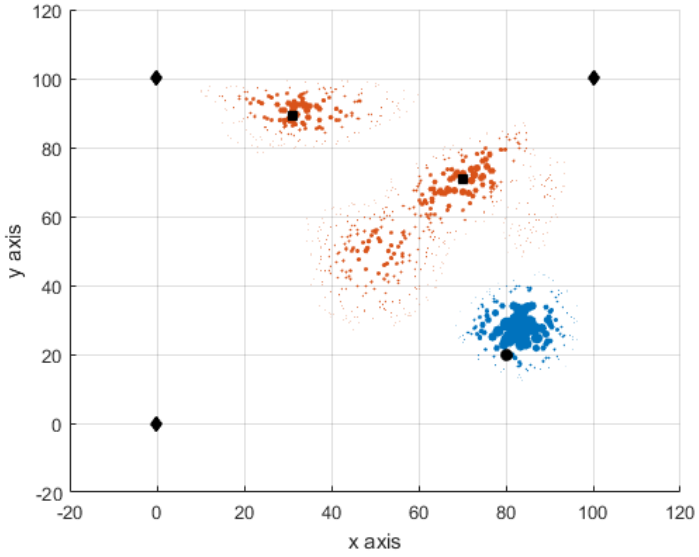

FIGURE 5.10: Marginal distribution with $\sigma_\theta^2 = \sigma_\phi^2 = 1$ deg^2 with the distributed method [125]. The diamonds, squares and circle represent the true positions of the 3 BSs, 2 scatterers and the user respectively.

5.5.6 Results and analysis

In Figs. 5.9 and 5.10, we plot the marginal distributions of the user and the scatterers with blue and orange scatter points, as formulated in equations (5.34a) and (5.34b) respectively. Since, as said earlier, we are dealing with particles rather than the continuous distribution, the size of blue and orange circles represents the weights associated with the corresponding particles. We also plot the true positions of the BSs, the scatterers and the user for comparison. Between the two figures, we can clearly see that the particle clouds in our proposed method can separate the two scatterers and the user unlike the distributed BP. The reason is that in our method, as we can deduce from equation (5.25b), only the particles with non zero probabilities according to equation (5.21) with respect to all the BSs are passed on from the factor $\boldsymbol{v}$ to the variable $\boldsymbol{a}$ in the factor graph. Hence, in this step, before the data association loop, we do some sort of initial filtering with respect to all the BSs. On the contrary, in the distributed method, the filtering is done with respect to only one single BS before the data association loop, and then further filtering is done later during the collection while passing the message from v_k to $\boldsymbol{s}_k$. Filtering before the loop reduces the propagation of any error during the data association loop.

Following this discussion, in Fig. 5.11, we plot the empirical CDF of the root mean squared error (RMSE) between the true and estimated positions of the user and scatterers. We calculate the RMSE by taking the distance between the true

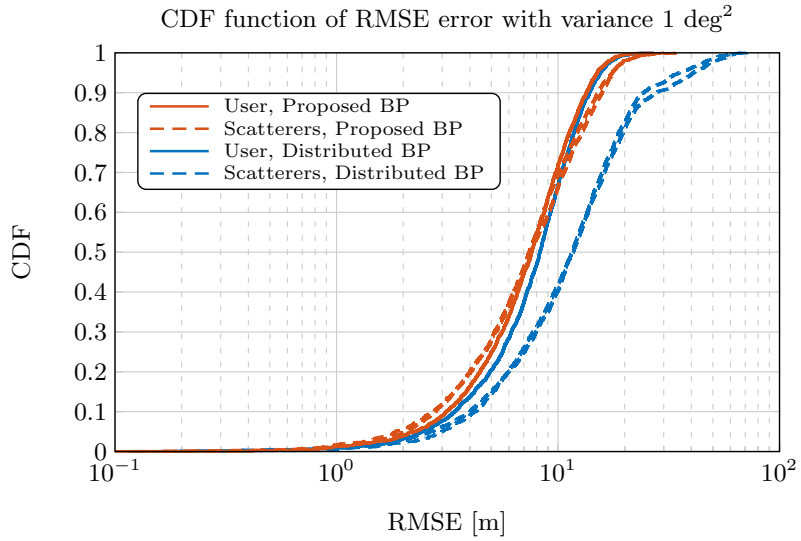

FIGURE 5.11: CDF plot comparison of the RMSE error between the proposed centralized and the distributed BP based methods with 1 deg^2 variance.

and the mean particle position. As we can see, the proposed centralized method performs better than the distributed method especially when it comes to estimating the position of the scatterer due to the limited error propagation in the data association phase.

Regarding the total number of messages between the two approaches, in the distributed method, we pass $\mathcal{O}(NL^2)$ messages, versus in the centralized approach $\mathcal{O}\left(L^{N+1}\right)$ messages. Hence, the centralized approach has better performance and low communication overhead, but at the price of a higher complexity cost. The distributed method exhibits less complexity, but requires the exchange of particle clouds among BSs.

5.6 Chapter conclusions

In this chapter we considered two different applications leveraging on the the multipath angles estimation, namely channel estimation and SLAM.

Firstly, we presented a low latency solution for channel estimation in the context of mm-Wave systems, with the aid of AoD and AoA information. Exploiting the inherently sparse properties of the mm-Wave channel, where the number of multipath components is limited, we showed that the localization based method outperforms other existing methods such as the exhaustive and iterative multi-resolution search based channel estimation approaches. Simulation results in a canonical scenario illustrated some latency gains accordingly.

One of the limitations of our channel estimation algorithm in comparison with the two existing methods is that we still need to have a means of measuring the angles corresponding to each paths.

Secondly, we proposed a BP based method to solve the problem of mm-Wave SLAM using only angular measurements in a system with multiple BSs and scatterers and a user node. To reach this objective, we firstly formulated the corresponding posterior distribution and then the factor graph including the problem of data association. By running the message passing algorithm in the graph, numerical results demonstrated that even without any a-priori distribution on the positions of the user and the scatterers, one can achieve relatively high accuracy. In comparison with methods from the literature where the data association problem is solved in a distributed manner separately at different BSs and requiring additional range measurements, we showed that our centralized data association approach provides a better estimation accuracy, mostly in terms of scatterers positioning.

Regarding our work on SLAM, as a future work we would like to consider a model including uncertainty in the user orientation and false alarms (*i.e.*, the fact that observed AoA measurements may not result from any of the modeled scattering points), which would provide an even more realistic assessment of the problem. In future, one could also consider coupling even more tightly the proposed mm-Wave multipath channel estimation method of section 5.4 with angle-based simultaneous localization and mapping algorithms from section 5.5.

Chapter 6

Conclusions and future perspectives

6.1 Main conclusions

In conclusion, the mm-Wave technology makes a strong case for accommodating the arduous demands of low latency high data rate services for 5G, but is thwarted by the propagation characteristics at such high frequencies. To remedy this propagation problem and thus enable mm-Wave for 5G, localization and location-aided directionality can both play a crucial role. In addition, some of the properties of mm-Wave communications are highly suitable for localization, generating an important interdependence of the two ingredients. Motivated by this importance of directionality in mm-Wave and the symbiotic relationship between the two functionalities, in this thesis, we investigated how to facilitate this interdependence and beyond, how to improve synergies between the two functionalities.

We started out by firstly exploring the relationship between beamforming and localization in chapter 2. We characterized the optimal beamforming, specifically optimal beam alignment, while minimizing different localization error cost functions firstly in a simple single-user single carrier scenario and then later in a multi-user scenario with multiple subcarriers. The localization optimal beamformer was later used in chapter 3 in order to characterize the localization-communication trade-off. The considered localization error cost functions were characterized as functions of the CRLBs of various estimated location-dependent radio estimates. The optimization provides the necessary freedom to adjust on-demand the underlying transmit waveform, as well as to iteratively refine localization performances regardless of the users' location (and thus possibly, to enable a spatially homogeneous quality of service). Moreover, by exploiting the frequency diversity over the multiple subcarriers by means of a power allocation scheme, we also illustrated the critical effect of frequency on localization. In the multi-user case, we also looked into different ways in which the beam power can be allocated to each user depending on different fairness criteria.

After tackling the localization optimal beamforming problem, we then investigated the possibility of integrating localization and communication functionalities in the same system in chapter 3. In this regard, we considered two distinct possibilities, depending if one service explicitly takes the input from another (joint services), or not (standalone services). In the standalone case, we studied the trade-off between the data and localization services while budgeting time and frequency resources in a multi-user scenario. Allocating more resources for the data communication phase instead of localization implies, forthrightly, a higher data rate but, concurrently, also higher localization error bounds (PEB and OEB). In the latter case, we studied the scenario when the two services are integrated jointly in a system and hence impact the performance of each other. In this case, we not only look at time and frequency resource sharing like in the first scenario, but also assess the impact of localization accuracy on the communication phase in terms of the rate coverage probability which is impacted by localization estimation induced beam alignment errors. Unlike the previous scenario, in this case the trade-off was intricate as the communication performance does not only rely on allocating more resource but also on accurate beam alignment which in turn leads to a better localization performance. We concluded this chapter by raising the need for not only proper beam alignment, as suggested in chapter 2, and optimal time/frequency resource allocation, but also a proper beamwidth optimization.

Motivated by the previous study, we then, in chapter 4, proposed an optimal beamwidth selection policy maximizing the rate coverage performance of a mmWave network in a joint localization and communication context. We formulated the localization performance and consequently the beam alignment errors at both BS and UE in terms of performance bounds of delay and AoA estimation. Based on these alignment errors, we first characterized the downlink rate performance (in terms of rate coverage probability) of a network deployed along the streets of an urban environment, before characterizing the previously mentioned non-trivial trade-off. Based on this trade-off, we described an optimal beamwidth selection strategy. Additionally, we also investigated the localization-based initial beam selection problem as a part of the initial access scheme. We proposed an iterative beam alignment and width based initial access assisted by the performance bounds of delay and AoA estimates. In comparison with state-of-the-art contributions, this new method significantly reduces the beam selection overhead which can be crucial to many 5G applications.

Finally, in chapter 5, we presented two distinct applications of localization (in particular AoD and AoA estimation) namely multipath channel estimation and

SLAM which, in turn, could both aid further mm-Wave communications. Firstly, it is crucial to understand the channel between the transmitter and the receiver as it can be beneficial to both localization and communication functionalities. Hence, we exploited localization and the iterative beam alignment and width adjustment algorithm, similarly to the one implemented during the initial access phase, to capture the geometric and sparse nature of the multipath mm-Wave channel. We showed that using localization instead of the conventional beam sweeping based beam training models allows us to significantly reduce the channel estimation duration to maintain an estimation quality. We then looked into SLAM techniques while using only AoD and AoA information to estimate the positions of the mobile user and different scatterers in order to map the environment in a multi-BS scenario. We considered a factor-graph representation of the SLAM problem (including data association between the observed angle measurements and their "scattering sources") and used a message passing algorithm in the form of BP to show that we can obtain a good localization performance even while not utilizing the distance measurements. We showed that with our method, we can estimate the positions more accurately than equivalent decentralized message passing techniques, while also reducing communication overhead.

Overall, in our thesis, we presented different aspects of the intricate relationship between localization and communications in mm-Wave systems and showed these functionalities can be beneficial to each other at different stages of the block diagram introduced on Fig. 1.7 in chapter 1.

6.2 Future perspectives

This thesis paves the way for several future directions of research, some of which are discussed in this section.

6.2.1 Channel and signal assumptions

In our work, we have made different assumptions regarding the mm-Wave channel model and such assumptions can be improved in the future.

- **Channel coefficients:**

  In chapters 2 and 3, we considered a frequency flat channel coefficient. Considering a frequency dependent channel model in chapter 2 would introduce a new dimension to the power allocation problem across the subcarriers. In contrast to just allocating the power at the extremities of the spectrum, we would also

need to consider the channel strength at each subcarrier and jointly decide on giving preference to certain subcarriers. Similarly, in section 3.4.2 of chapter 3, we considered the allocation of localization oriented pilots on the extremities of the spectrum. Like in the previous case, with the frequency dependent channel coefficient, we need to further optimize the subcarriers to allocate the pilots, in this case not only for localization but also for communication. The subcarrier allocation would also depend upon the QoS requirement for both data communication and localization phases.

- **Multipath exploitation:**

  Likewise, in chapters 2, 3 and 4, we have considered a simplistic channel model with only the direct path. Considering that, firstly, there are only few dominant paths in mm-Wave channel and secondly, the beams are narrow (such as in the above mentioned chapters), we can assume that the direct path is the only dominant path [58, 65]. However, considering a multipath channel model, similarly to chapter 5, we can improve both localization and communication performances especially in the case of blockages. Under NLOS conditions, in chapter 2, we could optimally align the beam with respect to an alternative path in case of blockage to avoid outage. Similarly, in the initial access algorithm, one can exploit the multipath in conjunction with AoD estimation to reduce beam alignment errors in case of blockages and instead rely on alternative paths rather than proceeding with larger beamwidth due to degraded localization performances. Similarly, the reduced beam alignment error would improve the SINR and rate coverage performance in chapters 3 and 4.

- **Blockage model:**

  Blockages play an important role in the context of mm-Wave as we have already described in chapter 1. Hence, it is important that in the future we accurately model the blockage in our analyses. For instance, in chapter 2, we did not consider any blockage model. In the future, in conjunction with the previously mentioned multipath channel model, we can incorporate the blockage model in order to find the optimal beamforming. For instance, a relevant beamforming strategy could consist in transmitting multiple beams corresponding to the different paths to avoid blockage, or alternatively, performing continuously multipath channel estimation in order to timely switch the main beam from the missing direct path to a significant secondary path. In the second part of chapter 3 and chapter 4, we however model the blockage

with a LOS ball model which is popular in the mm-Wave literature due to its simplicity[82, 98]. In the future, we can choose a more accurate model, for instance the ones recommended in the technical report (Release 14) of 3GPP [53] where both self (human) and dynamic (vehicles) blockages are modelled.

- **Interference in localization:**

  Similarly, in the context of interference at the user from multiple BSs, we have considered it only in the communication phase. However, in the case of localization, since we considered that the BSs use orthogonal resources for transmitting the localization pilots in chapters 3 and 4, we assume no interference, also in line with other works in the literature. The assumption was made with the expectation that even though interference would indeed degrade the localization performance, the trends of beam alignment error and accordingly the rate coverage performance would still stay the same. Consequently, the insights derived from the work would still be crucial despite the simplification. For deriving more accurate conclusions however, the derivation of the CRLB for the estimation of location-dependent variables in presence of interference and its subsequent impact on communication performance could be an interesting axis of research.

- **Sectorized beamforming model:**

  In chapters 3, 4 and 5 we have considered a sectorized beamforming model for simplicity. It is common in the literature to make such simplifications [56, 82, 99]. One problem in contrast to more realistic beamforming models is that all the beamwidths cannot be supported depending on the antenna array used and hence we have to resort to an approximation such as in [90] and [91]. Hence, the performance while considering such assumptions may not exactly match the figures of the reality, even though it gives a good idea of the trends. Hence, in the future, it would be more interesting to extend our analysis considering realistic beamforming models like in chapter 2.

- **Antenna architecture:**

  In our work, we have considered the analog beamforming architecture, given its low power consumption and its relatively low hardware complexity compared to hybrid and digital architectures. The downside of the analog architecture however is the inability to multiplex multiple streams of data for multiple users at the same time owing to its single RF chain. Hence, the hybrid architecture has been recently gaining popularity in the literature. Due

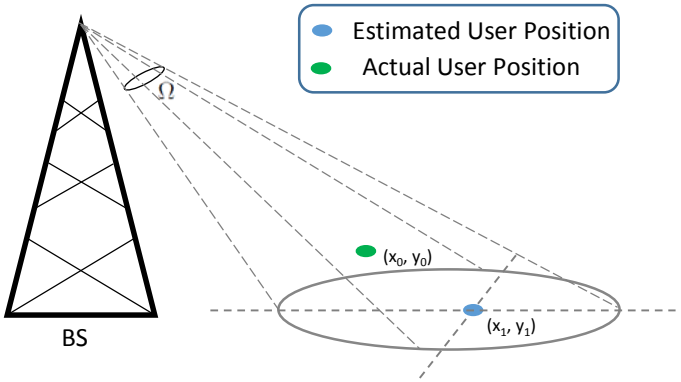

FIGURE 6.1: Extension of the beam-selection error model into two dimensions.

to the channel sparsity in mm-Wave, only a few RF chains are required for having a complete access to the dominant paths, and hence it is still within reasonable power and complexity constraint. Thus, in the future, it could be worth envisaging an architecture endowed with multiple RF chains so as to fully exploit this diversity in the context of both localization and communication.

6.2.2 Scenario assumptions

- **1D vs 2D model:**

  In chapters 3 and 4, we considered a one dimensional model for emulating the mm-Wave network inspired from the network operators' plans to deploy the first generation of mm-Wave small cells along the roads in urban areas. As an example, let us note that Verizon has announced plans to deploy 5G on 101 street lights in Sacramento, focused on fixed broadband service with plans of offering mobile service later [132]. Similarly, AT&T has announced plans to deploy 5G on 170 outdoor small cells on lamp posts in San Jose for mobile access [133]. In such scenarios, the stochastic geometry based one dimensional model assumed in our thesis can be utilized by a network operator to derive system design insights and use them as a starting point to further fine-tune the deployment and the operational parameters.

  However, our work can be extended in the 2D case with the beam coverage as shown in Fig. 6.1 in an area defined by the solid angle Ω and can be an interesting axis of work for the future. Such beams can be supported by a planar array.

  To be more concrete, we can can take the example of the beam selection error, and show how the concepts developed in this thesis can be extended. In the

2D case, the beam-selection error for a user (see Fig. 6.1) can be defined as the probability that the actual location of the user (x_0, y_0) is outside the beam selected according to the estimated position (x_1, y_1). In a similar way, the other concepts that are developed in this thesis, such as the beam dictionary, misalignment error probability, SINR coverage probability, and the initial access procedure can be extended for the 2D case.

- **Equal heights of the BSs:**

  Our network model in chapters 3 and 4 follows from the development that Verizon and AT&T have both announced plans to deploy 5G infrastructure on lampposts for fixed wireless network [132] and mobile access [133], respectively. Accordingly, we have assumed that the height of the lampposts (and consequently, the BSs) are the same throughout the network. However, the consideration of different heights can be an interesting aspect to study in our network for future works. Specifically, with a BS installed at a higher altitude would have a larger geographical coverage, but at the cost of reduced power at the users. In our model, the effect of varying the height can be incorporated by either an assumption on the distribution of the heights of instalment, or by assuming a discrete set of installation heights.

- **Mobility model:**

  The issue of mobility is a very important aspect for communication networks in general, and a fortiori for mm-Wave networks. In this context, it would be worth revisiting again both beam alignment and beamwidth selection problems accordingly. Hence, in the context of all the chapters, adding mobility model on top of our framework would provide interesting ideas for future work. We can integrate a user (and even scatterers in a multipath model) tracking algorithm that can be used to have continuous position information at various time instances running on top of the proposed framework, without any deep modification of the latter. In this regard, Bayesian filters such as Extended Kalman filters or particle filters (*e.g.*, [134, 135]) are popular tools for tracking the evolution of localization variables and/or user's position. Estimating user position with respect to mobility directly impacts the variance of the estimated localization variables (assumed a priori in our algorithms), that could be taken into account while considering the beam selection errors and accordingly the beam width and alignment optimization. In addition, the position estimates based on the channel estimation and SLAM approaches proposed in chapter 5 can be an input to tracking algorithms, similarly to [134].

Regarding the work on SLAM in chapter 5, we could further incorporate the mobility model according to some dynamic state space characterization of the user mobility. Such model in the context of SLAM has been implemented in [125] in the vehicular context. In such cases, we would have an iterative factor-graph formulation, for each time index, feeding from the both the location information from the previous time stamp and the new measurements.

However, again, it is important to note that this neither imposes any deep modification of the proposed method in our thesis, nor contradict related findings in terms of performance. In other words, we believe UE tracking and location-based beam optimization are not mutually exclusive but on the contrary, the former could even be further beneficial to the latter in future variants of our solution.

- **Localization algorithms:**

  In our work, we considered the different techniques to estimate location-dependent variables from the literature. Although we can treat the channel estimation as a localization estimation problem similarly to [51], we have no specific localization algorithm has been explicitely designed in the very context. For instance, for delay estimation, we could rely on generic methods and metrics such as RSSI, ToA or TDoA. Similarly, for AoD and AoA estimations we considered mainly AoA estimation algorithms such as MUSIC or ESPRIT in uplink and downlink respectively.

  Hence, it would be also interesting to investigate more specific algorithms, that can in turn act as an input to beamforming and thus to the initial access, resource allocation, channel estimation and SLAM procedures. One could further use the algorithm and hence the estimates of the location dependent variables in conjunction with the classical positioning algorithms such as trilateration or triangulation in order to position the user and the scatterers.

6.2.3 Experimental validations

A selection of the solutions reported in this thesis could be validated experimentally, relying on the complete mm-Wave proof-of-concept system currently under development at CEA-Leti. The latter includes hardware antenna systems (*e.g.*, integrated steerable transmit arrays) in the Ka band (ranging from 17.7 – 21.2 GHz and 27.5 – 31.0 GHz) [136, 137]. This would also offer new opportunities for the exploitation of yet largely under exploited features such as tunable antenna polarization, which

could be beneficial when interpreting the received signal from a localization perspective (thus enriching further the localization estimation and mapping problems accordingly). An adaptation of our algorithmic proposals, as well as a revision of a few related working assumptions, would be also needed (*e.g.*, assuming quantized phase terms, and other real RF impairments or implementation characteristics). In terms of tested environments and scenarios, one could consider a gradually complex and controlled approach. As a starting point, preliminary tests could be conducted within an anechoic chamber, mostly for functional validation purposes. Then, more realistic operating contexts could be envisaged, such as urban in-street vehicular scenarios. In the latter case specifically, since antenna arrays are strapped onto the car body, the car's absolute orientation could be derived directly out of AoA estimation with respect to a BS (or a mm-Wave-enabled Road Side Unit). Moreover, the limited degrees of freedom in terms of car attitude and movement (i.e., resulting in a constrained pseudo-2D problem) is expected to simplify both angular estimation and user tracking problems. Finally, generally, the localization functionality could be assisted from extra on-board sensors and navigation systems (GPS, odometry, IMU), for instance while assuming coarse a priori location information in our initial access approach and/or simply for redundancy purposes.

Appendix A

Proofs of chapter 2

A.1 Proof that coefficients $k_1 > 0$ and $k_2 > 0$

To prove that the coefficients k_1 and k_2 in equations (2.10) and (2.12) are always positive, we have to prove that $\alpha\beta - \gamma^2 \geq 0$ and hence

$$N_r\zeta_2 > \zeta_1^2, \tag{A.1}$$

where ζ is defined in (2.13). From this definition,

$$N_r\zeta_2 = \frac{N_r^2(N_r+1)(2N_r+1)}{6}. \tag{A.2}$$

Similarly,

$$\zeta_1^2 = \frac{N_r^2(N_r+1)^2}{4}. \tag{A.3}$$

Comparing the above two equations,

$$N_r\zeta_2 \gtreqless \zeta_1^2, \tag{A.4a}$$

$$4N_r + 2 \gtreqless (3N_r+1) + 2. \tag{A.4b}$$

Then, $4N_r > 3N_r + 1$ and k_1 and k_2 are positive for all $N_r > 1$ as a consequence.

A.2 Proof that $\boldsymbol{x}^T\boldsymbol{Z}\boldsymbol{x} > 0$

It has been established that $\boldsymbol{Z} \in \mathbb{R}^{N\times N}$. Let (n_p, n_q) be any component of the matrix $\boldsymbol{Z}$. It is

$$\boldsymbol{Z}(n_p, n_q) = \alpha\beta\frac{n_p^2}{\lambda_{n_q}^2} - \gamma^2\frac{n_p n_q}{\lambda_{n_p}\lambda_{n_q}}, \tag{A.5a}$$

$$\boldsymbol{Z}(n_q, n_p) = \alpha\beta\frac{n_q^2}{\lambda_{n_p}^2} - \gamma^2\frac{n_q n_p}{\lambda_{n_q}\lambda_{n_p}}. \tag{A.5b}$$

In the term $\boldsymbol{x}^T\boldsymbol{Z}\boldsymbol{x}$, the coefficient of $x_{n_p}x_{n_q}$ is given by

$$\boldsymbol{Z}(n_p, n_q) + \boldsymbol{Z}(n_q, n_p), \tag{A.6a}$$

$$= \frac{(\alpha\beta - \gamma^2)(n_p^2\lambda_{n_p}^2 + n_q^2\lambda_{n_q}^2) + (\gamma n_p\lambda_{n_p} + \gamma n_q\lambda_{n_q})^2}{\lambda_{n_p}^2\lambda_{n_q}^2}. \tag{A.6b}$$

Since $\alpha\beta - \gamma^2 \geq 0$ (from Appendix A.1) for $N_r > 1$, we can say that $\boldsymbol{x}^T\boldsymbol{Z}\boldsymbol{x}$ is always positive.

A.3 Components of the FIM per sub-carrier

Let $\boldsymbol{F}_n = \boldsymbol{f}_n\boldsymbol{f}_n^H$ and $\dot{\boldsymbol{a}}_{\mathrm{Tx},u} = d\boldsymbol{a}_{\mathrm{Tx},u}/d\theta$. By assuming the centroid of the antenna array as the reference point in equation (2.25), we have the relation $\boldsymbol{a}_{\mathrm{Tx}}^H\boldsymbol{F}\dot{\boldsymbol{a}}_{\mathrm{Tx}} = 0$ similar to [59, 72]. Hence, the components of the FIM in equation (2.27), are as

follows.

$$\psi_n(\tau_u,\tau_u) = 4\pi^2\rho_{u,n}\frac{n^2B^2}{N^2}|h_u|^2 d_{0,u}\boldsymbol{a}^H_{\mathrm{Tx},u}\boldsymbol{F}_n\boldsymbol{a}_{\mathrm{Tx},u}, \tag{A.7a}$$

$$\psi_n(\tau_u,\theta_u) = 2\pi\rho_{u,n}\frac{nB}{N}|h_u|^2 d_{0,u}\Re\{j\dot{\boldsymbol{a}}^H_{\mathrm{Tx},u}\boldsymbol{F}_n\boldsymbol{a}_{\mathrm{Tx},u}\}, \tag{A.7b}$$

$$\psi_n(\tau_u,\phi_u) = 2\pi\rho_{u,n}\frac{nB}{N}|h_u|^2 d_{1,u}\Re\{j\boldsymbol{a}^H_{\mathrm{Tx},u}\boldsymbol{F}_n\boldsymbol{a}_{\mathrm{Tx},u}\}, \tag{A.7c}$$

$$\psi_n(\tau_u,h_{R,u}) = 2\pi\rho_{u,n}\frac{nB}{N}d_{0,u}\Re\{jh^*_u\boldsymbol{a}^H_{\mathrm{Tx},u}\boldsymbol{F}_n\boldsymbol{a}_{\mathrm{Tx},u}\}, \tag{A.7d}$$

$$\psi_n(\tau,h_{I,u}) = -2\pi\rho_{u,n}\frac{nB}{N}d_{0,u}\Re\{h^*_u\boldsymbol{a}^H_{\mathrm{Tx},u}\boldsymbol{F}_n\boldsymbol{a}_{\mathrm{Tx},u}\}, \tag{A.7e}$$

$$\psi_n(\theta_u,\theta_u) = \rho_{u,n}|h_u|^2 d_{0,u}\dot{\boldsymbol{a}}^H_{\mathrm{Tx},u}\boldsymbol{F}_n\dot{\boldsymbol{a}}_{\mathrm{Tx},u}, \tag{A.7f}$$

$$\psi_n(\theta_u,\phi_u) = 0, \tag{A.7g}$$

$$\psi_n(\theta_u,h_{R,u}) = 0, \tag{A.7h}$$

$$\psi_n(\theta_u,h_{I,u}) = 0, \tag{A.7i}$$

$$\psi_n(\phi_u,\phi_u) = \rho_{u,n}|h_u|^2 d_{2,u}\boldsymbol{a}^H_{\mathrm{Tx},u}\boldsymbol{F}_n\boldsymbol{a}_{\mathrm{Tx},u}, \tag{A.7j}$$

$$\psi_n(\phi_u,h_{R,u}) = \rho_{u,n}\Re\{h_u d_{1,u}\}\boldsymbol{a}^H_{\mathrm{Tx},u}\boldsymbol{F}_n\boldsymbol{a}_{\mathrm{Tx},u}, \tag{A.7k}$$

$$\psi_n(\phi_u,h_{I,u}) = \rho_{u,n}\Im\{h_u d_{1,u}\}\boldsymbol{a}^H_{\mathrm{Tx},u}\boldsymbol{F}_n\boldsymbol{a}_{\mathrm{Tx},u}, \tag{A.7l}$$

$$\psi_n(h_{R,u},h_{R,u}) = \rho_{u,n}d_{0,u}\boldsymbol{a}^H_{\mathrm{Tx},u}\boldsymbol{F}_n\boldsymbol{a}_{\mathrm{Tx},u}, \tag{A.7m}$$

$$\psi_n(h_{R,u},h_{I,u}) = 0, \tag{A.7n}$$

$$\psi_n(h_{I,u},h_{I,u}) = \rho_{u,n}d_{0,u}\boldsymbol{a}^H_{\mathrm{Tx},u}\boldsymbol{F}_n\boldsymbol{a}_{\mathrm{Tx},u}, \tag{A.7o}$$

where, $\rho_{u,n} = 2P_{Tx,u}T_s\xi_u|s_n|^2/N_0$, h^*_u is the complex conjugate of the channel coefficient, and

$$d_{0,u} = \left|\left|\boldsymbol{w}^H_u\boldsymbol{a}_{\mathrm{Rx},u}\right|\right|^2_2, \tag{A.8a}$$

$$d_{1,u} = \boldsymbol{a}_{\mathrm{Rx},u}\boldsymbol{w}^H_u\frac{d}{d\phi}\boldsymbol{w}^H_u\boldsymbol{a}_{\mathrm{Rx},u}, \tag{A.8b}$$

$$d_{2,u} = \left|\left|\frac{d}{d\phi}\boldsymbol{w}^H_u\boldsymbol{a}_{\mathrm{Rx},u}\right|\right|^2_2. \tag{A.8c}$$

A.4 Components of the FIM for all the sub-carriers

For the multiple sub-carrier case, we take advantage of the symmetry of the sub-carriers, beamformers, combiners and the data s_n to formulate the FIM as follows.

$$\psi(\tau_u, \tau_u) = 4\pi^2 \sigma_u \frac{B^2}{N^2} |h_u|^2 d_{0,u} \boldsymbol{a}_{\mathrm{Tx},u}^H \boldsymbol{X}_\tau \boldsymbol{a}_{\mathrm{Tx},u}, \tag{A.9a}$$

$$\psi(\tau_u, \theta_u) = 0, \tag{A.9b}$$

$$\psi(\tau_u, \phi_u) = 0, \tag{A.9c}$$

$$\psi(\tau_u, h_{R,u}) = 0, \tag{A.9d}$$

$$\psi(\tau, h_{I,u}) = 0, \tag{A.9e}$$

$$\psi(\theta_u, \theta_u) = \sigma_u |h_u|^2 d_{0,u} \dot{\boldsymbol{a}}_{\mathrm{Tx},u}^H \boldsymbol{X} \dot{\boldsymbol{a}}_{\mathrm{Tx},u}, \tag{A.9f}$$

$$\psi(\theta_u, \phi_u) = 0, \tag{A.9g}$$

$$\psi(\theta_u, h_{R,u}) = 0, \tag{A.9h}$$

$$\psi(\theta_u, h_{I,u}) = 0, \tag{A.9i}$$

$$\psi(\phi_u, \phi_u) = \sigma_u |h_u|^2 d_{2,u} \boldsymbol{a}_{\mathrm{Tx},u}^H \boldsymbol{X} \boldsymbol{a}_{\mathrm{Tx},u}, \tag{A.9j}$$

$$\psi(\phi_u, h_{R,u}) = \sigma_u \Re\{h_u d_{1,u}\} \boldsymbol{a}_{\mathrm{Tx},u}^H \boldsymbol{X} \boldsymbol{a}_{\mathrm{Tx},u}, \tag{A.9k}$$

$$\psi(\phi_u, h_{I,u}) = \sigma_u \Im\{h_u d_{1,u}\} \boldsymbol{a}_{\mathrm{Tx},u}^H \boldsymbol{X} \boldsymbol{a}_{\mathrm{Tx},u}, \tag{A.9l}$$

$$\psi(h_{R,u}, h_{R,u}) = \sigma_u d_{0,u} \boldsymbol{a}_{\mathrm{Tx},u}^H \boldsymbol{X} \boldsymbol{a}_{\mathrm{Tx},u}, \tag{A.9m}$$

$$\psi(h_{R,u}, h_{I,u}) = 0, \tag{A.9n}$$

$$\psi(h_{I,u}, h_{I,u}) = \sigma_u d_{0,u} \boldsymbol{a}_{\mathrm{Tx},u}^H \boldsymbol{X} \boldsymbol{a}_{\mathrm{Tx},u}, \tag{A.9o}$$

where,

$$\sigma_u = \frac{2 P_{\mathrm{Tx},u} T_s \xi_u}{N_0}, \tag{A.10}$$

and $\boldsymbol{X}_\tau = \sum_{n=-N/2}^{N/2} |s_n|^2 n^2 \boldsymbol{F}_n$, and $\boldsymbol{X} = \sum_{n=-N/2}^{N/2} |s_n|^2 \boldsymbol{F}_n$.

A.5 Derivation of localization error

From equation (2.28), we have the FIM matrix as:

$$\boldsymbol{J}_u = \left(\begin{array}{cc|ccc} \psi(\tau_u,\tau_u) & 0 & 0 & 0 & 0 \\ 0 & \psi(\theta_u,\theta_u) & 0 & 0 & 0 \\ \hline 0 & 0 & \psi(\phi_u,\phi_u) & \psi(\phi_u,h_{R,u}) & \psi(\phi_u,h_{I,u}) \\ 0 & 0 & \psi(\phi_u,h_{R,u}) & \psi(h_{R,u},h_{R,u}) & 0 \\ 0 & 0 & \psi(\phi_u,h_{I,u}) & 0 & \psi(h_{I,u},h_{I,u}) \end{array}\right) \tag{A.11a}$$

$$= \left(\begin{array}{c|c} \boldsymbol{\psi}_{1,u} & \boldsymbol{0}_{2\times 3} \\ \hline \boldsymbol{0}_{3\times 2} & \boldsymbol{\psi}_{4,u} \end{array}\right), \tag{A.11b}$$

where $\mathbf{0}_{m\times n}$ represents a m by n zero matrix.

Now transforming the FIM $\boldsymbol{J}_u$ to the basis $\boldsymbol{\mu}$ from $\boldsymbol{\eta}$, we have the relation $\boldsymbol{J}_{\boldsymbol{\mu},u} = \boldsymbol{T}_u \boldsymbol{J}_u \boldsymbol{T}_u^T$ where,

$$\boldsymbol{T}_u = \left(\begin{array}{cc|c|cc} \cos(\theta_u)/c & -\sin(\theta_u)/d_u & -\sin(\theta_u)/d_u & 0 & 0 \\ \cos(\theta_u)/c & \cos(\theta_u)/d_u & \cos(\theta_u)/d_u & 0 & 0 \\ \hline 0 & 0 & -1 & 0 & 0 \\ 0 & 0 & 0 & 1 & 0 \\ 0 & 0 & 0 & 0 & 1 \end{array}\right) = \left(\begin{array}{c|c} \boldsymbol{T}_{1,u} & \boldsymbol{T}_{2,u} \\ \hline \mathbf{0}_{3\times 2} & \boldsymbol{T}_{4,u} \end{array}\right), \quad \text{(A.12)}$$

where $d_u = ||\boldsymbol{p}_u - \boldsymbol{q}_u||_2$.

Hence, we can now write

$$\begin{aligned} \boldsymbol{J}_{\boldsymbol{\mu},u} = \boldsymbol{T}_u \boldsymbol{J}_u \boldsymbol{T}_u^T &= \begin{bmatrix} \boldsymbol{T}_{1,u} & \boldsymbol{T}_{2,u} \\ \mathbf{0}_{3\times 2} & \boldsymbol{T}_{4,u} \end{bmatrix} \begin{bmatrix} \boldsymbol{\psi}_{1,u} & \mathbf{0}_{2\times 3} \\ \mathbf{0}_{3\times 2} & \boldsymbol{\psi}_{4,u} \end{bmatrix} \begin{bmatrix} \boldsymbol{T}_{1,u}^T & \mathbf{0}_{2\times 3} \\ \boldsymbol{T}_{2,u}^T & \boldsymbol{T}_{4,u}^T \end{bmatrix}, && \text{(A.13a)} \\ &= \begin{bmatrix} \boldsymbol{T}_{1,u} & \boldsymbol{T}_{2,u} \\ \mathbf{0}_{3\times 2} & \boldsymbol{I}_3 \end{bmatrix} \begin{bmatrix} \boldsymbol{\psi}_{1,u} & \mathbf{0}_{2\times 3} \\ \mathbf{0}_{3\times 2} & \tilde{\boldsymbol{\psi}}_{4,u} \end{bmatrix} \begin{bmatrix} \boldsymbol{T}_{1,u}^T & \mathbf{0}_{2\times 3} \\ \boldsymbol{T}_{2,u}^T & \boldsymbol{I}_3 \end{bmatrix}, && \text{(A.13b)} \\ &= \tilde{\boldsymbol{T}}_u \tilde{\boldsymbol{J}}_u \tilde{\boldsymbol{T}}_u^T, && \text{(A.13c)} \end{aligned}$$

where, $\tilde{\boldsymbol{J}}_u$ is a diagonal matrix and $\tilde{\boldsymbol{\psi}}_{4,u} = \boldsymbol{T}_{4,u} \boldsymbol{\psi}_{4,u} \boldsymbol{T}_{4,u}^T$ which is equal to

$$\tilde{\boldsymbol{\psi}}_{4,u} = \boldsymbol{T}_{4,u} \boldsymbol{\psi}_{4,u} \boldsymbol{T}_{4,u}^T = \begin{bmatrix} \psi(\phi_u, \phi_u) & 0 & 0 \\ 0 & \psi(h_{R,u}, h_{R,u}) & 0 \\ 0 & 0 & \psi(h_{I,u}, h_{I,u}) \end{bmatrix}. \quad \text{(A.14)}$$

Now, in order to calculate the CRLB, we need to find $\boldsymbol{J}_{\boldsymbol{\mu},u}^{-1}$.

$$\boldsymbol{J}_{\boldsymbol{\mu},\boldsymbol{u}}^{-1} = \tilde{\boldsymbol{T}}_u^{-T} \tilde{\boldsymbol{J}}_u^{-1} \tilde{\boldsymbol{T}}_u^{-1}, \quad \text{(A.15)}$$

where $\tilde{\boldsymbol{T}}_u^{-T} = \left(\tilde{\boldsymbol{T}}_u^{-1}\right)^T$. Using Schur's complement to calculate the inverse,

$$\tilde{\boldsymbol{T}}_u^{-1} = \begin{bmatrix} \boldsymbol{T}_{1,u} & \boldsymbol{T}_{2,u} \\ \mathbf{0}_{3\times 2} & \boldsymbol{I}_3 \end{bmatrix}^{-1} = \begin{bmatrix} \boldsymbol{T}_{1,u}^{-1} & -\boldsymbol{T}_{5,u} \\ \mathbf{0}_{3\times 2} & \boldsymbol{I}_3 \end{bmatrix}, \quad \text{(A.16)}$$

and, $\boldsymbol{T}_{5,u} = \boldsymbol{T}_{1,u}^{-1}\boldsymbol{T}_{2,u}$ where

$$\boldsymbol{T}_{1,u}^{-1} = \frac{cd_u}{\cos^2(\theta_u) + \cos(\theta_u)\sin(\theta_u)} \begin{bmatrix} \cos(\theta_u)/d_u & \sin(\theta_u)/d_u \\ -\cos(\theta_u)/c & \cos(\theta_u)/c \end{bmatrix} = k_u \begin{bmatrix} t_{11,u} & t_{12,u} \\ t_{21,u} & t_{22,u} \end{bmatrix}. \tag{A.17}$$

Hence, we can formulate $\boldsymbol{T}_{5,u}$ as,

$$\boldsymbol{T}_{5,u} = \boldsymbol{T}_{1,u}^{-1}\boldsymbol{T}_{2,u} = \begin{bmatrix} 0 & 0 & 0 \\ 1 & 0 & 0 \end{bmatrix}. \tag{A.18}$$

From the above expressions, we can finally formulate $\boldsymbol{J}_{\boldsymbol{\mu},\boldsymbol{u}}^{-1}$ as

$$\boldsymbol{J}_{\boldsymbol{\mu},\boldsymbol{u}}^{-1} = \begin{bmatrix} \boldsymbol{T}_{1,u}^{-T}\boldsymbol{\psi}_{1,u}^{-1}\boldsymbol{T}_{1,u}^{-1} & -\boldsymbol{T}_{1,u}^{-T}\boldsymbol{\psi}_{1,u}^{-1}\boldsymbol{T}_{5,u} \\ -\boldsymbol{T}_{5,u}^{T}\boldsymbol{\psi}_{1}^{-1}\boldsymbol{T}_{1,u} & \boldsymbol{T}_{5,u}^{T}\boldsymbol{\psi}_{1}^{-1}\boldsymbol{T}_{5,u} + \tilde{\boldsymbol{\psi}}_{4}^{-1} \end{bmatrix}, \tag{A.19}$$

where,

$$\boldsymbol{T}_{1,u}^{-T}\boldsymbol{\psi}_{1,u}^{-1}\boldsymbol{T}_{1,u}^{-1} = k_u^2 \begin{bmatrix} t_{11}^2\psi^{-1}(\tau_u,\tau_u) + t_{21}^2\psi^{-1}(\theta_u,\theta_u) & \\ & t_{12}^2\psi^{-1}(\tau_u,\tau_u) + t_{22}^2\psi^{-1}(\theta_u,\theta_u) \end{bmatrix}, \tag{A.20}$$

and,

$$T_{5,u}^{T}\boldsymbol{\psi}_{1}^{-1}\boldsymbol{T}_{5,u} = \begin{bmatrix} \psi^{-1}(\theta_u,\theta_u) & 0 & 0 \\ 0 & 0 & 0 \\ 0 & 0 & 0 \end{bmatrix}. \tag{A.21}$$

Consider γ to be the homogeneity factor with unit m^2/rad^2. We can write the localization error as $L_u = \text{trace}[\boldsymbol{J}_{\eta}^{-1}]_{1:3}$ as

$$L_u = \text{PEB}_u^2 + \gamma\text{OEB}_u^2, \tag{A.22a}$$

$$= \underbrace{k_u^2 t_{11}^2\psi^{-1}(\tau_u,\tau_u) + k_u^2 t_{21}^2\psi^{-1}(\theta_u,\theta_u)}_{\text{From } \boldsymbol{J}_{\boldsymbol{\mu},u}^{-1}(1,1)} + \underbrace{k_u^2 t_{12}^2\psi^{-1}(\tau_u,\tau_u) + k_u^2 t_{22}^2\psi^{-1}(\theta_u,\theta_u)}_{\text{From } \boldsymbol{J}_{\boldsymbol{\mu},u}^{-1}(2,2)}$$

$$+ \underbrace{\gamma\psi^{-1}(\theta_u,\theta_u) + \gamma\psi^{-1}(\phi,\phi)}_{\text{From } \boldsymbol{J}_{\boldsymbol{\mu},u}^{-1}(3,3)}, \tag{A.22b}$$

$$= k_{\tau,u}\psi^{-1}(\tau_u,\tau_u) + k_{\theta,u}\psi^{-1}(\theta_u,\theta_u) + k_{\phi,u}\psi^{-1}(\phi_u,\phi_u). \tag{A.22c}$$

A.6 Convex reformulation of the AoD constraint

In equation (2.38c) consider $u = \dot{\boldsymbol{a}}_u^H \boldsymbol{X}_N \dot{\boldsymbol{a}}_u$, $v = \dot{\boldsymbol{a}}_u^H \boldsymbol{X}_N \boldsymbol{a}_u$, $w = \boldsymbol{a}_u^H \boldsymbol{X}_N \boldsymbol{a}_u$ and $k = \alpha_{\theta,u}\zeta_\theta$. Then,

$$u - \frac{|v|^2}{w} \geq k, \tag{A.23a}$$

$$w(u-k) \geq v^H v, \tag{A.23b}$$

$$4w(u-k) \geq 4v^H v, \tag{A.23c}$$

$$4w(u-k) + w^2 + (u-k)^2 \geq (2|v|)^2 + w^2 + (u-k)^2, \tag{A.23d}$$

$$((u-k)+w)^2 \geq (2|v|)^2 + w^2 + (u-k)^2 - 2w(u-k), \tag{A.23e}$$

$$((u-k)+w)^2 \geq (2|v|)^2 + ((u-k)-w)^2, \tag{A.23f}$$

$$((u-k)+w) \geq \sqrt{(2\Re(v))^2 + (2\Im(v))^2 + ((u-k)-w)^2}, \tag{A.23g}$$

$$(u-k+w) \geq \left\| \begin{bmatrix} 2\Re(v) \\ 2\Im(v) \\ (u-k-w) \end{bmatrix} \right\|_2 . \tag{A.23h}$$

Appendix B

Proofs of chapter 3

B.1 Data rate optimal beamforming in multi-user case

Consider an analog beamformer with 1 RF chain that transmits beams sequentially to multiple users users across time *i.e.* one user at a time. Hence, with such consideration, for user-u, from the signal model in equation (2.26), we can express SNR as:

$$\mathrm{SNR}_u = \frac{1}{N_0}\sum_{n=n_1}^{n_N} P_{\mathrm{Tx}}|\boldsymbol{w}_u^H \boldsymbol{H}_{u,n}\boldsymbol{f}_{n,u}|^2|s_n|^2, \tag{B.1a}$$

$$= \frac{1}{N_0}\sum_{n=n_1}^{n_N} \frac{P_{\mathrm{Tx}}}{\xi_u}|s_n|^2|h_u|^2|\boldsymbol{w}_u^H \boldsymbol{a}_{\mathrm{Rx},u}|^2\boldsymbol{a}_{\mathrm{Tx},u}^H\boldsymbol{F}_{u,n}\boldsymbol{a}_{\mathrm{Tx},u}, \tag{B.1b}$$

$$= \frac{1}{N_0}\boldsymbol{a}_{\zeta,u}^H\boldsymbol{X}_{N,u}\boldsymbol{a}_{\zeta,u}, \tag{B.1c}$$

where,

$$\boldsymbol{a}_{\zeta,u} = \begin{bmatrix}\zeta_u|s_{n_1}|\boldsymbol{a}_{\mathrm{Tx},u}^T & \cdots & \zeta_u|s_{n_N}|\boldsymbol{a}_{\mathrm{Tx},u}^T\end{bmatrix}^T \in \mathbb{C}^M, \tag{B.2}$$

and $\zeta_u = \sqrt{\frac{P_{\mathrm{Tx}}}{\xi_u}}|h_u||\boldsymbol{w}_u^H\boldsymbol{a}_{\mathrm{Rx},u}|$.

The sum rate for U users, can now be formulated as

$$\mathrm{R} = \sum_{u=1}^{U} R_u = \sum_{u=1}^{U}\frac{T_u}{T_C}\log_2\left(1+\mathrm{SNR}_u\right), \tag{B.3a}$$

$$= \sum_{u=1}^{U}\frac{T_u}{T_C}\log_2\left(1+\frac{\boldsymbol{a}_{\zeta,u}^H\boldsymbol{X}_{N,u}\boldsymbol{a}_{\zeta,u}}{N_0}\right). \tag{B.3b}$$

where, T_u is the fraction of time allocated for data communication phase for a particular user. Mathematically $\sum_{u=1}^{U} T_u = T_C$. The optimization can then be

formulated similarly to [89] as follows

$$(P): \quad \max_{\boldsymbol{X}_N, T_u} \quad R \tag{B.4a}$$

subject to:

$$R_u \geq r_0, \tag{B.4b}$$

$$\sum_{u=1}^{U} T_u = T_C, \tag{B.4c}$$

(2.36b)-(2.36g).

Since we consider beamforming with respect to one user at a time, we can separate the optimization problem (P) into two separate optimization problems $(P1)$ and $(P2)$, the first one concerning optimal beamforming vector per user and the second concerning the allocation of time T_u depending on the minimum rate requirement constraint for the u-th user in the sum rate maximization.

The first optimization problem $(P1)$ can be formulated as:

$$(P1): \max_{\boldsymbol{X}_{N,u}} \quad \text{SNR}_u \tag{B.5a}$$

subject to:

(2.36b)-(2.36g).

The above optimization problem $(P1)$ concerns the beamforming optimization in a given direction for a particular user. The solution to the problem is a well known problem in the literature [62, 138] referred to as conventional beamformer (CBF), expressed as follows:

$$\boldsymbol{X}^*_{N,u} = \text{diag}(\boldsymbol{F}^*_u, \boldsymbol{F}^*_u, \cdots, \boldsymbol{F}^*_u), \tag{B.6}$$

where, $\boldsymbol{F}^*_u = \boldsymbol{f}^*_u \boldsymbol{f}^{*H}_u$ and

$$\boldsymbol{f}^*_u = \frac{\boldsymbol{a}_{\zeta,u}}{||\boldsymbol{a}_{\zeta,u}||^2_2}. \tag{B.7}$$

Since the SNR expression is not dependent on the subcarrier frequency, the optimal beamformer is the same for the beamformers across all the subcarriers.

Now given the optimal beamforming vector for each user, we need to determine how much fraction of time T_C should be allocated to each user. Accordingly, the

second optimization problem can be written as:

$$(P2): \max_{T_u} \quad R \tag{B.8a}$$

subject to:

$$\boldsymbol{X}_{N,u} = \boldsymbol{X}^*_{N,u} \tag{B.8b}$$

(B.4b),(B.4c).

For the problem $(P2)$, the solution would be to allocate the time firstly to fulfill the minimum rate requirement per user from equation (B.4b), then to allocate all the remaining time to the user with highest SNR_u in order to maximize the sum rate. Hence the optimal solution would be:

$$T^*_u = \frac{r_0}{\log_2(1+\mathrm{SNR}_u)} T_C + z^*_u, \tag{B.9}$$

where,

$$z^*_u = \begin{cases} \delta T_C & \text{if } \mathrm{SNR}_u = \max\left(\mathrm{SNR}_1, \cdots, \mathrm{SNR}_U\right) \\ 0 & \text{otherwise} \end{cases} \tag{B.10}$$

where, $\delta = 1 - \sum_{u=1}^{U} r_0/\log_2(1+\mathrm{SNR}_u)$.

B.2 Derivation of beam-selection error

Beam-selection error occurs for a user in coverage of the beam j of beamwidth ω_k when the estimated position lies outside the beam j. Thus, the probability of beam-selection error, in case the user is estimated to be located at $\hat{d}$, is computed as:

$$\mathcal{P}_{BS,j,k}\left(d, \sigma_d^2\right) = \mathbb{P}\left(\hat{d} < d_{L_{jk}}\right) + \mathbb{P}\left(\hat{d} > d_{R_{jk}}\right) \tag{B.11a}$$

$$= 1 - \mathcal{Q}\left(\frac{d_{L_{jk}} - d}{\sigma_d}\right) + \mathcal{Q}\left(\frac{d_{R_{jk}} - d}{\sigma_d}\right). \tag{B.11b}$$

Accordingly, the average beam-selection error of any user for which the j-th beam is selected for service is given by:

$$\bar{\mathcal{P}}_{BS,j,k} = \int_{d_{L_{jk}}}^{d_{R_{jk}}} \mathcal{P}_{BS,j,k}(x) f_d(x) dx. \tag{B.12}$$

Finally, the average beam-selection error for the localization based beam-selection scheme with a beam-dictionary size of k is calculated as:

$$\bar{\mathcal{P}}_{BS} = \frac{1}{\lambda} \sum_{j=1}^{k} \bar{\mathcal{P}}_{BS,j,k}. \tag{B.13}$$

B.3 Derivation of SINR coverage probability

Let x be the distance between the base of the serving BS and the UE and $z_0 = \sqrt{x^2 + h_B^2}$ be the distance between the BS and the UE. Likewise, let d_k, $k \geq 1$ represent the distance between the base of the k-th interfering BS and the UE. Likewise, let $z_k = \sqrt{d_k^2 + h_B^2}$, $\forall k$ be the distance between the k-th BS and the UE. Similarly, h_k represents the complex channel coefficient between the k-th BS and the UE. In the following analysis, i and i' represents the index of BSs in LOS and NLOS respectively.

Firstly, we consider the case when the main lobe of both the serving BS and the UE beams are aligned with each other (*i.e.* no beam selection error). Let $G = \gamma_{Tx}(\omega_{Tx})\gamma_{Rx}(\omega_{Rx})$. The SINR Coverage probability at a threshold γ in case of no beam-selection error, referred to as $\mathcal{T}_0$ is calculated as:

$$\mathcal{T}_0(x,\gamma) = \mathbb{P}\left(\text{SINR} \geq \gamma\right) \tag{B.14a}$$

$$= \mathbb{P}\left(\frac{P_{Tx} K G z_0^{-\alpha_L} |h_0|^2}{\sigma_N^2 + P_{Tx} K g^2 \left(\sum_{i \in \xi_L \setminus \{0\}} z_i^{-\alpha_L} |h_i|^2 + \sum_{i' \in \xi_N} z_{i'}^{-\alpha_N} |h_{i'}|^2\right)} \geq \gamma\right), \tag{B.14b}$$

$$= \mathbb{P}\left(|h_0|^2 \geq \frac{\gamma\sigma_N^2 + \gamma P_{Tx} K g^2 \left(\sum_{i \in \xi_L \setminus \{0\}} z_i^{-\alpha_L} |h_i|^2 + \sum_{i' \in \xi_N} z_{i'}^{-\alpha_N} |h_{i'}|^2\right)}{P_{Tx} K G z_0^{-\alpha_L}}\right), \tag{B.14c}$$

$$= \mathop{\mathbb{E}}_{\xi_L, \xi_N, h_i, h_{i'}} \left[\exp\left(-\frac{\gamma\sigma_N^2}{P_{Tx} K G z_0^{-\alpha_L}} - \frac{\gamma g^2 \sum_{i \in \xi_L \setminus \{0\}} z_i^{-\alpha_L} |h_i|^2}{G z_0^{-\alpha_L}} - \frac{\gamma g^2 \sum_{i' \in \xi_N} z_{i'}^{-\alpha_N} |h_{i'}|^2}{G z_0^{-\alpha_L}}\right)\right], \tag{B.14d}$$

$$= \zeta \mathop{\mathbb{E}}_{|h_i|^2, \xi_L \setminus \{0\}} \left[\exp\left(-\frac{\gamma g^2 \sum\limits_{i \in \xi_L \setminus \{0\}} z_i^{-\alpha_L} |h_i|^2}{G z_0^{-\alpha_L}}\right)\right] \mathop{\mathbb{E}}_{|h_{i'}|^2, \xi_N} \left[\exp\left(-\frac{\gamma g^2 \sum\limits_{i' \in \xi_N} z_{i'}^{-\alpha_N} |h_{i'}|^2}{G z_0^{-\alpha_L}}\right)\right], \tag{B.14e}$$

where, $\zeta = \exp\left(-\frac{\gamma\sigma_N^2}{P_{Tx}KGz_0^{-\alpha_L}}\right)$. Now the terms corresponding to the LOS and the NLOS case can be evaluated separately as:

$$\mathop{\mathbb{E}}_{|h_i|^2,\xi_L\setminus\{0\}}\left[\exp\left(-\frac{\gamma g^2\sum\limits_{i\in\xi_L\setminus\{0\}} z_i^{-\alpha_L}h_i}{Gz_0^{-\alpha_L}}\right)\right] = \mathop{\mathbb{E}}_{\xi_L}\left[\prod_{i\in\xi_L\setminus\{0\}}\mathop{\mathbb{E}}_{|h_i|^2}\left[\exp\left(-\frac{\gamma g^2 z_i^{-\alpha_L}|h_i|^2}{Gz_0^{-\alpha_L}}\right)\right]\right], \tag{B.15a}$$

$$\overset{(a)}{=} \exp\left(-\int_x^{d_S} 1-\mathbb{E}_{|h_i|^2}\left[\exp\left(-\frac{\gamma g^2(y^2+h_B^2)^{-\alpha_L/2}|h_i|^2}{Gz_0^{-\alpha_L}}\right)\right]2\lambda y dy\right), \tag{B.15b}$$

$$= \exp\left(-\int_x^{d_S}\frac{\gamma g^2(y^2+h_B^2)^{-\alpha_L/2}}{Gz_0^{-\alpha_L}+\gamma g^2(y^2+h_B^2)^{-\alpha_L/2}}2\lambda y dy\right) = A_{L0}(x,\gamma), \tag{B.15c}$$

where (a) follows as a result of the proof according to [139, Theorem 4.9]. The integral in (a) is only over the z_i (and not over z_0) as the expectation is over all the interfering BSs in LOS.

With the same reasoning,

$$\mathbb{E}_{h_{i'},\xi_N}\left[\exp\left(-\frac{\gamma g^2\sum_{i'\in\xi_N} z_{i'}^{-\alpha_N}|h_{i'}|^2}{Gz_0^{-\alpha_L}}\right)\right]$$
$$= \exp\left(-\int_{d_S}^{\infty}\frac{\gamma g^2(y^2+h_B^2)^{-\alpha_N/2}}{Gz_0^{-\alpha_L}+\gamma g(y^2+h_B^2)^{-\alpha_N/2}}2\lambda(y-d_S)dy\right) = A_{NL0}(x,\gamma) \tag{B.16}$$

Likewise, in the case of beam selection error, we can derive the coverage probability $\mathcal{T}_{BS}$ by replacing G with g^2 since here we assume that main lobes of both BS and the UE are not aligned. Then, from the theorem of total probability, the SINR coverage at a distance x is calculated. Conditioning on the user lying between d_{L_i} and d_{R_i} completes the proof.

Appendix C

Proofs of chapter 4

C.1 Derivation of CRLB for distance and AoA

We consider the received signal model similarly to that as in equation (3.14). Similarly to chapter 3 and [62], let the power spectral density of the transmit signal be symmetric and equal to $T_s/2\pi B$, where, T_s and B are the time duration and the bandwidth of $s(t)$.

The FIM $\boldsymbol{J}$ from [52] and [62] for the estimation of the mentioned variables are given below.

$$\boldsymbol{J} = \begin{bmatrix} J_{d,d} & 0 & 0 & 0 \\ 0 & J_{\phi,\phi} & J_{h_R,\phi} & J_{h_I,\phi} \\ 0 & J_{\phi,h_R} & J_{h_R,h_R} & 0 \\ 0 & J_{\phi,h_I} & 0 & J_{h_I,h_I} \end{bmatrix}, \tag{C.1}$$

in which:

$$J_{d,d} = \zeta G_{Rx}(\omega_{Rx}) G_{Tx}(\omega_{Tx}) \frac{B^2\pi^2}{3c^2}, \tag{C.2a}$$

$$J_{\phi,\phi} = \zeta |\dot{\boldsymbol{a}}_{Rx}^H(\phi)\boldsymbol{w}|^2 G_{Tx}(\omega_{Tx}), \tag{C.2b}$$

$$J_{h_R,\phi} = \frac{\zeta}{|h|^2} \mathbb{R}\left\{h \boldsymbol{a}_{Rx}^H(\phi)\boldsymbol{w}\boldsymbol{w}^H \dot{\boldsymbol{a}}_{Rx}(\phi)\right\} G_{Tx}(\omega_{Tx}), \tag{C.2c}$$

$$J_{h_R,h_R} = \zeta G_{Rx}(\omega_{Rx}) G_{Tx}(\omega_{Tx}), \tag{C.2d}$$

$$J_{h_I,\phi} = \frac{\zeta}{|h|^2} \mathbb{I}\left\{h \boldsymbol{a}_{Rx}^H(\phi)\boldsymbol{w}\boldsymbol{w}^H \dot{\boldsymbol{a}}_{Rx}(\phi)\right\} G_{Tx}(\omega_{Tx}), \tag{C.2e}$$

$$J_{h_I,h_I} = \zeta G_{Rx}(\omega_{Rx}) G_{Tx}(\omega_{Tx}), \tag{C.2f}$$

where $\zeta = 2\mathrm{SNR}_L B(1-\beta)T_F / G_{Tx}(\omega_{Tx}) G_{Rx}(\omega_{Rx})$ and $\dot{\boldsymbol{a}}_{Rx}(\phi) = \partial \boldsymbol{a}_{Rx}(\phi)/\partial\phi$.

Finally, the CRLBs for the estimation of the distance (by inverting the first element of $\boldsymbol{J}$) and the AoA (using Schur's decomposition [58]) can be written as

follows:

$$\sigma_d^2 = \left(\zeta G_{Rx}(\omega_{Rx}) G_{Tx}(\omega_{Tx}) \frac{B^2 \pi^2}{3c^2} \right)^{-1}, \tag{C.3a}$$

$$\sigma_\phi^2 = \left(\zeta G_{Tx}(\omega_{Tx}) \left(|\dot{\boldsymbol{a}}_{Rx}^H(\phi) \boldsymbol{w}(\omega_{Rx})|^2 - \frac{|\boldsymbol{a}_{Rx}^H(\phi) \boldsymbol{w}(\omega_{Rx}) \boldsymbol{w}^H(\omega_{Rx}) \dot{\boldsymbol{a}}_{Rx}(\phi)|^2}{G_{Rx}(\omega_{Rx})} \right) \right)^{-1}. \tag{C.3b}$$

Bibliography

[1] X. Li et al. "The Future of Mobile Wireless Communication Networks". In: *2009 International Conference on Communication Software and Networks*. Feb. 2009, pp. 554–557. DOI: 10.1109/ICCSN.2009.105.

[2] *Ericsson mobility report*. https://www.ericsson.com/assets/local/mobility-report/documents/2019/ericsson-mobility-report-june-2019.pdf. June 2019.

[3] T. S. Rappaport, J. N. Murdock, and F. Gutierrez. "State of the Art in 60-GHz Integrated Circuits and Systems for Wireless Communications". In: *Proceedings of the IEEE* 99.8 (Aug. 2011), pp. 1390–1436. ISSN: 0018-9219. DOI: 10.1109/JPROC.2011.2143650.

[4] Gabriel Brown. "Exploring 5G new radio: Use cases capabilities & timeline". In: (2016).

[5] Nokia Networks. *5G use cases and requirements*. 2014.

[6] J. G. Andrews et al. "What Will 5G Be?" In: *IEEE Journal on Selected Areas in Communications* 32.6 (June 2014), pp. 1065–1082. ISSN: 0733-8716. DOI: 10.1109/JSAC.2014.2328098.

[7] GSMA Intelligence. "Understanding 5G: Perspectives on future technological advancements in mobile". In: *White paper* (2014), pp. 1–26.

[8] ITUR WP5D. *Minimum requirements related to technical performance for IMT-2020 radio interface (s)*. Feb. 2017.

[9] S. A. Busari et al. "Millimeter-Wave Massive MIMO Communication for Future Wireless Systems: A Survey". In: *IEEE Communications Surveys Tutorials* 20.2 (Dec. 2017), pp. 836–869. ISSN: 1553-877X. DOI: 10.1109/COMST.2017.2787460.

[10] I. Parvez et al. "A Survey on Low Latency Towards 5G: RAN, Core Network and Caching Solutions". In: *IEEE Communications Surveys Tutorials* 20.4 (2018), pp. 3098–3130. ISSN: 1553-877X. DOI: 10.1109/COMST.2018.2841349.

[11] C. E. Shannon. "A mathematical theory of communication". In: *The Bell System Technical Journal* 27.3 (July 1948), pp. 379–423. ISSN: 0005-8580. DOI: 10.1002/j.1538-7305.1948.tb01338.x.

[12] Resolution Com 6/20. *Provisional Final Acts WRC-15. WRC-15. Geneva: ITU.* https://www.itu.int/dms_pub/itu-r/opb/act/R-ACT-WRC.11-2015-PDF-E.pdf.

[13] T. S. Rappaport et al. "Millimeter Wave Mobile Communications for 5G Cellular: It Will Work!" In: *IEEE Access* 1 (2013), pp. 335–349. ISSN: 2169-3536. DOI: 10.1109/ACCESS.2013.2260813.

[14] Q. C. Li et al. "5G Network Capacity: Key Elements and Technologies". In: *IEEE Vehicular Technology Magazine* 9.1 (Mar. 2014), pp. 71–78. ISSN: 1556-6072. DOI: 10.1109/MVT.2013.2295070.

[15] F. Al-Ogaili and R. M. Shubair. "Millimeter-wave mobile communications for 5G: Challenges and opportunities". In: *2016 IEEE International Symposium on Antennas and Propagation (APSURSI)*. June 2016, pp. 1003–1004. DOI: 10.1109/APS.2016.7696210.

[16] Yong Niu et al. "A survey of millimeter wave communications (mmWave) for 5G: opportunities and challenges". In: *Wireless Networks* 21.8 (Nov. 2015), pp. 2657–2676. ISSN: 1572-8196. DOI: 10.1007/s11276-015-0942-z. URL: https://doi.org/10.1007/s11276-015-0942-z.

[17] *E-Band Technology.* https://www.e-band.com/index.php?id=86. Accessed: 26-06-2019.

[18] H. T. Friis. "A Note on a Simple Transmission Formula". In: *Proceedings of the IRE* 34.5 (May 1946), pp. 254–256. ISSN: 0096-8390. DOI: 10.1109/JRPROC.1946.234568.

[19] Z. Pi and F. Khan. "An introduction to millimeter-wave mobile broadband systems". In: *IEEE Communications Magazine* 49.6 (June 2011), pp. 101–107. ISSN: 0163-6804. DOI: 10.1109/MCOM.2011.5783993.

[20] A. V. Alejos, M. G. Sanchez, and I. Cuinas. "Measurement and Analysis of Propagation Mechanisms at 40 GHz: Viability of Site Shielding Forced by Obstacles". In: *IEEE Transactions on Vehicular Technology* 57.6 (Nov. 2008), pp. 3369–3380. ISSN: 0018-9545. DOI: 10.1109/TVT.2008.920052.

[21] X. Ge et al. "5G Ultra-Dense Cellular Networks". In: *IEEE Wireless Communications* 23.1 (Feb. 2016), pp. 72–79. ISSN: 1536-1284. DOI: 10.1109/MWC.2016.7422408.

[22] Per-Simon Kildal. *Foundations of antenna engineering: a unified approach for line-of-sight and multipath*. Artech House, 2015.

[23] S. Sun et al. "MIMO for millimeter-wave wireless communications: beamforming, spatial multiplexing, or both?" In: *IEEE Communications Magazine* 52.12 (Dec. 2014), pp. 110–121. ISSN: 0163-6804. DOI: 10.1109/MCOM.2014.6979962.

[24] R. W. Heath et al. "An Overview of Signal Processing Techniques for Millimeter Wave MIMO Systems". In: *IEEE Journal of Selected Topics in Signal Processing* 10.3 (Apr. 2016), pp. 436–453. ISSN: 1932-4553. DOI: 10.1109/JSTSP.2016.2523924.

[25] H. Inanoglu. "Multiple-Input Multiple-Output System Capacity: Antenna and Propagation Aspects". In: *IEEE Antennas and Propagation Magazine* 55.1 (Feb. 2013), pp. 253–273. ISSN: 1045-9243. DOI: 10.1109/MAP.2013.6474541.

[26] A. Alkhateeb et al. "MIMO Precoding and Combining Solutions for Millimeter-Wave Systems". In: *IEEE Communications Magazine* 52.12 (Dec. 2014), pp. 122–131. ISSN: 0163-6804. DOI: 10.1109/MCOM.2014.6979963.

[27] I. A. Hemadeh et al. "Millimeter-Wave Communications: Physical Channel Models, Design Considerations, Antenna Constructions, and Link-Budget". In: *IEEE Communications Surveys Tutorials* 20.2 (2018), pp. 870–913. ISSN: 1553-877X. DOI: 10.1109/COMST.2017.2783541.

[28] David Tse and Pramod Viswanath. *Fundamentals of wireless communication*. Cambridge university press, 2005.

[29] Richard B Kershner and Frank T McClure. "The Legacy of Transit: A Dedication". In: *JOHNS HOPKINS APL TECHNICAL DIGEST* 19.1 (1998), p. 3.

[30] C. J. Hegarty and E. Chatre. "Evolution of the Global Navigation Satellite System (GNSS)". In: *Proceedings of the IEEE* 96.12 (Dec. 2008), pp. 1902–1917. ISSN: 0018-9219. DOI: 10.1109/JPROC.2008.2006090.

[31] V. M. Perez-Colado et al. "Learning analytics for location-based serious games". In: *2018 IEEE Global Engineering Education Conference (EDUCON)*. Apr. 2018, pp. 1192–1200. DOI: 10.1109/EDUCON.2018.8363365.

[32] M. Pourhomayoun, Z. Jin, and M. Fowler. "Spatial sparsity based indoor localization in wireless sensor network for assistive healthcare". In: *2012 Annual International Conference of the IEEE Engineering in Medicine and Biology Society*. Aug. 2012, pp. 3696–3699. DOI: 10.1109/EMBC.2012.6346769.

[33] Stefania Bartoletti et al. *5G Localization and Context-Awareness*. https://www.5gitaly.eu/wp-content/uploads/2019/01/5G-Italy-White-eBook-5G-Localization.pdf.

[34] Yihong Qi, H. Kobayashi, and H. Suda. "Analysis of wireless geolocation in a non-line-of-sight environment". In: *IEEE Transactions on Wireless Communications* 5.3 (Mar. 2006), pp. 672–681. ISSN: 1536-1276. DOI: 10.1109/TWC.2006.1611097.

[35] Alessio Fascista, Angelo Coluccia, and Giuseppe Ricci. "Mobile Positioning in Multipath Environments: a Pseudo Maximum Likelihood approach". In: *arXiv e-prints*, arXiv:1808.00857 (Aug. 2018), arXiv:1808.00857. arXiv: 1808.00857 [eess.SP].

[36] Zafer Sahinoglu. *Ultra-wideband positioning systems*. Cambridge university press, 2008.

[37] S. A. Shaikh and A. M. Tonello. "Localization based on angle of arrival in EM lens-focusing massive MIMO". In: *2016 IEEE 6th International Conference on Consumer Electronics - Berlin (ICCE-Berlin)*. Sept. 2016, pp. 124–128. DOI: 10.1109/ICCE-Berlin.2016.7684736.

[38] F. Rusek et al. "Scaling Up MIMO: Opportunities and Challenges with Very Large Arrays". In: *IEEE Signal Processing Magazine* 30.1 (Jan. 2013), pp. 40–60. ISSN: 1053-5888. DOI: 10.1109/MSP.2011.2178495.

[39] F. Lemic et al. "Localization as a feature of mmWave communication". In: *2016 International Wireless Communications and Mobile Computing Conference (IWCMC)*. Sept. 2016, pp. 1033–1038. DOI: 10.1109/IWCMC.2016.7577201.

[40] Jie Xiong, Karthikeyan Sundaresan, and Kyle Jamieson. "ToneTrack: Leveraging Frequency-Agile Radios for Time-Based Indoor Wireless Localization". In: *Proceedings of the 21st Annual International Conference on Mobile Computing and Networking*. MobiCom '15. Paris, France: ACM, 2015, pp. 537–549. ISBN: 978-1-4503-3619-2. DOI: 10.1145/2789168.2790125. URL: http://doi.acm.org/10.1145/2789168.2790125.

[41] COST Action CA15104, IRACON, Troels Pedersen, and Bernard Henri Fleury. *Whitepaper on New Localization Methods for 5G Wireless Systems and the Internet-of-Things*. English. Other. 2018.

[42] A. Dammann, R. Raulefs, and S. Zhang. "On prospects of positioning in 5G". In: *2015 IEEE International Conference on Communication Workshop (ICCW)*. June 2015, pp. 1207–1213. DOI: 10.1109/ICCW.2015.7247342.

[43] H. Wymeersch et al. "5G mmWave Positioning for Vehicular Networks". In: *IEEE Wireless Communications* 24.6 (Dec. 2017), pp. 80–86. ISSN: 1536-1284. DOI: 10.1109/MWC.2017.1600374.

[44] R. M. Buehrer, H. Wymeersch, and R. M. Vaghefi. "Collaborative Sensor Network Localization: Algorithms and Practical Issues". In: *Proceedings of the IEEE* 106.6 (June 2018), pp. 1089–1114. DOI: 10.1109/JPROC.2018.2829439.

[45] J Meredith. "Study on channel model for frequency spectrum above 6 GHz". In: *Technical report, 3GPP TR 38.900* (2016).

[46] C. Gustafson et al. "On mm-Wave Multipath Clustering and Channel Modeling". In: *IEEE Transactions on Antennas and Propagation* 62.3 (Mar. 2014), pp. 1445–1455. ISSN: 0018-926X. DOI: 10.1109/TAP.2013.2295836.

[47] S. Geng et al. "Millimeter-Wave Propagation Channel Characterization for Short-Range Wireless Communications". In: *IEEE Transactions on Vehicular Technology* 58.1 (Jan. 2009), pp. 3–13. ISSN: 0018-9545. DOI: 10.1109/TVT.2008.924990.

[48] Iain Jameson. *Time delay estimation*. Tech. rep. Defence Science and Technology Organisation, Australia, 2006.

[49] R. Mendrzik et al. "Harnessing NLOS Components for Position and Orientation Estimation in 5G Millimeter Wave MIMO". In: *IEEE Transactions on Wireless Communications* 18.1 (Jan. 2019), pp. 93–107. ISSN: 1536-1276. DOI: 10.1109/TWC.2018.2877615.

[50] C. Gentner et al. "Multipath Assisted Positioning with Simultaneous Localization and Mapping". In: *IEEE Transactions on Wireless Communications* 15.9 (Sept. 2016), pp. 6104–6117. ISSN: 1558-2248. DOI: 10.1109/TWC.2016.2578336.

[51] A. Shahmansoori et al. "Position and Orientation Estimation Through Millimeter-Wave MIMO in 5G Systems". In: *IEEE Transactions on Wireless Communications* 17.3 (Mar. 2018), pp. 1822–1835. ISSN: 1536-1276. DOI: 10.1109/TWC.2017.2785788.

[52] A. Shahmansoori et al. "5G Position and Orientation Estimation through Millimeter Wave MIMO". In: *2015 IEEE Globecom Workshops (GC Wkshps)*. Dec. 2015, pp. 1–6. DOI: 10.1109/GLOCOMW.2015.7413967.

[53] 3GPP Radio Access Network Working Group et al. *Study on channel model for frequencies from 0.5 to 100 GHz (Release 15)*. Tech. rep. 3GPP TR 38.901.

[54] H. Wymeersch, J. Lien, and M. Z. Win. "Cooperative Localization in Wireless Networks". In: *Proceedings of the IEEE* 97.2 (Feb. 2009), pp. 427–450. ISSN: 1558-2256. DOI: 10.1109/JPROC.2008.2008853.

[55] M. Z. Win et al. "Network localization and navigation via cooperation". In: *IEEE Communications Magazine* 49.5 (May 2011), pp. 56–62. ISSN: 1558-1896. DOI: 10.1109/MCOM.2011.5762798.

[56] A. Alkhateeb et al. "Channel Estimation and Hybrid Precoding for Millimeter Wave Cellular Systems". In: *IEEE Journal of Selected Topics in Signal Processing* 8.5 (Oct. 2014), pp. 831–846. ISSN: 1932-4553. DOI: 10.1109/JSTSP.2014.2334278.

[57] Z. Xiao et al. "Hierarchical Codebook Design for Beamforming Training in Millimeter-Wave Communication". In: *IEEE Transactions on Wireless Communications* 15.5 (May 2016), pp. 3380–3392. ISSN: 1536-1276. DOI: 10.1109/TWC.2016.2520930.

[58] N. Garcia, H. Wymeersch, and D. T. M. Slock. "Optimal Precoders for Tracking the AoD and AoA of a mmWave Path". In: *IEEE Transactions on Signal Processing* 66.21 (Nov. 2018), pp. 5718–5729. ISSN: 1053-587X. DOI: 10.1109/TSP.2018.2870368.

[59] Anastasios Kakkavas et al. "5G Downlink Multi-Beam Signal Design for LOS Positioning". In: *CoRR* abs/1906.01671 (2019). arXiv: 1906.01671. URL: http://arxiv.org/abs/1906.01671.

[60] *IEEE Standard for Information technology–Telecommunications and information exchange between systems–Local and metropolitan area networks–Specific requirements-Part 11: Wireless LAN Medium Access Control (MAC) and Physical Layer (PHY) Specifications Amendment 3: Enhancements for*

Very High Throughput in the 60 GHz Band. Nov. 2012. DOI: 10.1109/IEEESTD.2012.6392842.

[61] F. Maschietti et al. "Robust Location-Aided Beam Alignment in Millimeter Wave Massive MIMO". In: *GLOBECOM 2017 - 2017 IEEE Global Communications Conference*. Dec. 2017, pp. 1–6. DOI: 10.1109/GLOCOM.2017.8254901.

[62] G. Destino and H. Wymeersch. "On the trade-off between positioning and data rate for mm-wave communication". In: *2017 IEEE International Conference on Communications Workshops (ICC Workshops)*. May 2017, pp. 797–802. DOI: 10.1109/ICCW.2017.7962756.

[63] C. Jeong, J. Park, and H. Yu. "Random access in millimeter-wave beamforming cellular networks: issues and approaches". In: *IEEE Communications Magazine* 53.1 (Jan. 2015), pp. 180–185. ISSN: 0163-6804. DOI: 10.1109/MCOM.2015.7010532.

[64] V. Desai et al. "Initial beamforming for mmWave communications". In: *2014 48th Asilomar Conference on Signals, Systems and Computers*. Nov. 2014, pp. 1926–1930. DOI: 10.1109/ACSSC.2014.7094805.

[65] N. Garcia et al. "Location-aided mm-wave channel estimation for vehicular communication". In: *2016 IEEE 17th International Workshop on Signal Processing Advances in Wireless Communications (SPAWC)*. July 2016, pp. 1–5. DOI: 10.1109/SPAWC.2016.7536855.

[66] C. N. Barati et al. "Initial Access in Millimeter Wave Cellular Systems". In: *IEEE Transactions on Wireless Communications* 15.12 (Dec. 2016), pp. 7926–7940. DOI: 10.1109/TWC.2016.2609384.

[67] P. Xia et al. "Practical Antenna Training for Millimeter Wave MIMO Communication". In: *2008 IEEE 68th Vehicular Technology Conference*. Sept. 2008, pp. 1–5. DOI: 10.1109/VETECF.2008.253.

[68] O. E. Ayach et al. "Spatially Sparse Precoding in Millimeter Wave MIMO Systems". In: *IEEE Transactions on Wireless Communications* 13.3 (Mar. 2014), pp. 1499–1513. ISSN: 1536-1276. DOI: 10.1109/TWC.2014.011714.130846.

[69] A. Alkhateeb, G. Leus, and R. W. Heath. "Limited Feedback Hybrid Precoding for Multi-User Millimeter Wave Systems". In: *IEEE Transactions on Wireless Communications* 14.11 (Nov. 2015), pp. 6481–6494. ISSN: 1536-1276. DOI: 10.1109/TWC.2015.2455980.

[70] S. Malla and G. Abreu. "Transmission strategies in multi-user millimeter wave systems". In: *2017 International Symposium on Wireless Communication Systems (ISWCS)*. Aug. 2017, pp. 54–59. DOI: 10.1109/ISWCS.2017.8108161.

[71] A. Guerra, F. Guidi, and D. Dardari. "Single-Anchor Localization and Orientation Performance Limits using Massive Arrays: MIMO vs. Beamforming". In: *IEEE Transactions on Wireless Communications* (July 2018), pp. 1–1.

[72] Anastasios Kakkavas et al. "Performance Limits of Single-Anchor mm-Wave Positioning". In: *CoRR* abs/1808.08116 (2018). arXiv: 1808.08116. URL: http://arxiv.org/abs/1808.08116.

[73] Y. Shen and M. Z. Win. "Fundamental Limits of Wideband Localization-Part I: A General Framework". In: *IEEE Transactions on Information Theory* 56.10 (Oct. 2010), pp. 4956–4980.

[74] Y. Shen, H. Wymeersch, and M. Z. Win. "Fundamental Limits of Wideband Localization- Part II: Cooperative Networks". In: *IEEE Transactions on Information Theory* 56.10 (Oct. 2010), pp. 4981–5000. DOI: 10.1109/TIT.2010.2059720.

[75] A. Guerra, F. Guidi, and D. Dardari. "Single Anchor Localization and Orientation Performance Limits using Massive Arrays: MIMO vs. Beamforming". In: *2015 IEEE International Conference on Communication Workshop (ICCW)*. June 2015, pp. 853–858. DOI: 10.1109/ICCW.2015.7247282.

[76] Zhi Quan Luo et al. "Semidefinite Relaxation of Quadratic Optimization Problems". In: *IEEE Signal Processing Magazine* 27.3 (May 2010), pp. 20–34. ISSN: 1053-5888. DOI: 10.1109/MSP.2010.936019.

[77] T. S. Rappaport et al. "Wideband Millimeter-Wave Propagation Measurements and Channel Models for Future Wireless Communication System Design". In: *IEEE Transactions on Communications* 63.9 (Sept. 2015), pp. 3029–3056. ISSN: 0090-6778. DOI: 10.1109/TCOMM.2015.2434384.

[78] Sophocles J Orfanidis. "Antenna Arrays". In: *Electromagnetic waves and antennas*. Rutgers University New Brunswick, NJ, 2002, pp. 1100–1110.

[79] Miguel Sousa Lobo et al. "Applications of second-order cone programming". In: *Linear Algebra and its Applications* 284.1 (1998). International Linear Algebra Society (ILAS) Symposium on Fast Algorithms for Control, Signals and Image Processing, pp. 193–228. URL: http://www.sciencedirect.com/science/article/pii/S0024379598100320.

[80] Frank Kelly. "Charging and rate control for elastic traffic". In: *Transactions on Emerging Telecommunications Technologies* 8.1 (1997), pp. 33–37.

[81] K. Witrisal et al. "High-Accuracy Localization for Assisted Living: 5G systems will turn multipath channels from foe to friend". In: *IEEE Signal Processing Magazine* 33.2 (Mar. 2016), pp. 59–70. DOI: 10.1109/MSP.2015.2504328.

[82] Tianyang Bai and Robert W Heath. "Coverage and Rate Analysis for Millimeter-Wave Cellular Networks". In: *IEEE Transactions on Wireless Communications,* 14.2 (2015), pp. 1100–1114.

[83] Sung Nok Chiu et al. *Stochastic geometry and its applications*. John Wiley & Sons, 2013.

[84] Francois Baccelli and Bartlomiej Blaszczyszyn. *Stochastic Geometry and Wireless Networks, Volume II - Applications*. Ed. by Baccelli et al. Vol. 2. Foundations and Trends in Networking: Vol. 4: No 1-2, pp 1-312. Stochastic Geometry and Wireless Networks, Volume I - Theory; see http://hal.inria.fr/inria-00403039. NoW Publishers, 2009, p. 209. DOI: 10.1561/1300000026. URL: https://hal.inria.fr/inria-00403040.

[85] H. Elshaer et al. "Downlink and Uplink Cell Association With Traditional Macrocells and Millimeter Wave Small Cells". In: *IEEE Trans. Wireless Commun.* 15.9 (July 2016), pp. 6244–6258.

[86] Young Jin Chun, Mazen O Hasna, and Ali Ghrayeb. "Modeling heterogeneous cellular networks interference using poisson cluster processes". In: *IEEE Journal on Selected Areas in Communications* 33.10 (2015), pp. 2182–2195.

[87] G. Ghatak, A. De Domenico, and M. Coupechoux. "Modeling and Analysis of HetNets with mm-Wave Multi-RAT Small Cells Deployed along Roads". In: *IEEE GLOBECOM 2017*. Dec. 2017, pp. 1–7. DOI: 10.1109/GLOCOM.2017.8254855.

[88] Seongah Jeong et al. "Beamforming design for joint localization and data transmission in distributed antenna system". In: *IEEE Transactions on Vehicular Technology* 64.1 (2015), pp. 62–76.

[89] D. Kumar et al. "On Trade-off Between 5G Positioning and mmWave Communication in a Multi-user Scenario". In: *2018 8th International Conference on Localization and GNSS (ICL-GNSS)*. June 2018, pp. 1–5. DOI: 10.1109/ICL-GNSS.2018.8440904.

[90] G. E. Garcia et al. "Transmitter Beam Selection in Millimeter-Wave MIMO With In-Band Position-Aiding". In: *IEEE Transactions on Wireless Communications* 17.9 (Sept. 2018), pp. 6082–6092. DOI: 10.1109/TWC.2018.2854583.

[91] G. E. Garcia et al. "Fast in-Band Position-Aided Beam Selection in Millimeter-Wave MIMO". In: *IEEE Access* 7 (2019), pp. 142325–142338. DOI: 10.1109/ACCESS.2019.2944579.

[92] *AT&T, San Jose Agree on New Wireless Infrastructure to Facilitate 5G*. Apr. 2018. URL: https://www.radioworld.com/trends-1/at-t-san-jose-agree-on-new-wireless-infrastructure-to-facilitate-5g.

[93] J. G. Andrews et al. "Modeling and Analyzing Millimeter Wave Cellular Systems". In: *IEEE Transactions on Communications* 65.1 (Jan. 2017), pp. 403–430. ISSN: 0090-6778. DOI: 10.1109/TCOMM.2016.2618794.

[94] A. Dammann et al. "Optimizing waveforms for positioning in 5G". In: *2016 IEEE 17th International Workshop on Signal Processing Advances in Wireless Communications (SPAWC)*. July 2016, pp. 1–5. DOI: 10.1109/SPAWC.2016.7536783.

[95] S. Singh, R. Mudumbai, and U. Madhow. "Interference Analysis for Highly Directional 60-GHz Mesh Networks: The Case for Rethinking Medium Access Control". In: *IEEE/ACM Transactions on Networking* 19.5 (Oct. 2011), pp. 1513–1527. ISSN: 1063-6692. DOI: 10.1109/TNET.2011.2122343.

[96] Harry L Van Trees. *Detection, estimation, and modulation theory*. John Wiley & Sons, 2004.

[97] Vera Ignatevna Pagurova. *Tables of the exponential integral*. Vol. 8. Pergamon Press, 1961.

[98] Marco Di Renzo. "Stochastic geometry modeling and analysis of multi-tier millimeter wave cellular networks". In: *IEEE Transactions on Wireless Communications* 14.9 (2015), pp. 5038–5057.

[99] Andrew M Hunter, Jeffrey G Andrews, and Steven Weber. "Transmission Capacity of ad hoc Networks with Spatial Diversity". In: *IEEE Trans. Wireless Commun.* 7.12 (Dec. 2008), pp. 5058–5071.

[100] H. Shokri-Ghadikolaei et al. "Millimeter Wave Cellular Networks: A MAC Layer Perspective". In: *IEEE Trans. Wireless Commun.* 63.10 (Oct. 2015), pp. 3437–3458. ISSN: 0090-6778. DOI: 10.1109/TCOMM.2015.2456093.

[101] J. Talvitie et al. "Novel Algorithms for High-Accuracy Joint Position and Orientation Estimation in 5G mmWave Systems". In: *2017 IEEE Globecom Workshops (GC Wkshps)*. Dec. 2017, pp. 1–7. DOI: 10.1109/GLOCOMW.2017.8269069.

[102] Andreas Roessler. "Cell search and cell selection in UMTS LTE". In: *White paper, Rhode & Schwarz* (2009).

[103] M. Giordani et al. "Comparative analysis of initial access techniques in 5G mmWave cellular networks". In: *2016 Annual Conference on Information Science and Systems (CISS)*. Mar. 2016, pp. 268–273. DOI: 10.1109/CISS.2016.7460513.

[104] C. N. Barati et al. "Directional Cell Discovery in Millimeter Wave Cellular Networks". In: *IEEE Transactions on Wireless Communications* 14.12 (Dec. 2015), pp. 6664–6678. DOI: 10.1109/TWC.2015.2457921.

[105] A. Capone, I. Filippini, and V. Sciancalepore. "Context Information for Fast Cell Discovery in mm-wave 5G Networks". In: *Proceedings of European Wireless 2015; 21th European Wireless Conference*. May 2015, pp. 1–6.

[106] G. Ghatak, A. De Domenico, and M. Coupechoux. "Coverage Analysis and Load Balancing in HetNets With Millimeter Wave Multi-RAT Small Cells". In: *IEEE Trans. Wireless Commun.* 17.5 (May 2018), pp. 3154–3169. ISSN: 1536-1276. DOI: 10.1109/TWC.2018.2807426.

[107] Orikumhi Igbafe et al. "Location-aware Beam Alignment for mmWave Communications". In: *arXiv preprint arXiv:1907.02197* (2019).

[108] M. Bartlett. "Periodogram analysis and continuous spectra". In: *Biometrika* 37.1/2 (1950), pp. 1–16.

[109] J. Capon. "High-resolution frequency-wavenumber spectrum analysis". In: *Proc. IEEE* 57.8 (Aug. 1969), pp. 1408–1418. ISSN: 0018-9219. DOI: 10.1109/PROC.1969.7278.

[110] R. Schmidt. "Multiple emitter location and signal parameter estimation". In: *IEEE Transactions on Antennas and Propagation* 34.3 (Mar. 1986), pp. 276–280. DOI: 10.1109/TAP.1986.1143830.

[111] Yanpeng Yang et al. "Fast and Reliable Initial Access with Random Beamforming for mmWave Networks". In: *CoRR* abs/1812.00819 (2018). arXiv: 1812.00819. URL: http://arxiv.org/abs/1812.00819.

[112] Y. Li et al. "Design and Analysis of Initial Access in Millimeter Wave Cellular Networks". In: *IEEE Transactions on Wireless Communications* 16.10 (Oct. 2017), pp. 6409–6425. DOI: 10.1109/TWC.2017.2723468.

[113] M. Hussain and N. Michelusi. "Throughput optimal beam alignment in millimeter wave networks". In: *2017 Information Theory and Applications Workshop (ITA)*. Feb. 2017, pp. 1–6. DOI: 10.1109/ITA.2017.8023460.

[114] M. Koivisto et al. "Joint Device Positioning and Clock Synchronization in 5G Ultra-Dense Networks". In: *IEEE Transactions on Wireless Communications* 16.5 (May 2017), pp. 2866–2881. DOI: 10.1109/TWC.2017.2669963.

[115] R. Mendrzik, H. Wymeersch, and G. Bauch. "Joint Localization and Mapping Through Millimeter Wave MIMO in 5G Systems". In: *2018 IEEE Global Communications Conference (GLOBECOM)*. Dec. 2018, pp. 1–6. DOI: 10.1109/GLOCOM.2018.8647451.

[116] Z. Abu-Shaban et al. "Error Bounds for Uplink and Downlink 3D Localization in 5G mmWave Systems". In: *IEEE Transactions on Wireless Communications* 17.8 (Aug. 2018), pp. 4939–4954. DOI: 10.1109/TWC.2018.2832134.

[117] S. Hur et al. "Millimeter Wave Beamforming for Wireless Backhaul and Access in Small Cell Networks". In: *IEEE Transactions on Communications* 61.10 (Oct. 2013), pp. 4391–4403. ISSN: 0090-6778. DOI: 10.1109/TCOMM.2013.090513.120848.

[118] M. Kokshoorn et al. "Millimeter Wave MIMO Channel Estimation Using Overlapped Beam Patterns and Rate Adaptation". In: *IEEE Transactions on Signal Processing* 65.3 (Feb. 2017), pp. 601–616. ISSN: 1053-587X. DOI: 10.1109/TSP.2016.2614488.

[119] A. Alkhateeb, G. Leus, and R. W. Heath. "Compressed sensing based multi-user millimeter wave systems: How many measurements are needed?" In: *2015 IEEE International Conference on Acoustics, Speech and Signal Processing (ICASSP)*. Apr. 2015, pp. 2909–2913. DOI: 10.1109/ICASSP.2015.7178503.

[120] J. Lee, G. Gil, and Y. H. Lee. "Exploiting spatial sparsity for estimating channels of hybrid MIMO systems in millimeter wave communications". In: *2014 IEEE Global Communications Conference*. Dec. 2014, pp. 3326–3331.

[121] S. Malla and G. Abreu. "Channel estimation in millimeter wave MIMO Systems: Sparsity enhancement via reweighting". In: *2016 International Symposium on Wireless Communication Systems (ISWCS)*. Sept. 2016, pp. 230–234. DOI: 10.1109/ISWCS.2016.7600906.

[122] Arash Shahmansoori et al. "Tracking Position and Orientation through Millimeter Wave Lens MIMO in 5G Systems". In: *CoRR* abs/1809.06343 (2018). arXiv: 1809.06343. URL: http://arxiv.org/abs/1809.06343.

[123] M. Ulmschneider et al. "Multipath assisted positioning in vehicular applications". In: *2016 13th Workshop on Positioning, Navigation and Communications (WPNC)*. Oct. 2016, pp. 1–6. DOI: 10.1109/WPNC.2016.7822850.

[124] Christian Gentner et al. "Positioning using terrestrial multipath signals and inertial sensors". In: *Mobile Information Systems* 2017 (2017).

[125] M. Frohle, C. Lindberg, and H. Wymeersch. "Cooperative localization of vehicles without inter-vehicle measurements". In: *2018 IEEE Wireless Communications and Networking Conference (WCNC)*. Apr. 2018, pp. 1–6. DOI: 10.1109/WCNC.2018.8377047.

[126] J. L. Williams and R. A. Lau. "Convergence of loopy belief propagation for data association". In: *2010 Sixth International Conference on Intelligent Sensors, Sensor Networks and Information Processing*. Dec. 2010, pp. 175–180. DOI: 10.1109/ISSNIP.2010.5706750.

[127] Yibo Wu et al. "Cooperative Localization with Angular Measurements and Posterior Linearization". In: *arXiv preprint arXiv:1907.04700* (2019).

[128] Stijn Wielandt and Lieven Strycker. "Indoor multipath assisted angle of arrival localization". In: *Sensors* 17.11 (2017), p. 2522.

[129] Frank R Kschischang, Brendan J Frey, Hans-Andrea Loeliger, et al. "Factor graphs and the sum-product algorithm". In: *IEEE Transactions on information theory* 47.2 (2001), pp. 498–519.

[130] Alexander Ihler, John III, and Alan Willsky. "Loopy Belief Propagation: Convergence and Effects of Message Errors." In: *Journal of Machine Learning Research* 6 (May 2005), pp. 905–936.

[131] Florian Meyer et al. "Message passing algorithms for scalable multitarget tracking". In: *Proceedings of the IEEE* 106.2 (2018), pp. 221–259.

[132] *Samsung and Verizon announce first 5G customer trials set to begin in Q2 2017*. 2017. URL: https://news.samsung.com/global/samsung-and-verizon-announce-first-5g-customer-trials-set-to-begin-in-q2-2017.

[133] *AT&T, San Jose Agree on New Wireless Infrastructure to Facilitate 5G*. Apr. 2018. URL: https://www.radioworld.com/trends-1/at-t-san-jose-agree-on-new-wireless-infrastructure-to-facilitate-5g.

[134] A. Shahmansoori et al. "Tracking Position and Orientation Through Millimeter Wave Lens MIMO in 5G Systems". In: *IEEE Signal Processing Letters* 26.8 (Aug. 2019), pp. 1222–1226. DOI: 10.1109/LSP.2019.2925969.

[135] V. Va, H. Vikalo, and R. W. Heath. "Beam tracking for mobile millimeter wave communication systems". In: *2016 IEEE Global Conference on Signal and Information Processing (GlobalSIP)*. Dec. 2016, pp. 743–747.

[136] L. Di Palma et al. "Circularly-Polarized Reconfigurable Transmitarray in Ka-Band With Beam Scanning and Polarization Switching Capabilities". In: *IEEE Transactions on Antennas and Propagation* 65.2 (Feb. 2017), pp. 529–540. ISSN: 1558-2221. DOI: 10.1109/TAP.2016.2633067.

[137] A. Clemente et al. "Electronically-Steerable Transmitarray Antennas for Ka-Band". In: *2019 13th European Conference on Antennas and Propagation (EuCAP)*. Mar. 2019, pp. 1–4.

[138] M. Bengtsson and B. Ottersten. "Optimal and Suboptimal Transmit Beamforming". In: *Handbook of Antennas in Wireless Communications*. CRC Press, 2001, pp. 18-1–18-33. ISBN: 9780849301247.

[139] Martin Haenggi. *Stochastic geometry for wireless networks*. Cambridge University Press, 2012.

UNIVERSITE BRETAGNE LOIRE / MATHSTIC

UNIVERSITÉ DE RENNES 1

Titre : Fonctions conjointes de localisation et de communication dans les réseaux 5G en bandes millimétriques

Mot clés : 5G, bandes millimétriques, localisation, communication, formation de faisceau, partage de ressources

Résumé : Dans ce travail de thèse, on se proposait d'explorer les synergies inhérentes entre services de radiolocalisation et de communication au sein de systèmes sans fil en bandes millimétriques (mm-Wave). Ces derniers sont actuellement pressentis pour couvrir les besoins de la cinquième génération (5G) de réseaux en termes de débits et de charges utiles. Un objectif général consistait alors à montrer comment ces deux fonctions pouvaient s'avérer mutuellement bénéfiques. Tout d'abord, nous avons étudié comment la formation de faisceau (au sens du pré-codage) pouvait contribuer à améliorer les performances de localisation, pour des systèmes multi-porteuses mono- et multi-utilisateurs. En particulier, en s'appuyant sur les performances théoriques de localisation au sens de la limite inférieure de Cramér-Rao (CRLB), nous avons montré qu'il était possible, au moyen d'une formation de faisceau optimisée, d'améliorer l'estimation de variables radio intermédiaires, telles que le délai, l'angle de départ (AoD) et/ou l'angle d'arrivée (AoA) du signal transmis, et in fine, l'estimation de la position et/ou de l'orientation du mobile. Nous avons ensuite considéré le problème de la coexistence des deux services, en envisageant différentes stratégies de budgétisation et de partage de ressources, en temps et en fréquence. A cette occasion, nous avons illustré la présence de compromis non-triviaux entre les performances de localisation et de communication. Nous avons alors proposé des schémas d'allocation de ressources et d'optimisation des faisceaux (en termes de largeur et/ou d'alignement), permettant d'assurer conjointement le meilleur niveau de performances pour les deux services. Nous avons enfin étudié la possibilité d'exploiter explicitement l'information de localisation ainsi acquise, en particulier pour l'accès initial, l'estimation de canaux multi-trajets, ou encore la localisation et la cartographie simultanées (SLAM). En comparaison d'approches plus conventionnelles, nous avons montré comment les performances de telles applications pouvaient être améliorées en termes de précision, de latence et/ou de complexité calculatoire.

Title: Joint Localization and Communication in 5G Millimeter Wave Networks

Keywords: 5G, millimeter wave, localization, communication, beamforming, resource sharing

Abstract: In this thesis, we investigate different facets of localization and communication services motivated by the symbiosis between them in the millimeter wave (mm-Wave) context for the fifth generation (5G) of wireless communications. Our aim is twofold: first, show that this duality is mutually beneficial to both services, and second, aim towards a co-existence to capture these benefits in order to bring forth mm-Wave as a strong contender for 5G. First, we look into how beamforming, an integral part of mm-Wave communications, can aid in improving the localization performance. After characterizing the localization performance in terms of Cramér-Rao lower bound (CRLB), we show that with optimized beamforming, the estimation of localization variables (delay, angle of departure (AoD) and angle of arrival(AoA)) improves. Then we consider the problem of co-existence of the two services together in the same system while sharing time and frequency resources. We study the non-trivial trade-off between the performances of the two services during this resource budgeting. Then, relying on this trade-off, we design an optimal resource allocation scheme while also optimizing the beamwidth in order to ascertain high performance in terms of both localization and communication. In the same context, we also look into different applications of this improved location information namely initial access, channel estimation and simultaneous localization and communication (SLAM). We show that the related performances improve in terms of quality, latency and/or complexity in comparison to the conventional methods.

Fonctions conjointes de localisation et de communication dans les réseaux 5G en bandes millimétriques

1 Introduction

L'augmentation exponentielle de la demande en matière de services à haut débit de données et à très faible latence font aujourd'hui apparaître la radio en bandes millimétriques (mm-Wave) comme une technologie clé de la 5ème génération (5G) de réseaux cellulaires [1], du fait des larges bandes passantes disponibles dans cette gamme de fréquences [2]. Cependant, les transmissions mm-Wave, comme le vérifie l'équation de Friis, se caractérisent par de fortes pertes d'atténuation en fonction de la distance parcourue par l'onde, ainsi que par une grande sensibilité aux phénomènes de masquage. Les techniques de formation de faisceaux, qui mettent en oeuvre des réseaux d'antennes ultra directifs et compacts, permettent d'apporter les gains en puissance nécessaires pour compenser ces pertes et ainsi améliorer le rapport signal sur bruit en réception (signal-to-noise ratio (SNR)) [3]. Du fait de cette forte directivité, les fonctions de localisation et de communication sont intimement liées et inter-dépendantes.

Certaines propriétés intrinsèques des communications en bandes mm-Wave s'avèrent du reste bénéfiques à la localisation [4, 5]. Typiquement, une large bande fréquentielle et un grand nombre d'éléments au sein du réseau d'antennes permettent des résolutions élevées, respectivement dans les domaines temporel et angulaire. De même, la faible densité du canal de propagation en composantes multi-trajets implique un niveau réduit de perturbations et d'interférence pour l'estimation des métriques radio topo-dépendantes. Enfin, la densification des réseaux permet de s'appuyer sur un grand nombre de stations de base pouvant faire office de nœuds d'ancrage géo-référencés. Réciproquement, les informations de localisation peuvent être exploitées pour améliorer certaines fonctions de communication, a fortiori compte tenu de la nature fortement géométrique du canal mm-Wave. La localisation peut ainsi être utilisée pour assister la formation de faisceau elle-même, accélérer

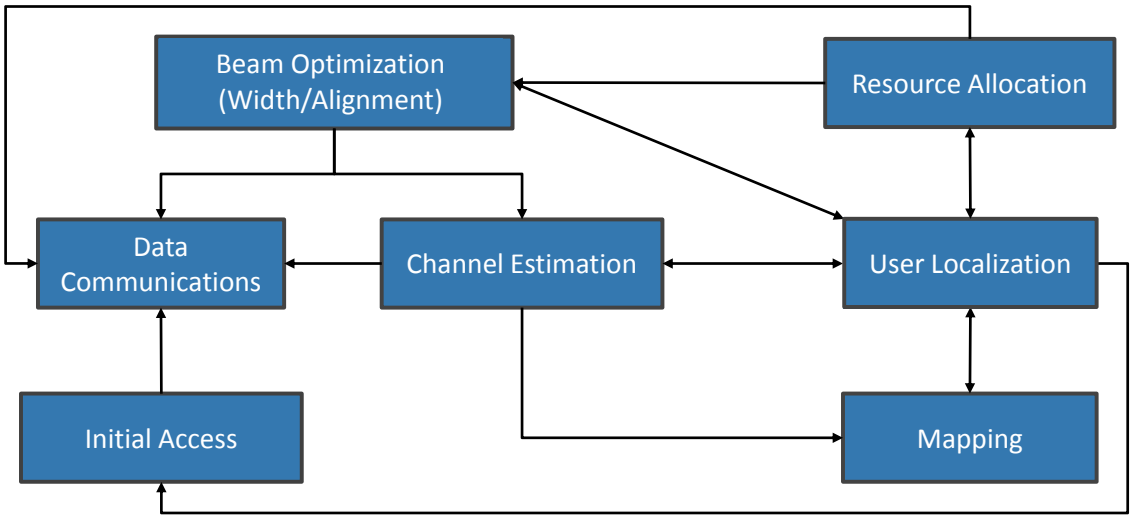

FIGURE 1: Illustration des différentes facettes de l'interdépendance entre services de localisation et de communication, au sein d'un système sans fil 5G en bande millimétrique.

l'estimation du canal ou encore la phase d'accès initial au réseau. Motivés par cette relation symbiotique, nous étudions dans notre thèse différents compromis entre fonctions de communication et de localisation, comme le montre la figure 1. In fine, l'objectif consiste à pourvoir et à optimiser de manière conjointe les deux types de services au sein d'un seul et même système mm-Wave.

2 Formation de faisceau adaptée à la localisation

Une première partie de ce travail de thèse portait sur l'optimisation de la formation de faisceau (au sens du pré-codage) vis-à-vis des performances de localisation, en complexifiant graduellement le scénario d'étude (en fonction du nombre de fréquences porteuses, du nombre d'utilisateurs et du type de métriques radio estimées).

Dans un premier temps, nous avons étudié une stratégie de formation de faisceau permettant de minimiser la limite inférieure de la borne de Cramer-Rao (CRLB) caractérisant l'estimation de l'angle d'arrivée (AoA) et du temps d'arrivée (ToA) dans un scénario multi-porteuses et mono-utilisateur, en l'abordant sous l'angle d'un problème d'allocation fréquentielle de puissance. Par la suite, nous avons considéré un scénario multi-utilisateurs, qui plus est, en introduisant l'estimation de variables radio supplémentaires, à savoir l'angle de départ (AoD) ainsi que les coefficients complexes du canal (i.e., en complément des variables AoA et ToA). Nous avons alors calculé une forme simplifiée de la borne CRLB pour chacun des paramètres estimés indépendamment, avant d'exprimer une erreur "composite" de

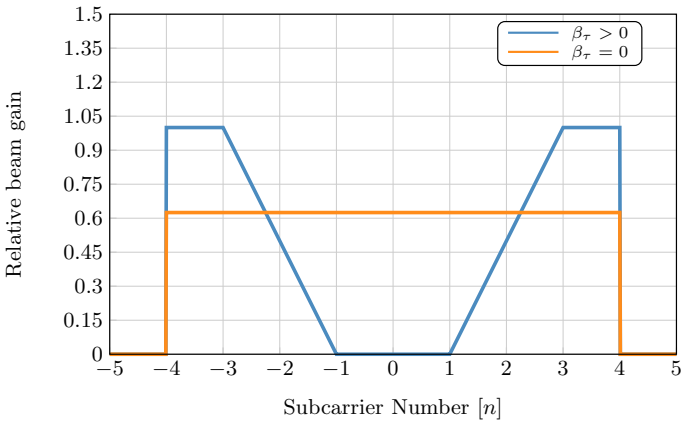

FIGURE 2: Allocation de puissance par sous-porteuse pour différentes valeurs de β_τ.

localisation sous la forme d'une combinaison linéaire intégrant les bornes théoriques précédentes. Enfin, cette erreur "composite" a été introduite comme fonction de coût pour l'optimisation de faisceau dans les deux cas. La flexibilité de cette fonction de coût permet de mettre l'accent, au choix, sur l'une ou l'autre des variables radio intermédiaires estimées, ou encore sur la position finale en résultant.

Dans le contexte multi-utilisateurs, nous avons également considéré des stratégies d'allocation de ressource basées sur différents critères d'équité (en particulier, des stratégies de type *min-max* et *proportional fairness*). Ces stratégies permettent une gestion optimale du faisceau entre utilisateurs en fonction de contraintes applicatives a priori, tout en appliquant globalement la même approche d'optimisation que dans le cas mono-utilisateur.

A titre d'exemple, la figure 2 illustre une allocation de puissance en fonction de la fréquence, respectivement en tenant compte ou en ignorant les composantes liées à l'estimation du ToA au sein de la fonction de coût (resp. via les coefficients $\beta_\tau > 0$ ou $\beta_\tau = 0$). Il apparaît alors que pour un coefficient $\beta_\tau > 0$, une majeure partie de la puissance disponible est allouée aux deux extrémités du spectre, augmentant d'autant la largeur de bande effective et ainsi la capacité de résolution temporelle du système (pour peu que les ambiguïtés spatiales aient été correctement résolues). En revanche, pour l'estimation de l'AoD et de l'AoA, dans la mesure où la fréquence ne joue aucun rôle selon le modèle sous-jacent de signal utilisé, on note une répartition uniforme de la puissance sur l'ensemble des sous-porteuses. Sur la figure 3, nous présentons le résultat de l'optimisation de la formation de faisceau pour le scénario canonique multi-utilisateurs de la figure 4. Nous observons alors des niveaux variables de puissance transmise dans les directions des trois utilisateurs distincts, en fonction de la stratégie d'équité considérée et de la qualité relative de chaque lien (selon la distance et l'orientation vis-à-vis de la stations de base).

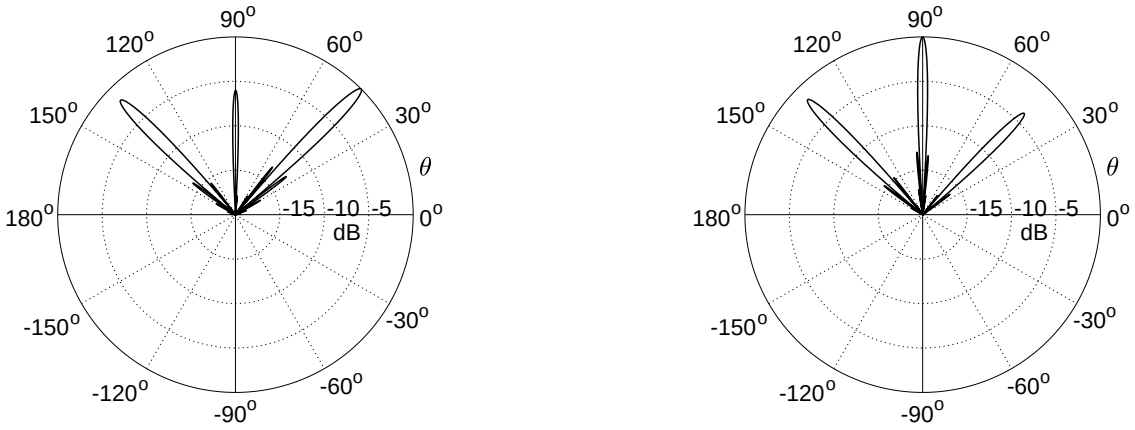

FIGURE 3: Exemple de faisceaux optimisés au sens de l'erreur de localisation dans un cas multi-utilisateurs, selon les stratégies d'équité (a) min-max et (b) proportionnelle.

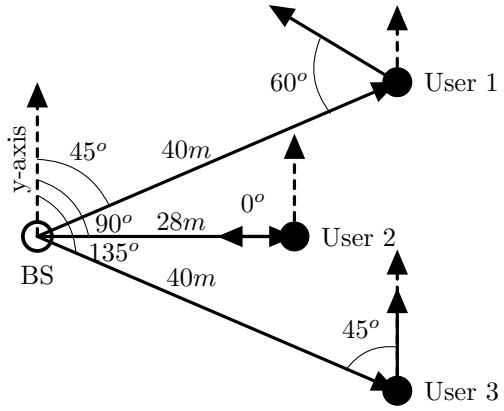

FIGURE 4: Exemple de scénario canonique impliquant une BS et 3 utilisateurs mobiles, avec des positions et orientations relatives distinctes vis-à-vis de la BS.

3 Étude du compromis entre services de localisation et de communication

Après avoir cherché à optimiser la formation de faisceau au sens d'une minimisation de l'erreur de localisation, nous nous sommes concentrés sur la manière dont les services de localisation et de communication peuvent être intégrés et opérés au sein d'un même système, étant donné un budget en ressources limité a priori (temps, fréquence, puissance). Nous avons d'abord considéré le cas de services de localisation et de communication indépendants, pour lequel nous avons évalué a posteriori le résultat de différentes stratégies statiques/fixes de partage des ressources, en temps et en fréquence notamment. Pour un tel système, budgétiser a priori trop des ressources pour le service de transmission de données par rapport au service

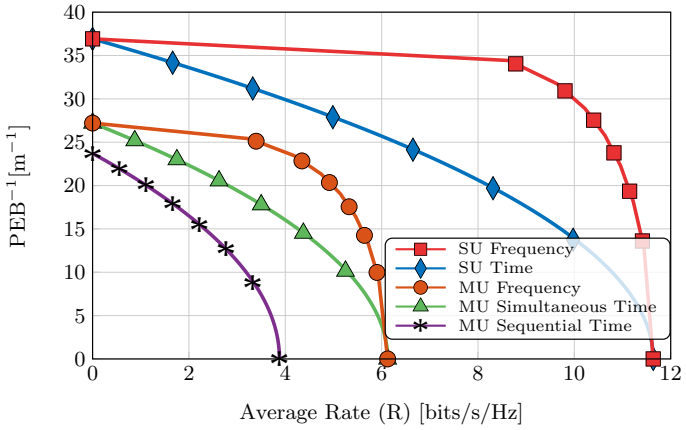

FIGURE 5: Illustration du compromis entre l'inverse de la borne théorique d'erreur de positionnement, PEB, et le débit de données moyen, R, pour diverses stratégies de répartition des ressources en fréquence et en temps et pour des scénarios mono- et multi-utilisateurs (chaque courbe est iso-budget).

de localisation mène, de manière triviale, à des débits plus élevés, mais aussi à des erreurs d'estimation de la position et de l'orientation beaucoup plus importantes. Dans un second temps, en considérant les deux services comme interdépendants, nous avons caractérisé le meilleur compromis possible entre services, non seulement pour le partage des ressources en temps et en fréquence, mais aussi pour la largeur de faisceau.

En raison de l'interdépendance des deux services, la phase de communication peut s'appuyer sur la phase de localisation afin d'optimiser la largeur de faisceau et donc de maximiser les performances de communication en termes de SINR et de probabilité de couverture pour un débit cible donné.

Sur la figure 5, on représente de manière concrète le compromis entre performances de localisation et performances de communication (exprimées respectivement comme l'inverse de la borne théorique d'erreur de positionnement, PEB, et le débit moyen, R), et ce, pour des services purement indépendants. Chaque courbe iso-budget résulte d'une stratégie spécifique de partage des ressources en temps ou en fréquence (i.e., étant fixés a priori un certain budget total de ressources, ainsi qu'un certain facteur de partage de ces mêmes ressources entre services). En jouant sur le facteur de partage des ressources β, il est alors possible de parcourir ces courbes pour satisfaire le niveau de performance cible pour l'un ou l'autre des services. A première vue, le partage fréquentiel semble globalement plus favorable en mode *standalone*.

Au-delà du seul facteur d'allocation de ressources (β), l'exemple de la figure 6 met en évidence que la largeur du faisceau (ou de manière équivalente, le nombre total de faisceaux requis pour couvrir une cellule en DL) peut également jouer un

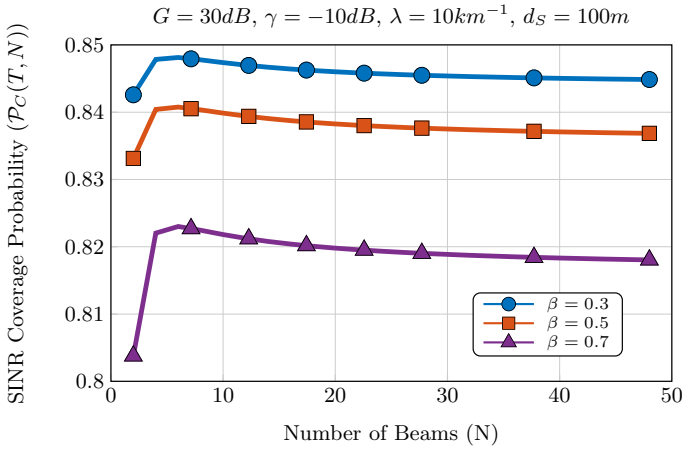

FIGURE 6: Probabilité de couverture en SINR, $\mathcal{P}_C(\gamma, N)$, en fonction du nombre total de faisceaux permettant de couvrir une cellule en DL, N (et donc, en fonction de la taille de ces mêmes faisceaux), pour différentes valeurs du facteur de partage des ressources entre services de communication et de localisation, β.

rôle prépondérant vis-à-vis des performances de communication.

4 Optimisation du faisceau pour des services conjoints de localisation et de communication

Après avoir constaté la présence de compromis entre services de localisation et de communication, nous avons ensuite cherché à formuler et à résoudre conjointement les problèmes d'allocation de ressources et d'optimisation de faisceau (i.e., au sens d'une sélection du faisceau et de sa largeur), en supposant que cette dernière pouvait s'appuyer sur l'information mise à disposition lors de la phase de localisation.

A cet effet, en traitant d'un cas canonique (e.g., déploiement de BSs le long des rues en milieu urbain), nous avons formulé un nouveau problème d'optimisation, en cherchant à maximiser les performances de communication sous la contrainte d'une erreur de localisation inférieure à un seuil critique (e.g., reflétant les besoins d'une application topo-dépendante). Pour un instant donné, le résultat de cette optimisation permet alors de déterminer la meilleure largeur de faisceau, ainsi qu'un facteur d'allocation de ressources améliorant les performances "instantanées" de localisation et de communication. En exploitant cette procédure dans un contexte itératif et donc, en supposant la répétition de l'enchaînement des phases de localisation et de communication en régime établi, on assure ainsi le raffinement et le contrôle continu de la qualité des deux services.

Nous nous sommes également intéressés plus spécifiquement au problème d'accès initial, en gardant à l'esprit les exigences de la 5G en matière de faible latence. Dans

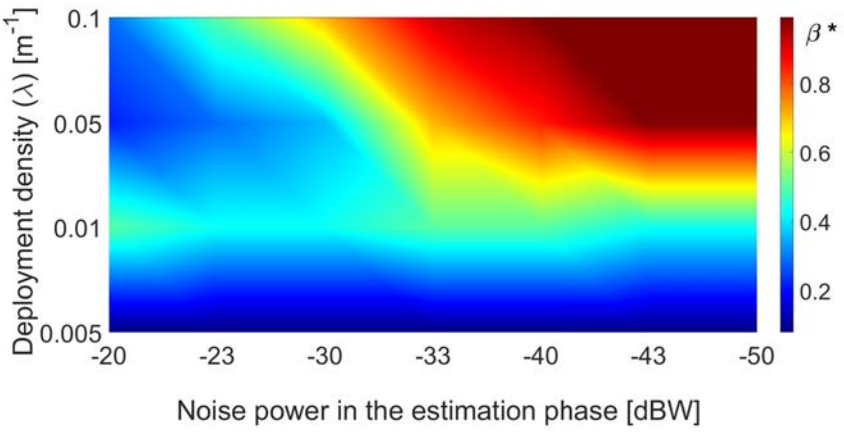

FIGURE 7: Valeur optimisée du facteur de partage de ressources β en fonction de la densité de déploiement des BSs et du niveau de bruit.

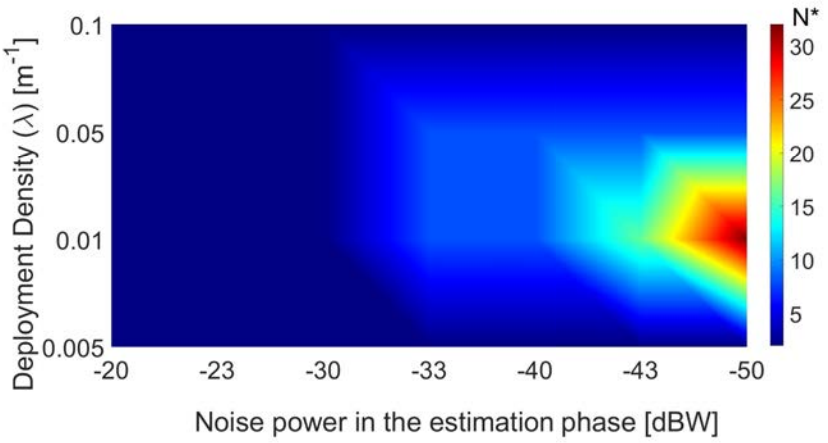

FIGURE 8: Taille optimisée du dictionnaire des faisceaux (inversement liée à largeur du faisceau) en fonction de la densité de déploiement des BSs et du niveau de bruit.

ce contexte, nous avons, là encore, exploité l'information de localisation de manière itérative pour la sélection initiale de faisceau. Nous avons alors comparé cette approche avec des méthodes de sélection et d'apprentissage de faisceau classiques, à savoir les méthodes itératives de recherche exhaustive et hiérarchique.

Sur les figures 7 et 8, on représente respectivement le facteur d'allocation des ressources optimisé, ainsi que la largeur de faisceau optimisée, et ce, pour deux paramètres clés du réseau (i.e., densité de déploiement des BSs en ordonnées et bruit d'estimation en abscisses). Comme on peut le noter, la méthode proposée permet de dégager des solutions optimisées a priori non triviales, dépendant grandement de la configuration du réseau. La figure 9, quant à elle, permet de comparer la durée de la procédure d'accès initial pour atteindre une certaine résolution spatiale donnée (via la sélection de faisceau), entre une approche s'appuyant sur l'information de

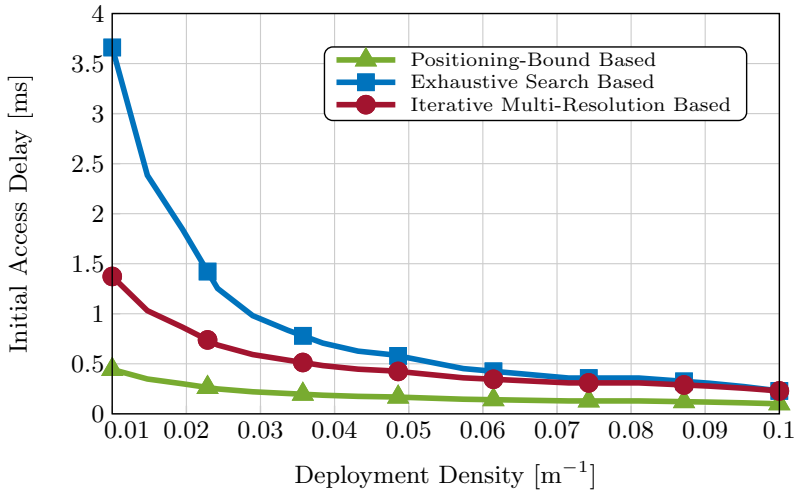

FIGURE 9: Comparaison du délai de la phase d'accès initial en fonction de la densité de déploiement du réseau, pour la stratégie proposée de sélection/d'apprentissage de faisceaux s'appuyant sur l'information de localisation et pour des stratégies itératives conventionnelles de recherche de faisceaux (i.e., exhaustive et hiérarchique).

localisation et des méthodes itératives conventionnelles. La méthode proposée à base de localisation, en particulier dans le cas d'un déploiement moins dense du réseau, semble alors surpasser assez nettement les méthodes existantes.

De manière générale, le schéma mis en avant permet, notamment pour les opérateurs, d'adapter au mieux la stratégie de sélection de faisceaux, étant donnée un déploiement de réseau.

5 Applications s'appuyant sur l'estimation angulaire multi-trajets

Nous avons enfin étudié les problèmes d'estimation de canal multi-trajets mmWave et de localisation et cartographie simultanées (SLAM), en exploitant dans les deux cas l'information angulaire AoD et AoA, qui est disponible par défaut dans le cadre de communications mmWave.

Dans le premier cas, nous avons proposé un algorithme d'estimation de canal mettant à profit la nature géométrique et la faible densité du canal multi-trajets mmWave, par le biais d'algorithmes d'acquisition comprimée. Nous avons montré en particulier que l'exploitation d'une information de localisation a priori -même erronée- en lieu et place de méthodes classiques d'apprentissage de faisceaux basées sur un balayage, permettait de réduire considérablement la durée et la complexité de cette phase critique d'estimation du canal, comme on peut le voir sur la figure 10.

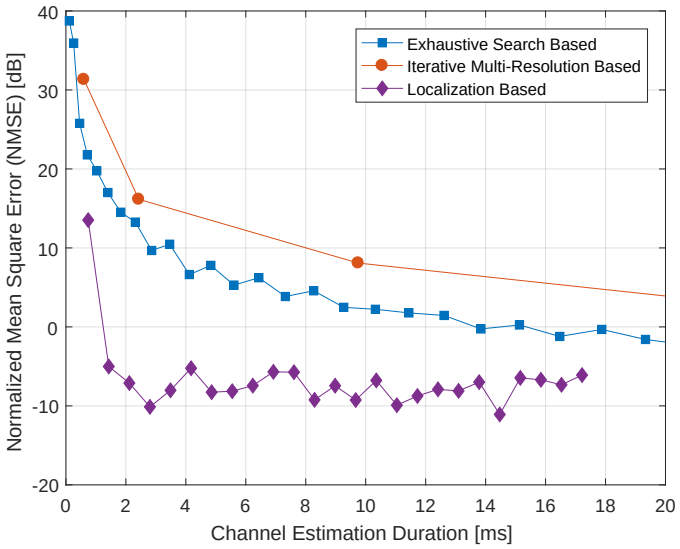

FIGURE 10: Erreur quadratique moyenne normalisée (NMSE) d'estimation du canal multi-trajets mmWave pour la méthode proposée s'appuyant sur l'information de localisation et deux méthodes de recherche conventionnelles, en fonction de la durée.

Dans le second cas d'application, nous avons utilisé les angles AoA/AoD estimés pour quelques composantes multi-trajets (i.e., issues de la phase précédente d'estimation de canal) afin d'estimer conjointement la position de l'utilisateur et celles de surfaces ou d'obstacles passifs dans l'environnement, rétro-diffusant l'onde transmise. En considérant plusieurs stations de base, nous avons alors utilisé une approche centralisée de type "passage de messages", basée sur des méthodes de propagation de croyances (BP) et une représentation du problème sous forme de *factor-graph*. Nous avons alors comparé la précision obtenue et la complexité (y compris en termes de trafic de signalisation) avec celles de méthodes SLAM distribuées existantes, exploitant les mêmes données d'entrée.

Sur la figure 10, on note qu'avec une méthode basée sur la localisation, l'erreur d'estimation du canal multi-trajets diminue plus rapidement que les autres méthodes. Ce gain de temps pourrait être crucial, en particulier dans le contexte des applications 5G à faible latence et/ou pour des scénarios dynamiques (e.g., en situation de mobilité).

Sur l'exemple de la figure 11, on remarque que la méthode BP centralisée proposée s'avère plus performante que sa variante distribuée, notamment en ce qui concerne l'estimation de la position des points de rétro-diffusion de l'environnement. Cela est principalement dû au fait que la méthode centralisée mutualise naturellement l'information de plusieurs BSs, permettant ainsi de réduire la propagation des erreurs de l'algorithme BP, et ce, en intervenant très tôt dans la séquence des messages passés (i.e., en opérant une forme de pré-filtrage d'information).

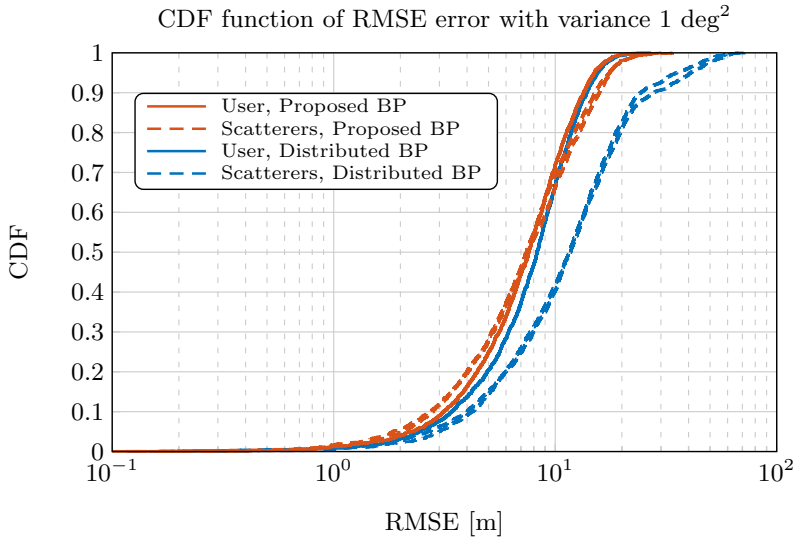

FIGURE 11: Fonction de distribution cumulative de l'erreur de positionnement de l'utilisateur et des points de rétro-diffusion de l'onde, pour la méthode BP centralisée proposée et pour la méthode distribuée existante, en supposant une variance de 1 deg^2 sur les mesures AoA/AoD multi-trajets admises en entrée.

6 Conclusions et perspectives

Dans ce travail de thèse, nous avons présenté des arguments et des résultats allant dans le sens d'une coexistence symbiotique entre localisation et communications au sein d'un même système mmWave. Nous avons illustré différents aspects de la relation complexe unissant ces deux services (e.g., sous l'angle de l'optimisation du pré-codage, de la sélection de faisceau, menée conjointement à l'allocation de ressources, ou encore de l'estimation de canal multi-trajets), en mettant en évidence leurs bénéfices mutuels, ainsi que l'existence de compromis pratiques.

Dans le cadre de futurs travaux, on envisage d'étendre les modèles sous-jacents utilisés (e.g., prise en compte des obstructions radio, coefficient de canal variable). De même, on se propose de traiter des scénarios véritablement dynamiques, en cherchant à assurer la poursuite de l'utilisateur mobile et des paramètres de canaux associés. Enfin, on vise une validation expérimentale de certaines contributions de la thèse (e.g., accès initial à faible latence, estimation du canal multi-trajets à basse complexité), en s'appuyant en particulier sur des dispositifs antennaires à 26-28GHz développés récemment au CEA-Leti.

Bibliography

[1] T. S. Rappaport et al. "Millimeter Wave Mobile Communications for 5G Cellular: It Will Work!" In: *IEEE Access* 1 (2013), pp. 335–349. ISSN: 2169-3536. DOI: 10.1109/ACCESS.2013.2260813.

[2] Z. Pi and F. Khan. "An introduction to millimeter-wave mobile broadband systems". In: *IEEE Communications Magazine* 49.6 (June 2011), pp. 101–107. ISSN: 0163-6804. DOI: 10.1109/MCOM.2011.5783993.

[3] O. E. Ayach et al. "Spatially Sparse Precoding in Millimeter Wave MIMO Systems". In: *IEEE Transactions on Wireless Communications* 13.3 (Mar. 2014), pp. 1499–1513. ISSN: 1536-1276. DOI: 10.1109/TWC.2014.011714.130846.

[4] Stefania Bartoletti et al. *5G Localization and Context-Awareness*. https://www.5gitaly.eu/wp-content/uploads/2019/01/5G-Italy-White-eBook-5G-Localization.pdf.

[5] COST Action CA15104, IRACON, Troels Pedersen, and Bernard Henri Fleury. *Whitepaper on New Localization Methods for 5G Wireless Systems and the Internet-of-Things*. English. Other. 2018.